Fibroblast Growth Factor Receptor 3 in Bladder Cancer - Perpetrator or Passenger?

Ryan James Ellison

Doctor of Philosophy

University of York

Biology

September 2024

Abstract

FGFR3 mutations are frequent in bladder cancer, where they are associated with lower stage and grade of disease, better prognosis, reduced risk of progression, and tumours which retain urothelial differentiation features.
While existing dogmata state that FGFR3 mutations must have a causative role in driving proliferation in urothelial carcinogenesis due to the frequency with which they occur, there is little evidence to support this, and in fact numerous studies suggest that FGFR3 mutation cannot drive urothelial proliferation.

With this in mind, the aims of this work were:

- To explore factors that control FGFR3 expression in normal urothelium, including urothelial differentiation status and growth factor signalling
- To examine the effect(s) of FGFR3 overexpression and mutation on normal urothelium

These questions were investigated using urothelial tissue and normal human urothelial (NHU) cells derived from this tissue. These NHU cells were used both in the undifferentiated state (modelling proliferative urothelium and/or basal/squamous tumours) as well as the differentiated state (modelling mitotically-quiescent *in situ* urothelium). FGFR3 protein and transcript were observed in urothelial tissue but not in proliferative NHU cells, where growth factor signalling is dominated by EGFR. Inhibition of EGFR resulted in expression of functional, glycosylated FGFR3 which could be stimulated by ligand.

Overexpression of the most common FGFR3 mutation in bladder cancer (FGFR3-S249C) in differentiated NHU cells did not drive urothelial proliferation, as measured by expression of the cell cycle marker *MKI67*.

This work showed that FGFR3 expression is negatively regulated by EGFR activity, but only in a proliferative undifferentiated urothelial context. The fact that FGFR3 mutation was unable to drive urothelial proliferation represents the first evidence in a non-cancerous human urothelial cell model that FGFR3 mutation does not drive proliferation during urothelial tumour initiation. This questions the role of FGFR3 mutation in the initiation of bladder cancer.

Contents

Abstract **3**
Contents **4**
List of abbreviations 10
List of Figures **13**
List of Tables **17**
Acknowledgements **18**
Author's Declaration **19**
1. Introduction **20**
1.1 The Urothelium 20
1.1.1 Structure and function of the urothelium 20
1.2 Bladder cancer 22
1.2.1 Grading and Staging of Bladder Cancer 22
1.2.2 NMIBC vs MIBC 24
1.2.3 Stratification strategy for management of NMIBC and MIBC 25
1.2.4 Overview of NMIBC and MIBC classification 26
1.2.5 Molecular Pathways of BLCA development 26
1.2.5.1 - The two pathways model 26
1.2.5.2 - Additional mutations and field cancerization 27
1.2.6 Upper Tract Urothelial Carcinoma 29
1.3 Growth Factors and Growth Factor Receptors in urothelial repair, development, and cancer 29
1.3.1 EGFR family in normal urothelium 30
1.3.2 EGFR family in BLCA 31
1.4 Fibroblast Growth Factor Receptor 3 32
1.4.1 The Fibroblast Growth Factor Family 32
1.4.2 FGFR3 in the normal urothelium 33
1.4.2.1 Control of FGFR3 expression 33
1.4.2.1.1 Expression and role of FGFR3 in urothelial tissue 33
1.4.2.1.2 Regulation of FGFR3 expression in normal and neoplastic urothelium 33
1.4.2.1.3 Regulation of FGFR3 expression in non-urothelial tissues 34
1.4.2.1.4 Alternative Splicing of FGFR3 35
1.4.2.1.5 Glycosylation of FGFR3 protein 37
1.4.2.2 Activation and localisation of FGFR3 37
1.4.2.2.1 Canonical signalling pathways activated downstream of FGFR3 37
1.4.2.2.2 Localisation and activation of FGFR3 in cell models 39
1.4.2.2.3 Localisation and activation of FGFR3 in urothelial tissue 41
1.4.3 FGFR3 in Bladder Cancer 41
1.4.3.1 FGFR3 point mutations are associated with tumours of lower stage and grade 44
1.4.3.2 FGFR3 gene fusions 49
1.4.4 Association of FGFR3 expression with urothelial differentiation in BLCA 50

1.4.5 Current Models of FGFR3 activation in urothelial carcinogenesis.....50
1.4.5.1 Effects of FGFR3 mutation in cell models..... 50
1.4.5.2 Mouse models of FGFR3 mutation in urothelium..... 51
1.5 Experimental Platform - Normal Human Urothelial (NHU) cells..... 53
1.5.1 Phenotypes of NHU cells in culture..... 53
1.5.2 Differentiation of NHU cells..... 58
1.5.3 Serum and calcium-mediated differentiation of NHU cells..... 58
1.6 Thesis Aims..... 59
2. Materials and Methods.....61
2.1 General..... 61
2.1.1 H2O and Buffers..... 61
2.1.2 List of Suppliers..... 61
2.1.3 Stock Solutions..... 62
2.2 Tissue culture..... 66
2.2.1 Overview..... 66
2.2.2 Ethical Approval for Sample Collection and details of donor tissue used 66
2.2.3 Urothelial Samples, cell culture, and storage..... 70
2.2.4 Chemical agonists and antagonists used in experiments..... 71
2.2.5 Differentiation of NHU cells..... 72
2.2.6 Generation of transduced NHU cells..... 73
2.3 Western blotting..... 73
2.3.1 Cell Harvesting..... 73
2.3.2 Protein Quantification..... 73
2.3.3 SDS Polyacrylamide Gel Electrophoresis (PAGE)..... 74
2.3.4 Western blotting to detect protein..... 75
2.3.5 Titration of C-terminal FGFR3 and pFRS2 antibodies for use in western blotting..... 76
2.4 Molecular Biology..... 77
2.4.1 General..... 77
2.4.2 RNA extraction..... 77
2.4.3 DNAse digest..... 78
2.4.4 cDNA synthesis..... 78
2.4.5 Gel electrophoresis..... 78
2.4.6 Real-time quantitative PCR (RT-qPR)..... 79
2.4.7 Plasmids used for generation of FGFR3-transduced cell lines..... 79
2.5 Histology..... 80
2.5.1 Tissue Fixation..... 80
2.5.2 Embedding of Tissue in Paraffin Wax..... 80
2.5.3 Sectioning of Tissue Blocks..... 80
2.5.4 Haematoxylin and Eosin (H&E) Staining..... 80
2.6 - Immunohistochemistry..... 81
2.6.1 Antigen retrieval..... 81
2.6.2 Antibody Labelling..... 81
2.6.3 Imaging and microscopy..... 82

2.7 Immunofluorescence..... 82
2.7.1 Slide preparation and fixation..... 82
2.7.2 Antibody Labelling..... 83
2.7.3 Imaging and microscopy.....84
2.8 Bioinformatics..... 84
2.8.1 Datasets used in this thesis generated by others within the Jack Birch Unit..... 84
2.8.2 External datasets used in this thesis..... 85
2.9 Statistical Analysis.....85
2.10 Generation of Transduced NHU cell lines..... 86
2.10.1 Source of FGFR3-containing vectors..... 86
2.10.2 Generation and verification of FGFR3 expression plasmids..... 86
2.10.3 Transduction and selection of NHU cells.....90
3. Investigation of factors which regulate FGFR3 transcript and protein expression in normal urothelium.....92
3.1 Aims and Objectives.....92
3.2 Experimental Design..... 93
3.2.1 Investigation of factors with the potential to influence FGFR3 transcript and/or protein expression in NHU cells..... 93
3.2.1.1 EGFR downstream signalling activity..... 93
3.2.1.2 Cholera Toxin and potential for Protein Kinase A activity..... 93
3.2.1.3 Urothelial differentiation..... 93
3.2.2 Analysis of FGFR3 transcript variants expressed in urothelial tissue and in NHU cells.....94
3.3 Results..... 95
3.3.1 Selection of BLCA cell lines for an FGFR3 protein expression positive control 95
3.3.2 Analysis of FGFR3 transcript and protein expression in urothelial tissue and NHU cells.....96
3.3.2.1 FGFR3 transcript expression in urothelial tissue and NHU cells from bladder and ureter tissue.....96
3.3.2.2 FGFR3 protein expression in urothelial tissue.....98
3.3.3 Investigation of factors which regulate expression of FGFR3 transcript and protein in NHU cells.....101
3.3.3.1 Cell confluence produced a slight increase in FGFR3 protein expression in undifferentiated NHU cells.....101
3.3.3.2 EGFR inhibition resulted in expression of FGFR3 protein.....104
3.3.3.3 Inhibition of the EGFR downstream signalling cascade.....110
3.3.2.4 Presence of cholera toxin in cell culture media had no significant effect on FGFR3 protein expression..... 111
3.3.3.5 FGFR3 protein was not expressed in differentiated NHU cells.....112
3.3.3.6 Activity of Peroxisome Proliferator-Activated Receptor Gamma (PPARγ) and Retinoic Acid Receptor Gamma (RARγ) inhibited expression of FGFR3 protein..... 115
3.3.4 Characterisation of FGFR3 transcript and protein expressed in urothelial tissue and NHU cells..... 117
3.3.4.1 Multiple different FGFR3 transcript isoforms were expressed in

urothelial tissue..... 117
3.3.4.2 FGFR3 protein expressed in NHU cells following EGFR inhibition was glycosylated..... 119
3.4 Summary..... 120
3.5 Discussion..... 121
3.5.1 What factors regulate expression of FGFR3 in urothelial tissue and in vitro urothelial cell models?..... 121
3.5.1.1 Repression of FGFR3 transcript and protein expression by EGFR and ERK activity..... 121
3.5.1.2 The potential mechanism of EGFR-ERK repression of FGFR3..... 121
3.5.1.3 EGFR/ERK-mediated repression of FGFR3 does not entirely explain FGFR3 expression patterns in urothelial tissue and NHU cells..... 122
3.5.2 Comparison of FGFR3 and EGFR family expression in urothelial tissue.... 123
3.5.3 Expression of FGFR3 in bladder vs ureter tissue..... 123
3.5.4 Analysis of FGFR3 transcript isoforms expressed in urothelial tissue..... 124
3.5.5 Glycosylation of FGFR3 in NHU cells..... 125
3.5.6 Does FGFR3 have a role in urothelial tissue?..... 126
3.5.7 Potential limitations of this work..... 126
4. Activation and localisation of FGFR3 protein in NHU cells..... 128
4.1 Aims and Objectives..... 128
4.2 Experimental Design..... 128
4.2.1 Use of Fibroblast Growth Factor 9 (FGF9) to activate FGFR3..... 128
4.2.2 Localisation of FGFR3 protein in NHU cells with and without activation..... 129
4.2.3 Localisation of FGFR3 protein in Urothelial tissues..... 130
4.3 Results..... 131
4.3.1 Expression of FGFR3 but not other FGFRs increased significantly in NHU cells in response to EGFR inhibition..... 131
4.3.2 Titration of FGF9 for activation of FGFR3 protein..... 132
4.3.3 Activation of FGFR3 protein expressed in EGFR-inhibited NHU cells..... 133
4.3.4 FGFR3 protein localisation in urothelial tissues..... 135
4.3.4.1 Titration of FGFR3 antibodies for immunohistochemical labelling of urothelial tissue and selection of controls..... 135
4.3.4.2 FGFR3 protein was expressed evenly throughout the layers of the urothelium in six tissue samples..... 139
4.3.5 Localisation of FGFR3 protein in NHU cells..... 143
4.3.5.1 Titration of FGFR3 antibodies for immunofluorescence labelling of NHU cells and selection of controls..... 143
4.3.5.2 FGFR3 protein showed cytoplasmic and perinuclear localisation within EGFR-inhibited NHU cells, regardless of FGFR3 activation status..... 151
4.4 - Summary..... 163
4.5 - Discussion..... 164
4.5.1 Signalling pathways activated downstream of FGFR3 in NHU cells..... 164
4.5.2 Variability of FGFR3 protein expression withinNHU cell cultures..... 164
4.5.3 Localisation of FGFR3 in urothelium..... 166
4.5.4 Potential limitations of this study..... 168
5. Effects of FGFR3 mutational activation in Bladder Cancer and urothelial cells.. 169

5.1 Aims and Objectives....169
5.2 Experimental Design.... 170
5.2.1 Experimental use of FGFR3-transduced NHU cell lines.... 170
5.2.2 Use of MKI67 transcript and Ki67 protein as markers of urothelial proliferation 171
5.2.3 Assessment of proliferation status in bladder cancer cohorts.... 172
5.3 Results.... 174
5.3.1 Phenotype of FGFR3-overexpressing NHU cells in culture.... 174
5.3.2 Assessment of FGFR3 protein overexpression and activity in transduced NHU cells....177
5.3.3 Overexpression of wild-type or S249C mutant FGFR3 did not significantly alter proliferation of differentiated NHU cells....179
5.3.4 Localisation of mutant FGFR3 and wild-type FGFR3 in differentiated NHU cells.... 181
5.3.5 FGFR3 mutations were associated with significantly lower expression of cell cycle-associated transcripts in NMIBC and MIBC....185
5.4 Summary.... 192
5.5 Discussion.... 193
5.5.1 Is FGFR3 mutation capable of driving urothelial proliferation? Contradictions in the literature....193
5.5.2 FGFR3 mutations were associated with lower expression of proliferation marker transcripts in both NMIBC and MIBC.... 194
5.5.3 FGFR3 mutations have been associated with reduced proliferation in other tissues.... 195
5.5.4 Lack of PIK3K activation downstream of FGFR3 - implications for BLCA...196
5.5.5 Potential limitations of this study.... 196
6. Discussion.... 198
6.1 Thesis Overview....198
6.2 Different acquisition and roles of FGFR3 mutations in NMIBC vs MIBC.....199
6.3 The link between FGFR3 mutations, urothelial differentiation, and immunosuppression in MIBC....202
6.4 Limitations of this study....204
6.5 Strengths of this study....204
6.6 Future Work....205
6.7 Conclusions....206
7. Appendix....207
Appendix A - Representative uncropped western blots.... 207
FGFR3....207
Phospho-ERK....208
Phospho-FRS2....209
Phospho-EGFR.... 210
Phospho-Akt.... 211
Phospho-ERBB2.... 212
ZO-3.... 213
Cytokeratin 13.... 214
Cytokeratin 14.... 215

B-actin..... 216
Appendix B - Titration of Cetuximab and Lapatinib in NHU cells..... 217
Titration of Cetuximab.....217
Titration of Lapatinib..... 220
Appendix C - Original assessment of FGFR3 protein expression in all 8 donor samples 224
8. References.....225

List of abbreviations

ABS	Adult Bovine Serum
APOBEC	apolipoprotein B mRNA-editing enzyme, catalytic polypeptide
AU	Arbitrary Units
Ba/Sq	Basa/Squamous
BCG	Bacillus Calmette–Guérin
BLCA	Bladder Cancer
BMP	Bone Morphogenic Protein
BPE	Bovine Pituitary Extract
BSA	Bovine Serum Albumin
CIS	Carcinoma in Situ
CK	Cytokeratin
CT	Cholera Toxin
DAG	diacylglycerol
DEPC	Diethyl pyrocarbonate
DMEM	Dulbecco's Modified Eagle Medium
DMSO	Dimethyl Sulfoxide
DNA	Deoxyribonucleic acid
DTT	dithiothreitol
DUSP	Dual-specificity phosphatase
EDTA	ethylenediaminetetraacetic acid
EGF	Epidermal Growth Factor
EGFR	Epidermal Growth Factor Receptor
EORTC	European Organization for Research and Treatment of Cancer
ERBB	Erythroblastic Oncogene B
ERK	Extracellular signal-regulated kinase
FGF	Fibroblast Growth Factor
FGFR	Fibroblast Growth Factor Receptor
FGFRL1	FGF-receptor-like 1
FRS2	FGFR substrate 2
HB-EGF	Heparin-binding EGF
HEPES	4-(2-hydroxyethyl)-1-piperazineethanesulfonic acid
hTERT	human telomerase reverse transcriptase
IF	Immunofluorescence
IFN	Interferon
IHC	Immunohistochemistry

IP3	inositol triphosphate
KSFM	Keratinocyte Serum Free Media
KSFMc	KSFM Complete
LAMP1	lysosome associated protein 1
LumP	Luminal Papillary
MAPK	Mitogen-activated protein kinase
MEK	MAPK/ERK kinase
MHC	Major histocompatibility complex
MIBC	Muscle-invasive BLCA
NHU	Normal Human Urothelial
NMIBC	Non muscle-invasive BLCA
PAGE	Polyacrylamide Gel Electrophoresis
PBS	Phosphate-buffered saline
PCR	Polymerase chain reaction
PD-L1	Programmed Death Ligand 1
PI3K	Phosphoinositide 3-kinase
PIP2	phosphatidylinositol
PLC	phospho-lipase C
PPAR	Peroxisome Proliferator-Activated Receptor
PVDF	polyvinylidene difluoride
RNA	Ribonucleic acid
RPMI	Roswell Park Memorial Institute
RTK	Receptor tyrosine kinase
RT-PCR	Reverse transcriptase PCR
SDS	sodium dodecyl sulphate
SHH	Sonic Hedgehog
SPRY	Sprouty
SRA	Sample Reducing Agent
STAT	signal transducer and activator of transcription
TBS	Tris Buffered Saline
TCGA	The Cancer Genome Atlas
TER	Transepithelial electrical resistance
TGF	Transforming growth factor
TPM	Transcripts per million
TURBT	Trans-urethral resection of the bladder tumour
UPK	Uroplakin
UTR	Untranslated region

UTUC	Upper Tract Urothelial Carcinoma
WT	Wild-type
ZO	Zonula Occludens

List of Figures

Figure 1.1 - Cross-section of the urothelium ……21
Figure 1.2 - Staging of bladder cancer based on tumour invasiveness……23
Figure 1.3 - Summary of outcomes, recurrence, and progression risk for NMIBC and MIBC……25
Figure 1.4 - The two proposed molecular pathways by which BLCA develops……...27
Figure 1.5 - Additional mutations which may play a role in the evolution of BLCA…….28
Figure 1.6 - Alternative splicing of FGFR3……36
Figure 1.7 - Canonical FGFR3 signalling pathways……38
Figure 1.8 - Negative regulation mechanisms of FGFR3 signalling……..39
Figure 1.9 - Three main Mechanisms of *FGFR3* alteration in Bladder Cancer……43
Figure 1.10 - Mechanism of FGFR3 activation following point mutation and sites of most common *FGFR3* point mutations……44

Figure 2.1 - Examples of healthy vs unhealthy appearances in NHU cell cultures…….71
Figure 2.2 - Titration of C-terminal FGFR3 antibody for western blotting using NHU cell lysate……....77
Figure 2.3 - Titration of pFRS2 antibody for western blotting using RT112 BLCA cell lysate……77
Figure 2.4 - Plasmid map of pLXSP vector control used to generate transduced NHU cell lines……87
Figure 2.5 - Plasmid map of wildtype FGFR3 used to generate transduced NHU cell lines……88
Figure 2.6 - Sequence of 249 region of wild type FGFR3 plasmid……89
Figure 2.7 - Plasmid map of S249C mutant FGFR3 used to generate transduced NHU cell lines……89
Figure 2.8 - Sequence of 249 region of S249C mutant FGFR3 plasmid……90
Figure 2.9 - DNA electrophoresis gel of the plasmids used to transduce NHU cells……91
Figure 2.10 - Process of how NHU cells were transduced to generate NHU cell lines which stably overexpressed FGFR3……91
Figure 2.11 - Representative images of transduced NHU cells under puromycin selection……92

Figure 3.1 - In a panel of BLCA cell lines FGFR3 protein expression was greatest in RT112 BLCA cells……..96

Figure 3.2 - Expression of *FGFR3* and *EGFR* family transcripts in urothelial tissue and NHU cells……..……..…….98
Figure 3.3 - FGFR3 protein was expressed in urothelial tissue……..99
Figure 3.4 - Histology of urothelial tissue samples used for western blotting……100
Figure 3.5 - Expression of FGFR3 protein in undifferentiated vs differentiated NHU cells…….103
Figure 3.6 - Cell micrograph images of undifferentiated and differentiated NHU cells….104
Figure 3.7 - FGFR3 protein expression in NHU cells was triggered by EGFR inhibition…….105-106
Figure 3.8 - FGFR3 protein expression in NHU cells was inversely correlated to ERK phosphorylation……107
Figure 3.9 - Cell culture images of NHU cells with and without EGFR inhibition……..108
Figure 3.10 - Expression of *FGFR3* transcript in NHU cells with and without EGFR inhibition……109
Figure 3.11 - Expression of FGFR3 protein in NHU cells following 72 h inhibition of EGFR using tyrosine kinase inhibitors PD153035 or AG1478 or EGFR-neutralising antibody cetuximab……..110
Figure 3.12 - Expression of FGFR3 protein in NHU cells following 72 h inhibition of EGFR downstream signalling pathway components……..111
Figure 3.13 - FGFR3 Expression in NHU cells following EGFR inhibition with and without the presence of cholera toxin in the growth medium……..……112
Figure 3.14 - Expression of *EGFR* family members in NHU cells following urothelial differentiation……113
Figure 3.15 - FGFR3 protein was not detected in differentiated NHU cells with or without inhibition of EGFR family member tyrosine kinase activity……115
Figure 3.16 - Expression of FGFR3 protein was significantly reduced by activation of PPARg or RARγ compared to a DMSO vehicle control……117
Figure 3.17 - Breakdown of FGFR3 transcript expressed in bladder urothelial tissue into individual isoforms……..……..……119
Figure 3.18 - Deglycosylation of FGFR3 protein expressed in NHU cells following EGFR inhibition……120

Figure 4.1 - Expression of FGFRs in NHU cells with and without EGFR inhibition……132
Figure 4.2 - Dose dependent activation of FGFR3 by FGF9 in NHU cells……..……133
Figure 4.3 - Activation of FGFR3 in EGFR-inhibited NHU cells over a 120 min time-course……..135

Figure 4.4 - Titration of FGFR3 N-terminal antibody in urothelial and control tissues……137-138
Figure 4.5 - Titration of FGFR3 C-terminal antibody in urothelial and control tissues…..139
Figure 4.6 - Localisation of FGFR3 protein within urothelial tissue……..141
Figure 4.7 - Experimental controls for immunohistochemical analysis of FGFR3 protein within urothelial tissues……142
Figure 4.8 - Titration of FGFR3 N-terminal antibody in RT112 BLCA cells…….145-146
Figure 4.9 - Titration of FGFR3 C-terminal antibody in RT112 BLCA cells…….147-148
Figure 4.10 - Titration of LAMP1 antibody in RT112 BLCA cells……..149-150
Figure 4.11 - Titration of Calnexin antibody in RT112 BLCA cells……151-152
Figure 4.12 - FGFR3 protein expression was variable across a population of NHU cells…….154-155
Figure 4.13 - Localisation of FGFR3 within NHU cells……..……158
Figure 4.14 - Localisation of FGFR3 within NHU cells compared with lysosomal marker LAMP1……159
Figure 4.15 - Localisation of FGFR3 within NHU cells compared with endoplasmic reticulum marker calnexin……...160
Figure 4.16 - Localisation of FGFR3 within RT112 positive control BLCA cell lines…….161
Figure 4.17 - Localisation of LAMP1 and Calnexin in NHU cells treated with and without PD153035 and FGF9……..163

Figure 5.1 - Experimental schematic for treatment of *FGFR3*-overexpressing NHU cell lines……172
Figure 5.2 - Phase contrast images of undifferentiated transduced NHU cells in culture……176
Figure 5.3 - Phase contrast images of Y2946 transduced NHU cells in culture during differentiation……177
Figure 5.4 - Expression and activation of FGFR3 in transduced NHU cells……..179
Figure 5.5 - Expression of proliferation marker *MKI67* was not significantly changed by overexpression of wild-type or S249C mutant FGFR3 vs vector-only controls……180
Figure 5.6 - Nuclear Ki67 index of transduced differentiated NHU cellswas not significantly changed by overexpression of wild-type or S249C mutant FGFR3 vs vector-only control……..181
Figure 5.7 - N-terminal localisation of both wild-type and S249C mutant FGFR3 protein was perinuclear in differentiated NHU cells……..183

Figure 5.8 - C-terminal localisation of both wild-type and S249C mutant FGFR3 protein was cytoplasmic and perinuclear in differentiated NHU cells……184
Figure 5.9 - FGFR3 immunofluorescence in pLXSP vector-only control NHU cells…….185
Figure 5.10 - FGFR3 mutations were associated with significantly lower expression of cell cycle-associated transcripts in UROMOL NMIBC tumours……...186
Figure 5.11 - FGFR3 mutations were associated with significantly lower expression of cell cycle-associated transcripts in Class 2a and Class 2b UROMOL NMIBC tumours……..187
Figure 5.12 - FGFR3 mutations were associated with significantly lower expression of cell cycle-associated transcripts in Stage T1 UROMOL NMIBC tumours……..188
Figure 5.13 - FGFR3 mutations were associated with significantly lower expression of cell cycle-associated transcripts in mostly high-grade vs low-grade UROMOL NMIBC tumours……..189
Figure 5.14 - FGFR3 mutations were associated with significantly lower expression of cell cycle-associated transcripts in TCGA MIBC tumours……190
Figure 5.15 - FGFR3 mutations were associated with significantly lower expression of cell cycle-associated transcripts in LumP but not Ba/Sq TCGA MIBC tumour…….191
Figure 5.16 - FGFR3 mutations were associated with significantly lower expression of cell cycle-associated transcripts in TCGA MIBC tumours regardless of tumour stage……192

Figure 6.1 - Schematic representation of how *FGFR3* mutations may occur independently in NMIBC and MIBC rather than progressing from NMIBC……...201
Figure 6.2 - PPARγ would theoretically link *FGFR3* mutation to both the luminal differentiation and immune desert phenotypes in MIBC tumours…….204

List of Tables

Table 1.1 - Factors which have been previously identified in the literature to either promote or repress expression of FGFR3 transcript and/or protein……..34
Table 1.2 - List of common FGFR3 mutations in BLCA and region of receptor they affect……...……46-48
Table 1.3 - Markers of differentiated and undifferentiated phenotypes in normal urothelium and bladder cancer……..…....54-57

Table 2.1 - List of suppliers…….……61-62
Table 2.2 - Information on NHU cell lines and donor tissue used in this thesis…….67-70
Table 2.3 - List of chemical agonists and antagonists used in this study……..72
Table 2.4 - List of antibodies used for western blotting……..75-76
Table 2.5 - List of antibodies used for immunohistochemistry…….82
Table 2.6 - List of antibodies used for immunofluorescence microscopy……..84
Table 2.7 - Datasets used in this thesis generated by others within the Jack Birch Unit…85
Table 2.8 - External datasets used in this thesis……...86

Table 4.1 - Variables representing colocalisation of FGFR3 N- and C-terminus and FGFR3 C-terminus and LAMP1 or Calnexin……..157-158

Table 5.1 - Genes chosen as markers of cell cycle activity……...173-174

Acknowledgements

Firstly, I would like to thank my partner Rhiannon and my family, particularly my parents. Without their moral and financial support this PhD would not have been possible.
I would like to thank my supervisors - Professor Jenny Southgate, Dr Simon Baker and Dr Gareth Evans - as well as my TAP member Dr Andrew Holding, for their support and advice.

I would like to thank all of my colleagues and friends in the Jack Birch Unit. They have provided such a wonderful environment to work and study in, and I believe I have genuinely made friends for life.

Thanks also go to the staff in the Biology department for providing a wonderful study environment. Particular thanks go to the staff at Cookies: Jenny, Jo and Louis.
I would like to thank York Against Cancer for funding my PhD, and most importantly a heartfelt thanks to all of the patients and their families who donated tissue. Without them this research could not have been possible.

Author’s Declaration

I declare that this thesis is a presentation of original work and I am the sole author. Where others have contributed to this work, appropriate credit has been given. This work has not previously been presented for a degree or other qualification at this University or elsewhere. All sources are acknowledged as references.

1. Introduction

1.1 The Urothelium

1.1.1 Structure and function of the urothelium

The urothelium is the specialised epithelial lining of the bladder, ureter, renal pelvis and proximal urethra of the urinary tract [reviewed by Jafari and Rohn, 2022]. The urothelium acts to provide a tight urinary barrier to prevent the passage of toxic components of urine (such as urea) to the surrounding tissues [reviewed by Kreft et al., 2010]. The human urothelium is composed of 3-6 layers of cells and can be divided into basal, intermediate, and superficial layers (Fig. 1.1) based on different morphology [Jost et al., 1989b]. Basal cells are the smallest and possess the smallest, most-condensed nuclei - cells become larger with larger nuclei towards the superficial layer [Jost et al., 1989b]. Basal and intermediate cells are mononuclear, while superficial cells can be either mononuclear or binuclear [Jost et al., 1989b]. Urothelial layers can also be distinguished by the differential expression of cytokeratins [reviewed by Southgate et al., 1999], tight junction [Acharya et al., 2004, Varley et al., 2006] and uroplakin [Wu et al., 1990, Yu et al., 1990] proteins. Superficial cells contain tight junctions on their lateral surfaces and an asymmetric unit membrane on their luminal surface, which together form the tight urinary barrier [Jost et al., 1989b].

The urothelium typically has a low cell turnover and is mitotically quiescent [Martin, 1972, Jost et al, 1989a, Jost et al, 1989b], however the urothelium can enter a regenerative state following damage, e.g. exposure to cytotoxic agents or during catheterisation [de Boer et al., 1994, Simeonova et al., 2000].

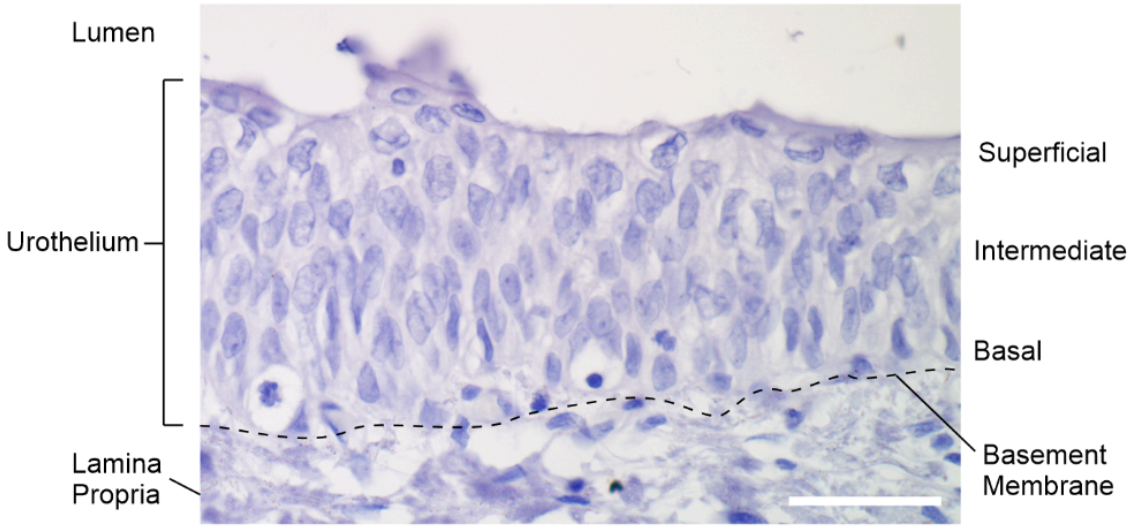

Figure 1.1 - Cross-section of the urothelium - Urothelial layers are labelled, as well as the approximate location of the basement membrane dividing the urothelium from underlying lamina propria (dotted black line). Human urothelial tissue section stained with haematoxylin and eosin to identify cell nuclei and cytoplasm respectively. Scale bar (white line) is 50 μm.

1.2 Bladder cancer

Urothelial cancers originate from the epithelial lining of the bladder and urinary tract, the urothelium. The majority of urothelial cancers are Bladder Cancer (BLCA), with a much smaller percentage (0.7-1.7%) being Upper Tract Urothelial Carcinoma (UTUC) [reviewed by Petros, 2020].

Around 10,000 people are diagnosed with BLCA each year in the UK, with over 5,000 deaths per year [Cancer Research UK, 2020]. In the UK, 73% of BLCA cases are in men and 27% in women [Cancer Research UK, 2020], and this reflects the global trend of increased incidence in men [reviewed by Dobruch et al., 2016]. BLCA typically affects older individuals, with more than 80% of UK cases occurring in those over 65 years old [reviewed by Mushtaq et al., 2019].

The main accepted risk factors for BLCA incidence are smoking [Freedman et al., 2011, Wilhelm-Benartzi et al., 2011] and occupational hazard, e.g. exposure to heavy metals and aromatic amines [reviewed by Al-Zalabani et al., 2016; Mushtaq et al., 2019].

The earliest sign of BLCA is typically blood in the urine. Diagnosis is usually made after observing a tumour through cystoscopy, as well as cytology and imaging [Davis et al., 2012, reviewed by Ahmadi and Daneshmand, 2021]. Cystoscopy involves insertion of a flexible camera up the urethra to view the luminal surface of the bladder. Cytology involves examining patient cells under a microscope to observe for cellular abnormalities that could indicate cancer. In BLCA, cytology is normally performed on cells present in urine voided by patients [reviewed by Shariat et al., 2008].

1.2.1 Grading and Staging of Bladder Cancer

In routine clinical practice, BLCAs are labelled using the TNM staging system, where TNM stands for Tumour, Node, Metastasis [Sobin et al., 2009, Cancer Research UK, 2022]. Tumour stage (given by a “T” value e.g. T1) describes how far the tumour has invaded into the bladder. Non-muscle-invasive BLCA (NMIBC) consists of Ta tumours contained entirely within the urothelium and T1 tumours which have breached the basement membrane beneath the urothelium (Fig. 1.2). Muscle-invasive BLCA (MIBC) consists of T2-T4 tumours; a T2 tumour which has invaded the muscle surrounding the bladder, a T3 tumour which has invaded the surrounding fatty tissue and a T4 tumour which has metastasized to at least one surrounding organ. In addition to T stages, non-invasive disease also contains Carcinoma in Situ (CIS), a flat lesion on the surface of the

urothelium, which is typically of high-grade and has a high likelihood of progression [Sobin et al., 2009, reviewed by Tang and Chang, 2015].

“Node” refers to whether the tumour has entered into a patient's lymph nodes. This typically signals worse prognosis as entering the lymph nodes allows cancer cells to travel around the body through the lymph network, leading to metastasis [reviewed by Pereira et al., 2015]. “Metastasis” refers to a cancer which has spread to another part of the body from the original site and typically this signifies worse prognosis [reviewed by Rosen and Sapra, 2020].

Tumours are also assigned a grade based on histology which reflects the differentiation of the tumour, ranging from G1 (well-differentiated and near-normal appearance) to G3 (poorly-differentiated) [reviewed by MacLennan et al., 2007]. Generally speaking, higher grade and stage tumours are more aggressive with a worse prognosis [reviewed by Lenis et al., 2020].

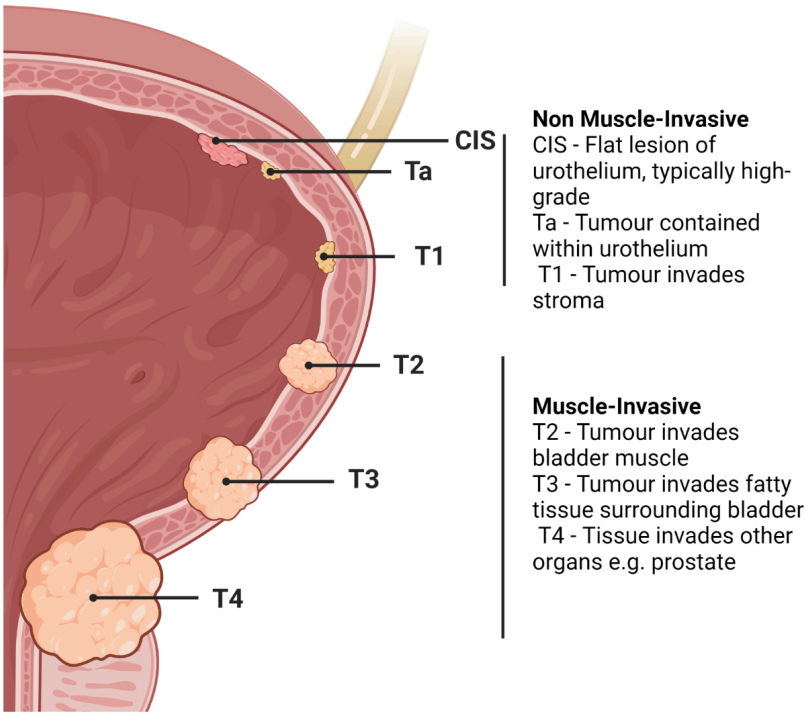

Figure 1.2 - Staging of bladder cancer based on tumour invasiveness - Adapted from Herranz et al., 2021 Figure 1 under Creative Commons 4.0 international.

1.2.2 NMIBC vs MIBC

Distinguishing between NMIBC and MIBC is useful due to their different behaviours, in terms of aggressiveness, prognosis, and treatment requirements (Fig. 1.3). NMIBC has a much better prognosis, with a 5-year survival rate between 71-97% [National Cancer Institute, 2023]. NMIBC is usually treated with trans-urethral resection of the bladder tumour (TURBT). This is a procedure in which the papillary growth is surgically removed during a cystoscopy. However, almost half of patients will suffer a recurrence within 2 years, and thus NMIBC requires frequent monitoring and additional surgeries [Böhle et al., 2003, Han and Gang, 2006].

NMIBC may also be treated with Bacillus Calmette–Guérin (BCG) if the NMIBC is judged to be high-risk. BCG is an attenuated strain of the bacterium *Mycobacterium bovis* also used as a vaccine for tuberculosis. BCG treatment is associated with reduced risk of recurrence or progression to MIBC. Although the mechanism of BCG is not fully understood, studies suggest that it works by stimulating the immune system in the proximity of the bladder tumour, leading to an immune response [reviewed by Jiang and Redelman-Sidi, 2022]. Intermediate and high-risk NMIBC can also be treated with intravesical (inserted directly into the bladder via a catheter) chemotherapy [reviewed by Porten et al., 2015] or with removal of part (partial cystectomy) or all of the bladder (radical cystectomy) following nonresponse to BCG [reviewed by Aminoltejari and Black, 2020].

MIBC is less frequent, with approximately 20% of patients presenting at this stage [reviewed by Patel et al., 2020]. Current therapeutic options for MIBC are limited and typically require extensive surgery with removal of part or all of the bladder and potentially surrounding organs and lymph nodes [reviewed by Lenis et al., 2020]. Bladder surgery is often preceded or followed by chemotherapy, as this has been shown to reduce the risk of recurrence and improve survival [Advanced Bladder Cancer Meta-analysis Collaboration, 2006].

Survival of MIBC is poor, with only 39% of patients surviving 5 years post-diagnosis, and survival dropping as low as 8% for metastatic MIBC [American Cancer Society, 2024]. As such there has been continued interest in increasing understanding of the underlying biology of MIBC, and of patient stratification into different molecular subtypes, to align patients better with treatments and understand the underlying drivers of disease to identify new targets for treatment [Lindgren et al., 2010, Sjodahl et al., 2012, Cancer Genome Atlas Research Network, 2014, Damrauer et al., 2014, Choi et al., 2014].

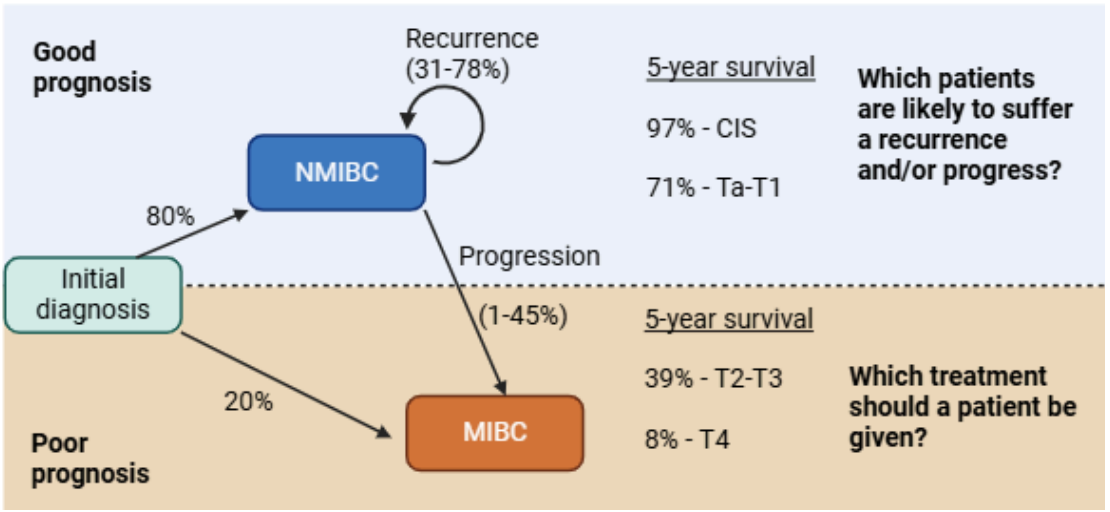

Figure 1.3 - Summary of outcomes, recurrence, and progression risk for NMIBC and MIBC - Major problems in NMIBC management include the frequency of recurrences, as well as predicting which patients will suffer a recurrence or progress to MIBC. In MIBC, the major problems are the lack of specific treatments and poor survival. All statistics are given at 5-year averages. Survival statistics were taken from American Cancer Society, 2024, recurrence and progression statistics were taken from Sylvester et al., 2006.

1.2.3 Stratification strategy for management of NMIBC and MIBC

NMIBC and MIBC pose different problems for clinicians (Fig. 1.3). In NMIBC, survival is good and rates of progression are relatively low, but it is difficult to predict which patients will suffer disease recurrence or progress to muscle-invasive disease [reviewed by Guerrero-Ramos et al., 2022]. This results in frequent invasive monitoring that is costly, and unnecessary for most patients. The majority of current research in NMIBC thus aims to allow for prediction of which patients are likely to suffer recurrence or progression. Patients at high risk of progression and/or recurrence can then be given additional treatments such as chemotherapy and BCG. Low-risk patients could then be monitored less frequently and spared from treatment.

MIBC is clinically very different, with a poor prognosis and mostly surgical treatments which could lead to poor quality of life. With MIBC-focused research, the aim of stratification is to identify characteristics (such as gene expression or mutations) that mark a patient as particularly suitable for a given treatment (e.g. targeted tyrosine kinase inhibitors or neutralising antibodies). This would allow for a precision medicine approach [reviewed by Gakis, 2020]. Despite a large number of studies identifying distinct

“molecular subtypes” in MIBC, these have yet to be integrated into routine clinical practice [Choi et al., 2014, Damrauer et al., 2014, Rebouissou et al., 2014, The Cancer Genome Atlas Research Network, 2014, Robertson et al., 2017, Marzouka et al., 2018, Kamoun et al., 2020].

1.2.4 Overview of NMIBC and MIBC classification

Generally, classification of both NMIBC and MIBC operates on an axis of luminal to basal, with luminal being associated with better prognosis and higher expression of urothelial differentiation markers, while basal tumours have a worse prognosis [reviewed by Zhu et al., 2020]. This “luminal” and “basal” terminology was originally coined in the field of breast cancer [Perou et al., 2000], and the luminal and basal subtypes of BLCA were originally identified based on their similarity to subtypes of breast cancer [Biton et al., 2014, Choi et al., 2014].

FGFR3 mutations are associated with luminal tumours in both NMIBC and MIBC, although this is clearer in MIBC. In the UROMOL NMIBC cohort, *FGFR3* mutations were associated with both the luminal Class 1 and the basal Class 3 [Lindskrog et al., 2021]. Similarly, analysis of T1 tumours found *FGFR3* mutations to be associated with a molecular subtype with low urothelial differentiation [Hurst et al., 2021]. As such, whether *FGFR3* mutations are strictly associated with luminal tumours is less clear in NMIBC. In MIBC, *FGFR3* mutations have been clearly associated with luminal tumours across many studies [Choi et al., 2014, Damrauer et al., 2014, Robertson et al., 2017, Marzouka et al., 2018, Kamoun et al., 2020]. The differences in which tumours *FGFR3* mutations are associated with in NMIBC vs MIBC could potentially indicate that *FGFR3* mutations have different effects in NMIBC vs MIBC.

1.2.5 Molecular Pathways of BLCA development

1.2.5.1 - The two pathways model

Due to the differences in gene expression, mutation, and other factors between MIBC and NMIBC, numerous groups have suggested that NMIBC and MIBC have different routes of origin [Spruck et al., 1994, Bakkar et al., 2003, van Rhijn et al., 2004]. Spruck et al. initially proposed that normal urothelium can become cancerous via two main pathways. The Ta/papillary pathway was at the time associated with loss of chromosome 9 alleles and mutations in *Fibroblast Growth Factor 3 (FGFR3)*, while *TP53* loss was associated with dysplasia and then CIS [Spruck et al., 1994]. Spruck et al., proposed that these 2

pathways converge when tumours advance to T1 and beyond. While this is a fairly simplified explanation of the molecular pathways of BLCA, the core structure proposed has remained mostly unchanged (Fig. 1.4).

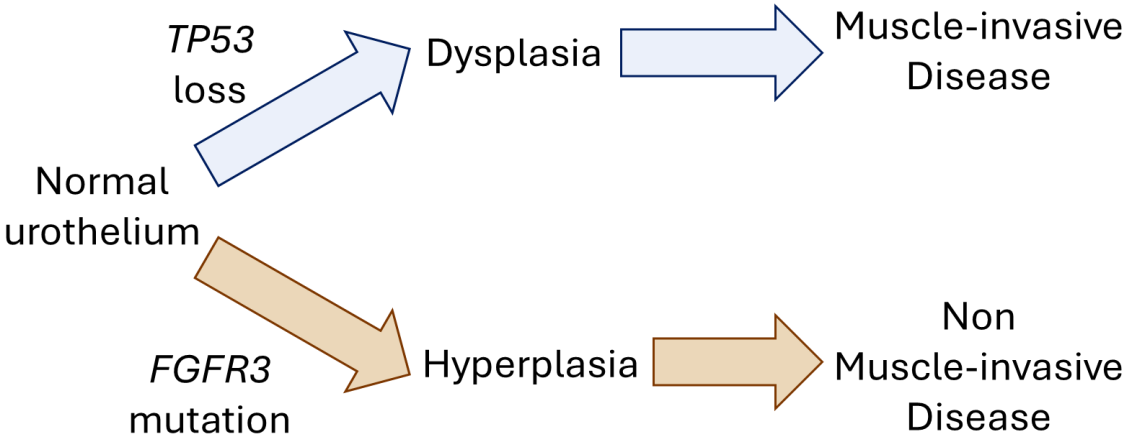

Figure 1.4 - The two proposed molecular pathways by which BLCA develops - *TP53* mutations are associated with the muscle-invasive pathway and specifically with dysplasia [Spruck et al., 1994, Bakkar et al., 2003, Van Rhin et al., 2004]. *FGFR3* mutations are associated with the non-muscle-invasive pathway and have been proposed to cause hyperplasia [van Rhijn et al., 2002, Bakkar et al., 2003, Van Rhijn et al., 2004, van Oers et al., 2006].

1.2.5.2 - Additional mutations and field cancerization

While the “two pathways” division of molecular pathways by which BLCA may evolve has remained relevant, several changes have been made following additional research (Fig 1.5). Firstly, several studies have indicated additional mutations that occur in urothelium before *FGFR3*, in what is termed the “Field Cancerization Effect” [Slaughter et al., 1953, reviewed by Wijewardhane et al., 2021]. This theory supposes that during an individual’s lifetime, the urothelium acquires a number of mutations due to exposure to carcinogens (e.g. from smoking or from consumption of aristolic acid) or from endogenous mutation processes (e.g. APOBEC cytidine deaminase activity; see Section 1.4.3.1) [Lawson et al., 2020, Li et al., 2020, Rozen et al., 2020]. Mutations acquired in this way are not sufficient to lead to cancer formation, and so the genetically-altered cells remain undetected as microscopically-normal urothelium [Lawson et al., 2020, Li et al., 2020, Rozen et al., 2020]. These mutations do however provide a selective advantage, leading to a clonal outgrowth of genetically altered cells which replace the normal surrounding urothelium. This results in clonal populations of cells which are “precancerous”. Should cells within

this population acquire a further mutation, such as in *TP53, PIK3CA,* or *RB1*, then the population may give rise to dysplasia, hyperplasia or a tumour (Fig. 1.5). Thus, these clonal populations of precancerous, microscopically normal urothelial cells can act as a source of tumour occurrences, recurrences and metastases [reviewed by Wijewardhane et al., 2021].

Common genetic alterations associated with the field cancerization effect include mutations in chromatin remodelling genes such as *KDM6A*, *KMT2D*, and *ARID1A* [Lawson et al., 2020, Li et al., 2020], as well as changes in DNA methylation which alter the expression genes involved in immune innate defence [Majewski et al., 2019]. Secondly, additional mutations have been identified which may be required for progression beyond hyperplasia and dysplasia. For example, *FGFR3* mutations are correlated with hyperplasia [van Rhijn et al., 2002, Bakkar et al., 2003, Van Rhijn et al., 2004, van Oers et al., 2006], but additional mutations in *STAG2* and *PIK3CA* [Taylor et al., 2013, reviewed by Inamura, 2018] may be required for progression to Ta, with *CDKN2* mutation proposed as being required for progression to T1 [Downes et al., 2017]. In the case of *TP53* mutations leading to dysplasia/CIS [Spruck et al., 1994, Bakkar et al., 2003, Van Rhin et al., 2004], it is now thought that additional mutations e.g. in *RB1* are required for progression to invasive disease [Kim et al., 2006].

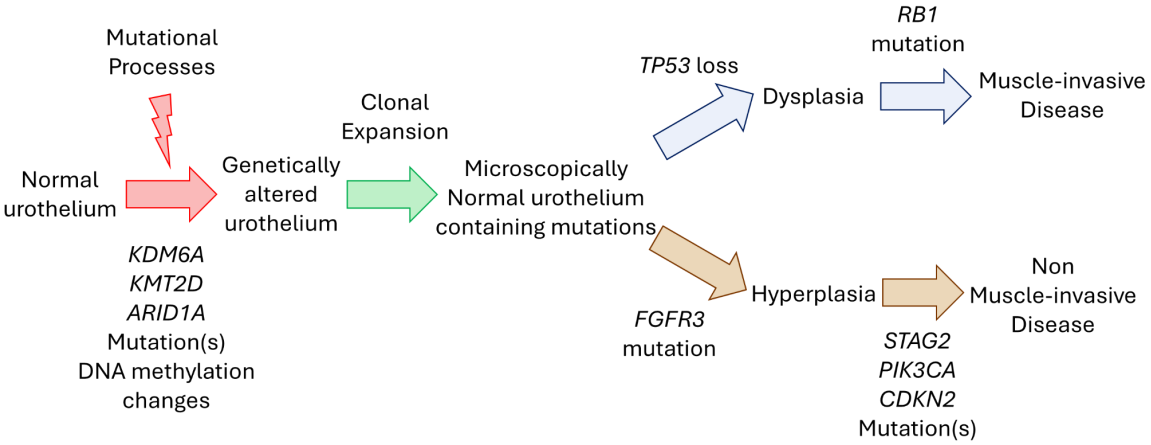

Figure 1.5 - Additional mutations which may play a role in the evolution of BLCA - Mutations in chromatin remodelling genes such as *KDM6A*, *KMT2D*, and *ARID1A* [Lawson et al., 2020, Li et al., 2020] as well as changes in DNA methylation status [Majewski et al., 2019] have been implicated in field cancerization. *RB1* mutations have been implicated in progression from dysplasia to muscle-invasive disease [Kim et al., 2006]. Mutations in *STAG2*, *PIK3CA*, and *CDKN2* have been implicated in the development of non muscle-invasive disease, such as T1 tumours [Taylor et al., 2013, Downes et al., 2017, reviewed by Inamura, 2018].

1.2.6 Upper Tract Urothelial Carcinoma

Although bladder and ureter tissue are morphologically similar, they have different embryological origins [reviewed by Liaw et al., 2018] and this is potentially reflected in differences between cancers of the bladder and ureter. Like BLCA, upper tract urothelial carcinoma (UTUC) is more common in the elderly and is more common in men than women [reviewed by Szarvas et al., 2016]. However, while BLCA survival is typically lower for women than men, survival rates have been observed as approximately equal between sexes for UTUC [reviewed by Szarvas et al., 2016]. UTUC also typically presents at a more advanced stage than BLCA, and has worse 5-year survival [reviewed by Kolawa et al., 2023].

The genetic alterations and phenotype of BLCA and UTUC are also different - UTUC is enriched for mutations in *FGFR3* and *HRAS*, while mutations in *TP53*, *RB1* and *ERBB2* are more common in BLCA [Audinet et al., 2019, Sfakianos et al., 2021]. Additionally, while BLCA consists of a number of different molecular subtypes, UTUC is enriched for Luminal Papillary tumours and the “immune desert” phenotype which is associated with *FGFR3* mutations [Robinson et al., 2019].

1.3 Growth Factors and Growth Factor Receptors in urothelial repair, development, and cancer

Several growth factor (receptor) families have been identified which play key roles in urothelial development and repair, including Epidermal Growth Factor Receptor (EGFR), Transforming Growth Factor β (TGF-β)/Bone Morphogenic Protein (BMP)/Smad, Wnt/β-Catenin, and Sonic Hedgehog (SHH) [Yu et al., 2002, Fleming et al., 2012, Haraguchi et al., 2012, Yang et al, 2014, Papafotiou et al., 2016]. These signalling pathways operate through a variety of paracrine (in cooperation with the underlying stroma) and autocrine signalling mechanisms [Varley et al., 2005, Jenkins et al., 2007, Shin et al., 2011]. These same families have also been found to participate in BLCA.

TGF-β signalling has been linked to aggressive BLCA phenotypes in multiple studies [Hung et al., 2008, Li et al., 2009, Stonjev et al., 2019], and increased expression of SMAD2 and SMAD4 has been with higher grade/stage and worse survival in BLCA [Stonjev et al., 2019. Overexpression [Kastris et al., 2009, Senol et al., 2015], nuclear localisation [Jang et al., 2010, Jing et al., 2014] and loss of plasma membrane localisation of β-catenin [Syrigos et al., 1998, Garcia del Muro et al., 2000, Kashibuchi et al., 2007] are

all associated with increased grade and stage in BLCA, as well as worse survival outcomes.

Thus urothelial development and repair pathways represent crucial normal processes which can be hijacked by cancers to drive growth and survival [He et al., 2012, Jing et al., 2014, Islam et al., 2015, Duenas et al., 2016, Martinez et al., 2017].

1.3.1 EGFR family in normal urothelium

The Epidermal Growth Factor Receptor (EGFR)/Erythroblastic Oncogene B (ERBB) family is a growth factor receptor family consisting of 4 members; ERBB1-4, with ERBB1 commonly referred to by its gene name - *EGFR* [reviewed by Wieduwilt and Moasser, 2008]. EGFR family members are crucial in development of cardiovascular, nervous, mammary and epithelial tissues by driving differentiation, proliferation and migration [reviewed by Casalini et al., 2004]. Mutation, amplification and overexpression of EGFR family members is also implicated in a number of cancers, particularly lung [reviewed by Bethune et al., 2010], breast [reviewed by Mitri et al., 2012] and bladder cancer [Chow et al., 1997, Chow et al., 2001, Cheng et al., 2002, Mason et al., 2009, Rebouissou et al., 2014].

The EGFR family members can be activated by a range of ligands, including epidermal growth factor (EGF) and transforming growth factor alpha (TGF-α); different EGFR family members have different ligand specificities [reviewed by Wieduwilt and Moasser, 2008]. Although EGFR family members have different ligand specificities and mechanisms of activation, they share downstream signalling pathways. EGFR family member activation can lead to downstream signalling via MAPK, PI3K-Akt, PLCγ, JAK-STAT and Src-FAK signalling pathways [reviewed by Jacobi et al., 2017].

The EGFR family members are differentially distributed throughout the layers of the urothelium [Chow et al., 1997, Uhlén M et al., 2015 and https://proteinatlas.org/]. EGFR protein is expressed mostly in the basal layer of the urothelium, while ERBB2 and ERBB3 are expressed most strongly in the plasma membrane of superficial urothelial cells. ERBB4 is also expressed in superficial cells. Studies measuring wound repair in explant cultures and urothelial cells following treatment with EGFR and/or ERBB2 (ant)agonists suggest that EGFR and ERBB2 play roles in driving proliferation and migration during urothelial wound repair [Bindels et al., 2002, Daher et al., 2003, Varley et al., 2005].

1.3.2 EGFR family in BLCA

EGFR mutations are rare events in BLCA with two studies failing to detect any *EGFR* mutations in their cohorts [Blehm et al., 2006, Chaux et al., 2012]. Amplifications in *EGFR* occur in 9-15% of MIBC and are associated with a basal/squamous molecular subtype [The Cancer Genome Atlas Research Network, 2014, Erikkson et al., 2017]. A number of studies have demonstrated that increasing expression of *EGFR* is associated with poor prognosis, invasiveness and disease progression in BLCA [Neal et al., 1990, Lipponen et al., 1994, Nyugen et al., 1994, Mellon et al., 1996, Popov et al., 2004, Kassouf et al., 2008, Hashimi et al., 2018, Sami et al., 2023].

In addition to the above associations, two studies have suggested that EGFR has a causal link with more advanced disease in BLCA. Cheng et al., 2002 observed that overexpression of *EGFR* in the urothelium of mice resulted in hyperplasia, showing that EGFR is capable of driving proliferation in the urothelium. Furthermore, when *EGFR* overexpression was combined with expression of SV40 large T antigen to inactivate p53 and pRB, mice developed high-grade tumours. Rebouissou et al., 2014 went on to show that the poor-prognosis Basal-Squamous MIBC tumours rely on EGFR activity for their growth and survival. Basal-squamous tumours showed high activity of EGFR, and basal-like BLCA cell lines were highly sensitive to EGFR inhibition. Together, these studies suggest that EGFR activity drives growth and survival in basal-squamous MIBC tumours.

The pattern of EGFR protein expression within the urothelium has also been observed to change in BLCA. In normal urothelium EGFR expression is restricted to the basal layer, while in tumours or neighbouring urothelium in patients with tumours, EGFR is expressed in all layers of the urothelium [Messing et al., 1987, Messing, 1990].

Although *ERBB2* amplifications and expression are associated with luminal MIBC [Eriksson et al., 2017, Robertson et al., 2017], multiple studies have failed to find any correlation between *ERBB2* (over)expression and prognosis, grade, stage, recurrence or progression [Underwood et al., 1995, Mellon et al., 1996, Jiminez et al., 2001, Kassouf et al., 2008].

Meta-analysis of 11 studies from the ONCOMINE cancer microarray database revealed changes in *EGFR*, *ERBB2* and *ERBB3* expression in NMIBC and MIBC vs normal urothelium [Mooso et al., 2015]. *EGFR* and *ERBB2* expression were not significantly different in NMIBC vs normal urothelium, but both were significantly over-expressed in

MIBC. *ERBB3* was overexpressed in both NMIBC and MIBC compared to normal urothelium.

1.4 Fibroblast Growth Factor Receptor 3

1.4.1 The Fibroblast Growth Factor Family

Fibroblast Growth Factor Receptors (FGFRs) are a family of receptor tyrosine kinase (RTK) proteins, which are activated following binding of Fibroblast Growth Factors (FGFs) [reviewed by Dai et al., 2019]. The *FGFR* gene family is composed of FGFR1-4, as well as FGF-receptor-like 1 (*FGFRL1*) [reviewed by Ornitz and Iroh, 2015]. FGFRs have key roles in all tissues of the body during development and organogenesis; deletion of FGFR1/2 in mice typically leads to fetal non-viability, while knockout of FGFR3 or individual FGFs causes a range of congenital anomalies [Colvin et al., 1996, Weinstein et al., 1998, Xu et al., 1998, Xu et al., 1999, Yu et al., 2003, Ohkubo et al., 2004].

FGFRs have a conserved structure consisting of 3 extracellular Immunoglobulin (Ig) loops, a transmembrane helix and an intracellular kinase domain [reviewed by Dai et al., 2019]. Ig loops 2 and 3 serve as binding sites for FGFs and differences in these domains determine the different ligand specificities, both in different FGFRs, and within alternatively spliced FGFR isoforms [Ornitz et al., 1996, Zhang et al., 2006]. *FGFRL1* shares all of these structural features, except that it contains no tyrosine kinase domain [reviewed by Trueb, 2011]. Although it possess a transmembrane helix for intramembrane insertion, FGFRL1 can be shed from the plasma membrane, where it has been shown to antagonise FGFR signalling by competing for binding to available FGFs [Steinberg et al., 2010].

Fibroblast Growth Factor Receptor 3 (FGFR3) has several roles in development, including formation of long bones and parts of the skull [reviewed by Ornitz and Marie, 2015]. FGFR3 activation suppresses chondrocyte growth [Colvin et al., 1996, Deng et al., 1996], and as such germline activating mutations of FGFR3 are associated with a variety of dwarfism conditions [Naski et al., 1998, Chen et al., 1999, Li et al., 1999, Wang et al., 1999, Iwata et al., 2001, Lee et al., 2017], while congenital loss-of-function FGFR3 mutations result in bone overgrowth and tall stature [Toydemir et al., 2006].

1.4.2 FGFR3 in the normal urothelium

1.4.2.1 Control of FGFR3 expression

1.4.2.1.1 Expression and role of *FGFR3* in urothelial tissue

Expression of *FGFR3* transcript by normal urothelium has received limited attention; most focus on FGFR3 has been in a cancer context due to the potential role(s) of FGFR3 in BLCA initiation and/or pathology [reviewed by Bogale, 2024]. Previous studies have compared expression of *FGFR3* transcript to other *FGFRs* in human urothelium [Tomlinson et al., 2007] or to other epithelia such as skin and cervix [Shi et al., 2023]. *FGFR3* was shown to be the most-expressed FGFR in ureter tissue [Tomlinson et al., 2007], and *FGFR3* expression in the bladder is somewhere between that of skin and exocervix [Shi et al., 2023]. However, *FGFR3* expression in bladder and ureter tissue has never been compared.

1.4.2.1.2 Regulation of *FGFR3* expression in normal and neoplastic urothelium

The factors which regulate expression of *FGFR3* in urothelial tissue are not fully understood, however several factors have been identified which modulate FGFR3 in NHU cells derived from urothelial tissue, and in BLCA (Table 1.1).

Another factor shown to negatively regulate *FGFR3* expression in BLCA cell lines is EGFR activity. In 97-7 and 94-10 BLCA cell lines inhibition of EGFR led to an increase in FGFR3 protein [Herrera-Abreu et al., 2013]. Additionally, stimulation of EGFR with Transforming growth factor α (TGFα) in RT112M cells repressed FGFR3 protein expression [Herrera-Abreu et al., 2013].

Sequencing of the *FGFR3* promoter region has also revealed a MYC binding site, suggesting that that MYC drives expression of *FGFR3* [Reinhold et al., 2004, Mahe et al., 2018]. Inhibition of MYC transcriptional activity in MGH-U3 and RT112 BLCA cell lines resulted in decreased *FGFR3* expression. Thus MYC positively regulated *FGFR3* expression - however the reverse was also demonstrated, as treatment with FGFR3 siRNA or the FGFR3 inhibitor PD17307 significantly reduced MYC expression [Mahe et al., 2018]. As such, *FGFR3* mutation and subsequent FGFR3 activity is implicated in driving MYC expression in BLCA, although this has yet to be demonstrated beyond *in vitro* models [reviewed by Bogale, 2024].

Table 1.1 - Factors which have been previously identified in the literature to either promote or repress expression of FGFR3 transcript and/or protein

Factor	Context	Effect(s) on FGFR3 expression	References
Protein Kinase A	RCJ rat chondrocyte cell line	Repressed expression of *FGFR3* transcript	McEwen et al., 1999
EGFR	97-7, 94-10 and RT112M BLCA cell lines	Repressed expression of *FGFR3* transcript and protein	Herrera-Abreu et al., 2013
microRNA99a	BLCA samples (correlation) NHU cells (direct intervention)	Repressed expression of *FGFR3* transcript and protein	Catto et al., 2009 Wu et al., 2014
Sp1 and Sp3	RCJ rat chondrocyte cell line	Promoted expression of *FGFR3* transcript	McEwen and Ornitz, 1998
Sp1, Sp3 and Sp4	253JB-V and KU7 BLCA cell lines	Promoted expression of FGFR3 protein	Chadalapaka et al., 2012]
Serum response factor	RCJ rat chondrocyte cell line	Promoted expression of *FGFR3* transcript	Reinhold et al., 2004
MYC	MGH-U3 and RT112 BLCA cell lines	Promoted expression of *FGFR3* transcript and protein	Mahe et al., 2018

1.4.2.1.3 Regulation of *FGFR3* expression in non-urothelial tissues

Outside of urothelial tissue, regulation of FGFR3 expression has been mostly studied in chondrocytes due to the role of FGFR3 in regulating bone development [Wen et al., 2016]. In the RCJ rat chondrocyte cell line, *FGFR3* transcript expression was shown to be under the control of the Sp family of transcription factors, as well as serum response factor [McEwen and Ornitz, 1998, Reinhold et al., 2004, Chadalapaka et al., 2012]. In the same cell line, *FGFR3* expression was repressed by protein kinase A activity [McEwen et al.,

1999]. Thus, these factors may also potentially regulate *FGFR3* expression in urothelial cells.

1.4.2.1.4 Alternative Splicing of *FGFR3*

All FGFRs are alternatively spliced as a mechanism to control their ligand specificity [Orr-Urtreger et al., 1993, Wuechner et al., 1996, Beer et al., 2000, Yeh et al., 2003]. *FGFR3* is alternatively spliced in the 3rd Ig domain to produce three main protein-coding isoforms: FGFR3 IIIb, FGFR3 IIIc, and FGFR3 Δ8-10 (Fig. 1.6) [Keegan et al., 1991, Avivi et al., 1993, Murgue et al., 1994, Johnston et al., 1995, Tomlinson et al., 2005]. For *FGFR3* IIIb and IIIc splice variants, exons 8 and 9 are mutually exclusive, with inclusion of exon 8 leading to production of IIIb, and inclusion of exon 9 producing IIIc (Fig. 1.6) [reviewed by Holzmann et al., 2012]. Exclusion of exons 8, 9 and 10 produces the Δ8-10 isoform which does not contain a transmembrane domain - this isoform was shown to be secreted from cells [Tomlinson et al., 2005]. FGFR3 Δ8-10 has also been proposed to negatively regulate FGFR3 signalling by competing for available ligand [Terada et al., 2001, Jang 2002, Tomlinson et al., 2005].

The FGFR3 IIIb and IIIc isoforms have different affinities for ligand, as their splicing occurs in the ligand-binding domain of *FGFR3* [Ornitz et al., 1996, Zhang et al., 2006]. It has been suggested based on BLCA cell line data that switching from FGFR3 IIIb to the more-promiscuous FGFR3 IIIc isoform during cancer development could provide a growth advantage over normal cells [Tomlinson et al., 2005]. However, *FGFR3* isoform switching has not been reported in any patient-based cancer datasets.

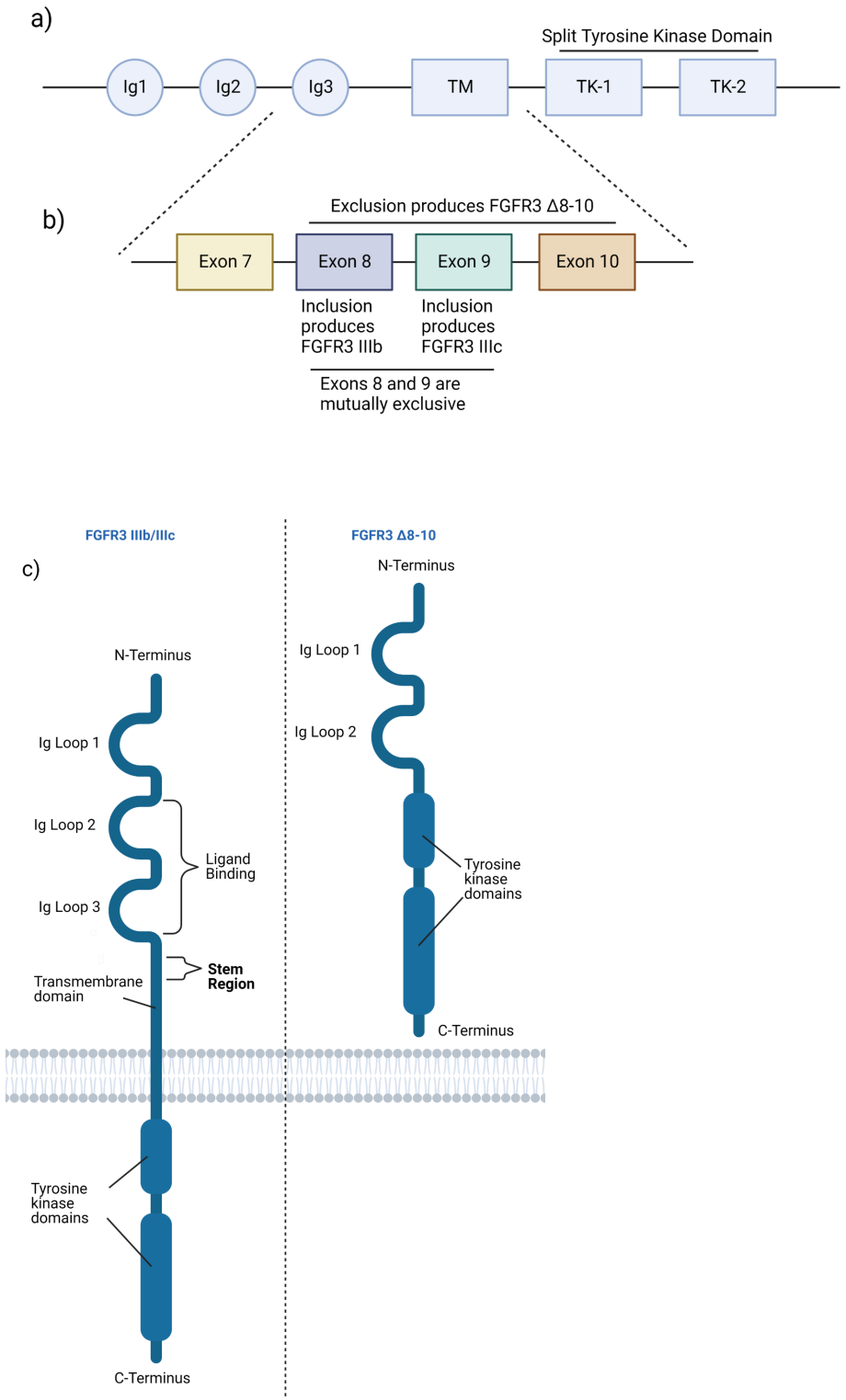

Figure 1.6 - Alternative splicing of FGFR3 - (a) Simplified structural diagram of *FGFR3* showing key features, (b) Exons 8-10 of *FGFR3* are alternatively spliced, (c) Simplified structure of the 3 main protein-coding isoforms of FGFR3: FGFR3 IIIb, FGFR3 IIIc, and FGFR3 Δ8-10. Figure adapted from Holzmann et al., 2012 under the Creative Commons Attribution Licence.

In summary, several potential regulators of *FGFR3* expression have been identified in non-urothelial cells/tissues and in BLCA, but whether these factors act to regulate FGFR3 in normal urothelium is unknown. In particular, EGFR activity was shown to repress expression of *FGFR3* in several BLCA cell lines, but the specific mechanism responsible for this was not determined.

1.4.2.1.5 Glycosylation of FGFR3 protein

Following translation, FGFR3 protein is post-translationally modified with glycosylation of several residues. Previous studies have focused on the glycosylation of FGFR3 IIIb/IIIc, which exists as three species: an unmodified FGFR3 species (98-105 kDa), an intermediate glycosylated species rich in mannose residues (115-120 kDa) and a mature glycosylated species (130 kDa) [Keegan et al., 1991, Lievens and Liboi, 2003, Lievens et al., 2004, Bonnaventure et al., 2007]. The variations in molecular weight reported for each species between studies are likely due to the relative insensitivity of a western blot for determining the exact molecular weight of a species. Six amino acids of FGFR3 have been identified which are N-glycosylated; mutation of these sites to prevent glycosylation resulted in FGFR3 being retained in the endoplasmic reticulum, suggesting that glycosylation may be crucial for correct localization of FGFR3 within cells [Hashimoto et al., 2024].

1.4.2.2 Activation and localisation of FGFR3

1.4.2.2.1 Canonical signalling pathways activated downstream of FGFR3

FGFR3 is activated by the binding of ligand (FGFs) to the receptor, which triggers FGFR3 monomers to dimerise, autophosphorylate and gain tyrosine kinase activity [Li et al., 2005, Chen and Hristova, 2011, Bocharov et al., 2013]. This sets off a cascade of phosphorylation events, commencing with FGFR substrate 2 (FRS2), an adaptor protein to all FGFRs which is localised to lipid rafts in the plasma membrane [Kouhara et al., 1997, Hadari et al., 1998, Ridyard and Robins, 2003, Limpert et al., 2007]. Phosphorylation sites on FRS2 recruit additional proteins such as Grb2 and PTPN11, which enables FGFR3 activation to signal along the PI3K-AKT and MAP kinase pathways [Kanai et al, 1997, Hart et al., 2001] (Fig. 1.7). Signal Transducer and Activator of Transcription (STAT) proteins and phospho-lipase C (PLC) gamma can also bind directly to phosphorylated residues on FGFR3 [Kanai et al, 1997, Hart et al., 2001, Chen et al., 2005].

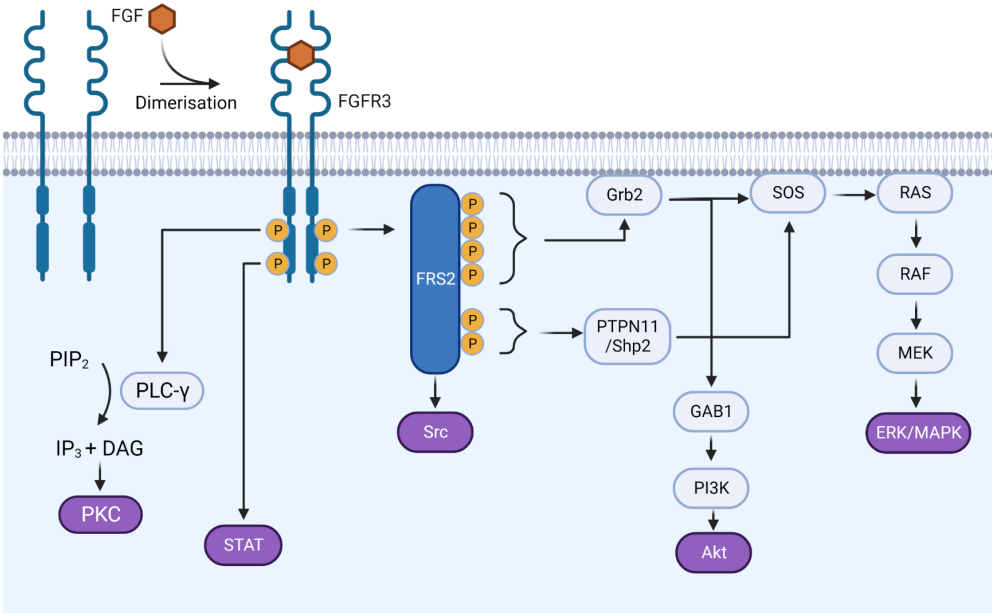

Figure 1.7 - Canonical FGFR3 signalling pathways - Common signalling pathway endpoints are shown in purple, with signalling pathway intermediates in light blue. DAG; diacylglycerol, PIP_2; phosphatidylinositol (4,5) bisphosphate, IP_3; inositol triphosphate. Information taken from Kanai et al, 1997, Kouhara et al., 1997, Ong et al., 1997, Hadari et al., 1998, Hart et al., 2001 and Chen et al., 2005.

Activity of FGFR3 is negatively regulated by the Sprouty (SPRY) and Dual-specificity phosphatase (DUSP) families of proteins [reviewed by Szybowska et al., 2021]. SPRY proteins are upregulated when ERK and SRC are activated downstream of FGFR3 and phosphorylate FRS2 on sites which prevent the binding of additional proteins, attenuating downstream signalling [Hanafusa et al., 2002, Li et al. 2004, Zhou et al., 2009] (Fig. 1.8). The DUSP family member DUSP6 is activated downstream of ERK, and attenuates FGFR3 signalling by de-phosphorylating ERK [Camps et al., 1998, Erekot et al., 2008]. Finally, FGFR3 activity can also be attenuated by targeting it for degradation - the E3-ubiquitin ligase c-Cbl can be recruited to active FGFR3-FRS2 signalling complexes through Grb2 [Cho et al., 2003]. This results in FGFR3 protein being ubiquitinated, internalised, and degraded [Monsonego-Ornan et al., 2002, Cho et al., 2003].

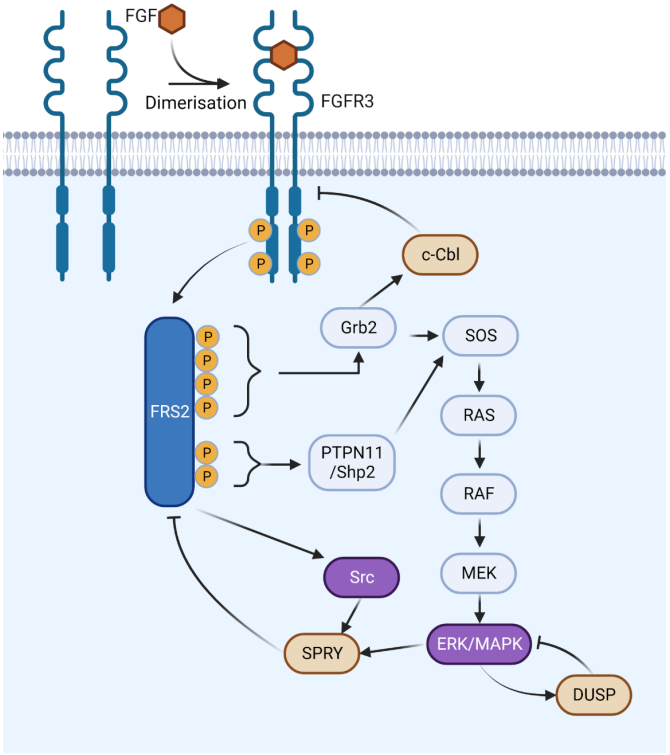

Figure 1.8 - Negative regulation mechanisms of FGFR3 signalling - Common signalling pathway endpoints are shown in purple, with signalling pathway intermediates in light blue, and negative feedback regulators are in orange. Information taken from [Camps et al., 1998, Hanafusa et al., 2002, Wong et al., 2002, Li et al. 2004, Erekot et al., 2008 and Zhou et al., 2009.

1.4.2.2.2 Localisation and activation of FGFR3 in cell models

Numerous studies have investigated the cellular localisation of FGFR3 and how this changes based on FGFR3 activity. These studies have used bone-derived cell lines such as RCJ (non-transformed rat chondrocytes) and U2OS (human osteosarcoma), as well as more general cell lines such as HeLa (cervical carcinoma), 293 (human embryonic kidney), and Cos7 (monkey kidney fibroblast-like line). Importantly, none of the cell lines used have endogenous expression of *FGFR3* - transient or stable transfection is always used to obtain expression of *FGFR3*.

FGFR3 protein has been observed to exist both intracellularly [Cho et al., 2003] and at the plasma membrane [Lievens et al., 2004, Ben-Zvi et al., 2006] by indirect immunofluorescence. Direct-labelling of proteins at the cell surface has also demonstrated that FGFR3 is located at the plasma membrane before being activated, and is then gradually internalised [Haugsten et al., 2005, Degnin et al., 2011].

There is some controversy about the timeframe over which FGFR3 is internalised and degraded following activation. Monseonego-Ornan et al., 2002 reported in RCJ cells that FGFR3 degradation was noticeable only 1 hour post-activation, and Haugsten et al., 2005 reported that at 2h post-activation in HeLa cells, 60% percent of total FGFR3 was still at the plasma membrane. Degnin et al., 2011 reported a much more rapid degradation in 293 cells, with all FGFR3 being lost from the plasma membrane by 90 minutes post-activation. This was supported by Haugsten et al., 2011 using U2OS cells, who claimed that total FGFR3 protein was depleted by 50% at 30 minutes post-activation, and by 80% at 2 h post-activation.

Due to differences in cell models and experimental approaches it is difficult to ascertain the reason behind the reported differences. What is consistent though is that internalisation and degradation of FGFR3 depends on its activation. FGFR3 ubiquitylation was shown to be proportional to receptor activity [Monsonego-Ornan et al., 2002], and kinase-dead FGFR3 remained localised at the plasma membrane following ligand stimulation [Degnin et al., 2011].

After internalisation, FGFR3 is trafficked through endosomes and is subject to both lysosomal and proteasomal degradation [Monsonego-Ornan et al., 2002, Cho et al., 2003, Haugsten et al., 2005, Ben-Zvi et al., 2006, Bonaventure et al., 2007]. The internalisation of FGFR3 following activation is dependent on both actin and dynamin-mediated endocytosis [Degnin et al., 2011, Haugsten et al., 2011].

Two studies have reported the effect of wild-type FGFR3 activation in modified NHU cells, although these did not examine the timing of FGFR3 activation or degradation. Both studies used undifferentiated NHU cells immortalised by retroviral expression of human telomerase reverse transcriptase (hTERT), then transduced to overexpress wild-type FGFR3. Di Martino et al., 2009 showed that FGFR3 activated with FGF1 could phosphorylate downstream FRS2, ERK, and PLCγ, all of which were strongly phosphorylated 5 minutes post-activation. FRS2 and PLCγ phosphorylation was stable at 15 minutes post-activation, while ERK phosphorylation had almost returned to baseline. Stability of ERK phosphorylation downstream of FGFR3 activation seems uncertain though, as a later report by the same group found that ERK was highly phosphorylated 24 h after FGFR3 activation [Lombardi et al., 2017].

1.4.2.2.3 Localisation and activation of FGFR3 in urothelial tissue

Four groups have previously described the expression and localisation of FGFR3 protein within urothelial tissue, with one group reporting no expression [Turo et al., 2015] and three groups reporting weak expression of FGFR3 throughout the whole urothelium [Tomlinson et al., 2007, Rotterud et al., 2007, Barbisan et al., 2008]. In all studies where FGFR3 protein was reported, FGFR3 was described as distributed evenly throughout the urothelial layers and with a cytoplasmic localisation within cells. This can be contrasted with another family of growth factor receptor tyrosine kinases expressed in urothelial tissue - the EGFR family. EGFR family proteins are localised to either the basal (EGFR) or superficial (ERBB2 and ERBB3) urothelium, and are restricted to the plasma membrane - as would be expected for a receptor [Chow et al., 1997]. These studies localised FGFR3 protein by immunohistochemical labelling using antibodies against either the N- or C-terminus of FGFR3.

In summary, the canonical signalling downstream of FGFR3 is well-understood, but has only been studied extensively in bone-derived cell lines. Furthermore, FGFR3 activation has not been studied in cells with endogenous expression of FGFR3. FGFR3 is understood to exist at the plasma membrane until its activation, at which point it is internalised and degraded. However, the speed of FGFR3 degradation and the time-frame over which FGFR3 signalling is active appears to vary with cell type. In contrast to the plasma membrane localisation observed in various cell models, FGFR3 protein expressed in urothelial tissue has been reported by multiple groups to have a cytoplasmic localisation. Together, these factors show that understanding of FGFR3 signalling and localisation within urothelial cells is lacking, justifying a more extensive characterisation in NHU cells.

1.4.3 FGFR3 in Bladder Cancer

FGFR3 is one of the most frequently altered genes in BLCA [reviewed by Ascione et al., 2023]. *FGFR3* is typically altered in BLCA in one of three ways: Point mutation of the *FGFR3* gene, overexpression of wild-type *FGFR3*, or fusion of the *FGFR3* gene (Fig. 1.9).

1. Point mutation leads to constitutive dimerisation and activation of FGFR3 (Fig. 1.10) - this has been demonstrated to drive overexpression of FGFR3 in BLCA cell lines [Bernard-Pierrot et al., 2005, Mahe et al., 2018] and FGFR3 mutant tumours frequently have FGFR3 overexpression [van Rhijn et al., 2020]. This constitutive FGFR3 activation has been shown to drive proliferation and gene expression patterns in BLCA cell line, xenograft models [Bernard-Pierrot et al.,

2005, Tomlinson et al., 2007, di Martino et al., 2009, Qing et al., 2009, di Martino et al., 2014, Mahe et al., 2018]. There is also some evidence that activating mutations in FGFR3 stabilise FGFR3 protein by preventing/slowing its degradation [Monsonego-Ornan et al., 2000, Monsonego-Ornan et al., 2002, Cho et al., 2003]. The most common *FGFR3* mutation is S249C, estimated to make up 62% of all *FGFR3* mutations in BLCA [Shi et al., 2019].The S249C mutation introduces a free cysteine residue that leads to erroneous disulphide bond formation between two FGFR3 monomers, causing constitutive dimerisation and activation (Fig. 1.10) [Bernard-Pierrot et al., 2005, Tomlinson et al., 2007].

2. MicroRNAs are a small, non-coding class of RNAs that function in transcriptional repression, typically by interacting with the 3' untranslated region (UTR) of target mRNA to induce translational repression [reviewed by O'Brien et al., 2018]. Catto et al., 2009, observed that microRNA-99a, predicted to target the 3' UTR of *FGFR3*, was inversely correlated with FGFR3 mRNA expression in BLCA patients. When NHU cells were transfected with anti-microRNAs to deplete microRNA-99a, FGFR3 protein expression increased three-fold, suggesting that microRNA may negatively regulate *FGFR3* expression in normal urothelium as well as BLCA [Catto et al., 2009]. Downregulation of microRNA-99a results in FGFR3 (over)expression without mutation [Catto et al., 2009, Wu et al., 2014]. Catto et al. proposed that microRNA-99a expression was lost in BLCA due to promoter methylation - methylation of DNA typically occurs in regions where a guanine repeatedly follows a cytosine (CpG islands) and this can negatively impact gene expression [reviewed by Moore et al., 2012]. The authors failed to detect any CpG islands in the microRNA-99a promoter region. However, expression of microRNA-99a was shown to increase by approximately five-fold when RT4 BLCA cells were treated to inhibit DNA methyltransferase [Catto et al., 2009].
3. Fusion of *FGFR3* to other genes (e.g. Transforming Acid Coil-coil 3; *TACC3*) can drive constitutive dimerisation and activation of FGFR3 [Nelson et al., 2016]; this fusion also typically removes the 3' UTR of *FGFR3* that is targeted by micro-RNAs, resulting in stabilisation of *FGFR3* mRNA and FGFR3 overexpression [Parker et al., 2013]. Although the result of fusion of *FGFR3* to other genes depends on the fusion partner, *TACC3* is by far the most common fusion partner for *FGFR3* in BLCA (Table 1.2).

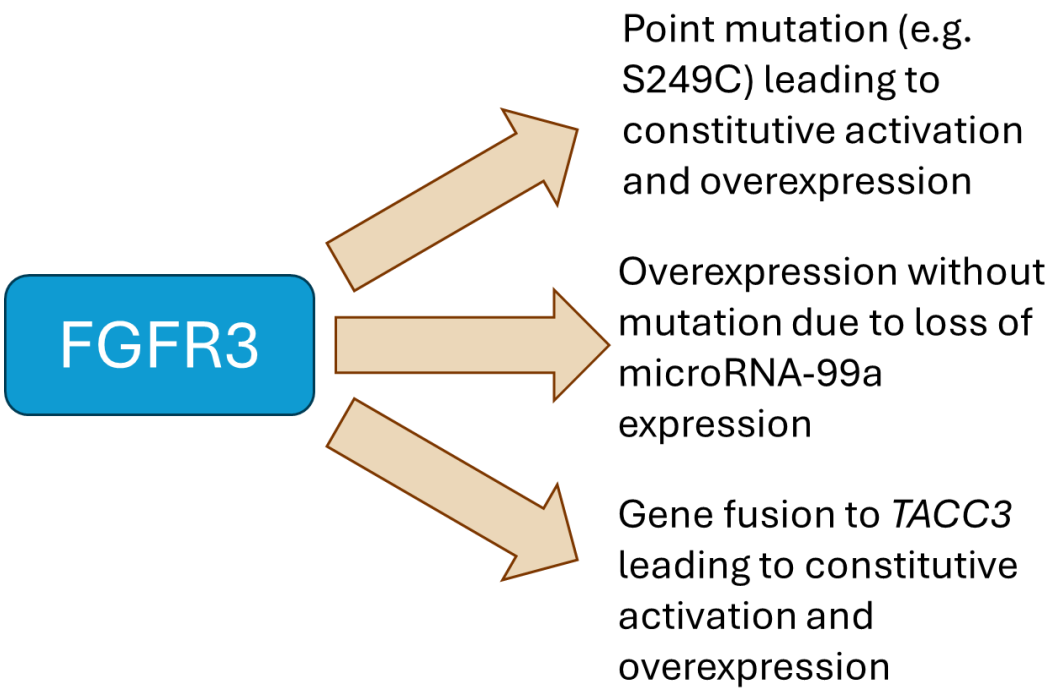

Figure 1.9 - Three main mechanisms of *FGFR3* alteration in Bladder Cancer

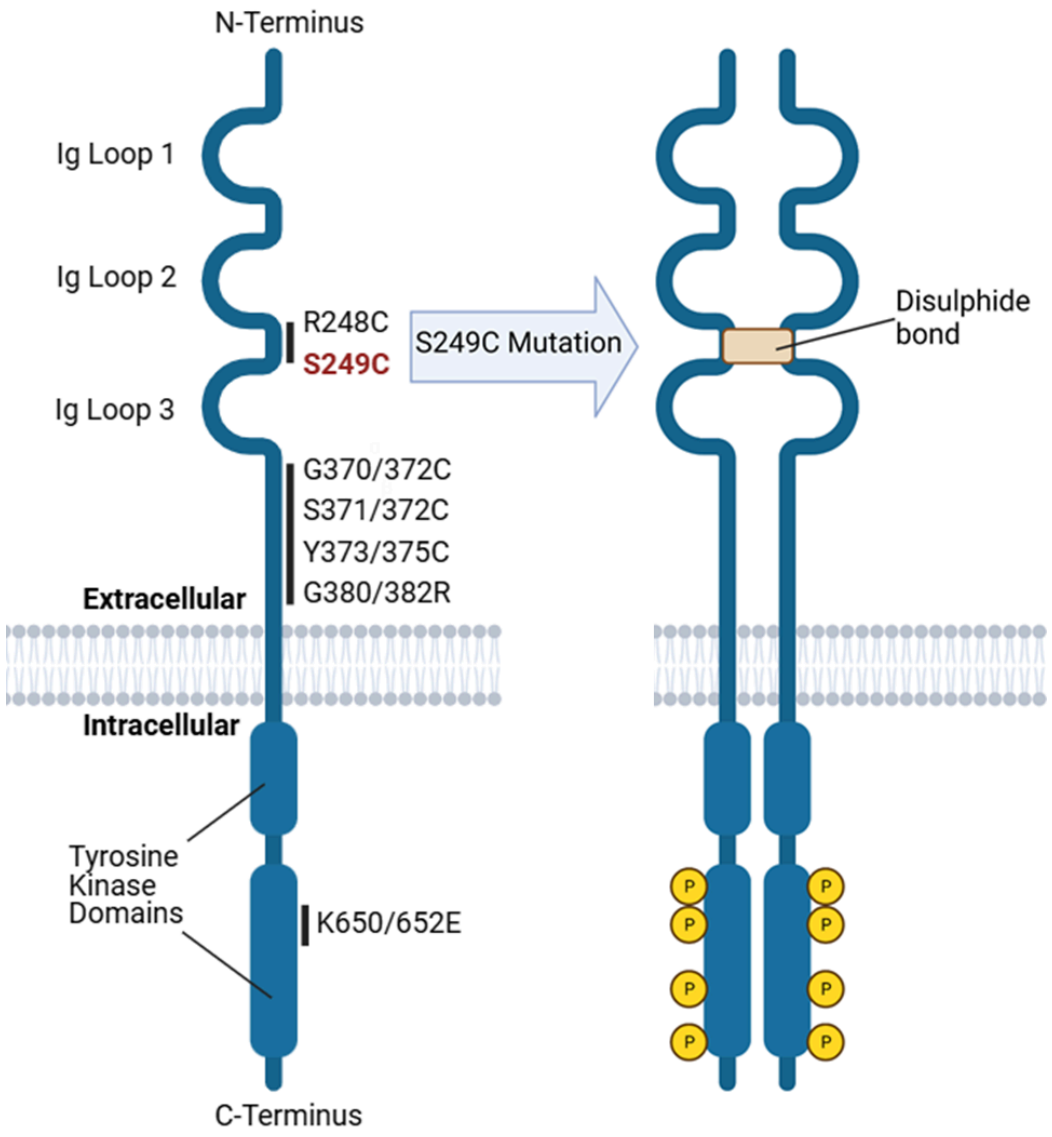

Figure 1.10 - Mechanism of FGFR3 activation following point mutation and sites of most common *FGFR3* point mutations - Where two numbers are given for the location of a mutation (e.g. G370/372C), this is the location in FGFR3 IIIc then FGFR3 IIIb, as is conventional in the literature.

1.4.3.1 *FGFR3* point mutations are associated with tumours of lower stage and grade

Point mutations are the most common *FGFR3* alteration, occurring in approximately 70% of NMIBC and 20% of MIBC [Mahe et al., 2018]. *FGFR3* mutations in BLCA are associated with lower stage and grade [Billerey et al., 2001, Hernandez et al., 2006, Lamy et al., 2006, Tomlinson et al., 2007, Junker et al., 2008], and are also associated with an improved prognosis/survival [van Rhijn et al., 2003, van Oers et al., 2007, van Rhijn et al., 2010, Robertson et al., 2017, Teo et al., 2020, Van Rhijn et al., 2020, Mertens et al.,

2022]. Additionally for NMIBC, *FGFR3* mutations are associated with a lower number of genetic mutations [Junker et al., 2008] and are less likely to progress [van Rhijn et al., 2003, Hernandez et al., 2006, Van Oers et al., 2007, Burger et al., 2008]. There have been mixed reports on the association of *FGFR3* mutations and disease recurrence. Hernandez et al., 2006 found that *FGFR3* mutations were associated with increased risk of recurrence in TaG1 tumours. However, several other studies have found no association between *FGFR3* mutation status and risk of disease recurrence [van Rhijn et al., 2003, Lamy et al., 2006, Van Oers et al., 2007, Burger et al., 2008, van Rhijn et al., 2010], and one study found that *FGFR3* mutant tumours were less likely to recur [van Rhijn et al., 2001]. In summary, the majority of studies to date have concluded that there is no clear link between the presence of *FGFR3* mutations and the likelihood of BLCA recurrence.

Out of all *FGFR3* point mutations in BLCA, S249C is the most common (Table 1.2), being three times more prevalent than the next most-frequent mutation, Y375C [Shi et al., 2019]. Shi et al. have hypothesised that this over-representation is due to apolipoprotein B mRNA-editing enzyme, catalytic polypeptide (APOBEC)-mediated mutagenesis. APOBEC represents a family of enzymes whose normal function is damage of viral DNA, but which has also been implicated in various cancers such as lung, breast, ovarian [reviewed by Swanton et al., 2015] and bladder [Shi et al., 2019]. Shi et al. demonstrated that the S249C mutation of *FGFR3* (nucleotide sequence TCC -> TGC) is the only recurrent BLCA *FGFR3* mutation that resembles an APOBEC mutation motif. Furthermore, by analysing mutational signatures in NMIBC tumours, the authors observed that tumours with an *FGFR3* mutation had a significantly higher APOBEC-associated mutational signature than tumours with any other type of *FGFR3* mutation. There was also a greater proportion of S249C mutations vs other *FGFR3* mutations in MIBC tumours with APOBEC activity vs those without APOBEC activity.

Mechanistically, Shi et al proposed that *FGFR3* is specifically targeted by APOBEC due to the propensity of the *FGFR3* genetic sequence to form hairpin loops when separated into single-stranded DNA during DNA replication. They observed that the base altered in the S249C mutation sits at the centre of a five-nucleotide single-stranded DNA loop, which would make it a target for APOBEC mutational activity - specifically APOBEC3A [Haradhvala et al., 2016, Sharma et al., 2017, Shi et al., 2019]. Shi et al then confirmed experimentally that the *FGFR3* sequence was deaminated by APOBEC using *in vitro* deamination assays. Following deamination of the target cytosine residue to a uracil, erroneous DNA repair mechanisms replace uracil with guanine, resulting in a TCC -> TGC substitution and an S249C mutation.

Table 1.2 - **List of common FGFR3 mutations in BLCA and region of receptor they affect**

Proportion of mutations in BLCA was taken from Shi et al., 2019, Supplementary table 2a. Point mutations are ordered numerically by location in the FGFR3 protein sequence. Where two numbers are given for the location of a mutation (e.g. G370/372C), this is the location in FGFR3 IIIc then FGFR3 IIIb, as is conventional in the literature.

Mutation	**Description**	**Region of receptor**	**Effect(s) of mutation on FGFR3 protein**	**Proportion of *FGFR3* mutations in BLCA**	**References**
R248C	Arginine substituted to Cysteine	Ligand-binding Immunoglobulin-like loops	Causes ligand-independent dimerisation, activation and phosphorylation of FGFR3	9%	Sorokin et al., 1994 Tavormina et al., 1995 Naski et al., 1996
S249C	Serine substituted to Cysteine	Ligand-binding Immunoglobulin-like loops	Causes ligand-independent dimerisation, activation and phosphorylation of FGFR3	62%	Bernard-Pierrot et al., 2005 Tomlinson et al., 2007
G370/372C	Glycine substituted to Cysteine	Transmembrane region	Causes ligand-independent dimerisation, activation and phosphorylation of FGFR3	5%	Rousseau et al., 1996 Adar et al., 2002
S371/373C	Serine substituted to Cysteine	Transmembrane region	Causes ligand-independent dimerisation, activation and phosphorylation of FGFR3	1%	Tavormina et al., 1995 Adar et al., 2002

Y373/375 C	Tyrosine substituted to Cysteine	Transmembrane region	Causes ligand-independent dimerisation, activation and phosphorylation of FGFR3	18%	Rousseau et al., 1996 Richelda et al., 1997 Ronchetti et al., 2001 Adar et al., 2002
G380/382 R	Glycine substituted to Arginine	Transmembrane region	Receptor becomes resistant to ligand-mediated internalisation and degradation, causing active receptor to signal for longer at the plasma membrane	1%	Naski et al., 1996 Webster and Donoghue, 1996 Monsonego-Ornan et al. 2000
K650/652 E	Lysine substituted to Glutamate	Tyrosine Kinase Domain	Glutamate stabilises the activation loop of the kinase domain and the receptor gains kinase activity without need for ligand. In some cell types, heavy phosphorylation of the mutant receptor results in it becoming trapped in the endoplasmic reticulum and unable to mature to the plasma membrane	1%<	Tavormina et al., 1995 Naski et al., 1996 Webster et al., 1996 Mohammadi et al., 1996 Hart et al., 2000 Ronchetti et al., 2001 Lievens and Liboi, 2003

TACC3 Fusion	Fusion to TACC3	Exon 18 of *FGFR3* fused to exon 11 of *TACC3*	FGFR3 can dimerise independent of ligand through the TACC3 fusion protein, as escapes regulation by microRNA	3%	Williams et al., 2012, Nelson et al., 2016

1.4.3.2 *FGFR3* gene fusions

The most common *FGFR3* gene fusion identified in BLCA is *TACC3*. *FGFR3-TACC3* represented 100% of *FGFR3* fusions in TCGA cohort of 406 MIBC tumours [TCGA, 2014 and Robertson et al., 2017], 75% of *FGFR3* fusions in a cohort of 105 high-risk NMIBC tumours [Pietzak et al., 2017], and 82% of *FGFR3* fusions in a cohort composed of 412 BLCA and 113 UTUC tumours [Guercio et al., 2023]. TACC3 is a microtubule-associated protein that is important for mitotic spindle assembly and proper chromosome segregation [Booth et al., 2011]. *TACC3* and *FGFR3* are located within 50 kb of each other on chromosome 4, hence their spatial proximity may favour recombination [Williams et al., 2013].

FGFR3-TACC3 occurs in approximately 2-3% of BLCAs [reviewed by Costa et al., 2016]. This fusion protein contains exons 1-18 of *FGFR3*, and exons 11 onwards of *TACC3* [Williams et al., 2013]. Almost the entirety of the FGFR3 protein is present, with the key absence being the region required for binding and activation of phospho-lipase c (PLC) gamma [Williams et al, 2013]. Studies in NIH-3T3 fibroblasts and immortalised NHU cells have confirmed that *FGFR3* point mutants (S249C, Y375C and K652E) resulted in PLCγ phosphorylation while FGFR3-TACC3 fusion did not [di Martino et al. 2009, Williams et al., 2013]. For TACC3, the majority of the protein is lost, but crucially, the domain(s) required for dimerisation and kinetochore-binding remain [Booth et al., 2011, Williams et al., 2013]. This has three key implications for FGFR3-TACC3 fusion proteins. Firstly, this allows FGFR3 to constitutively dimerise through the TACC3 dimerisation domain, without the need for ligand binding [Nelson et al. 2016]. These active FGFR3-TACC3 dimers can signal into the MAP kinase pathway, hence having similar activation effects to FGFR3 point mutants [Williams et al., 2013, Nelson et al., 2016, Chew et al., 2020].

Secondly, since the kinetochore-binding domain of TACC3 remains, FGFR3-TACC3 may dimerise with TACC3 at the mitotic spindle [Chew at al., 2020] or may leach wild-type TACC3 away from the mitotic spindle, leading to chromosome segregation defects and thus aneuploidy [Sarkar et al., 2017]. From this one might expect that FGFR3-TACC3 mutant tumours would display higher tumour mutational burden. In fact, in BLCA and glioblastoma, tumours with FGFR3-TACC3 fusions have lower tumour mutational burden than tumours without FGFR3-TACC3 [Nassar et al., 2018, Mata et al., 2020].

Finally, the FGFR3-TACC3 fusion protein does not contain the 3’ untranslated region (UTR) of *FGFR3* [Parker et al., 2013]. This 3’ UTR has been shown to be important for

negative regulation of *FGFR3* expression by miR-99a [Catto et al., 2009], and thus *TACC3* fusion releases *FGFR3* from miR-99a regulation, allowing for its overexpression [Parker et al., 2013].

1.4.4 Association of *FGFR3* expression with urothelial differentiation in BLCA

Several studies have reported that in BLCA, *FGFR3* expression is associated with BLCA tumours which also have high expression of urothelial differentiation markers, or expression or activity of transcription factors associated with urothelial differentiation, such as PPARɣ, RXRα or FOXA1 [Choi et al., 2014, Eriksson et al., 2014, Kamoun et al., 2020]. This suggests that *FGFR3* expression may be regulated by urothelial differentiation, or may be co-regulated alongside urothelial differentiation, for example by transcription factors that drive urothelial differentiation such as PPARɣ, FOXA1, and GATA3 [Varley et al., 2004, Varley et al., 2009, Fishwick et al., 2017].

1.4.5 Current Models of FGFR3 activation in urothelial carcinogenesis

In line with the “two pathways” model of BLCA development [Spruck et al., 1994], *FGFR3* mutations have been identified as an early event in BLCA and are associated with lower grade and stage disease [Billerey et al., 2001, Hernandez et al., 2006, Lamy et al., 2006, Tomlinson et al., 2007, Junker et al., 2008]. Based on the detection of *FGFR3* mutations in low grade/stage BLCA (particularly NMIBC) and urothelial hyperplasias, it has been proposed that *FGFR3* mutations lead to hyperplasia and are a causative event in urothelial carcinogenesis by driving proliferation [reviewed by Inamura et al., 2018].
In response to this hypothesis, several studies have investigated the effect(s) of *FGFR3* mutation in cell and animal models. These studies have aimed to understand the effects that mutant FGFR3 activity may have in normal and/or neoplastic urothelium, and whether *FGFR3* mutation in normal urothelium could drive urothelial carcinogenesis.

1.4.5.1 Effects of *FGFR3* mutation in cell models

A number of studies investigating the role(s) of mutant *FGFR3* in cancer cell lines have generally concluded that mutant FGFR3 activity is required to drive cell proliferation and cancer-like properties, i.e. oncogene addiction [Mahe et al., 2018]. However, the same is not true for normal human cells, e.g. NHU cells. Bernard-Perrot et al. showed that transfection of the constitutively-active *FGFR3* mutant FGFR3-S249C was able to transform NIH-3T3 mouse fibroblasts and induce a spindle-like morphology [Bernard-Pierrot et al., 2006]. Others have since demonstrated that interventions targeting

FGFR3 (such as anti-FGFR3 siRNA or tyrosine kinase inhibitors) in FGFR3-mutant BLCA cell lines reduces proliferation, cell viability, and ability to form colonies in soft agar [Tomlinson et al., 2007, Di Martino et al., 2009, Qing et al., 2009, Mahe et al., 2018].

FGFR3 expression (both mutant and wild-type) has also been examined *in vitro* in NHU cells. Di Martino et al showed that expression of mutant-active FGFR3 was unable to induce anchorage-independent growth in human telomerase reverse transcriptase (hTERT)-immortalised NHU cells (hTERT-NHU cells) but did result in higher saturation density at confluence [di Martino et al., 2009]. The authors suggested that mutant FGFR3 activity conferred some ability to overcome contact inhibition. In line with this hTERT-NHU cells transduced with mutant *FGFR3* showed a multilayer appearance versus the monolayer of control cultures [di Martino et al., 2009].

Further work supported the hypothesis that mutant *FGFR3* activity reduces contact inhibition by disrupting cell-cell interactions. hTERT-NHU cells transduced with *FGFR3-S249C* detached more readily from culture dishes than controls when trypsinized, and showed reduced expression of genes which contribute to the structure of desmosomes, adherens junctions and focal adhesions [di Martino et al., 2015]. These changes were reversed upon treatment of FGFR3-transduced cells with anti-FGFR3 siRNA, showing that the gene expression changes were driven by FGFR3-S249C activity. hTERT-NHU cells expressing mutant *FGFR3* also showed greater expression of the survival/anti-apoptotic proteins MCL1, BCL-XL and BCL2, suggesting that the increased saturation density at confluence may be due to reduced cell death versus controls [di Martino et al., 2009].

Thus overall, cell studies have shown that in a normal urothelial background, *FGFR3* mutation may contribute to a reduction in contact inhibition or a reduction in cell death, but cannot drive urothelial proliferation. This is in contradiction with the suggestion that *FGFR3* mutations have a precursor role in BLCA by driving urothelium into a proliferative state and thus causing hyperplasia [van Rhijn et al., 2020]

1.4.5.2 Mouse models of *FGFR3* mutation in urothelium

The majority of mouse studies have shown that expression of mutant *FGFR3* is unable to generate urothelial tumours or even hyperplasia. Constitutive expression of the mouse equivalents of the activating *FGFR3* mutants K650E or K650M did not cause hyperplasia or tumours and resulted in no increase in urothelial proliferation [Ahmad et al., 2011, Foth et al., 2014]. Combination of activating *Fgfr3* mutations with inactivating *Pten* mutations

(thus activating PI3K-AKT) resulted in urothelial hyperplasia [Foth et al., 2014], although combination of *FGFR3* mutations with *K-Ras* or *B-Catenin* did not [Ahmad et al., 2011]. Although expression of mutant *FGFR3* alone was unable to activate PI3K, it did result in an increase in ERK phosphorylation, and expression of the FGFR-negative feedback regulator Sprouty2 [Ahmad et al., 2011, Foth et al., 2014].

Constitutive or inducible expression of the activating human *FGFR3* mutant S249C in mice was also unable to urothelial proliferation, hyperplasia or tumours [Zhou et al., 2016, Foth et al., 2018]. In contrast to previous studies, *FGFR3* S249C alone was able to increase AKT phosphorylation [Zhou et al., 2016], but was unable to trigger urothelial hyperplasia when combined with inactivating *Pten* mutations [Foth et al., 2018]. FGFR3 K650E and S249C have been shown to have different mechanisms of activation and different downstream signalling potentials, which could potentially explain these discrepancies [Liveens et al., 2004, Bonaventure et al., 2007, di Martino et al., 2009].

The only study to date which has demonstrated formation of urothelial hyperplasia and/or urothelial tumours in mice expressing *FGFR3*-activating mutations is Shi et al., 2022. Here the authors used constitutive expression of FGFR3-S249C in mice by placing FGFR3-S249C under the control of the mouse Uroplakin 2 promoter - the same approach as has been used in all previous studies. The authors reported that mice which expressed human *FGFR3-S249C* developed hyperplasia and/or low-grade papillary urothelial tumours, as relative expression of *FGFR3-S249C* increased. The *FGFR3*-mutant tumours which formed were genetically similar to luminal BLCAs [Shi et al., 2022]. Shi et al suggested that the tumorigenicity of *FGFR3-S249C* seen in their hands could be due to increased expression of *FGFR3* versus previous studies. However, as previous mouse studies have not quantified mutant *FGFR3* expression in a manner similar to that of Shi et al. this suggestion is impossible to test.

Thus, while the effects of combining *FGFR3-activating* mutations with other mutations is contested, almost all studies have concluded that mutational activation of *FGFR3* alone is not sufficient to trigger urothelial proliferation, hyperplasia or tumour formation.

1.5 Experimental Platform - Normal Human Urothelial (NHU) cells

1.5.1 Phenotypes of NHU cells in culture

Normal Human Urothelial (NHU) cells can adopt a variety of phenotypes when cultured, depending on the cell culture conditions. When cells of the urothelium are isolated in culture and grown in serum-free low-calcium (0.09 mM) conditions, they adopt a proliferative phenotype similar to the wound-repair program that exists in urothelial tissue [Varley et al., 2005]. These “undifferentiated” NHU cells grow as a monolayer where growth is driven by autocrine EGFR signalling, stimulated primarily by the amphiregulin ligand [Varley et al., 2005]. Undifferentiated NHU cells do not express markers of differentiated urothelium, such as Cytokeratin 13 (*KRT13*) or Uroplakin 3A (*UPK3A*) [Varley et al., 2004a, Varley et al., 2006, Southgate et al., 2007] . Instead, undifferentiated NHU cells express markers of squamous differentiation [Southgate et al., 1994] as seen in BLCA, such as *KRT14* [Harnden and Southgate, 1997, Southgate et al., 2007]. More information and additional differentiation markers are provided in Table 1.3 below.

Table 1.3 - Markers of differentiated and undifferentiated phenotypes in normal urothelium and bladder cancer

Gene	Associations in normal urothelium	References	Associations in BLCA	References
KRT20	>Expressed in superficial layer of urothelial tissue >Expression increased by *in vitro* differentiation of urothelial cells	De La Rosette et al., 2002, Varley et al., 2004, Southgate et al., 2007, Hustler et al., 2018	>Expression is associated with luminal subtype and non-response to chemotherapy in MIBC >Expression associated with expression or uroplakins	Sjodahl et al., 2012, Choi et al., 2014, Damrauer et al., 2014, Dadhania et al., 2016, Robertson et al., 2017
KRT13	>Expressed suprabasally in normal urothelium >Expression increased by *in vitro* differentiation of urothelial cells >Excluded from basal layer of urothelial tissue affected by metaplasia	Varley et al., 2004, Southgate et al., 2009, Bock et al., 2014	>Decreased expression in BLCA vs normal urothelium >Decreased expression associated with increased BLCA stage and grade	Schaafsma et al., 1990. Celis et al., 1996, Marsit et al., 2010, Worst et al., 2014, Lenartz et al., 2022
UPK3A	>Expression in urothelial	Southgate et al., 2007,	>Expression is	Lai et al., 2010,

	tissue restricted to apical membrane of superficial urothelium >>Expression increased by *in vitro* differentiation of urothelial cells	Varley et al., 2009, Bock et al., 2014	associated with luminal subtype >Elevated in urine of BLCA patients	Damrauer et al., 2014, Marzouka et al., 2018, Szymańska et al., 2018, Bernado et al., 2019
FOXA1	>Transcription factor motifs are enriched in *in vitro* differentiated urothelial cells >Expression increased by *in vitro* differentiation of urothelial cells >Expression in urothelial tissue increases when moving from basal to superficial layer >Required for *in vitro* differentiation-associated expression of uroplakins	Varley et al., 2009, Fishwick et al., 2017, Bock et al., 2014	>Expression is associated with luminal subtype and expression of PPARγ target genes	Eriksson et al., 2015, Dadhania et al., 2016, Robertson et al., 2017, Marzouka et al., 2018
GATA3	>Transcription factor	Bock et al., 2014,	>Expression is	Eriksson et al., 2015,

	motifs are enriched in *in vitro* differentiated urothelial cells >Required for *in vitro* differentiation-associated expression of *KRT13* >Expression increased by *in vitro* differentiation of urothelial cells	Fishwick et al., 2017	associated with luminal subtype and expression of PPARγ target genes	Dadhania et al., 2016, Robertson et al., 2017, Marzouka et al., 2018
KRT5	Expressed in basal urothelial layer	De La Rosette et al., 2002, Hustler et al., 2018	>Expression is associated with basal subtype and response to chemotherapy in MIBC >Expression associated with squamous differentiation in BLCA >Associated with expression of p63 target genes	Blaveri et al., 2005, Sjodahl et al., 2012, Choi et al., 2014, Damrauer et al., 2014, Eriksson et al., 2015, Dadhania et al., 2016, Robertson et al., 2017, Marzouka et al., 2018
KRT14	>Associated with squamous urothelial	Harnden and Southgate, 1997, Varley et al., 2004,	>Expression associated with squamous	Blaveri et al., 2005, Sjodahl et al., 2012, Choi

	differentiation >Not expressed in normal urothelial tissue >Expression decreased by *in vitro* differentiation of urothelial cells	Southgate et al., 2009	differentiation in BLCA >Associated with expression of p63 target genes	et al., 2014, Damrauer et al., 2014, Eriksson et al., 2015, Dadhania et al., 2016, Robertson et al., 2017, Marzouka et al., 2018

NHU cells are non-immortalised, finite cell lines and eventually undergo senescence when grown continuously in culture [Southgate et al., 1994, Shaw et al., 2005, Georgopoulos et al., 2011].Although undifferentiated NHU cells produce their own EGFR ligands, they are grown in keratinocyte serum-free medium (KSFM) supplemented with recombinant EGF to promote proliferation, as well as cholera toxin (CT) to promote plating efficiency and bovine pituitary extract (BPE) to provide growth factors necessary for survival [Hutton et al., 1993, Southgate et al., 1994, Southgate et al., 2002].

1.5.2 Differentiation of NHU cells

Undifferentiated NHU cells retain the capacity to become differentiated in culture and express markers associated with differentiated *in situ* urothelium. Two main methods have been published to induce urothelial cytodifferentiation - pharmacological-induced differentiation [Varley et al., 2004a, Varley et al., 2004b, Southgate et al., 2007, Fleming et al., 2012, Hustler et al., 2018], and differentiation using serum and physiological (2 mM) calcium [Cross et al., 2005, Fleming et al., 2012, Hustler et al., 2018].
NHU cells can be pharmacologically differentiated by combined activation of the nuclear receptor Peroxisome Proliferator-Activated Receptor γ (PPARγ) alongside inhibition of EGFR [Varley et al., 2004a, Varley et al., 2004b]. Previously, this pharmacological differentiation has been performed using the EGFR tyrosine kinase inhibitor PD153035 in combination with the PPARγ agonist troglitazone [Varley et al., 2004a, Varley et al., 2004b]. This treatment results in increased expression of urothelial differentiation markers *KRT13* and *KRT20* as well as a reduction in *KRT14* [Varley et al., 2004a, Varley et al., 2004b]. Other transcriptional changes include increased expression of the urothelial differentiation markers *UPK1b* and *UPKII*, as well as increased expression of *CLDN3* and the differentiation-associated transcription factors *IRF1*, *GATA3* and *FOXA1* [Varley et al., 2009, Fishwick et al., 2017]

1.5.3 Serum and calcium-mediated differentiation of NHU cells

When NHU cells are grown in media containing serum and physiological calcium (2mM) differentiation-associated gene expression changes occur, such as upregulation of *KRT13*, *UPK2*, *UPK3A* and *CLDN4*, as well as downregulation of *KRT14* [Cross et al., 2005, Fleming et al., 2012].

Key to differentiation of NHU cells with adult bovine serum and calcium (ABS-Ca^{2+}) is the adoption of key physiological properties of *in situ* urothelium. Epithelia are classically considered to have a “tight” barrier if they have a transepithelial electrical resistance (TER) of greater than 500 Ω.cm^2 [Frömter, 1972]. When grown on a semi-permeable membrane, ABS-Ca^{2+} differentiated NHU cells stratify and can form a barrier with a TER of 3000 Ω.cm^2 [Cross et al., 2005, Georgopoulos et al., 2011, Smith et al., 2015, Hinley et al., 2022]. Whereas undifferentiated NHU cells are highly proliferative, ABS-Ca^{2+} differentiated NHU cells and *in situ* urothelium are both mitotically quiescent [Varley et al., 2005, Baker et al., 2022].

1.6 Thesis Aims

The overall aim(s) of this project were to characterise the expression of FGFR3 in urothelium and examine the effects of FGFR3 activation in urothelial cells, both through ligand and mutational activation. The goal was to increase understanding of what role *FGFR3* mutational activation plays in urothelial carcinogenesis.

Specific thesis objectives were :

- Determine the factors controlling expression of *FGFR3* in the normal urothelium (Chapter 3)
    - Characterise expression of *FGFR3* in urothelial tissue from bladder and ureter, and urothelial cell models derived from urothelial tissue
    - Investigate how expression of *FGFR3* expression can be achieved experimentally by manipulation of growth factor receptor signalling and urothelial differentiation
- Characterise activation of FGFR3 in urothelial cells (Chapter 4)
    - Assess the downstream signalling cascade following FGFR3 activation in urothelial cells
    - How does activation affect FGFR3 localisation in urothelial cells?
    - How does FGFR3 localisation in urothelial cells compare to urothelial tissues?
- Determine the role (if any) of *FGFR3* mutational activation in tumour initiation in the normal urothelium (Chapter 5)
    - In BLCA datasets, how is *FGFR3* mutation associated with markers of proliferation?
    - Generate retrovirally-transduced urothelial cell lines expressing the S249C mutant-active or wild-type *FGFR3*
    - Does overexpression of mutant-active FGFR3 drive quiescent urothelial cells into a proliferative state?

2. Materials and Methods

2.1 General

2.1.1 H_2O and Buffers

Water used in experiments and to make up buffers and stock solutions was purified using an ultrapure deionisation unit (SUEZ water). SUEZ water and buffers used for tissue culture were sterilised by autoclaving (112ºC for 20 minutes) prior to use.

2.1.2 List of Suppliers

Table 2.1 - List of suppliers

Supplier	Location	Website
Abcam	Cambridge, United Kingdom	https://www.abcam.com/
Bio-rad	Hercules, California, United States	https://www.bio-rad.com/
Cambridge Bioscience	Cambridge, United Kingdom	https://www.bioscience.co.uk/
Cayman Chemical	Ann Arbor, Michigan, United States	https://www.caymanchem.com/
Cell Signalling Technology	Danvers, Massachuesets, United States	https://www.cellsignal.com/
ITW reagents	Barcelona, Spain	https://www.itwreagents.com/rest-of-world/en/home-rw
Leica Biosystems	Sheffield, United Kingdom	https://www.leicabiosystems.com/
LI-CORi-cor	Lincoln, Nebraska, United States	https://www.licor.com/
Merck Millipore	Burlington, Massachusetts,	https://www.merckmillipore.

	United States	com/GB/en
Origene	Rockville, Maryland, United States	https://www.origene.com/
Plasmidsaurus	Arcadia, California, United States	https://www.plasmidsaurus.com/
Qiagen	Hilden, Germany	https://www.qiagen.com/
Santa Cruz Biotechnology	Dallas, Texas, United States	https://www.scbt.com/home
Sarstedt	Nümbrecht, Germany	https://www.sarstedt.com/en/
Sigma Aldrich	St. Louis, Missouri, United States	https://www.sigmaaldrich.com/GB/en
Stratech	Ely, United Kingdom	https://www.stratech.co.uk/
Thermofisher Scientific	Waltham, Massachusetts, United States	https://www.thermofisher.com/uk/en/home.html
Tocris - Bio-techne	Bristol, United Kingdom	https://www.tocris.com/
Vector Laboratories	Oxford, United Kingdom	https://www.2bscientific.com/Suppliers/Vector-Laboratories?gad_source=1&gclid=CjwKCAjwkuqvBhAQEiwA65XxQC1JDgN3gwhm1rbdjChet2iclXfgbzy-jYWYilJyDVfE774j1pc84xoCxdsQAvD_BwE

2.1.3 Stock Solutions

General

PBS

10 x PBS tablets (Thermo Fisher) in 1 L was adjusted to pH 7.3 and autoclaved before use.

TBS

Tris	1.21 g (10 mM)
NaCl	8.18 g 140 mM)
dH_2O	to 1 L

TBST was made by adding 0.1% Tween to TBS. Both were adjusted to pH 7.4 and stored at ambient temperature.

Cell culture

EDTA

Made up with 0.1% (w/v) EDTA in PBS and autoclaved before use.

Transport medium

500 mL HBSS
5 mL 1 M HEPES (final concentration 10 mM)
1 mL Traysol (500,000 KIU)

Stripper Medium

500 mL HBSS
5 mL 1 M HEPES (final concentration 10 mM)
1 mL Traysol (500,000 KIU)
50 mL 1% EDTA (final concentration 0.1%)

Collagenase IV

Collagenase was dissolved in transport medium to a concentration of 100 U/mL. This was aliquoted and stored at -20°C.

Trypsin versene

200 mL trypsin
4 mL 1% EDTA
176 mL HBSS

Trypsin versene was aliquoted and stored at -20°C.

Trypsin Inhibitor

100 mg of trypsin inhibitor was dissolved in 5 mL D-PBS then filter sterilised, then aliquoted and stored at -20°C.

Molecular Biology

10x TAE Buffer
108 g Tris
55 g Boric Acid
20 mL 1M EDTA
Made up to 1 L with dH_2O

10X solution was stored at ambient temperature and then diluted further 1:10 in dH_2O to make the working solution.

Western Blotting

SDS Sample buffer

10 mL Glycerol (20% v/v)
1 g SDS (2% w/v)
6.2 5mL Tris-HCl (pH 6.8) – 1 M stock diluted 1:8 = 125 mM
0.42 g Sodium fluoride (NaF)
18.4 mg Sodium orthovanadate (Na_3O_4V)
0.446 g tetra-Sodium pyrophosphate ($Na_4P_2O_7$)
dH_2O up to 50 mL

SDS sample buffer was stored in 1 mL aliquots at -20°C. Before use SDS sample buffer was completed by addition of 1M BTT to a final concentration of 0.2% and protease inhibitor cocktail.

Transfer Buffer

Tris	1.45 g (12 mM)
Glycine	7.2 g (96 mM)
Methanol	200 mL (20%)
dH_2O	to 1L

Transfer buffer was made up fresh at time of use and chilled on ice.

Ponceau Red

5 g Ponceau

10 mL glacial acetic acid

dH_2O up to 100 mL

Immunofluorescence

Antibody Diluent

25 mL 2 M Tris (pH 7.6)

50 mL 3 M NaCl

10 mL 10% (w/v) Sodium Azide Solution

10 mL 10% (w/v) BSA in TBS

Made up to 1 L with dH_2O

Solution was then stored at 4°C.

Immunohistochemistry

Scott's Tap Water

100 mL 20% $MgSO_4$ (final concentration 2%)

50 mL $NAHCO_3$ (final concentration 0.35%)

850 mL dH_2O

Hematoxylin

3 g Haematoxylin

20 mL 100% Ethanol

0.3 g Sodium Iodate

1g Citric Acid

50 g Chloral Hydrate

50 g Aluminium Potassium Sulphate

850 mL dH_2O

120 mL glycerol

Solution was filtered prior to use.

Citric Acid

2.4g citric acid (final concentration 10 mM)

1050 mL dH2O

Solution was adjusted to pH 6.

2.2 Tissue culture

2.2.1 Overview

Tissue culture work was performed in class II laminar flow hoods, using aseptic technique. Surfaces were cleaned with 70% (v/v) ethanol before and after use. NHU cell cultures were maintained in Keratinocyte Serum Free Media (KSFM; Gibco and ThermoFisher), supplemented with 5 ng/mL recombinant human epidermal growth factor (EGF), 50 µg/mL bovine pituitary extract (BPE) and 30 ng/mL cholera toxin, unless stated otherwise. The addition of these supplements forms “complete” KSFM (KSFMc). KSFMc was replaced on cells every 2-3 days.

Cultures were maintained in HeraCell 240 incubators (Thermo Scientific) at 37^{o}C in a humidified atmosphere with 5% CO_2 in air. Waste cells and medium were aspirated by vacuum into a Buchner flask containing 10% (w/v) virkon sterilising agent for decontamination.

2.2.2 Ethical Approval for Sample Collection and details of donor tissue used

Human urothelial specimens of ureter, collected under NHS Research Ethics Committee approval Leeds (East) REC 99/095 for the anonymous use of excess tissue following renal transplant surgery was used for immunohistochemistry and the experimental studies reported here, including generation of finite NHU cell lines. In addition, sections of formalin-fixed paraffin-embedded renal pelvis and bladder were accessed from URoBank (NHS REC approved research tissue bank 16/YH/0396 containing specimens collected with patient informed consent) and used anonymously for immunohistochemistry. Local institutional research approval for these activities was granted by the University of York Department of Biology Ethics Committee.

Anonymous human urothelial specimens of ureter, renal pelvis and bladder were obtained with informed consent from patients. Tissue was collected under NHS Research Ethics Committee approvals Leeds (East) REC 99/095 and REC 16/YH/0396 (URoBank).

On arrival, samples were allocated a laboratory record number (referred to as “Y number”, e.g. Y2566). Each Y number used in this thesis, along with the procedure under which the tissue was collected, is shown in Table 2.2. Age and sex are given where known.

Table 2.2 - Information on NHU cell lines and donor tissue used in this thesis

Cell line	Tissue Type	Donor Age	Donor Sex	Procedure	Passage number(s)
Y1781	Ureter	23	Male	Renal Transplant	P3
Y2863	Ureter	48	Male	Renal Transplant	P3
Y2843	Ureter	47	Male	Renal Transplant	P5
Y2324	Ureter	76	Female	Renal Transplant	P3
Y1827	Ureter	20	Male	Renal Transplant	P4
Y1971	Ureter	15	Male	?	P6
Y2442	Ureter	44	Female	Renal Transplant	P3
Y2698	Ureter	40	Female	Renal Transplant	P4
Y1237	Ureter	73	Male	Nephrectomy	P3
Y1359	Ureter	46	Male	Nephrectomy	P3
Y1909	Ureter	55	Female	Nephrectomy	P3
Y2717	Ureter	64	Male	Renal Transplant	P3
Y2777	Ureter	72	Male	Renal Transplant	P4
Y3000	Ureter	12	?	?	P4
Y3149	Ureter	31	Male	Renal Transplant	P3
Y3058	Ureter	58	?	Renal Transplant	P4
Y3059	Ureter	39	Male	Renal Transplant	P4
Y3161	Ureter	?	?	Renal Transplant	P5
Y1096	Ureter	75	Male	?	P4

Y1837	Ureter	54	Female	Renal Transplant	P3
Y2855	Ureter	53	Male	Renal Transplant	P4
Y2391	Ureter	49	Female	Renal Transplant	P5
Y2392	Ureter	43	Female	Renal Transplant	P3
Y2396	Ureter	?	Male	Renal Transplant	P4
Y2514	Ureter	45	Female	Renal Transplant	P4
Y2639	Ureter	?	Male	Renal Transplant	P4
Y2960	Ureter	44	Male	Renal Transplant	P3
Y2958	Ureter	64	Female	Renal Transplant	P3
Y2787	Ureter	41	Male	Renal Transplant	P4
Y2788	Ureter	34	Female	Renal Transplant	P3
Y2513	Ureter	46	Female	Renal Transplant	P3
Y2641	Ureter	32	Male	Renal Transplant	P4
Y2642	Ureter	63	Male	Renal Transplant	P6
Y2055	Ureter	42	Female	Renal Transplant	P3
Y2052	Ureter	55	Male	Renal Transplant	P4
Y1393	Ureter	60	Male	Renal Transplant	P3
Y2946	Ureter	52	Male	Renal Transplant	P7
Y2653	Ureter	56	Male	Renal Transplant	P8
Y2712	Ureter	?	Female	Renal Transplant	P8
Y2281	Bladder	?	Female	Cystoscopy	P0
Y2306	Bladder	68	Female	Cystoscopy	P0
Y2307	Bladder	26	Female	Cystoscopy	P0
Y2319	Bladder	65	Female	Cystoscopy	P0
Y2320	Bladder	50	Female	Cystoscopy	P0
Y2336	Bladder	?	?	Cystoscopy	P0
Y2337	Bladder	?	?	Cystoscopy	P0
Y2338	Bladder	?	?	Cystoscopy	P0
Y2339	Bladder	?	?	Cystoscopy	P0

Y2340	Bladder	66	Female	Cystoscopy	P0
Y2361	Bladder	?	Female	Cystoscopy	P0
Y2371	Bladder	64	Female	Cystoscopy	P0
Y2383	Bladder	55	Female	Cystoscopy	P0
Y2384	Bladder	39	Female	Cystoscopy	P0
Y2389	Bladder	68	Female	Cystoscopy	P0
Y2390	Bladder	44	Female	Cystoscopy	P0
Y2439	Bladder	77	Female	Cystoscopy	P0
Y2440	Bladder	59	Female	Cystoscopy	P0
Y2470	Bladder	62	Female	Bladder Biopsy	P0
Y2499	Bladder	52	Female	Flexible Cystoscopy	P0
Y2510	Bladder	25	Female	Flexible Cystoscopy	P0
Y2520	Bladder	?	?	Flexible Cystoscopy	P0
Y2521	Bladder	?	?	Flexible Cystoscopy	P0
Y2534	Bladder	74	Male	Rigid Cystoscopy	P0
Y2537	Bladder	61	Female	Rigid Cystoscopy	P0
Y2538	Bladder	37	Female	Rigid Cystoscopy	P0
Y2551	Bladder	57	Female	Rigid Cystoscopy	P0
Y2552	Bladder	70	Female	Rigid Cystoscopy	P0
Y2553	Bladder	59	Female	Rigid Cystoscopy	P0
Y2560	Bladder	41	Female	Rigid Cystoscopy	P0
Y2571	Bladder	16	Female	Flexible Cystoscopy	P0
Y2574	Bladder	63	Female	Rigid Cystoscopy	P0
Y2577	Bladder	49	Female	Flexible Cystoscopy	P0
Y2578	Bladder	78	Female	Flexible Cystoscopy	P0
Y2589	Bladder	40	Female	Rigid Cystoscopy	P0
Y2590	Bladder	61	Female	Rigid Cystoscopy	P0
Y2595	Bladder	54	Female	Rigid Cystoscopy	P0
Y2610	Bladder	?	Female	Rigid Cystoscopy	P0

Y2611	Bladder	74	Female	Flexible Cystoscopy	P0
Y2612	Bladder	57	Female	Flexible Cystoscopy	P0
Y2620	Bladder	66	Female	Flexible Cystoscopy	P0
Y2631	Bladder	67	Female	Rigid Cystoscopy	P0
Y2632	Bladder	54	Female	Rigid Cystoscopy	P0
Y2638	Bladder	51	Female	Flexible Cystoscopy	P0
Y2643	Bladder	35	Male	Rigid Cystoscopy	P0
Y2796	Bladder	77	Female	Bladder Prolapse	P0
Y2391	Ureter	?	Female	?	P0
Y2392	Ureter	?	Female	?	P0
Y2396	Ureter	?	Male	?	P0
Y1171	Ureter	?	?	?	P0
Y1174	Ureter	?	?	?	P0
Y1178	Ureter	?	?	?	P0

2.2.3 Urothelial Samples, cell culture, and storage

Primary urothelium cell cultures were established from urological specimens as previously described [Southgate et al., 1994]. Samples were stripped of fat and connective tissue in sterile petri dishes using scissors and forceps. The remaining sample was incubated in media containing 0.1 % (w/v) ethylenediaminetetraacetic acid (EDTA) for 4 hrs at 37^{o}C to dissociate the urothelium from the basement membrane. After incubation, sheets of urothelium were collected from basement membrane using forceps, then pelleted via centrifugation and resuspended in 2 mL (9200 units per mL) collagenase IV in Hank's balanced salt solution (HBSS) with Calcium, Magnesium, 4-(2-hydroxyethyl)-1-piperazineethanesulfonic acid (HEPES) (pH 7.6) to disaggregate cells, and incubated at 37^{o}C for 20 minutes. Cells were then collected by centrifugation and seeded at a density of at least 4x10^{4} cells/cm^{2} in KSFMc medium.

NHU cells were passaged when they reached (near) confluence by incubating cell monolayers in 0.1% (w/v) EDTA in PBS for 5 minutes at 37^{o}C. Cells were then incubated in 0.3-1mL, depending on flask size, of HBSS containing 0.25% (w/v) trypsin and 0.02%

(w/v) EDTA for 2 minutes at 37°C or until cells were visibly detached from each other and from the dish/flask. Cells were harvested into 5 mL KSFMc containing 1.5mg/mL trypsin inhibitor. Cells were then centrifuged at 1200 rpm for 4 minutes, supernatant aspirated and resuspended in KSMFc before being split into fresh flasks/dishes. Cells were passaged using ratios of 1:2 to 1:3. Unless stated otherwise, all experiments were performed on cells of passage 1-6.

For long-term storage, cells were trypsinized and then resuspended in freeze mix; this was composed of the normal media the cells were grown in plus 10% serum and 10% DMSO. Cells were resuspended to a concentration of 1 million cells per 1 mL and then frozen in 1 mL aliquots in cryo vials (ThermoFisher). Cryo vials were then placed in a Mr. Frosty Freezing container (ThermoFisher) which was stored at -80°C for 24 h. Following this, cryo vials were transferred to a dewar and stored under liquid nitrogen.

When selecting NHU cell lines for use in experiments, NHU cell lines were chosen which were of a suitable passage number and displayed a normal phenotype when viewed under a microscope, consisting of a “cobblestone” morphology and cells with bright borders, rather than a flat appearance (Fig. 2.1). Selected cells also showed an approximate cell doubling time of 24 h.

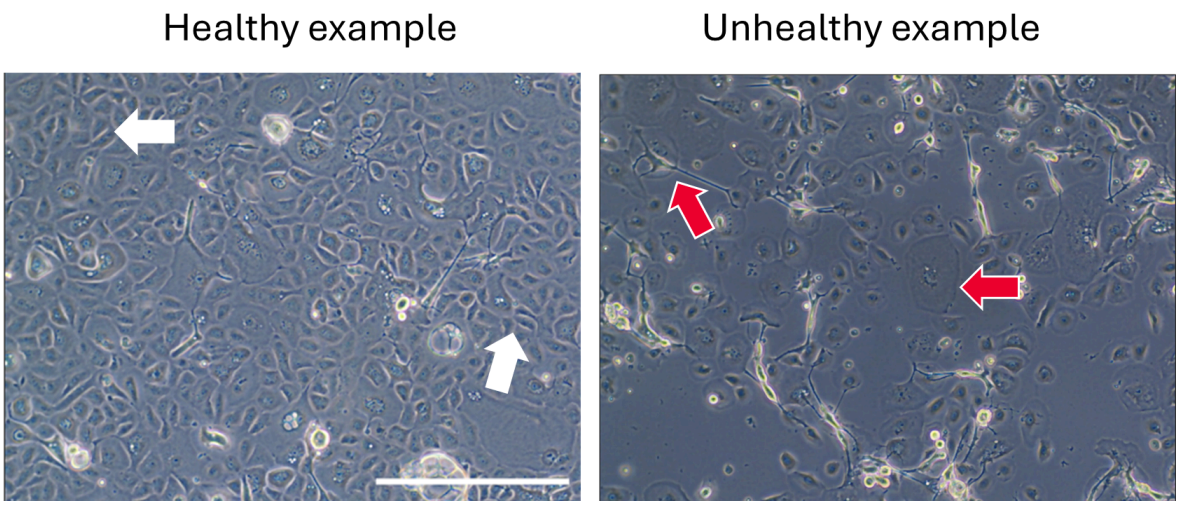

Figure 2.1 - Examples of healthy vs unhealthy appearances in NHU cell cultures - Healthy cell culture images are shown on the left, with examples of cells with bright borders and “cobblestone” morphology highlighted with white arrows. Unhealthy cell appearances are shown on the right, with flat unhealthy cells highlighted with red arrows. Scale bar (white line) represents 200 µm.

2.2.4 Chemical agonists and antagonists used in experiments

Details of chemical agonists and antagonists used are given in Table 2.3. DMSO was used as a vehicle control, at 0.1% (v/v) concentration, to match final concentration of DMSO in agonist/antagonist conditions. DMSO concentration was kept constant across all experiments. Compounds were solubilised in tissue culture grade DMSO and frozen at -20^{o}C in individual aliquots for long-term storage. See table below for more information. Chemical antagonists were titrated to determine the lowest concentration at which effective inhibition was achieved.

Table 2.3 - List of chemical agonists and antagonists used in this study

Name	**Target**	**Function**	**Supplier**	**Concentration used at**	**Solvent**
PD153035	EGFR	Antagonist	Merck Millipore	1 μM	DMSO
Lapatinib	EGFR/ERBB2	Antagonist	Stratech	1 μM	DMSO
AG1478	EGFR	Antagonist	Calbiochem	1 μM	DMSO
FR180204	ERK1/2	Antagonist	Tocris	1 μM	DMSO
Trametinib	MEK1/2	Antagonist	Tocris	10 nM	DMSO
Cetuximab	EGFR	Neutralising Antibody	Cambridge Bioscience	1 μg/mL	DMSO
T0070907	PPARγ	Antagonist	Cambridge Bioscience	5 μM	DMSO
Troglitazone	PPARγ	Agonist	R&D Systems	1 μM	DMSO
LY2955303	RARγ	Antagonist	Tocris	10 nM	DMSO
BMS961	RARγ	Agonist	Tocris	10 nM	DMSO

2.2.5 Differentiation of NHU cells

NHU cells were differentiated as described in Cross et al, 2005. Cells were established in KSFMc medium until they reached confluence, at which point cells were changed into KSFMc supplemented with 5% adult bovine serum (ABS). Cells were grown in KSFMc + 5% ABS for 5 days and then media changed to KSFMc + 5% ABS + 2 mM calcium, and grown for a further 7 days, before being used for experiments.

2.2.6 Generation of transduced NHU cells

PT67 packaging cells transfected with either pLXSP vector, or WT FGFR3 or S249C mutant FGFR3, were grown to post-visual confluence in Dulbecco's Modified Eagle Medium (DMEM). Once post-confluent, PT67 cells were media changed into DMEM: (Roswell Park Memorial Institute) RPMI 50:50 and incubated for 16 h. Following incubation, virus-containing medium was filtered with a 0.45 μM filter before mixing with Polybrene to a final concentration of of 8 μg/mL. Actively-proliferating NHU cells were then incubated in virus-containing medium for 8 h. 48 h after incubation, transduced NHU cells were passaged and placed into KSFMc containing 1 μg/mL puromycin antibiotic for selection. NHU cells were then cultured until the accompanying mock-transduced flask was completely dead. Stable retroviral transduction was confirmed (cells no longer produce virus) by incubating independent NHU cells with media from transduced NHU cells and then placing in KSFMc containing puromycin.

2.3 Western blotting

2.3.1 Cell Harvesting

Cells cultured for protein samples were grown either in 10 cm dishes (10 mL medium per dish), 6-well plates (3 mL medium per well), T25 flasks (5mL medium per flask) or T75 flasks (10 mL medium per flask). Upon reaching desired time-point or cell confluence, cells were washed twice in cold Phosphate-buffered saline (PBS), before being harvested in 50-200 μL of lysis buffer. Lysis buffer was made by mixing 2X sodium dodecyl sulphate (SDS) sample buffer with 1 M dithiothreitol (DTT) diluted 1:77, and protease inhibitor cocktail diluted 1:100 (both obtained from Sigma).

Sample plates were kept on ice and cold lysis buffer added, then cells were scraped off using cell scrapers. Lysates were collected into chilled 1.5 mL Eppendorf tubes, then either frozen at -20^{o}C for later processing, or immediately processed. For processing, lysates were sonicated using an ultrasonic processor for 2 x ten-second bursts, resting in

an ice bath for 10 seconds in between. Samples were then cooled on ice for 30 minutes, before being centrifuged at 14,000 rpm for 30 mins at 4°C, to separate lysate from SDS. Lysates were then pipetted to clean tubes and stored at -20°C until use.

2.3.2 Protein Quantification

Protein concentration of lysates was determined for normalisation of loading volumes for western blotting, using a Pierce™ Coomassie (Bradford) Protein Assay Kit (ThermoFisher). Two mg/mL Bovine Serum Albumin (BSA) was sequentially diluted in SUEZ water to create protein standards of 1000, 750, 500, 250, 125, 25, and 0 (water only) µg/mL. 10 µL of each standard was loaded in duplicate into a 96-well plate, along with duplicates of 10 µL of protein lysate diluted 1:12.5 in SUEZ water. Coomassie reagent was warmed to room temperature and then 200 µL was added to each well. Plates were then shaken for 30 seconds by a Multiskan Ascent plate reader before having absorbance read at 570 nm. Absorbance reading of BSA standards was used to generate a standard curve which was used to calculate the protein concentration of each lysate.

2.3.3 SDS Polyacrylamide Gel Electrophoresis (PAGE)

20 µg of protein lysate (unless stated otherwise) was prepared for SDS-PAGE by mixing with 4X NuPAGE Lithium Dodecyl Sulphate (LDS), 10X NuPAGE Sample Reducing Agent (SRA) and SUEZ water to a volume of 25 µL. All NuPAGE reagents, gels and gel tanks were purchased from invitrogen. Samples were then denatured at 70°C for 10 minutes, before cooling on ice for 2 minutes and briefly spun to collect sample from tube lid. Samples were then loaded on 4-12% Bis-Tris Plus 1.0mm x10/12/15 well gels. Gels were placed inside mini gel tanks and submerged in NuPAGE MOPS running buffer (diluted 1:20 with SUEZ water), before samples were loaded alongside 6 or 3 µL of Precision Plus Protein All Blue standards ladder (Bio-Rad). 200 µL NuPAGE antioxidant was added to inner chamber of gel tank before running to keep proteins reduced throughout electrophoresis. SDS-PAGE was performed at 200 (10 and 12-well gels) or 150 v (15-well gels) for between 45 to 90 minutes to allow proteins to migrate fully down the gel, based on size.

For western blotting, protein-immoblising polyvinylidene difluoride (PVDF) membrane was cut to a rectangle roughly 7x10cm and washed in methanol for 30 seconds, rinsing in deionised water, then equilibrating in transfer buffer. PVDF membrane was sandwiched with the gel, between filter paper and sponges inside a Mini Blot module (Invitrogen), in the order of: Cathode, sponge, filter paper, SDS-PAGE gel, PVDF membrane, filter paper, sponge, anode. Air bubbles were removed using a mini roller. Filled mini blot module was

then inserted into gel tank, and the inner and outer chamber filled with ice-cold transfer buffer. Transfer was performed for 90-120 minutes based on number of samples, at 20 v, in an ice bath. After transfer, membranes were washed with TBS, then reversibly stained with Ponceau Red solution for 10 seconds and washed in deionised water to visualise protein bands and confirm transfer.

2.3.4 Western blotting to detect protein

To prevent non-specific antibody binding, membranes were blocked at room temperature for 1 h on an orbital shaker, using either Odyssey Block Buffer (Li-Cor) diluted 1:1 with TBS or 5% (w/v) non-fat milk powder (ITW reagents) in TBST, depending on primary antibody (see Table 2.4). Prior to use, antibodies were titrated on known positive controls to establish optimal usage concentration. In most cases, a positive control lysate was also run on the same blot. Secondary antibodies were tested by placing on blocked membranes without any primary antibody, to account for background due to secondary antibody nonspecificity. Primary antibodies were diluted either in Odyssey Block buffer 1:1 with TBST, or TBS + 0.1% BSA + 0.1% Azide, depending on blocking (odyssey antibodies in odyssey, Milk antibodies in TBS). Primary antibody was applied overnight at 4^{o}C on an orbital shaker. Membranes were then washed for 5 minutes x 4 with TBST to remove unbound primary antibody, before being incubated with secondary antibody for 1hr at room temperature on an orbital shaker, covered in tinfoil. Secondary antibodies were diluted in Odyssey block buffer 1:1 with TBST or TBS + 0.1% BSA + 0.1% Azide, as above. Membranes were then further washed in TBST as above, plus 1 x 5 minute wash in TBS, before scanning for fluorescent bands of secondary antibody using the Odyssey Sa Infrared Imaging System (Li-Cor). Image Studio version 5.2 software was used to visualise bands and determine relative protein expression between samples using densitometry analysis of band intensity.

Table 2.4 - List of antibodies used for western blotting

Antibody	Species	Supplier	Clone/Number	Conc. used at
FGFR3	Rabbit	Cell Signalling	4574	1:1000
pERK	Rabbit	Cell Signalling	9101	1:1000
pFRS2	Rabbit	Cell Signalling	3861	1:1000
pEGFR	Rabbit	Cell Signalling	3777P	1:1000

pAkt	Rabbit	Cell Signalling	9271S	1:1000
pERBB2	Rabbit	Cell Signalling	2247P	1:1000
EGFR	Mouse	Sigma	E3138	1:2000
ZO-3	Rabbit	Cell Signalling	3704	1:1000
CK13	Mouse	Origene	bm5047s	1:1000
CK14	Mouse	Biorad	MCA890	1:5000
β-actin	Mouse	Sigma	AC15	1:10,000
Anti-Mouse IgG Alexa680	Goat	Molecular Probes	A21057	1:10,000
Anti-Rabbit IgG DyLight 800	Goat	Cell Signalling	5151P	1:30,000

2.3.5 Titration of C-terminal FGFR3 and pFRS2 antibodies for use in western blotting

Prior to experiments, antibodies against the N-terminus of FGFR3 and pFRS2 were titrated, based on manufacturer-recommended concentrations. All other antibodies, including FGFR3 C-terminal antibody, were titrated prior to the start of this work.
For titration of FGFR3 C-terminal antibody, NHU cells treated with either a DMSO control or the EGFR inhibitor PD153035 for 72 h were used (Fig. 2.2).

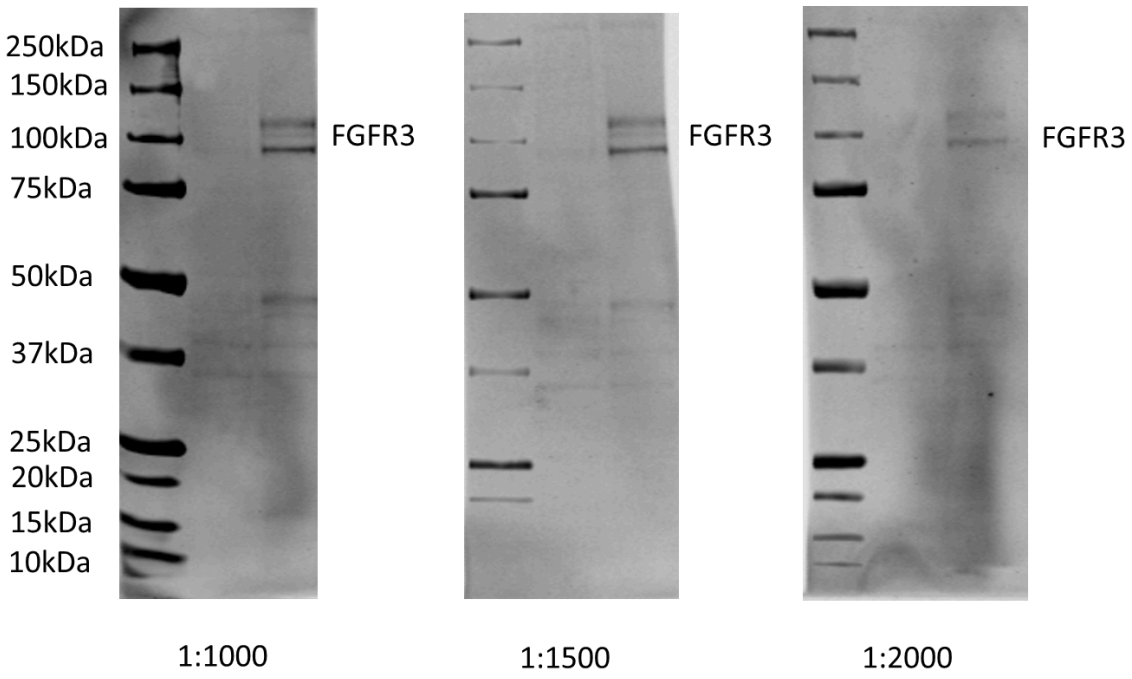

Figure 2.2 - Titration of C-terminal FGFR3 antibody for western blotting using NHU cell lysate

For pFRS2, RT112 BLCA cells were used (Fig. 2.3), as they have previously been reported to show FRS2 phosphorylation due to activity downstream of an FGFR3-TACC3 fusion protein [Williams et al., 2013].

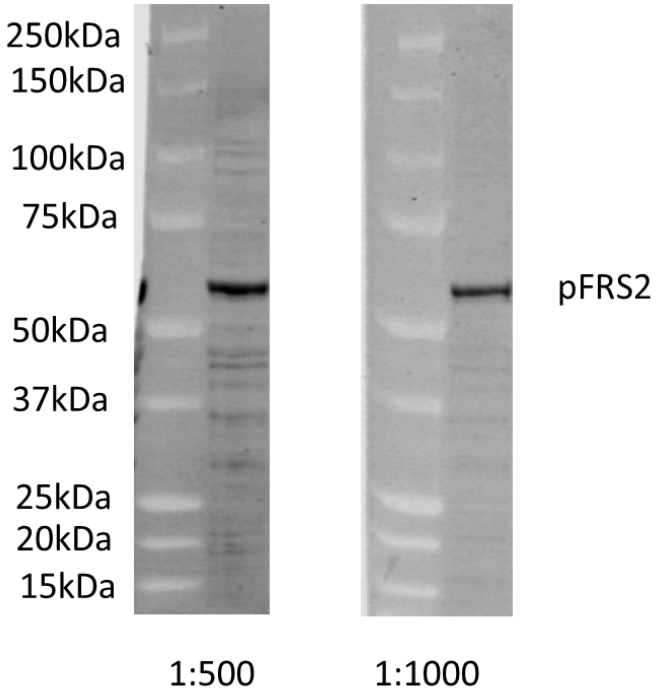

Figure 2.3 - Titration of pFRS2 antibody for western blotting using RT112 BLCA cell lysate

2.4 Molecular Biology

2.4.1 General

All RNA work was performed on a specific bench pre-cleaned with RNAseZap® wipes (Ambion). cDNA and PCR experiments were on a separate bench to avoid contamination. RNAse-free pipette tips, 1.5 mL and 500 µL tubes (Ambion) were used for all RNA work. SUEZ water (see above) was treated with 0.1% Diethyl pyrocarbonate (DEPC) overnight to remove RNAse enzymes, then autoclaved to remove DEPC from water.

2.4.2 RNA extraction

Cell medium was aspirated and cells washed once with ice-cold PBS before addition of TRIzol® Reagent (Life Technologies). Cells were then scraped from dishes using plastic cell scrapers. Resultant lysate was then either processed or frozen at -80^{o}C for future use. Upon thawing, lysates were incubated at room temperature for 5 mins to allow dissociation of nucleoprotein complexes. Chloroform was then added to solubilise the RNA. Samples were then centrifuged to phase-separate RNA, DNA and protein. RNA was collected by pipetting and other components were disposed of. RNA was then precipitated by serial washes of isopropanol and 75% (v/v) ethanol. Samples were then centrifuged and the supernatant disposed before allowing the resultant pellet to dry. Once dry, the pellet was resuspended in nuclease-free DEPC-treated water (see above). RNA was then stored at -80^{o}C or treated to remove DNA.

2.4.3 DNAse digest

A DNA-free™ kit (Ambion) was used to remove any contaminated DNA from RNA samples. RNA was treated with 2U/µL of rDNAse with DNAse buffer at a ratio of 1:10 buffer to RNA. RNA was then incubated at 37^{o}C for 30 minutes. DNAse inactivation reagent from the kit was then added and samples vortexed every 30 seconds for 2 minutes/ RNA was then centrifuged and supernatant taken to remove DNase and inactivation reagent.

At this point any samples intended for use in RNA-sequencing were treated with RNaseOUT™ Recombinant Ribonuclease Inhibitor (ThermoFisher) at 40 U per 30µL RNA.

Concentration of RNA in samples was determined using a NanoDrop™ UV spectrophotometer.

2.4.4 cDNA synthesis

50 ng poly(A)-tail-specific primers (Life Technologies) were annealed to 1 µg RNA at 65ºC 10 minutes. Master mix containing 2.5 mM $MgCl_2$, 10 mM DTT, 1 mM dNTP mix, First-strand buffer and SuperScript®II reverse-transcriptase (ThermoFisher) was added, then samples were incubated at 42ºC for 50 minutes followed by inactivation at 72ºC for 15 minutes. Samples were then diluted in DEPC-treated water.

2.4.5 Gel electrophoresis

Purified plasmid was separated by gel electrophoresis. Samples were run on an agarose gel, made from a solution of agarose and TBE buffer, with the percentage of agarose varying by DNA sample size. The solution was boiled using a microwave to dissolve the agarose powder (Melford Laboratories) before addition of the DNA gel stain SYBR Safe (Invitrogen) at 1:10,000. Gels were then poured into a cast and allowed to set by cooling. Set gels were then placed in a gel tank and submersed in 1x TBE buffer and DNA samples were electrophoresed next to a DNA ladder, which varied depending on the DNA sample size. Once the sample DNA had been adequately separated, the resultant bands were visualised with UV light.

2.4.6 Real-time quantitative PCR (RT-qPCR)

RT-qPCR master mixes were made up using 2x fast SYBR green master mix, forward and reverse primers each to a final concentration of 300 nM, and DEPC water to a final volume of 15 µL. One well of the fast SYBR green RT-qPCR used 15 µL of master mix and 5 µL of pre-diluted cDNA. Each gene target per cDNA sample was run in triplicate on a fast optical 96-well reaction plate (Applied Biosystems) and plates were sealed with an adhesive plastic cover.

Reactions were run on a QuantStudio RT-PCR system and analysed in qPCR Design and Analysis software (both thermo fisher). Each RT-qPCR reaction included an initial denaturing step at 95ºC for 20 seconds, followed by 40 cycles of DNA denaturation at 95ºC for 20 seconds and 20 seconds of elongation at 60ºC. An RT negative reaction was included for each gene target to confirm absence of non-specific amplification or genomic DNA contamination.

Expression of the housekeeping gene *GAPDH* was included with every RT+ sample as an internal loading control and was used to determine fold-change expression values. Data was analysed to determine the average Ct value per triplicate samples, to calculate the

difference in Ct value between the gene of interest and *GAPDH* housekeeping reference (ΔCt). ΔCt values were then normalised to sample *GAPDH* expression (ΔΔCt) and then fold changes in gene expression values were calculated (2- ΔΔCt).

2.4.7 Plasmids used for generation of FGFR3-transduced cell lines

Transduction of NHU cells was performed using PT67 cell lines previously-transduced with FGFR3-encoding plasmids of interest. Plasmids encoding for wild-type *FGFR3* IIIb or S249C-mutant *FGFR3* IIIb were a gift from Dr François Radvanyi.
To verify plasmid sequence, *E. coli* transformed with either pLXSP vector control, or pLXSP plasmid with an insertion of wild-type or S249C mutant *FGFR3* were spread on an agar plate containing puromycin. Colonies were then picked and expanded in media containing puromycin, after which plasmid DNA was collected using a plasmid mini kit (Qiagen). Following this, samples were sequenced by whole-plasmid sequencing (Plasmidsaurus). Sequencing confirmed that all 3 colonies picked for each construct contained the correct sequence: vector, wildtype or S249C *FGFR3*.

2.5 Histology

2.5.1 Tissue Fixation

All tissues used for experiments were fixed for 48-72 h in 10% neutral-buffered formalin unless stated otherwise. After the fixation period, tissues were transferred to 70% ethanol for storage until processing for embedding in paraffin wax, sectioning and staining.

2.5.2 Embedding of Tissue in Paraffin Wax

Before embedding, tissues were first dehydrated by washing in 70% ethanol, then 3 washes in 100% ethanol, 2 washes in isopropanol, and 4 washes in xylene. All washes were 10 minutes. After the final xylene wash, tissues were blotted dry and then transferred to molten paraffin wax at 60^{o}C. After 15 minutes, tissues were transferred to another wax pot, and this was repeated for a total of 4 wax treatments. Tissues were then embedded in a molten wax block that was allowed to set.

2.5.3 Sectioning of Tissue Blocks

Prior to sectioning, wax tissue blocks were cooled to -12^{o}C using a cold plate. Once cold, blocks were cut into 5 µm sections using a Leica RM2135 microtome. Sections were then placed on Superfrost Plus microscope slides using a water bath and left to dry overnight. After drying, slides were baked for 1 h to remove wax before any further processing.

2.5.4 Haematoxylin and Eosin (H&E) Staining

After baking, slides were de-waxed with 2 x 10-minute washes in xylene followed by 2 x 1-minute washes in xylene, then gradual rehydration with 3 x 1-minute absolute ethanol washes and 1 1-minute wash in 70% (v/v) ethanol. After this, sections were washed in running tap water for 1 minute, before staining with haematoxylin for 1 minute. After staining, slides were washed for 1 minute in running tap water, then 1 minute in Scott's tap water, and another 1-minute wash in running tap water. Slides were then eosin stained for 30 seconds (no eosin stain was applied for IHC), before being washed in running tap water. Slides were then gradually dehydrated through 1 x 70% ethanol wash, 3 x absolute ethanol washes, 2 x xylene washes, before finally being mounted with DPX mountant under glass coverslips.

2.6 - Immunohistochemistry

2.6.1 Antigen retrieval

Prior to antigen retrieval, slides were dewaxed in ethanol and xylene, as described for H&E staining above (Section 2.5.4). Slides were then blocked for 10 minutes with 3% hydrogen peroxide, before being washed for ten minutes in running tap water. For antigen retrieval, slides were either treated in a pressure cooker for 10 minutes at 50 kPa, in a 10mM Citric Acid buffer at pH 6, or Microwaved in a Pyrex dish for 13 minutes in 1 mM EDTA (pH 8). The optimal antigen retrieval method was determined for each antibody individually.

2.6.2 Antibody Labelling

Primary antibodies were titrated on positive control tissues to determine optimum antibody usage concentrations. A negative control treated with secondary antibody only, as well as a positive control tissue known to express the protein of interest was included in each experiment. The concentration at which primary antibodies was used is given in Table 2.5

Normal horse serum, amplifier antibody, ImmPRESS Excel reagent and DAB reagent were all supplied as part of an ImmPRESS Excel kit purchased from Vector Laboratories. Specific information on antibodies used is given in Table 2.5.

After antigen retrieval, slides were washed in running tap water, then placed in a slide rack. Slides were washed with TBST, then blocked with 100 µL 2.5% normal horse serum

for 20 minutes at room temperature. Each slide was then treated with 100 µL of primary antibody diluted in TBST and incubated overnight at 4°C.
After incubation, slides were washed 3 times with TBST and then incubated for 15 mins with 100 µL amplifier antibody at ambient temperature. Slides were then washed twice with TBST and incubated for 30 mins at room temperature with 100 µL ImmPRESS Excel reagent per slide. Slides were then washed once with TBST and then dH_2O, before incubation with DAB reagent for 5 minutes at room temperature. Slides were then rinsed in dH_2O and then tap water, before counterstaining in Haematoxylin for 1 second, then washing thoroughly in tap water. Slides were then cleared through ethanol and xylene and mounted with DPX, as described above for H&E staining. :

Table 2.5 - List of antibodies used for immunohistochemistry

Antibody	**Species**	**Supplier**	**Clone/Number**	**Conc. used at**	**Antigen retrieval method**
FGFR3 (N-terminal)	Mouse	Santa Cruz	sc-13121	1:50	Polymer Kit, Pressure Cooker Citric Acid
FGFR3 (C-terminal)	Rabbit	Cell Signalling	4574	1:50	Polymer Kit, Pressure Cooker Citric Acid

2.6.3 Imaging and microscopy

Immunohistochemical labelled was visualised on an Olympus BX60 bright field microscope and images were taken using an Olympus DP50 digital camera and cellSens Standard Micro Imaging Software (Olympus).

2.7 Immunofluorescence

2.7.1 Slide preparation and fixation

Sterilised 12-well glass slides were placed in 4-slide quadriPERM culture dishes (Sarstedt). Cells were seeded onto slides and then allowed to attach for 4 h before

flooding with media. Cells were grown to required density and treated as indicated. Once cells were ready, they were washed with ice-cold PBS and then fixed either using Methanol:Acetone (Me:Ac) 1:1 (v/v) or 10% Formalin (w/v).

For Me:Ac fixation, slides were fixed in Me:Ac for 30 seconds before air-drying. Slides were then either used immediately, or wrapped in clingfilm and stored at -20^{o}C until use. For formalin fixation, cells were fixed in 10% formalin (w/v) for ten minutes, then washed in PBS and used immediately or stored in PBS in a humid environment at 4^{o}C. Cells were permeabilised by washing slides PBS containing 0.5% (w/v) Triton X-100 before antibody labelling.

2.7.2 Antibody Labelling

Primary antibodies were titrated on a positive control to determine optimum antibody concentration. A secondary-only negative control was included in each experiment to account for fluorescence from just the secondary antibody. The concentration at which primary antibodies were used is given in Table 2.6.

A grease pen (Cell Path) was used to circle each well to prevent antibody cross-contamination. Each well was labelled with 30 µL of primary antibody diluted in (TBS), pH 7.6 with 0.1 % NaN_3 (Sigma-Aldrich, S8032) and 0.1% bovine serum albumin (BSA) (Thermo Fisher Scientific, 37520) and this was incubated overnight at 4^{o}C in a humid atmosphere. Primary antibody was then removed by pipetting and slides were washed twice with PBS (Formalin fixation) or PBS + 0.2% (v/v) Tween20 (PBST) (Me:Ac fixation). Secondary antibodies were then applied for 1h at room temperature, using the same dilution and volume as primary antibody, protected from light. Slides were then washed twice with PBS (formalin fixation) or PBST (Me:Ac fixation), then labelled with 0.1 µg/ml Hoechst 33258 diluted in PBS for 5 minutes to label cell nuclei. Slides were then washed in PBS followed by SUEZ water. A second Me:Ac fixation was performed for 30 seconds followed by air-drying. Once slides were dry, cover-slips were mounted using Prolong™ Gold antifade (Thermo Fisher Scientific, P36930) mountant, then allowed to dry overnight at ambient temperature.
Information on specific antibodies is given in Table 2.6 below:

Table 2.6 - List of antibodies used for immunofluorescence microscopy

Antibody	Species	Supplier	Clone/Number	Conc. used at
FGFR3 (N-terminal)	Mouse	Santa Cruz	sc-13121	1:50
FGFR3 (C-terminal)	Rabbit	Cell Signalling	4574	1:50
Ki67	Mouse	Leica	NCL-L-Ki67-MM1	1:400
MCM2	Rabbit	Cell Signalling	D7G11	1:1600
LAMP1	Mouse	Developmental Studies Hybridoma Bank	H4A3	1:40
Calnexin	Mouse	BD Biosciences	610523	1:500

2.7.3 Imaging and microscopy

Fluorescent labelling of slides was visualised using an Olympus BX60 epifluorescent microscope, under a 20x or 60x oil immersion objective. Images were taken using an Olympus DP50 digital camera and cellSens Standard Micro Imaging Software (Olympus).

2.8 Bioinformatics

2.8.1 Datasets used in this thesis generated by others within the Jack Birch Unit

Table 2.7 - Datasets used in this thesis generated by others within the Jack Birch Unit

Dataset	Samples	Sequencing Strategy	Publication	Accession
Benign Uropathies	80	44 * 75bp PE; HiSeq4000	Unpublished	-

		36 * 151bp PE; NovaSeq6000		
Baker_ABS-ca	9	101bp PE; HiSeq3000	Baker SC, Mason AS, Southgate J. Procarcinogen Activation and Mutational Signatures Model the Initiation of Carcinogenesis in Human Urothelial Tissues In Vitro. Eur Urol 2020 Aug;78(2):143-147. PMID: 32349929	ABS/Ca: (GEO) GSE146372 or (ENA) PRJNA610264 Undiff: (ENA) PRJNA847878
Nuclear Receptor	88	46 * 75bp PE; HiSeq4000 42 * 151bp PE; NovaSeq6000	Unpublished	-
P0-Ureters	3	101bp PE; HiSeq4000	Unpublished	-

2.8.2 External datasets used in this thesis

Table 2.8 - External datasets used in this thesis

Dataset	Samples	Publication	URL
TCGA_MIBC	408	Robertson et al., 2017	https://pubmed.ncbi.nlm.nih.gov/28988769/
UROMOL	535	Lindskrog et al.,	https://www.nature.

		2021	com/articles/s41467-021-22465-w

2.9 Statistical Analysis

GraphPad PRISM 9 was used to graph data and perform statistical tests where appropriate. Information regarding specific statistical tests as well as p values and levels of significance is given in the relevant figures. For transcriptomic data, all data points were plotted alongside the median value. For experiments using NHU cells, unless stated otherwise all experiments were performed in 3 distinct biological replicates using independent cell lines; mean values were graphed with error bars representing one standard deviation. The identifying “Y number” of each NHU cell line used for a given experiment is provided in the relevant figures.

2.10 Generation of Transduced NHU cell lines

2.10.1 Source of *FGFR3*-containing vectors

Plasmids containing wild-ype *FGFR3* IIIb or S249C mutant *FGFR3* IIIb were a gift from Dr François Radvanyi.

2.10.2 Generation and verification of *FGFR3* expression plasmids

Plasmids containing empty vector (pLXSP), *FGFR3-wild-type* and *FGFR3-S249C* were generated previously by Nicola Shaw (Jack Birch Unit, University of York) [Shaw et al., 2005]. These plasmids were then verified by whole-plasmid sequencing.

To verify plasmid sequence, *E. coli* transformed with either pLXSP vector control, or pLXSP plasmid with an insertion of wild-type or S249C mutant *FGFR3* were spread on an agar plate containing puromycin. Colonies were then picked and expanded in media containing puromycin, after which plasmid DNA was collected using a plasmid mini kit (Qiagen). Following this, samples were sequenced by whole-plasmid sequencing (Plasmidsaurus). Sequencing confirmed that pLXSP vector was a vector-only control (Fig. 2.4). Looking at the FGFR3 294 codon position confirmed the wildtype and S249C mutant status (Fig. 2.5 - 2.8).

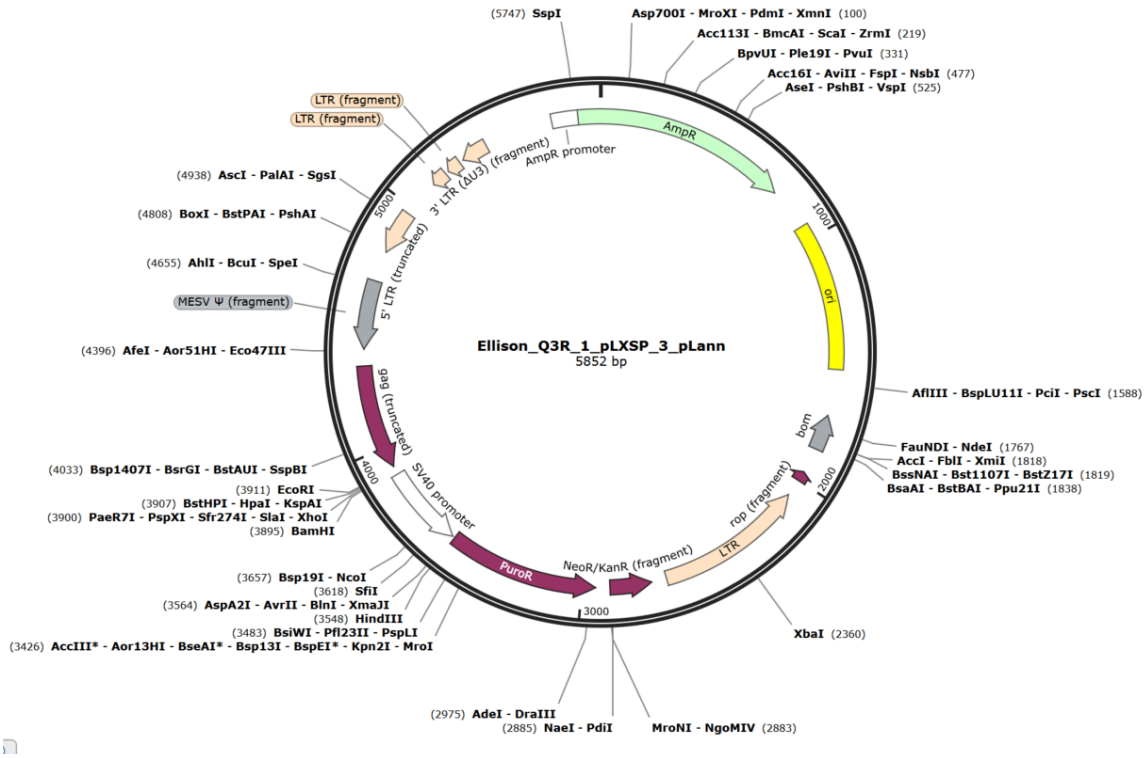

Figure 2.4 - Plasmid map of pLXSP vector control used to generate transduced NHU cell lines - Annotated plasmid map was produced using SnapGene Viewer software from a .gbk file obtained from plasmid sequencing. Restriction sites and plasmid features are annotated.

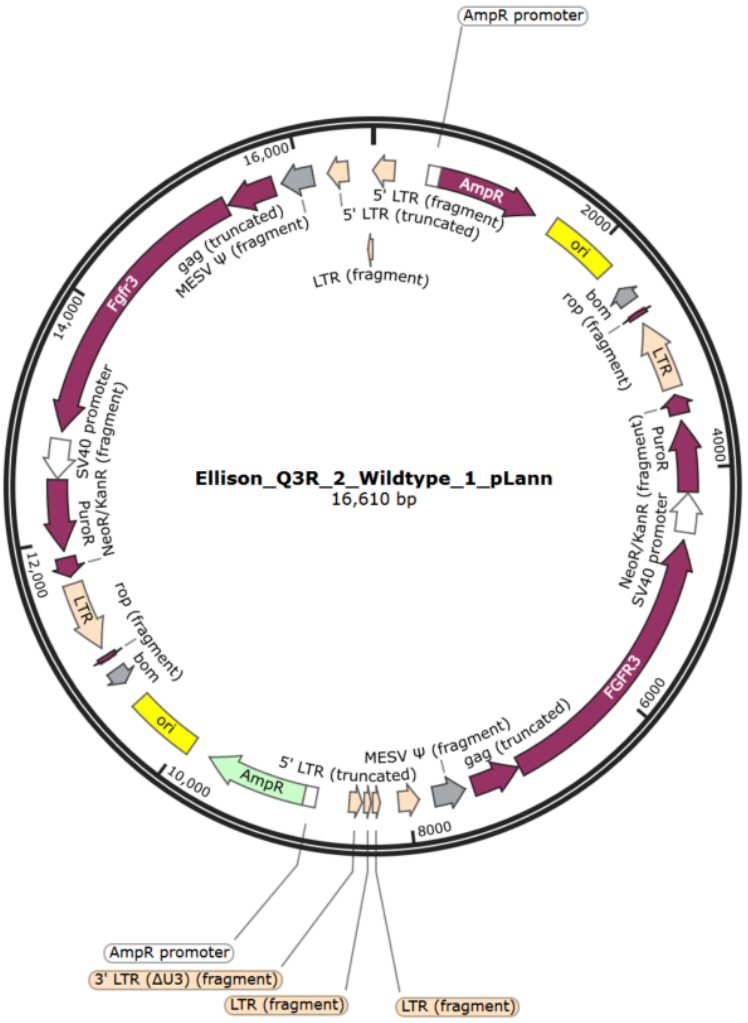

Figure 2.5 - Plasmid map of wildtype FGFR3 used to generate transduced NHU cell lines - Annotated plasmid map was produced using SnapGene Viewer software from a .gbk file obtained from plasmid sequencing. Restriction sites and plasmid features are annotated.

Figure 2.6 - Sequence of 249 region of wild type FGFR3 plasmid - Plasmid sequence was analysed in SnapGene Viewer software. The 249 codon is highlighted in red, showing the presence of the wild type Serine.

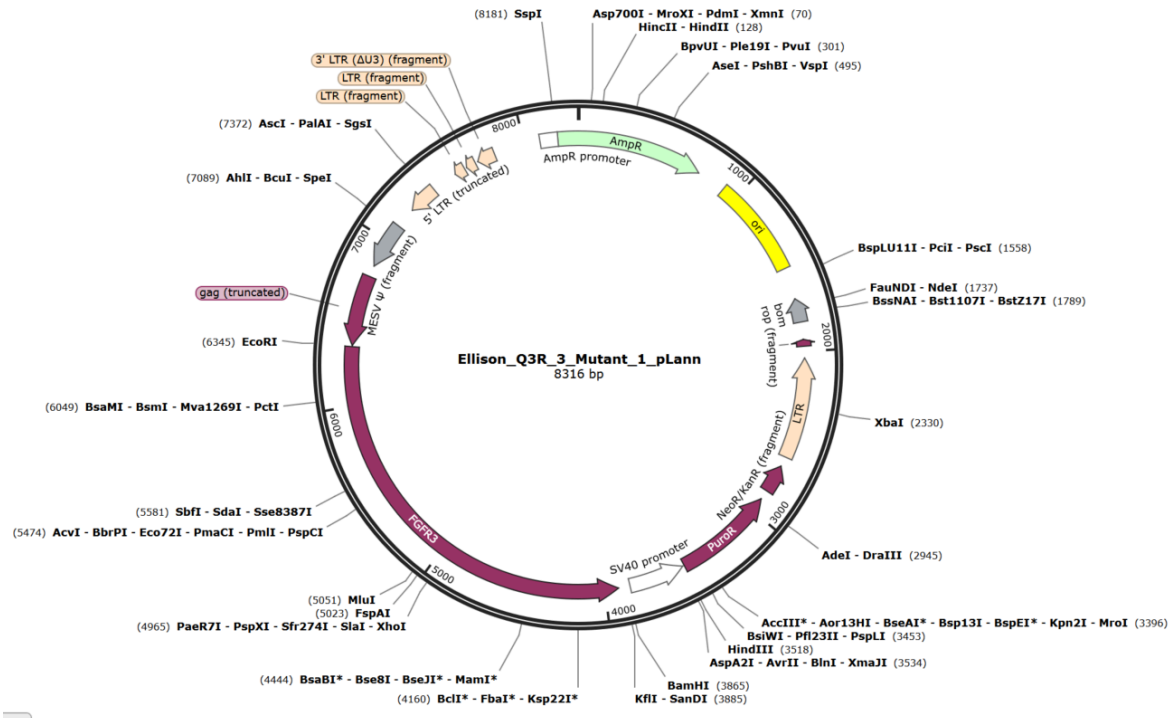

Figure 2.7 - Plasmid map of S249C mutant FGFR3 used to generate transduced NHU cell lines - Annotated plasmid map was produced using SnapGene Viewer software from a .gbk file obtained from plasmid sequencing. Restriction sites and plasmid features are annotated.

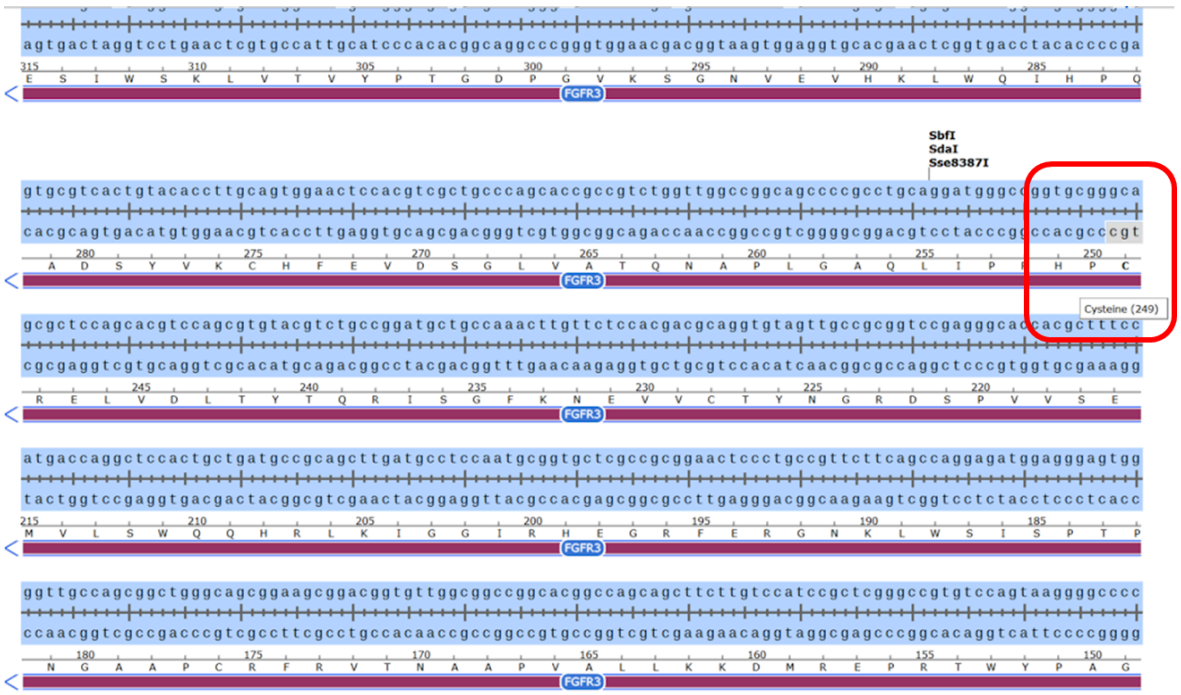

Figure 2.8 - Sequence of 249 region of S249C mutant FGFR3 plasmid - Plasmid sequence was analysed in SnapGene Viewer software. The 249 codon is highlighted in red, showing the presence of an S249C mutation.

The FGFR3 wild-type plasmid appeared to be approximately twice as large as the S249C FGFR3 plasmid, and contained two copies of the elements in the plasmid, compared to S249C FGFR3. This suggests that the wild-type FGFR3 plasmid may have somehow become duplicated. When plasmids were run on an electrophoresis gel, the wild-type FGFR3 plasmid appeared approximately twice as large as the S249C FGFR3 plasmid, confirming the sequencing results (Fig. 2.9).

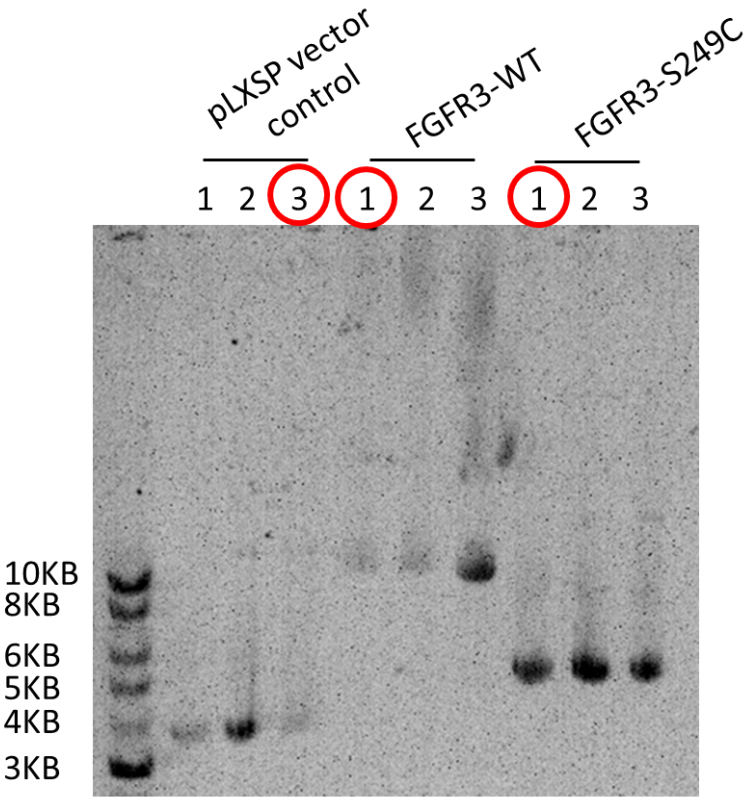

Figure 2.9 - DNA electrophoresis gel of the plasmids used to transduce NHU cells - Bacteria transformed with each of the indicated plasmids were grown on agar plates containing puromycin for antibiotic selection. Three colonies were picked from each plate, then one of each (indicated with a red circle) was sent for whole plasmid sequencing with Plasmidsaurus. Plasmids ran at a slightly lower than predicted molecular weight, most likely due to supercoiling.

2.10.3 Transduction and selection of NHU cells

Following validation, plasmids were transfected into PT67 packaging cell lines (Fig. 2.10). Following collection of virus from packaging cells, NHU cell lines derived from ureter tissue were transduced with empty vector, *FGFR3-wild-type* or *FGFR3-S249C* plasmids then selected with puromycin to kill non-transduced cells [Shaw et al., 2005]. The ureter-derived NHU cells lines Y2654, Y2712 and Y2946 were used for transduction.

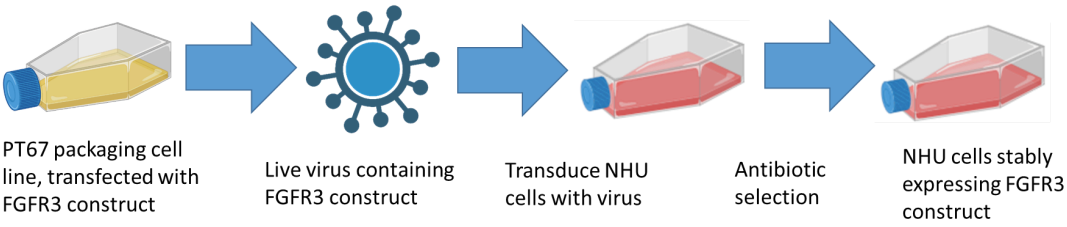

Figure 2.10 - Process of how NHU cells were transduced to generate NHU cell lines which stably overexpressed *FGFR3*

Mock-transduced cultures were included to track effectiveness of killing with puromycin (Fig. 2.11). Western blotting was used to confirm overexpression of wild-type or S249C FGFR3 in transduced NHU cells.

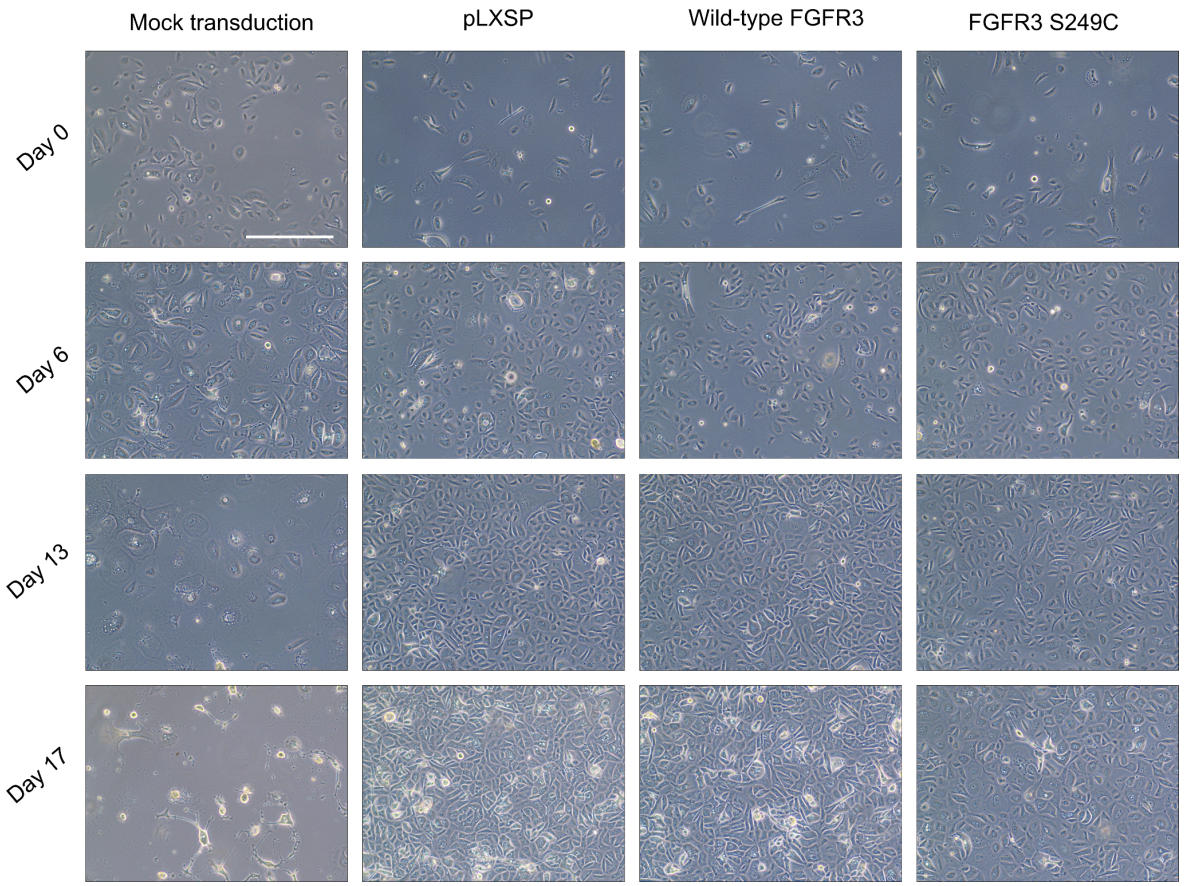

Figure 2.11 - Representative images of transduced NHU cells under puromycin selection - Scale bar is 200μm

3. Investigation of factors which regulate FGFR3 transcript and protein expression in normal urothelium

3.1 Aims and Objectives

The aim of this chapter was to identify factors which regulate the expression of FGFR3 transcript and protein in normal urothelium. Additionally, a broader characterisation of FGFR3 transcript and protein was attempted, by examining the different isoforms of *FGFR3* transcript and the glycosylation status of FGFR3 protein.

Specific objectives were:

- To characterise *FGFR3* transcript and protein expression in urothelial tissue and NHU cells derived from urothelium (Chapter 3.3.2)
    - To compare expression of *FGFR3* in bladder and ureter tissue
    - To compare expression of *FGFR3* to the *EGFR* family of growth factor receptors
- To determine factors which may regulate *FGFR3* expression in normal urothelium, such as EGFR (downstream) activity and urothelial differentiation (Chapter 3.3.3)
- Perform broader characterisation of FGFR3 transcript and protein expressed in urothelium by examining relative expression of *FGFR3* transcript isoforms and assessing the glycosylation status of FGFR3 protein (Chapter 3.3.4)

3.2 Experimental Design

Human urothelia from ureter (n=5) was examined *in situ* by western blotting of cell lysates from freshly-isolated urothelial tissue to quantify FGFR3 protein expression using verified antibodies against N- and C-terminal antigens. Initially, 8 donors were selected for testing of FGFR3 protein expression via western blot. However, 3 of these donors gave an excess of nonspecific signal when FGFR3 protein expression was assessed, and so an additional blot was performed using only 5 donors which gave a “clean” signal. The original test blot with all 8 donors is given in Appendix C.

3.2.1 Investigation of factors with the potential to influence FGFR3 transcript and/or protein expression in NHU cells

3.2.1.1 EGFR downstream signalling activity

To determine whether reported EGFR repression of FGFR3 expression was exclusive to BLCA or could also exist in normal urothelium, NHU cells were treated with an EGFR inhibitor (PD153035) and the effect on FGFR3 expression was measured. While testing the effect of EGFR inhibition on *FGFR3* expression, the exogenous EGF normally used in NHU cell culture was removed as previous work has shown that EGF-supplemented medium can overcome inhibitor treatments to activate MAPK signalling in NHU cells [Swiatkowski et al., 2003]. Hence, unless stated otherwise, all experiments conducted in this chapter used NHU cells grown without addition of EGF to the culture medium. EGFR and ERK phosphorylation were quantified and used as proxies for EGFR and ERK activity respectively.

3.2.1.2 Cholera Toxin and potential for Protein Kinase A activity

During NHU cell culture, media is supplemented with cholera toxin to improve cell plating efficiency and attachment [Southgate et al., 1994]. However, cholera toxin is known to activate PKA signalling indirectly through activation of adenylate cyclase [Cassel and Selinger, 1977]. Thus, to test if cholera toxin may influence *FGFR3* expression in NHU cells through PKA activation, experiments were performed where FGFR3 protein expression was assessed in NHU cells cultured with and without cholera toxin.

3.2.1.3 Urothelial differentiation

To investigate if *FGFR3* expression was regulated by urothelial differentiation, NHU cells were differentiated by culture in conditions of 5% Adult bovine serum (ABS) and 2 mM

calcium [Cross et al., 2005, reviewed by Baker et al., 2014]. See Chapter 2 for more detail.

3.2.2 Analysis of *FGFR3* transcript variants expressed in urothelial tissue and in NHU cells

FGFR3 transcript variant expression was assessed in urothelial RNAseq data representing isolated *in situ* urothelium or following growth *in vitro*, as differentiated or undifferentiated NHU cells. RNA-sequencing data was provided by Dr Simon Baker and Dr Andrew Mason (Jack Birch Unit, University of York) and was generated outside of this thesis. Specific datasets used were “Benign Uropathies”, “Baker_ABS-ca”, and “P0-Ureters”. Additional detail on these datasets is provided in Chapter 2. *FGFR3* transcripts were classified as either protein-coding or non protein-coding according to transcript classification rules from the Ensembl database. Genes containing an open reading frame were classified as “protein-coding”. *FGFR3* IIIb, IIIc and Δ8-10 were distinguished from other protein-coding transcripts due to their more extensive literature characterisation, versus almost no literature on non protein-coding *FGFR3* transcripts.

Transcript variants for which an open reading frame could not be defined were classed as “nonsense mediated decay”, “protein coding sequence not defined”, or “retained intron” (together “non protein-coding”). “Nonsense mediated decay” variants contained a coding sequence which finished >50 bp from a downstream splice site or if the transcript variant did not cover the full reference coding sequence (i.e. appears incomplete). “Protein coding sequence not defined” transcripts appeared to be protein coding, but did not have an open reading frame. “Retained intron” sequences contained sequences which appeared to be spliced out of other coding transcripts as introns.

Isoform-level transcript data was provided by Richard Gawne (Jack Birch Unit, University of York) and then analysed by me according to the above classification.

3.3 Results

3.3.1 Selection of BLCA cell lines for an FGFR3 protein expression positive control

To identify a suitable positive control for the expression of FGFR3 protein for the use of experiments, FGFR3 protein expression was probed using antibodies against the N- and C-terminus of FGFR3 in a panel of BLCA cell lines. BLCA cell lysate was previously generated by Dr Simon Baker (Jack Birch Unit, University of York). This identified detectable expression of FGFR3 protein in several of the BLCA cell lines tested, however the RT112 cell line showed particularly high FGFR3 protein expression (Fig. 3.1). This was consistent with previous reports of FGFR3 protein expression in RT112 BLCA cells [Williams et al., 2013].

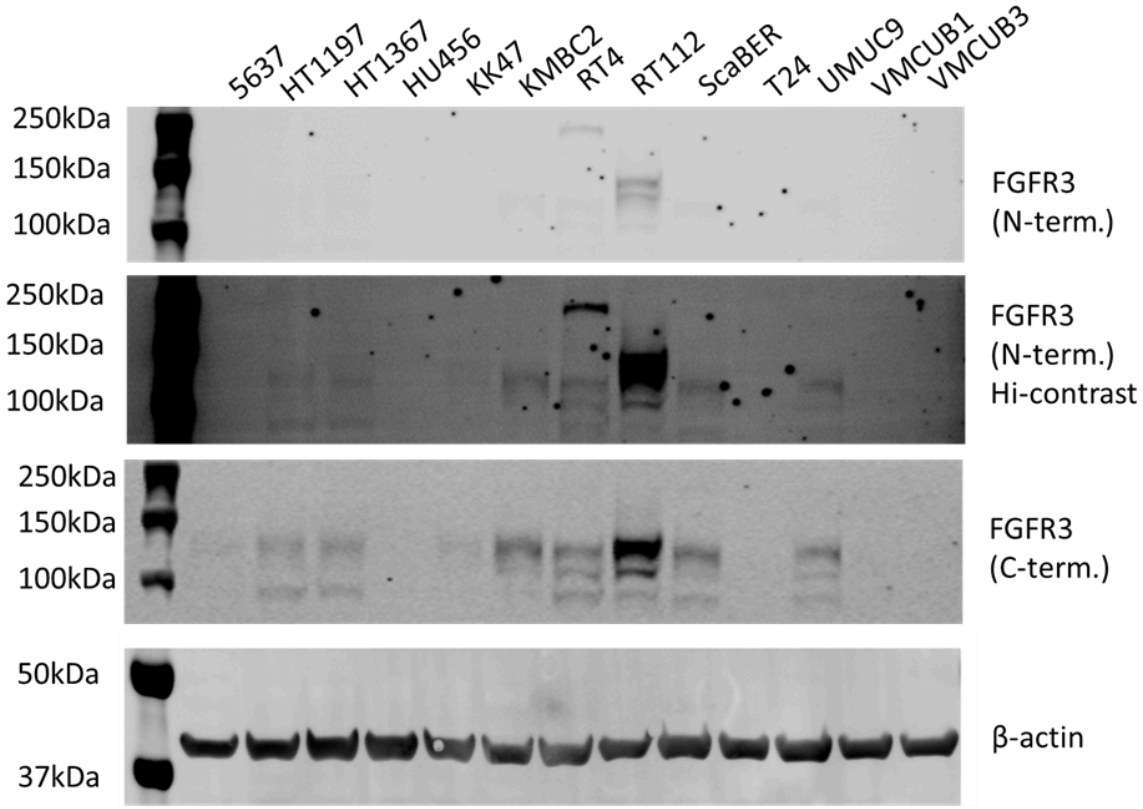

Figure 3.1 - In a panel of BLCA cell lines FGFR3 protein expression was greatest in RT112 BLCA cells - Cell lysates previously generated by Dr Simon Baker (Jack Birch Unit, University of York). 20 µg of protein was loaded for each sample. β-actin was used as a loading control to ensure equal protein between lanes.

3.3.2 Analysis of FGFR3 transcript and protein expression in urothelial tissue and NHU cells

3.3.2.1 *FGFR3* transcript expression in urothelial tissue and NHU cells from bladder and ureter tissue

Analysis of RNA-sequencing data (provided by Dr Simon Baker and Dr Andrew Mason) from different urothelial models showed that *FGFR3* transcript expression was significantly greater in freshly-isolated urothelial tissue than NHU cells, for both bladder but not ureter ($p<0.05$, Fig. 3.2a). Expression of *FGFR3* transcript was significantly more abundant in ureter than bladder urothelial tissue and *FGFR3* transcript expression was significantly more variable in ureter than bladder (both $p<0.05$, Fig. 3.2).

The expression of *EGFR* family member transcripts was used as a reference point for typical expression values of a growth factor receptor tyrosine kinase with known roles in normal urothelium. In bladder tissue, median *FGFR3* transcript expression was more than 1.5 times greater than all *EGFR* family members (Fig. 3.2).

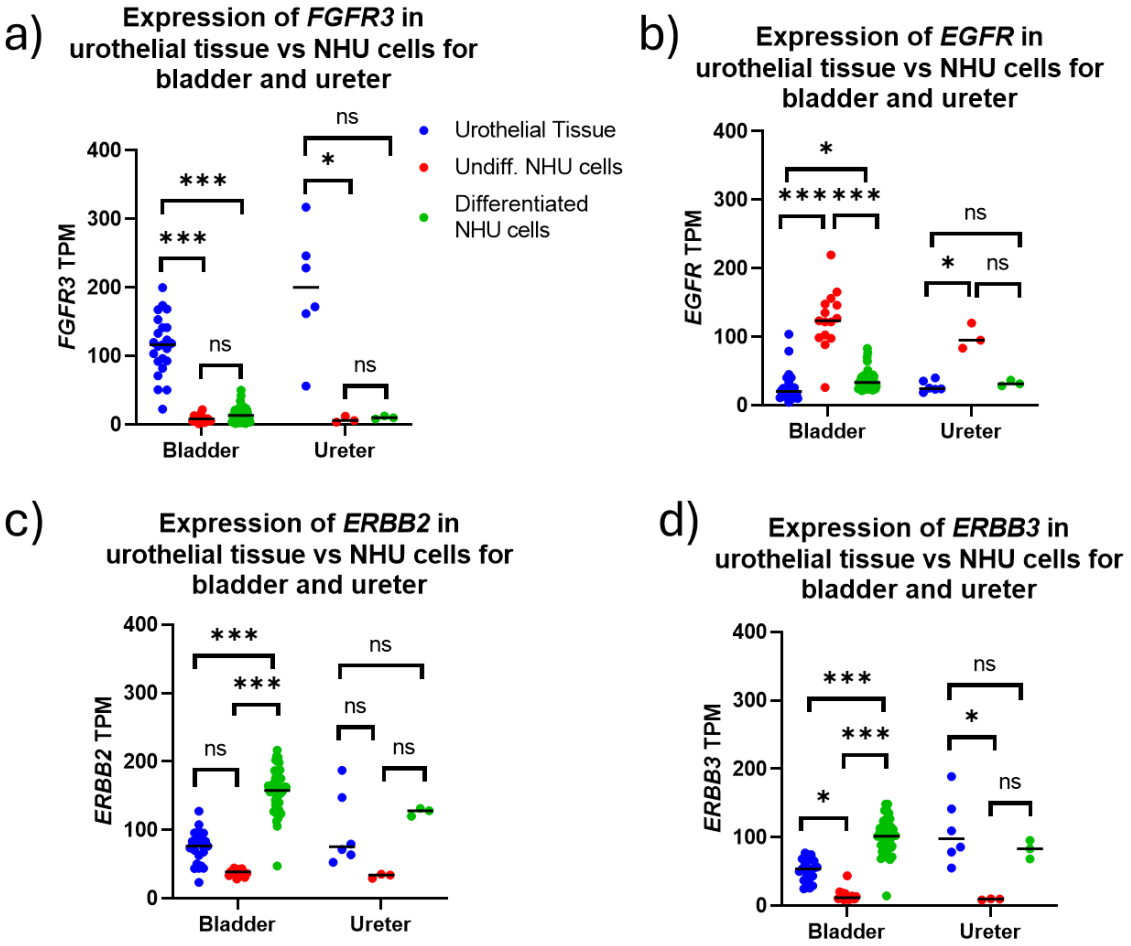

Figure 3.2 - Expression of *FGFR3* and *EGFR* family transcripts in urothelial tissue and NHU cells - (a) Comparison of *FGFR3* , (b) *EGFR*, (c) *ERBB2*, and (d) *ERBB3* expression in freshly isolated urothelium to NHU cells Black line shows the median expression value. Kruskal Wallis multiple comparisons test with Dunn's multiple comparisons as a post-hoc test was used to determine statistical significance. An F test was used to determine the variability of *FGFR3* expression. TPM; Transcripts per million. RNA-sequencing data was previously generated by Dr Simon Baker and Dr Andrew Mason.

3.3.2.2 FGFR3 protein expression in urothelial tissue

Following assessment of transcript, FGFR3 protein expression was assessed in five ureter tissue samples. FGFR3 protein expression showed a similarly high variability to *FGFR3* transcript expression, as FGFR3 protein was detected in three of five samples (Y2514, Y2639 and Y2642) and one positive sample (Y2642) showed much lower expression (Fig. 3.3). Tissue integrity of samples was confirmed by histology and by probing for urothelial tissue marker cytokeratin 13 (CK13) and superficial cell marker Zonula Occludens 3 (ZO-3; Fig. 3.3 and 3.4). Tissue samples showed small amounts of damage to the urothelium. Expression of superficial cell marker ZO-3 was only detected in two samples, suggesting that the superficial layer may have been lost. Thus, FGFR3 transcript and protein were detected in urothelial tissue.

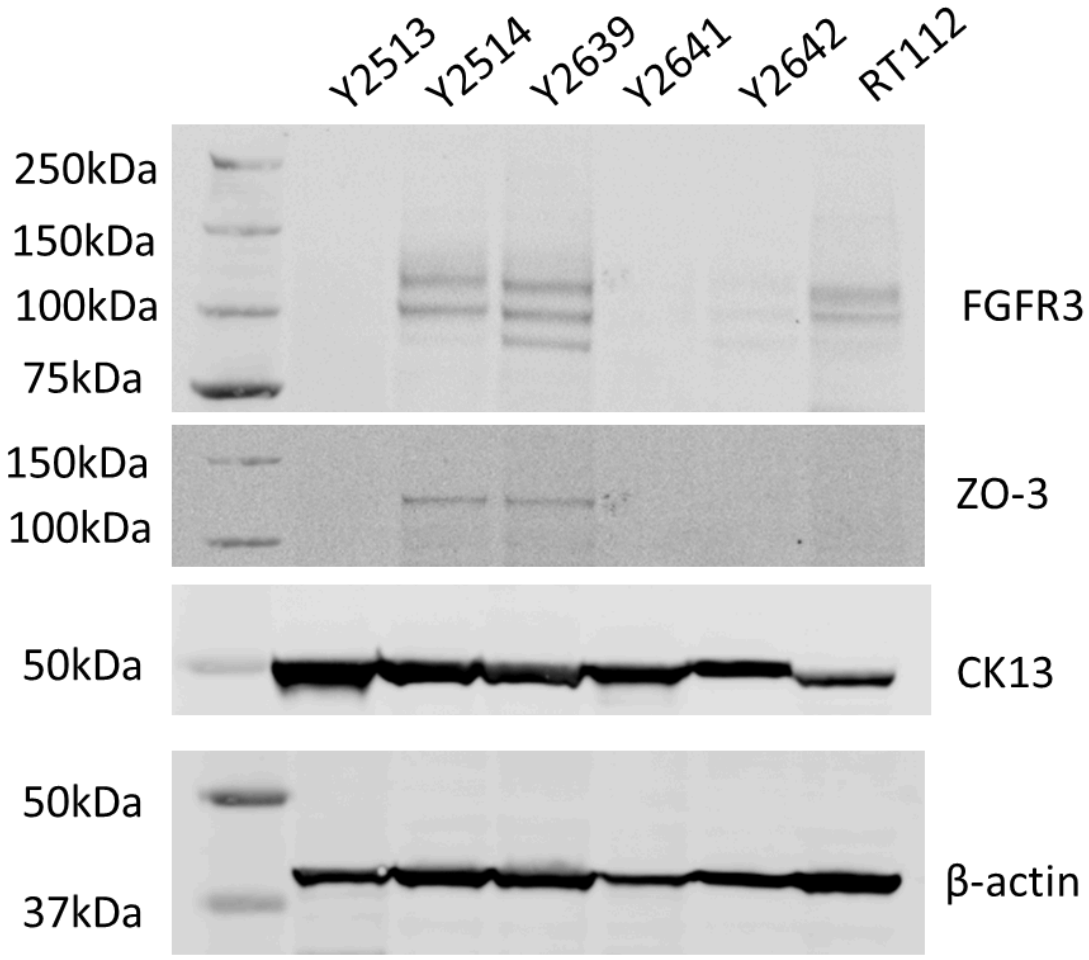

Figure 3.3 - FGFR3 protein was expressed in urothelial tissue - Western blot of urothelial tissue separated from stroma. Lysates were taken from freshly-isolated ureteric urothelium (n = 5). ZO-3 and CK13 were used as markers of urothelial tissue identity. 20 µg of protein was loaded for each sample. β-actin was used as a loading control to ensure equal protein between lanes. Lysate from the RT112 BLCA cell line was loaded as a

positive control for FGFR3 expression. Western blot shows 5 donors which were selected from a larger pool of 8 donors for running cleanly on a western blot. Full blot of all 8 donors is given in Appendix C.

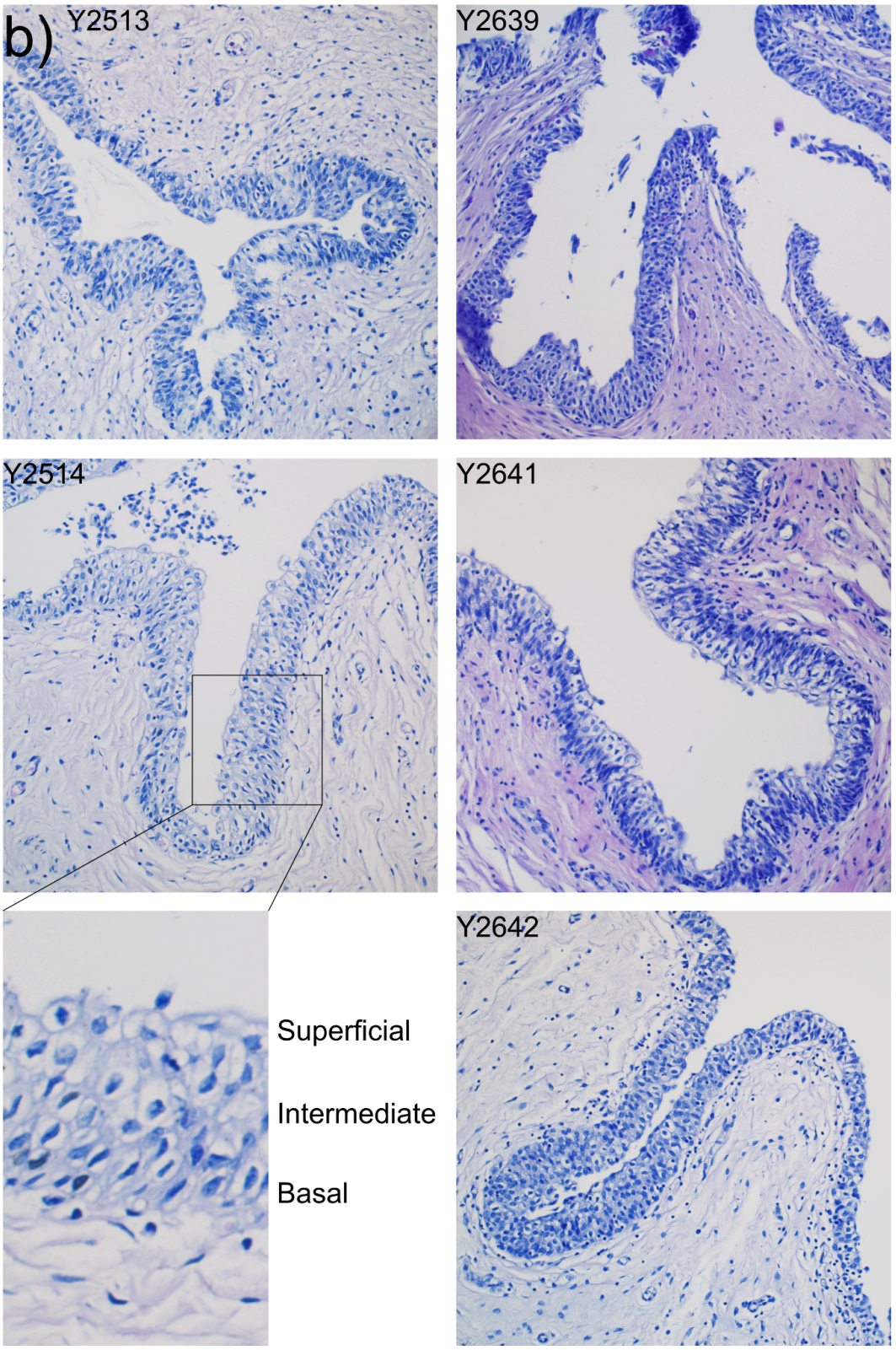

Figure 3.4 - Histology of urothelial tissue samples used for western blotting - images of hematoxylin and eosin stained sections showing integrity of ureter tissue samples. Scale bar (white line) represents 100 μm.

3.3.3 Investigation of factors which regulate expression of FGFR3 transcript and protein in NHU cells

3.3.3.1 Cell confluence produced a slight increase in FGFR3 protein expression in undifferentiated NHU cells

In order to assess whether NHU cell cycle state could affect FGFR3 protein expression, Three NHU cells (Y1237, Y1359, and Y1909) were grown to visual confluence, six days post-confluent, or were differentiated to induce mitotic quiescence. Given that EGFR and MAP kinase signalling has previously been implicated in repression of FGFR3 expression, EGFR and ERK phosphorylation was assessed for potential correlations to FGFR3 protein expression.

In confluent NHU cells, faint FGFR3 protein was detected in one cell line (Y1359)- at the same time, both EGFR and ERK were highly phosphorylated in all three cell lines (Figs. 3.5 and 3.6). In six days post-confluent NHU cells FGFR3 protein was detected in all three cell lines; at the same time, EGFR and ERK phosphorylation were both much lower (Figs. 3.5 and 3.6). FGFR3 protein was not detected in differentiated NHU cells, despite phosphorylation of EGFR and ERK that was comparable to post-confluent undifferentiated NHU cells (Fig. 3.5). Thus in undifferentiated but not differentiated NHU cells, FGFR3 protein expression appeared to be inversely related to ERK and EGFR phosphorylation.

FGFR3 protein expression was relatively low in undifferentiated NHU cells, but appeared to increase post-confluence where EGFR and ERK activity were reduced (Fig. 3.5). This in combination with previous observations that EGFR activity can repress expression of FGFR3 transcript and protein in BLCA cell lines led to the hypothesis that autocrine EGFR and ERK activity in NHU cells may have suppressed FGFR3 expression.

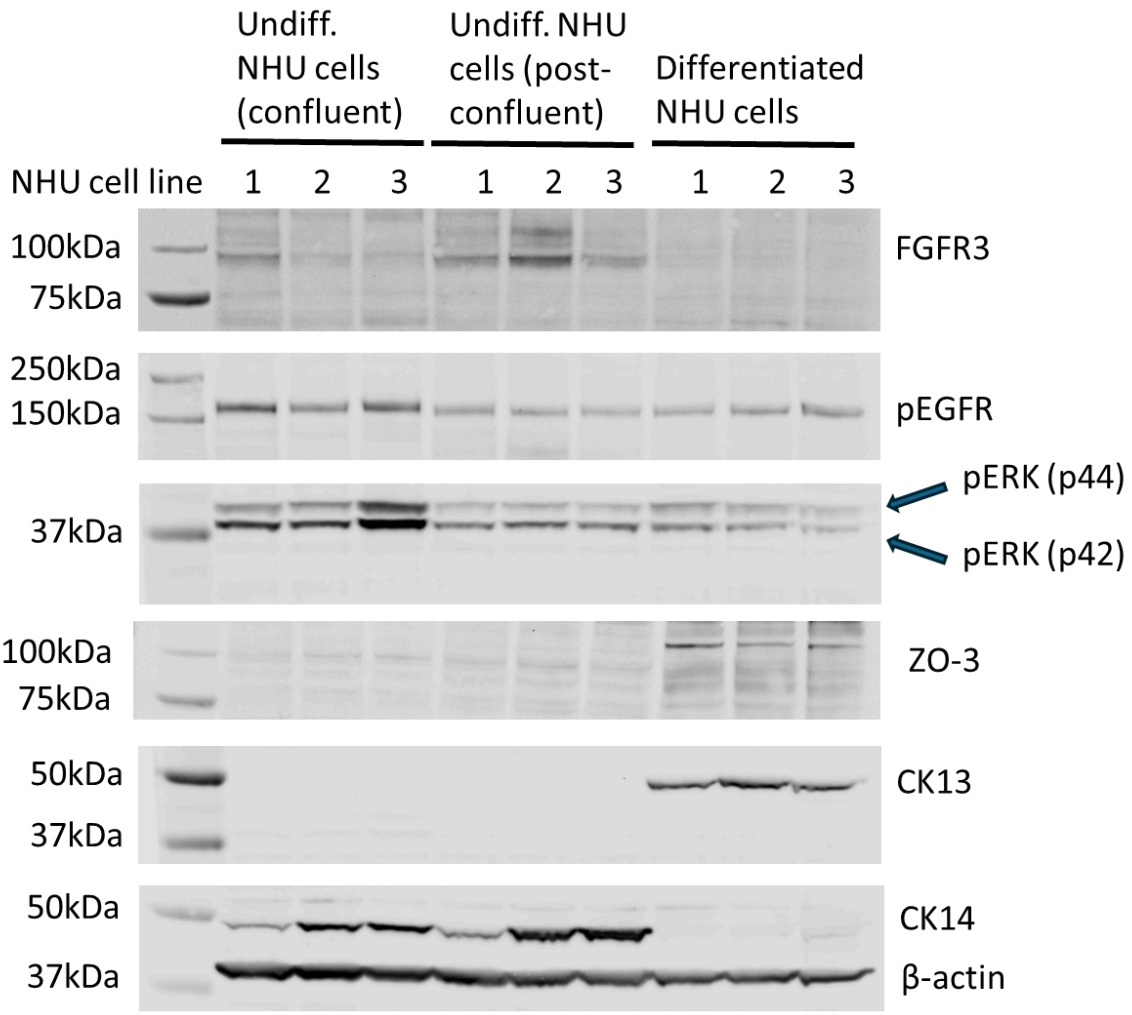

Figure 3.5 - Expression of FGFR3 protein in undifferentiated vs differentiated NHU cells - ZO-3 and CK13 were used as markers of urothelial differentiation, and CK14 was used as a squamous differentiation marker. 20 µg of protein was loaded for each sample. β-actin was used as a loading control to ensure equal protein between lanes. Independent experiments were performed on NHU cell lines Y1237 (1), Y1359 (2), and Y1909 (3) - all three are shown (n = 3). NHU cells were grown in Keratinocyte Serum-Free Medium supplemented with Bovine Pituitary Extract and Cholera Toxin.

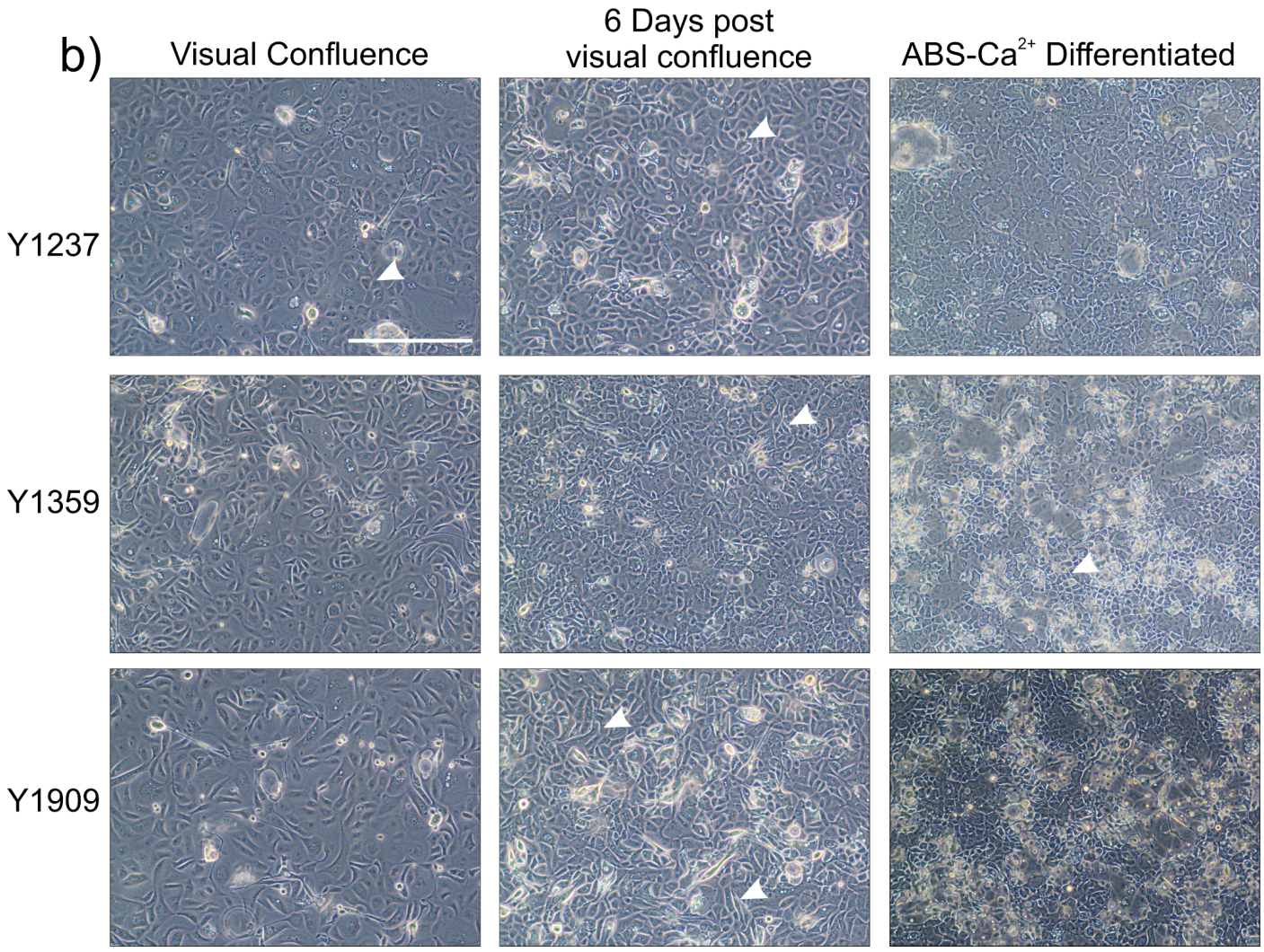

Figure 3.6 - Cell micrograph images of undifferentiated and differentiated NHU cells - Undifferentiated NHU cells are shown at various stages of confluence. Scale bar (white line) represents 200 µm. White arrowheads indicate cells which display bright borders.

3.3.3.2 EGFR inhibition resulted in expression of FGFR3 protein

To test the hypothesis that EGFR activity might repress expression of FGFR3 protein, NHU cells were EGFR-inhibited. Following inhibition of EGFR with the tyrosine kinase inhibitor PD153035 for 24 h, undifferentiated NHU cells displayed expression of FGFR3 protein which increased at 48 h and 72 h of treatment (Fig. 3.7). Similarly to the previous experiment, DMSO-treated control cultures showed faint FGFR3 protein expression when they reached visual confluence. EGFR phosphorylation varied but EGFR was clearly inhibited by PD153035, as seen by abolishment of ERK phosphorylation. Although FGFR3 protein did not appear to correlate with EGFR phosphorylation, there was a clear negative association between FGFR3 protein expression and ERK phosphorylation, particularly p44 ERK (Fig. 3.7). The relationship between FGFR3 protein expression and ERK phosphorylation was better fit by an inverse exponential than by linear regression (Fig. 3.8).

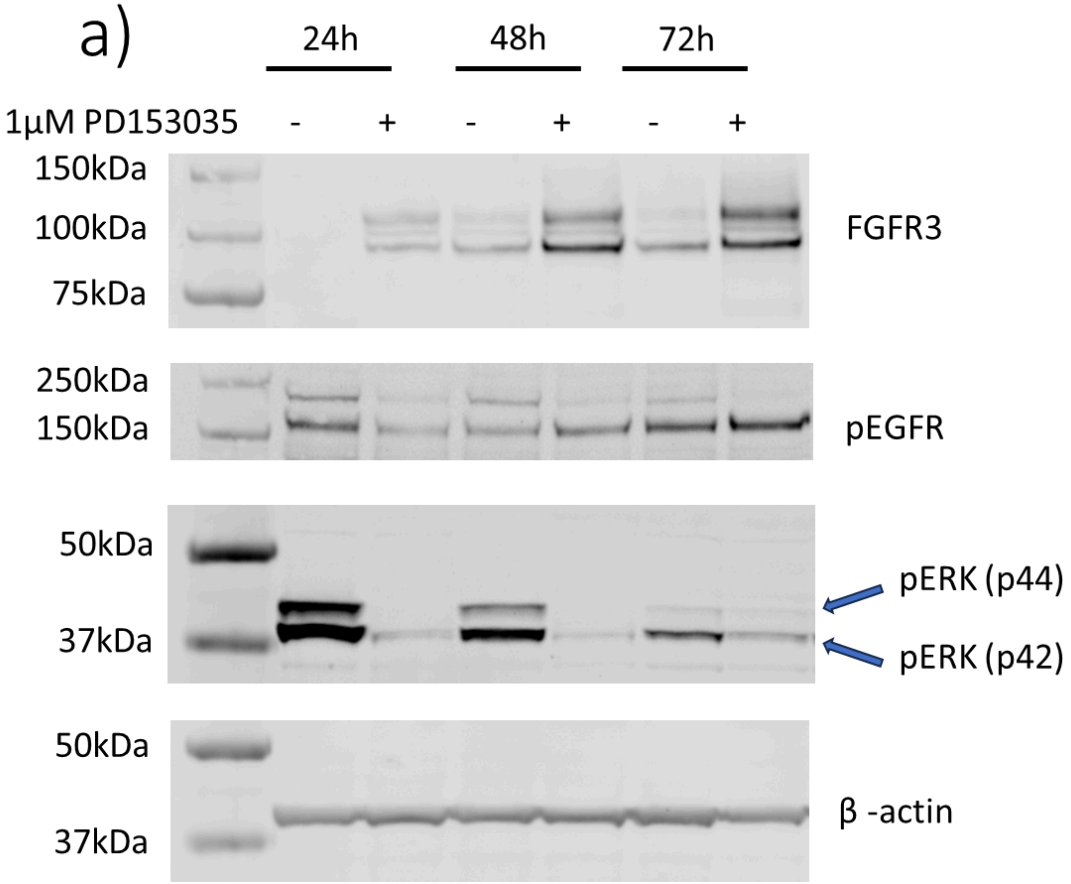

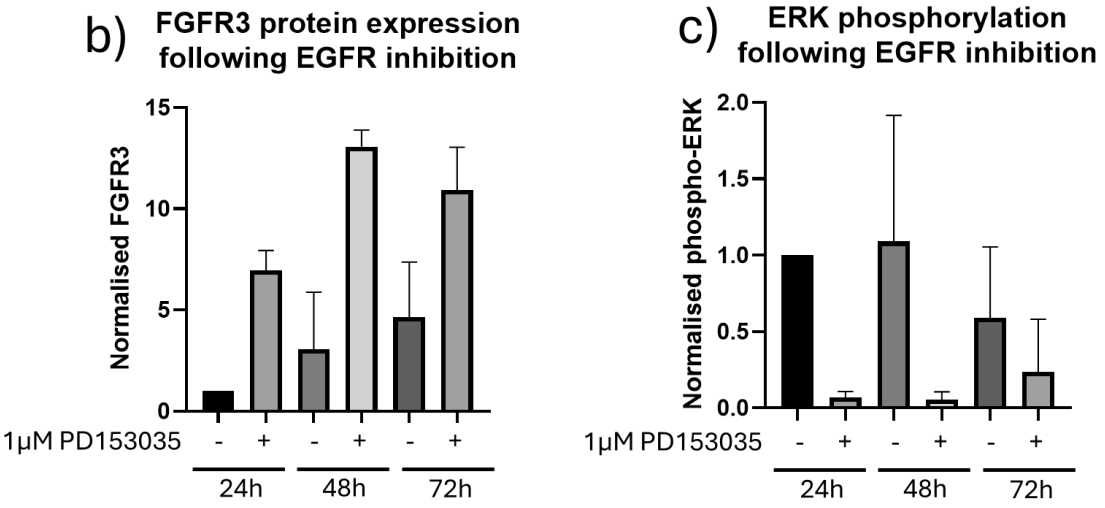

Figure 3.7 - FGFR3 protein expression in NHU cells was triggered by EGFR inhibition - (a) Western blot, (b) Densitometry of FGFR3 expression, (c) Densitometry of ERK phosphorylation. 20 μg of protein was loaded for each sample. β-actin was used as a loading control to ensure equal protein between lanes. EGFR inhibition was assessed by western blotting for EGFR and ERK phosphorylation. Error bars represent standard deviation. Independent experiments were performed in NHU cell lines Y3000, Y2777 and Y2717 (n = 3) - Y3000 is shown in (a) and data from all three lines compiled in (b) and (c).

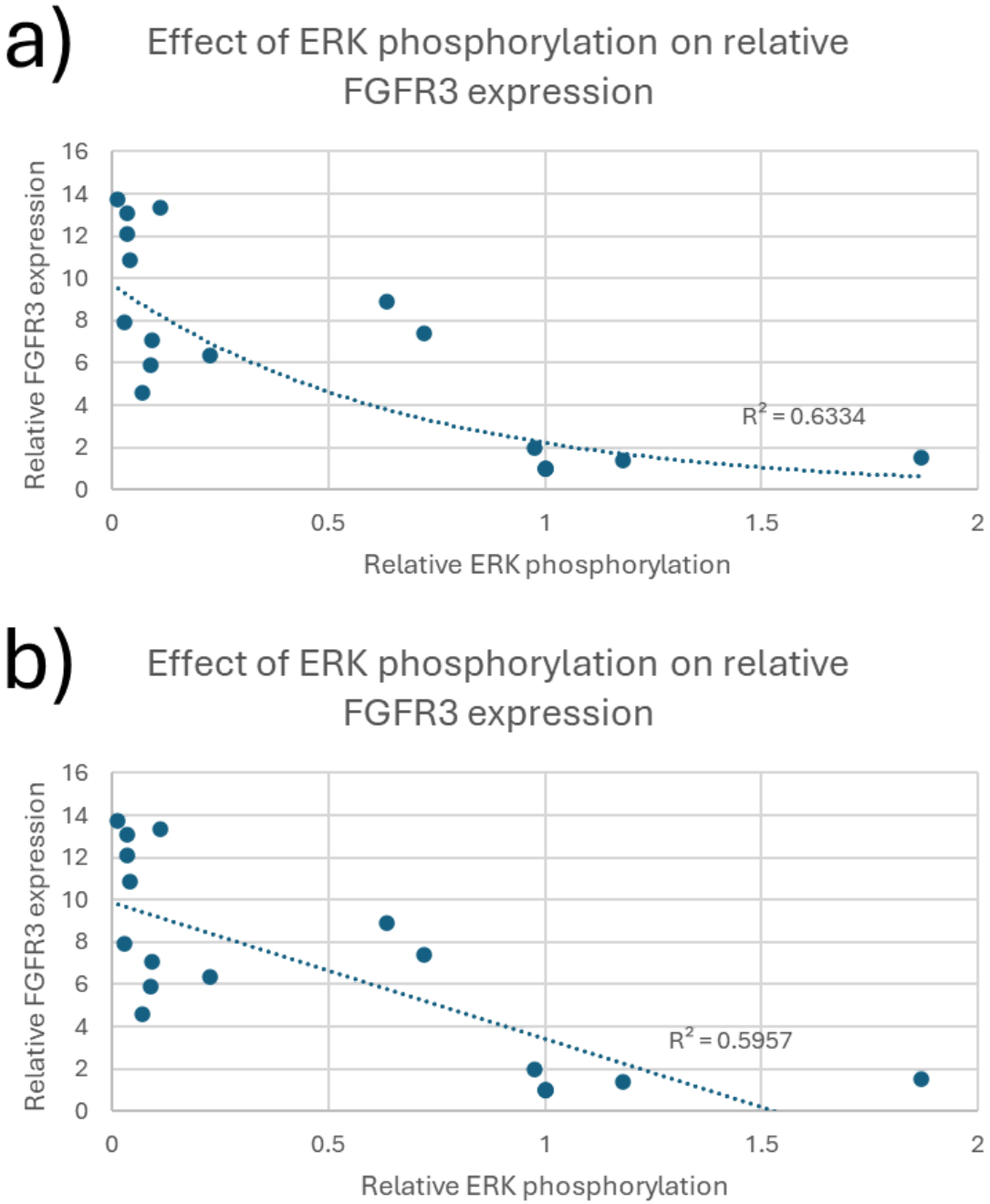

Figure 3.8 - FGFR3 protein expression in NHU cells was inversely correlated to ERK phosphorylation Correlation of FGFR3 protein expression against ERK phosphorylation fitted with both exponential (a) and linear (b) regression. Densitometry values for relative FGFR3 protein expression and relative ERK phosphorylation are plotted against each other. R squared represents the coefficient of determination in the regression models.

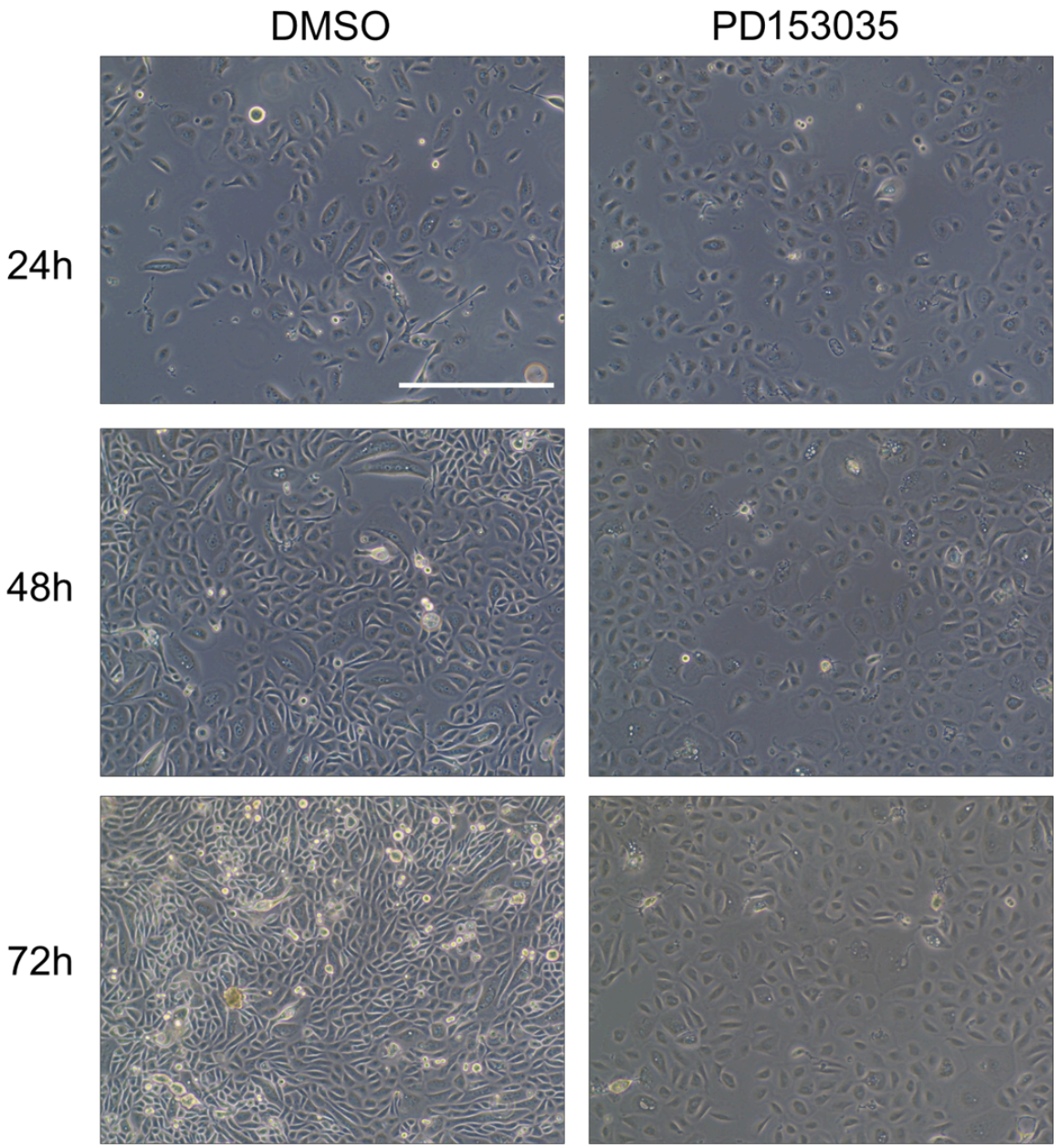

Figure 3.9 - Cell culture images of NHU cells with and without EGFR inhibition - Cell images are taken from Y3000. Scale bar is 200 μm. NHU cells were grown in Keratinocyte Serum-Free Medium supplemented with Bovine Pituitary Extract and Cholera Toxin.

To explore whether EGFR activity repressed FGFR3 expression at the transcript or protein level, EGFR inhibition experiments were repeated and *FGFR3* transcript examined. Semi-quantitative reverse-transcriptase PCR revealed the presence of *FGFR3* transcript in NHU cells not treated with EGFR inhibition, however EGFR inhibition did increase *FGFR3* expression (Fig. 3.10). At 24 h and 48 h, *FGFR3* expression was greater when EGFR was inhibited. However at 72 h, *FGFR3* expression appeared to be equal with and without EGFR inhibition. Hence, *FGFR3* transcript expression did not appear to be dependent upon EGFR activity at all time-points, unlike FGFR3 protein expression.

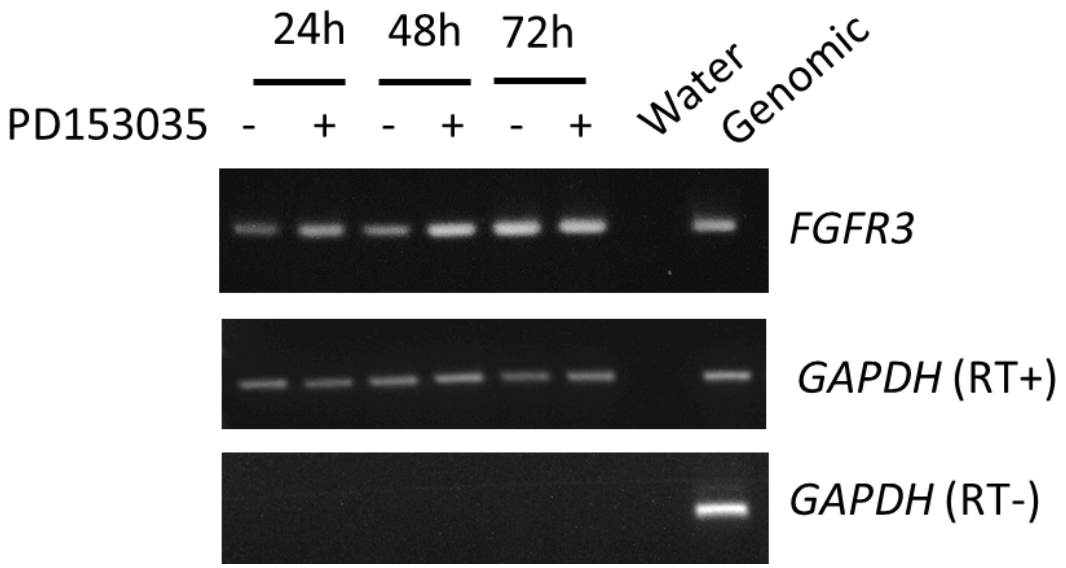

Figure 3.10 - Expression of *FGFR3* transcript in NHU cells with and without EGFR inhibition - *GAPDH* was used as a loading control (25 cycles). Experiment was performed in NHU cell line Y3000 (n = 1). 1 µg RNA from each sample was used for cDNA synthesis, after which cDNA was PCR amplified for 27 cycles. A genomic DNA control was used to confirm gene amplification by the primers used, a water negative control (no template) alongside controls in which reverse transcriptase was not added to the starting RNA (RT-) was used to confirm lack of genomic DNA contamination.

Finally, to verify that FGFR3 expression was truly due to EGFR inhibition and was not merely an effect of PD153035, NHU cells were EGFR-inhibited for 72 h with the additional EGFR tyrosine kinase inhibitor AG1478 and the EGFR-neutralising antibody cetuximab. Titration data for Cetuximab is presented in Appendix B. EGFR inhibition with PD153035 or AG1478 resulted in a greater than ten-fold increase in FGFR3 protein expression versus DMSO controls, while cetuximab increased FGFR3 protein expression by three-fold versus controls (Fig. 3.11).

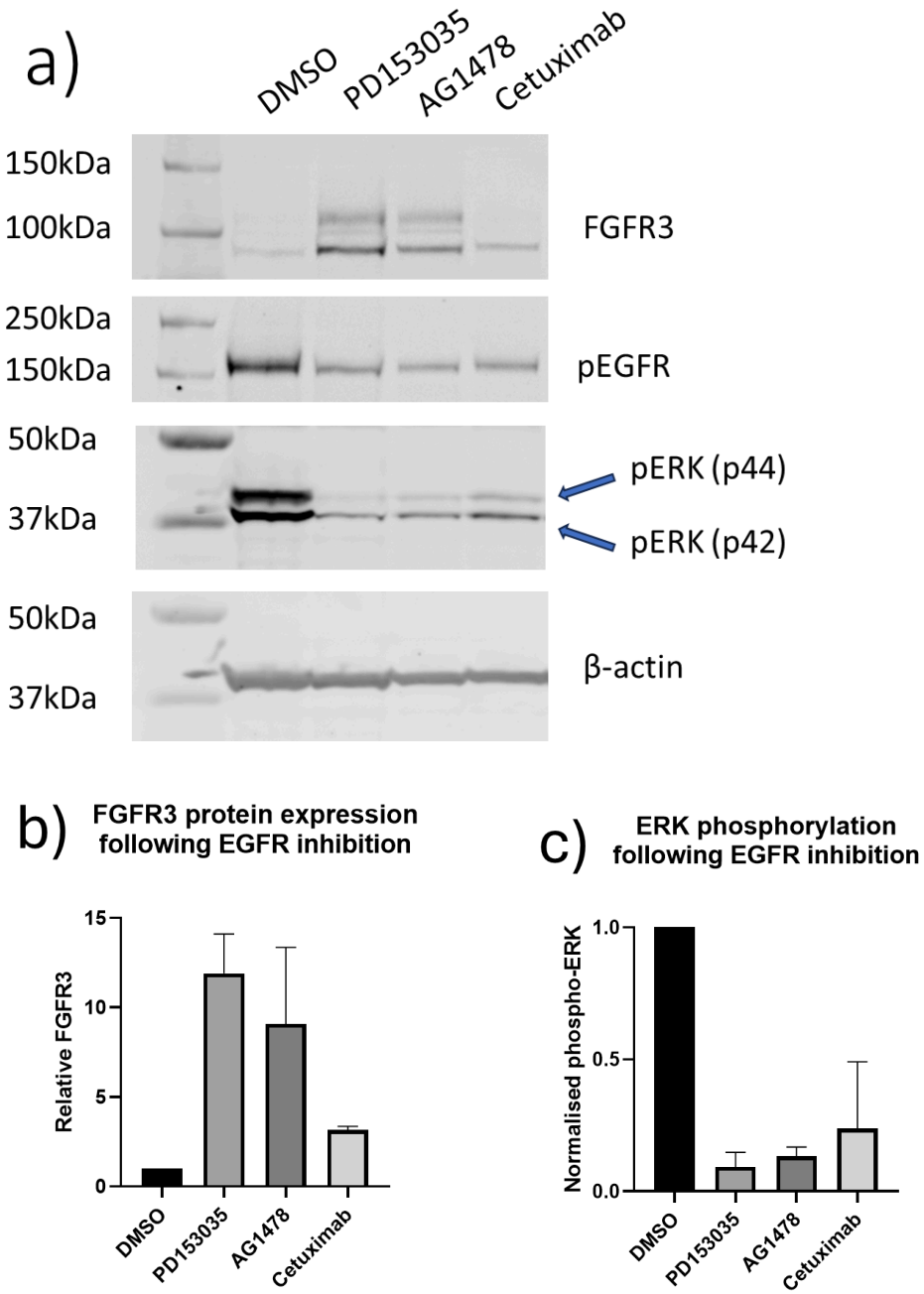

Figure 3.11 - Expression of FGFR3 protein in NHU cells following 72 h inhibition of EGFR using tyrosine kinase inhibitors PD153035 or AG1478 or EGFR-neutralising antibody cetuximab - (a) Western blot, (b) and (c) Densitometry of 3 NHU cell lines. 20 µg of protein was loaded for each sample. β-actin was used as a loading control to ensure equal protein between lanes. EGFR inhibition was assessed by western blotting for EGFR and ERK phosphorylation. Error bars represent standard deviation. Independent experiments were performed in NHU cell lines Y3000, Y3149 and Y1781 (n = 3) - Y1781 is shown in (a) and data from all three lines compiled in (b). NHU cells were grown in Keratinocyte Serum-Free Medium supplemented with Bovine Pituitary Extract and Cholera Toxin.

3.3.3.3 Inhibition of the EGFR downstream signalling cascade

Previous experiments showed that EGFR inhibition resulted in FGFR3 protein expression, and FGFR3 protein correlated inversely with ERK phosphorylation. From this it was hypothesised that the MAP kinase signalling pathway downstream of EGFR was responsible for repression of FGFR3 expression.

To test this hypothesis, NHU cells were treated for 72 h with the MEK inhibitor trametinib or the ERK inhibitor FR18204. Inhibition of either MEK or ERK resulted in FGFR3 protein expression comparable to FGFR3 expression following EGFR inhibition with PD153035 (Fig. 3.12).

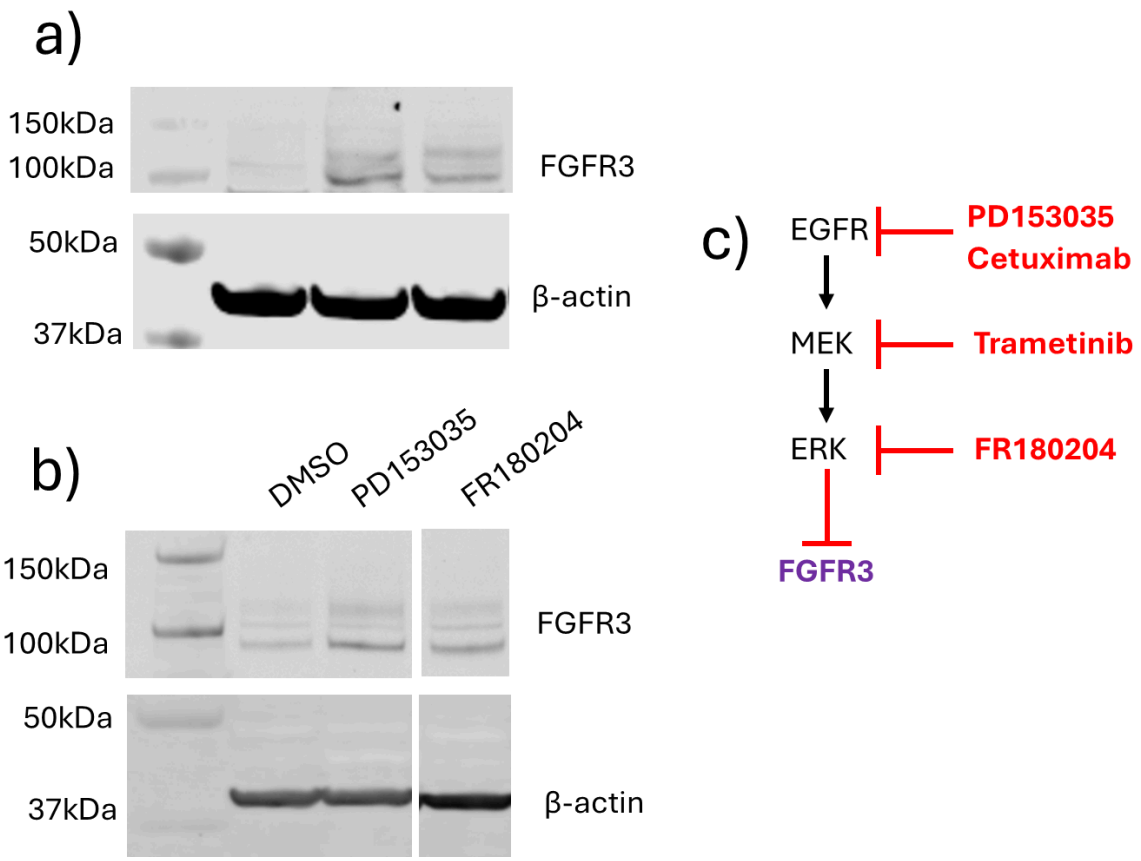

Figure 3.12 - Expression of FGFR3 protein in NHU cells following 72 h inhibition of EGFR downstream signalling pathway components - (a) Expression of FGFR3 protein in undifferentiated NHU cells following MEK inhibition with Trametinib and (b) ERK inhibition with FR180204, (c) diagram of the signalling components downstream of EGFR, and the small molecule inhibitors/antibodies directed against them in this study. RT112 BLCA cell line is a positive control for FGFR3 expression. 20 µg of protein was loaded for each sample. β-actin was used as a loading control to ensure equal protein between lanes. For (a), independent experiments were performed in NHU cell lines Y3000 and

Y3110 (n = 2) by Dr Rosalind Duke. For (b), independent experiments were performed in NHU cell lines Y3161, Y3058 and Y3059 (n = 3) - NHU cells were grown in Keratinocyte Serum-Free Medium supplemented with Bovine Pituitary Extract and Cholera Toxin.

3.3.2.4 Presence of cholera toxin in cell culture media had no significant effect on FGFR3 protein expression

To test if the relatively low expression of FGFR3 in NHU cells could be due to cholera toxin-mediated repression, NHU cells were grown for 72 h in KSFM with or without cholera toxin. Since EGFR inhibition was shown to robustly induce FGFR3 protein expression, EGFR inhibition was used as a positive control for FGFR3 expression. There was no significant change in the expression of FGFR3 protein with or without cholera toxin - FGFR3 protein was not expressed unless NHU cells were EGFR-inhibited (Fig. 3.13).

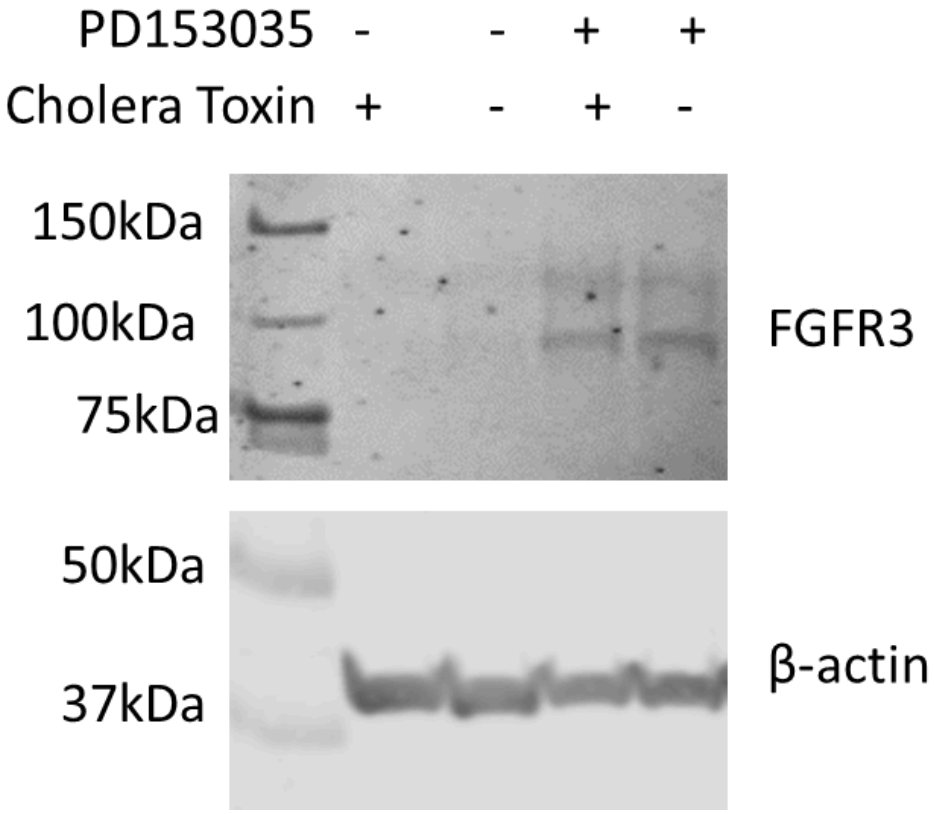

Figure 3.13 - FGFR3 Expression in NHU cells following EGFR inhibition with and without the presence of cholera toxin in the growth medium - 20 µg of protein was loaded for each sample. β-actin was used as a loading control to ensure equal protein between lanes. Experiment was performed in NHU cell line Y1096 (n = 1). NHU cells were grown in Keratinocyte Serum-Free Medium supplemented with Bovine Pituitary Extract.

3.3.3.5 FGFR3 protein was not expressed in differentiated NHU cells

Following the observation that inhibition of EGFR/ERK activity was sufficient to trigger FGFR3 protein expression in undifferentiated NHU cells, the same question was also tested in differentiated NHU cells. Given that ERBB2 and ERBB3 - which are capable of inducing ERK activity - are expressed in urothelial tissue (Fig. 3.2) [Chow et al., 1997, Uhlén M et al., 2015 and https://proteinatlas.org/], it was expected that they would be expressed in differentiated NHU cells. Expression of *ERBB2* and *ERBB3* in differentiated NHU was verified by examining RNA-sequencing data.

Differentiated NHU cells had significantly greater expression of *ERBB2* and *ERBB3* than undifferentiated NHU cells ($p<0.05$, Fig. 3.14). Thus since EGFR inhibition alone was unlikely to be sufficient to abolish ERK activity, differentiated NHU cells were treated with a combination of the EGFR inhibitor PD153035 as well as the EGFR family inhibitor lapatinib.

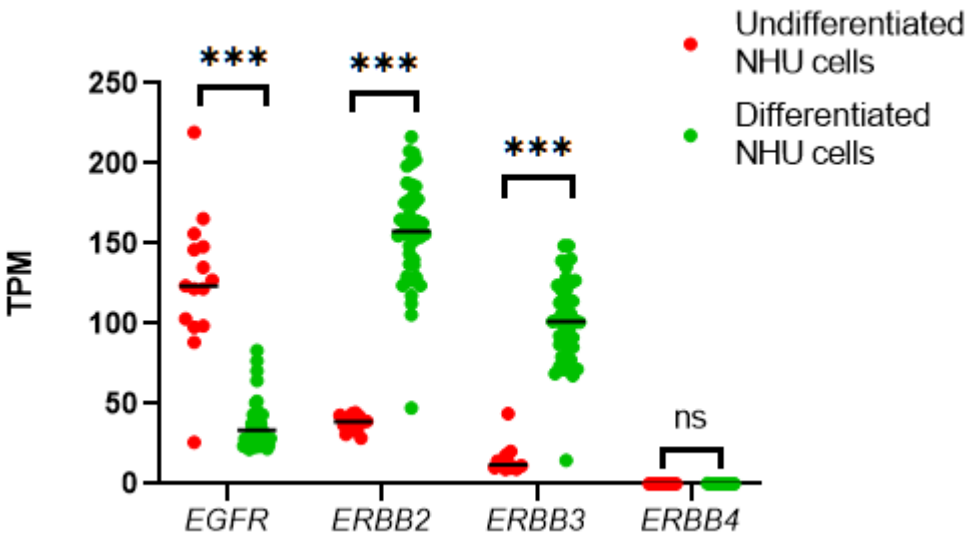

Figure 3.14 - Expression of *EGFR* family members in NHU cells following urothelial differentiation - Black line shows the median expression value. Wilcoxon matched-pairs signed rank test was used to determine statistical significance. TPM; Transcripts per million

Analysis of RNA sequencing data showed some expression of *FGFR3* in differentiated NHU cells (Fig. 3.2), however expression of FGFR3 protein could not be detected (Fig. 3.5). To test whether inhibition of ERK could also trigger FGFR3 protein expression in

differentiated urothelium, NHU cells were treated with a combination of PD153035 and lapatinib. Titration data for lapatinib are presented in Appendix B.

Treatment of differentiated NHU cells with PD153035 for 72 h did not affect phosphorylation of ERBB2 and only slightly reduced phosphorylation of ERK. Treatment with lapatinib was sufficient to abrogate ERBB2 phosphorylation but also only slightly reduced ERK phosphorylation. However, combination of PD153035 and lapatinib inhibited phosphorylation of ERBB2 and ERK.

Even when ERK phosphorylation was reduced to a similar degree that could produce FGFR3 protein expression in undifferentiated NHU cells, FGFR3 protein expression was not detected (Fig. 3.15). The use of 144 h treatments was generally more effective at inhibiting ERK phosphorylation. Unlike at 72 h, 144 h of PD153035 treatment strongly reduced ERK phosphorylation, and lapatinib alone was able to completely inhibit ERK phosphorylation for both p44 and p42 ERK. However, even when ERK phosphorylation was completely inhibited, FGFR3 protein was not detected (Fig. 3.15). Thus, inhibition of ERK activity was not sufficient to trigger FGFR3 protein expression in differentiated NHU cells.

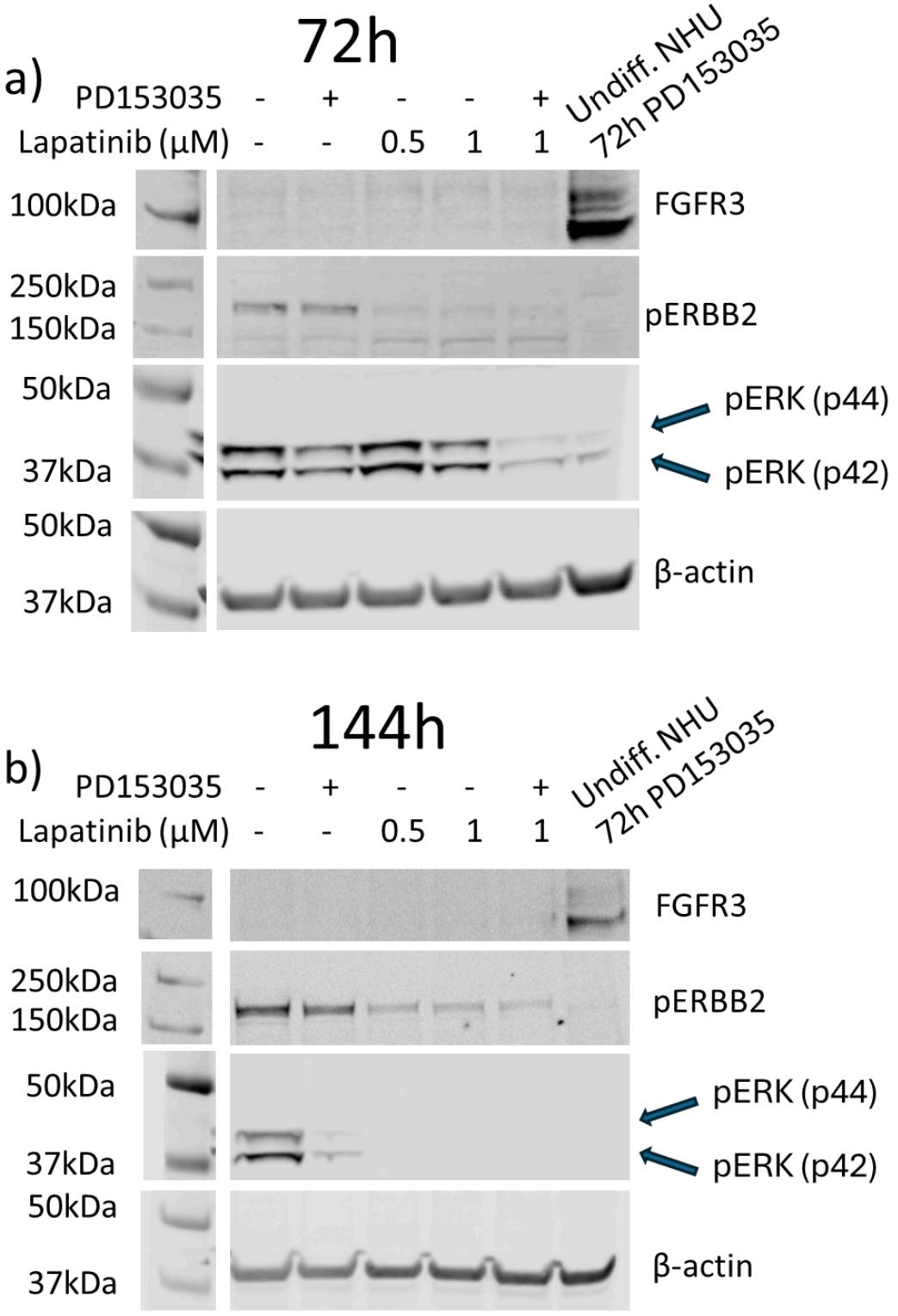

Figure 3.15 - FGFR3 protein was not detected in differentiated NHU cells with or without inhibition of EGFR family member tyrosine kinase activity - NHU cells were differentiated and then treated for (a) 72 h or (b) 144 h with PD153035 and/or lapatinib to inhibit EGFR and ERBB2/ERBB3 respectively. Lysate from undifferentiated NHU cells treated for 72 h with PD153035 was used as a positive control for FGFR3 expression. 20

μg of protein was loaded for each sample. β-actin was used as a loading control to ensure equal protein between lanes. EGFR family inhibition was assessed by western blotting for ERBB2 and ERK phosphorylation. For (a), experiment was performed in NHU cell line Y2885 (n = 1) and for (b) independent experiments were performed in Y2885, Y2843 and Y3000 (n = 3) - Y2885 is shown. NHU cells were grown in Keratinocyte Serum-Free Medium supplemented with Bovine Pituitary Extract and Cholera Toxin as well as 2 mM calcium and 5% adult bovine serum.

3.3.3.6 Activity of Peroxisome Proliferator-Activated Receptor Gamma (PPARγ) and Retinoic Acid Receptor Gamma (RARγ) inhibited expression of FGFR3 protein

Given the surprising result that urothelial differentiation did not lead to FGFR3 protein expression, further work was performed to determine why this might be. PPARγ has previously shown to be crucial for *in* vitro differentiation of NHU cells (see section 1.5.2) [Varley et al., 2004a, Varley et al., 2004b], and also in urothelial tissue [Liu et al., 2019]. Recent work has suggested that PPARγ activity is dependent upon activation of RARγ [Slip, 2023]. Thus, given the important roles of PPARg and RARγ activity in regulating gene expression during urothelial differentiation, it was queried as to whether their activity could impact expression of FGFR3.

PPARg or RARγ were activated or inhibited for 72 h, and the effect on FGFR3 protein expression was assessed via western blotting (Fig. 3.16). Inhibition of PPARγ with the synthetic antagonist T0070907 resulted in a small but significant increase in FGFR3 protein expression compared to the DMSO vehicle control. Inhibition of RARγ with the synthetic antagonist LY2955303 resulted in a highly variable increase in FGFR3 protein expression which did not reach significance. Activation of either PPARγ with the synthetic agonist Troglitazone or RARγ with the synthetic agonist BMS961 resulted in a significant decrease in FGFR3 protein expression. This is consistent with the hypothesis that PPARγ and/or RARγ activity inhibit expression of FGFR3 protein.

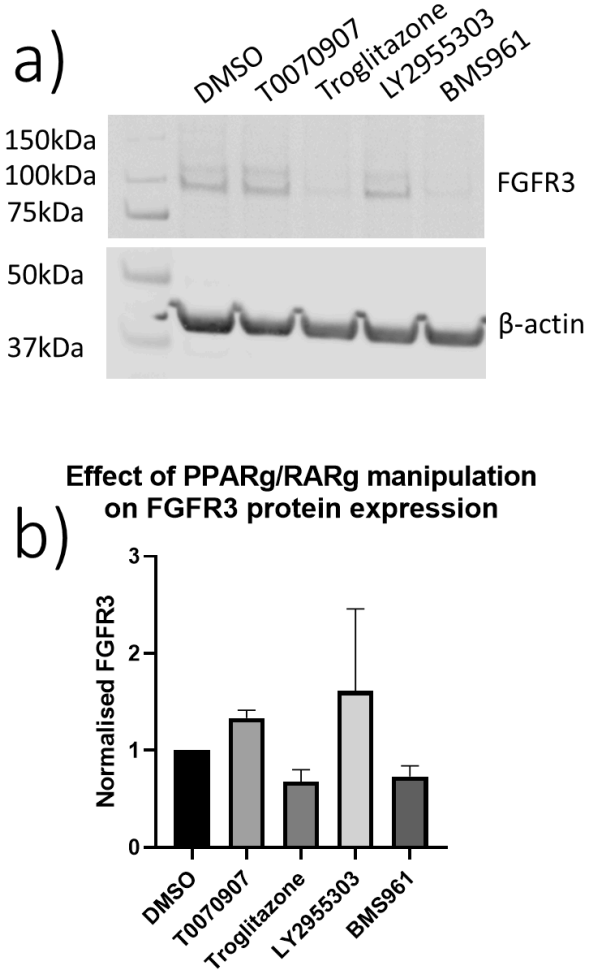

Figure 3.16 - Expression of FGFR3 protein was significantly reduced by activation of PPARg or RARγ compared to a DMSO vehicle control - (a) Western blot, (b) Densitometry of FGFR3 expression. 20 µg of protein was loaded for each sample. β-actin was used as a loading control to ensure equal protein between lanes. Error bars represent standard deviation. Independent experiments were performed in NHU cell lines Y3000, Y3103 and Y3149 (n = 3) - Y3000 is shown in (a) and data from all three lines compiled in (b).

3.3.4 Characterisation of FGFR3 transcript and protein expressed in urothelial tissue and NHU cells

3.3.4.1 Multiple different *FGFR3* transcript isoforms were expressed in urothelial tissue

A final step to characterise *FGFR3* expression in urothelium was to analyse the individual *FGFR3* transcript variants expressed in urothelial tissue, as well as the glycosylation status of FGFR3 protein expressed in NHU cells following EGFR-inhibition.

The only previous study which has examined *FGFR3* transcripts in urothelial tissue and NHU cells only assessed expression of *FGFR3* IIIb, IIIc, and Δ8-10 [Tomlinson et al., 2005]. Furthermore, given the highly-variable expression of *FGFR3* in ureter reported here, the fact that *FGFR3* transcript variants were previously examined in only three samples could mean that report showed an unrepresentative sample of *FGFR3* expression. Hence, RNA-sequencing of 22 samples was used here to assess expression of all ten identified *FGFR3* transcripts. The 22 samples used were: Y2439, Y2306, Y2307, Y2319, Y2320, Y2336, Y2337, Y2338, Y2339, Y2371, Y2383, Y2538, Y2589, Y2590, Y2595, Y2610, Y2340, Y2361, Y2366, Y2440, Y2631, Y2632. Details on these samples (including patient age and sex) is listed in Chapter 2.

Analysis of RNA-sequencing from ureter tissue revealed that *FGFR3* IIIb, IIIc and Δ8-10 in total comprised less than 50% of the total *FGFR3* transcripts expressed in urothelial tissue, with approximately 50% of total *FGFR3* transcript consisting of transcripts which did not code for protein (Fig. 3.17a). Despite this, *FGFR3* IIIb was still the transcript with the greatest median expression. When only FGFR3 IIIb, IIIc and Δ8-10 were considered *FGFR3* IIIb was the majority isoform, making up 66.31% of *FGFR3* transcript (Fig. 3.17c). This was compared to 10.93% for *FGFR3* Δ8-10 and 22.76% for *FGFR3* IIIc.

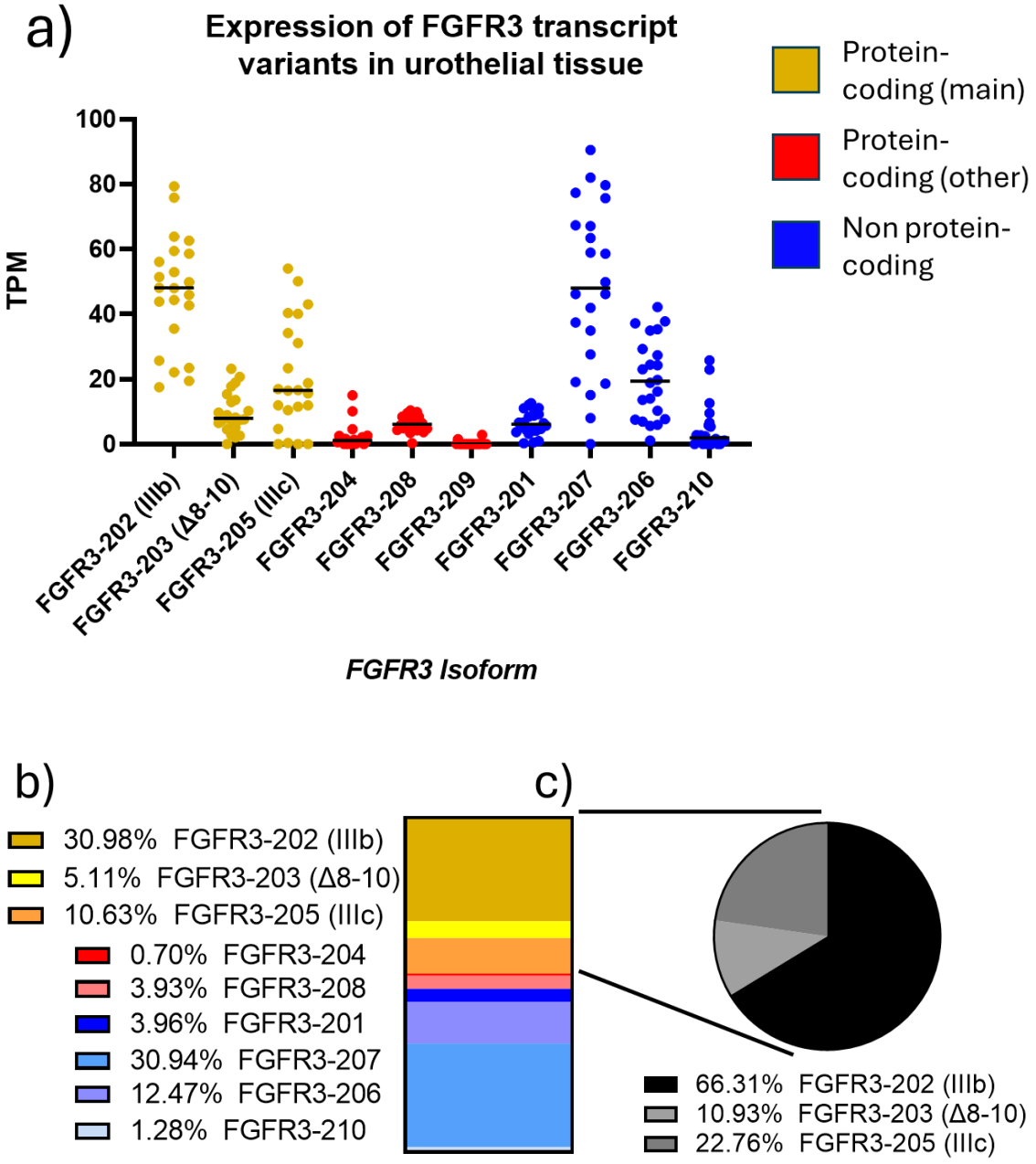

Figure 3.17 - Breakdown of FGFR3 transcript expressed in bladder urothelial tissue into individual isoforms - (a) Expression of each FGFR3 transcript variant in freshly-isolated urothelium, (b) proportion of total *FGFR3* transcript that each isoform makes up, (c) proportion of previously-reported protein coding isoforms that each of FGFR3 IIIb FGFR3 IIIc and FGFR3 Δ8-10 each make up. Isoforms in (a) and (b) are colour-coding according to their protein-coding status. Black line represents the median. TPM; Transcripts per million. Isoform-level transcript data was provided by Richard Gawne (Jack Birch Unit, University of York).

3.3.4.2 FGFR3 protein expressed in NHU cells following EGFR inhibition was glycosylated

FGFR3 protein expressed in EGFR-inhibited undifferentiated NHU cells was treated with PNGase F to remove N-linked glycosylation. Untreated FGFR3 protein ran as three bands by western blot, at approximately 110kDa, 100 kDa and 90 kDa (Fig. 3.18). FGFR3 which was de-glycosylated also ran as three bands, at approximately 90 kDa, 85 kDa and 80 kDa.

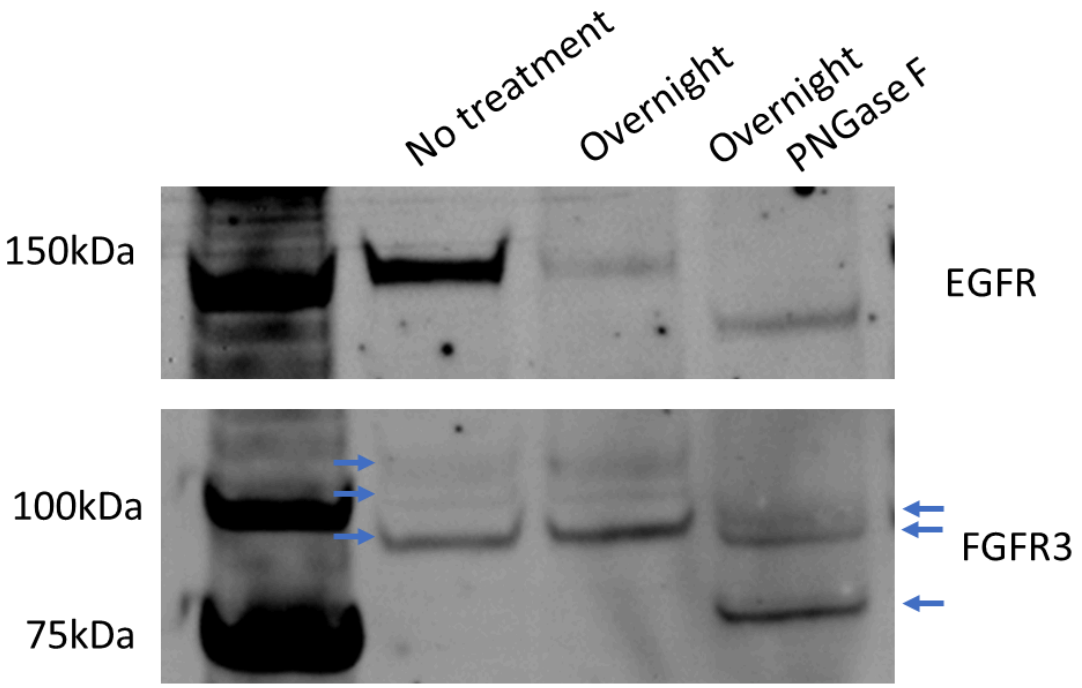

Figure 3.18 - Deglycosylation of FGFR3 protein expressed in NHU cells following EGFR inhibition - Lysate was taken from NHU cell line Y3000 (n = 1) treated for 72 h with EGFR inhibitor PD153035. "No treatment" samples were loaded without processing, "overnight" samples were first treated overnight with PBS (a control for overnight protein degradation), "Overnight PNGase F" samples were treated overnight with PNGase F to remove N-linked glycosylation.

3.4 Summary

- *FGFR3* transcript was expressed in bladder and ureter tissue. *FGFR3* expression was significantly greater and was more variable in ureter than bladder tissue. *FGFR3* expression was significantly greater in urothelial tissue compared to NHU cells for both bladder and ureter. Additionally, differentiation of NHU cells did not lead to detectable FGFR3 expression..
- In undifferentiated NHU cells, inhibition of EGFR with tyrosine kinase inhibitors or an EGFR-neutralising antibody resulted in an increased expression of FGFR3 transcript and protein. *FGFR3* transcript was expressed in the absence of protein expression induced by EGFR inhibition.
- EGFR/ERBB2/ERBB3 inhibition did not result in FGFR3 protein expression in differentiated NHU cells, even when ERK phosphorylation was completely abolished.
- Factors which were found to regulate FGFR3 protein expression included EGFR and downstream MEK and ERK activity, and FGFR3 protein expression was inversely correlated with ERK phosphorylation. Rather than promoting FGFR3 protein expression as was expected, urothelial differentiation reduced FGFR3 expression. The presence of cholera toxin in cell culture media did not affect FGFR3 expression.
- Ten *FGFR3* transcript isoforms were expressed in urothelial tissue, with the most expressed isoform being *FGFR3* IIIb. Almost half of total *FGFR3* transcripts did not code for protein.
- FGFR3 protein expressed in NHU cells following EGFR inhibition ran in three bands by western blot, at 110 kDa, 100 kDa, and 90 kDa. When FGFR3 protein was deglycosylated, three protein bands were observed which ran at 90 kDa, 85 kDa and 80 kDa.

3.5 Discussion

3.5.1 What factors regulate expression of *FGFR3* in urothelial tissue and *in vitro* urothelial cell models?

3.5.1.1 Repression of FGFR3 transcript and protein expression by EGFR and ERK activity

In proliferative NHU cell cultures FGFR3 protein expression was observed to inversely correlate with ERK phosphorylation. Inhibition of EGFR with tyrosine kinase inhibitors or a neutralising antibody abrogated ERK phosphorylation and resulted in FGFR3 protein expression. This confirms previous results in cancer cell lines [Ware et al., 2010, Herrera-Abreu et al., 2013] and demonstrates potential for FGFR3 to be repressed by EGFR activity in normal urothelium.

Downstream analysis using inhibition of MEK or ERK also resulted in FGFR3 protein expression, although comparatively less than when EGFR itself was inhibited. Herrera-Abreau et al saw similar results in RT112M and 97-1 BLCA cell lines, concluding that Src, Akt-PI3K and MAP kinase signalling all downstream of EGFR co-operated to repress FGFR3 expression [Herrera-Abreu et al., 2013].

3.5.1.2 The potential mechanism of EGFR-ERK repression of FGFR3

The exact mechanism by which EGFR/ERK signalling repressed FGFR3 transcript/protein expression is not clear. Undifferentiated NHU cells showed expression of *FGFR3* mRNA even without EGFR inhibition, suggesting that EGFR activity blocks FGFR3 translation rather than transcription. However, *FGFR3* transcript was still increased by EGFR inhibition and Herrera-Abreau et al observed that both FGFR3 transcript and protein were repressed by EGFR activity, which would favour the idea of transcriptional rather than translational regulation.

Another option for how EGFR/ERK represses FGFR3 may be through driving expression of microRNA-99a, which has been shown to negatively regulate FGFR3 transcript and protein expression in NHU cells and a variety of cancers [Catto et al., 2009, Chakrabarti et al., 2013, Jiang et al., 2014, Lin et al., 2019]. Tsai et al demonstrated that microRNA-99a was upregulated by ERK activity in T24 and 5637 BLCA cell lines [Tsai et al., 2020]. Thus, ERK activity downstream of EGFR could repress *FGFR3* expression by driving expression of microRNA-99a.

However, this theory is contradicted by the work of Herrera-Abreau. Firstly, when EGFR was hyperactivated with TGFα in RT112M cells the FGFR3-TACC3 fusion protein expressed in RT112M was suppressed. Since FGFR3-TACC3 does not contain the 3' UTR targeted by microRNA-99a [Parker et al., 2013], microRNA-99a is unlikely to be responsible for the repression of FGFR3 observed. Secondly, when the authors treated 97-7 BLCA cells with inhibitors to microRNA-99a, there was no change to FGFR3 expression [Herrera-Abreu et al., 2013].

Thus, there is contradictory evidence as to whether EGFR repression of FGFR3 is mediated by microRNA.

3.5.1.3 EGFR/ERK-mediated repression of FGFR3 does not entirely explain FGFR3 expression patterns in urothelial tissue and NHU cells

It must also be noted that the repression of FGFR3 transcript and protein expression by EGFR/ERK activity does not appear to be universally true. Here, EGFR was shown to repress FGFR3 expression in undifferentiated NHU cells, which have previously been shown to have high EGFR/ERK activity driven by autocrine signalling [Swiatkowski et al., 2003, Varley et al., 2005]. When this autocrine EGFR signalling was inhibited, FGFR3 was then expressed.

Differentiated NHU cells were found to express *ERBB2* and *ERBB3* as well as *EGFR*, similar to urothelial tissue [Chow et al., 1997, Uhlén M et al., 2015]. These cells showed ERK phosphorylation, likely downstream of these EGFR family members [reviewed by Jacobi et al., 2017]. However, when EGFR family members were inhibited and ERK phosphorylation entirely abolished, FGFR3 protein expression was not detected. This suggests that other factors may exist in differentiated NHU cells which suppress FGFR3 expression, and thus that inhibition of EGFR/ERK is not sufficient for FGFR3 expression in this context. Stimulation of the nuclear receptors PPARγ and RARγ (which are highly active during urothelial differentiation) reduced the expression of FGFR3 protein. Thus, it is possible that lack of FGFR3 protein expression in differentiated NHU cells (even when ERK activity was abolished) may be due to increased activity of PPARγ and RARγ in differentiated NHU cells.
Similarly, FGFR3 transcript and protein were expressed in urothelial tissue. While EGFR activity has not been previously investigated in urothelial tissue (for example by studying EGFR/ERK phosphorylation or downstream gene expression), studies have shown that

the EGFR ligands EGF, TGFα and HB-EGF are expressed in urothelium [Baskin et al., 1996, Mellon et al., 1996, Freeman et al., 1997, Varley et al., 2005]. Thus, it is likely that there is at least some level of EGFR activity in urothelial tissue, which exists alongside and does not completely repress FGFR3 expression. This agrees with the observation in undifferentiated NHU cells that FGFR3 protein and ERK phosphorylation were inversely related, suggesting that FGFR3 is not mutually exclusive with EGFR/ERK activity. Thus under this model, FGFR3 expression in urothelial tissue is possible due to the relatively lower EGFR/ERK activity compared to undifferentiated NHU cells. Alternatively, there could be some factor(s) present in urothelial tissue (for example, due to paracrine signalling from the underlying stroma) which are absent in NHU cell models. This would explain why FGFR3 transcript and protein were expressed in urothelial tissue but not in NHU cells (without EGFR inhibition).

3.5.2 Comparison of *FGFR3* and *EGFR* family expression in urothelial tissue

Although a role for FGFR3 in human urothelium is completely unknown, expression of FGFR3 in human urothelial tissue has been reported [Tomlinson et al., 2007, Shi et al., 2023]. As part of the characterisation of *FGFR3* expression in urothelial tissue, expression of *FGFR3* was compared with the better-understood EGFR family members *EGFR*, *ERBB2* and *ERBB3*. EGFR and ERBB2 in particular have been implicated in driving proliferation and migration during urothelial wound repair [Bindels et al., 2002, Daher et al., 2003]. Expression of *FGFR3* was significantly greater than *EGFR*, *ERBB2* and *ERBB3* in both ureter and bladder tissue.

3.5.3 Expression of *FGFR3* in bladder vs ureter tissue

While expression of *FGFR3* in ureter and bladder tissue have been previously reported separately, the two have never been compared. Bladder and ureter are morphologically similar tissues which both contain urothelium, but the two have different embryological origins [reviewed by Liaw et al., 2018] and their cancers (BLCA and UTUC respectively) tend to have different molecular properties [reviewed by Tomiyama et al., 2022].
Of key relevance to this study is the relative abundance of *FGFR3* mutations and overexpression in UTUC compared to BLCA [Bagrodia et al., 2016, Moss et al., 2017, Audinet et al., 2019, Robinson et al., 2019, Fuji et al., 2021, Shigeta et al., 2022]. While the underlying reasons for differences in BLCA and UTUC are not fully understood, here an *FGFR3*-based difference in bladder and ureter urothelium was observed. *FGFR3*

expression was significantly greater and significantly more varied in ureter tissue compared to bladder tissue.

It is conceivable that a higher “resting” level of *FGFR3* expression could result in a more central role for FGFR3 in UTUC compared to BLCA. Once an FGFR3 mutation occurs, that mutation would presumably have greater effect if the expression of FGFR3 is higher. For example, Shi et al previously demonstrated that when S249C mutant-active *FGFR3* was expressed in the urothelium of mice, mice developed bladder tumours more readily the greater the expression of mutant *FGFR3* [Shi et al., 2023].

3.5.4 Analysis of *FGFR3* transcript isoforms expressed in urothelial tissue

Isoform-level analysis of RNA-sequencing data confirmed expression of a number of different *FGFR3* isoforms. Tomlinson et al., 2005 analysed the expression of *FGFR3* IIIb, IIIc and ∆8-10 in urothelial tissue using RT-PCR and reported that *FGFR3* IIIb made up more than 95% of *FGFR3* expressed in urothelial tissue. Results here indicated that while *FGFR3* IIIb was still the majority isoform expressed, it makes up much less of the total *FGFR3* population than previously estimated (30.98% of total *FGFR3* transcript). Specifically, when only *FGFR3* IIIb, IIIc, and ∆8-10 were considered, *FGFR3* made up only 66.31% of the total *FGFR3* transcript. This is in comparison to Tomlinson et al., 2005, which reported that *FGFR3* IIIb made up for more than 95% of the total *FGFR3* transcript in urothelial tissue. This is likely due to several factors. Since Tomlinson et al probed *FGFR3* expression using RT-PCR, they were only able to assess expression of the three *FGFR3* isoforms they chose to examine, rather than the additional *FGFR3* isoforms seen here. However, even when only *FGFR3* IIIb, IIIc, and ∆8-10 isoforms are considered the proportion of *FGFR3* IIIc, and ∆8-10 in urothelial tissue was still shown to be higher than previously estimated. These differences may be due to the larger number of samples examined here (n = 22) - a large degree of variability was seen in total *FGFR3* transcript and also in individual isoforms, and so the smaller sample size used by Tomlinson (n = 6) means they could have obtained an unrepresentative sample of *FGFR3* isoform distribution.

It should be noted that about half of all *FGFR3* expression was composed of transcripts considered not to code for protein, according to the Ensembl database. Of these non-coding transcripts *FGFR3-207* made up the majority at 30.94% of total transcript. To

date, no literature has reported on the significance of FGFR3 transcripts other than *FGFR3* IIIb, IIIc and ∆8-10 in BLCA, the normal urothelium, or at all.

3.5.5 Glycosylation of FGFR3 in NHU cells

FGFR3 protein was expressed in NHU cells following treatment with EGFR tyrosine kinase inhibitors or an EGFR-neutralising antibody. This FGFR3 protein appeared as three bands - at approximately 110 kDa, 100 kDa, and 90 kDa. This pattern of expression agrees with previous studies [Keegan et al., 1991, Bonaventure et al., 2007, Gibbs and Legeai-Mallet, 2007, St-Germain et al., 2014, Hashimoto et al., 2024]. However, previous work suggests that these three bands represent mature glycosylated, intermediate glycosylated and non-glycosylated FGFR3 respectively (see Chapter 1). As such, when treated with PNGase-F to remove N-terminal glycosylation, these three species of FGFR3 would be expected to collapse into one band representing the non-glycosylated form [Bonaventure et al., 2007, Gibbs and Legeai-Mallet, 2007, St-Germain et al., 2014, Hashimoto et al., 2024].

However when FGFR3 protein expressed following EGFR inhibition was treated with PNGase-F, three bands remained. This suggests that the initial three bands of FGFR3 protein observed do not represent differentially glycosylated forms of the same protein, but rather different isoforms of FGFR3. The three bands present after deglycosylation were present as a pair of bands of very similar molecular weight at approximately 95 kDa and a third band at approximately 80 kDa. These results are very similar to those of Tomlinson et al., 2005, who also assessed expression of FGFR3 protein pre- and post-treatment with PNGase F. Tomlinson et al also performed their assessment in NHU cells, although they specifically used NHU cells grown to confluence, rather than the EGFR inhibition treatments used here. Tomlinson et al also used two antibodies to determine which protein band(s) represented the ∆8-10 isoform of FGFR3. Thus, the results obtained here can be informed by those of Tomlinson et al. The authors observed that when FGFR3 was immunoprecipitated using an antibody which could not bind FGFR3 ∆8-10, the band at ~90k Da was not present, while the bands at 100 and 100 kDa were.

All together, the previous literature would suggest that the protein bands expressed in NHU cells represent both the mature (110 kDa) and intermediate (100 kDa) glycosylated forms of FGFR3 IIIb, as well as a glycosylated form of FGFR3 ∆8-10 (90 kDa). Upon addition of PNGase F to remove glycosylation, the two glycosylated forms of FGFR3 IIIb collapsed into a collection of bands around 90 kDa, representing the non-glycosylated

form of FGFR3 IIIb. The reason for this collection of bands could be due to an incomplete deglycosylation reaction, leading to some species of FGFR3 IIIb which retained part of their glycosyl moieties. The band originally present at 90 kDa, representing glycosylated FGFR3 ∆8-10, shifted to 80 kDa, now representing non-glycosylated FGFR3 ∆8-10.

3.5.6 Does FGFR3 have a role in urothelial tissue?

Very few studies have examined the potential function of FGFR3 in urothelium. FGFR3 knockout mice did not have any urinary tract defects [Colvin et al., 1996], ruling out the role of FGFR3 in urothelial development (although it is possible that the lack of FGFR3 could have been compensated for by other FGFRs). The only other evidence is from individuals with congenital abnormalities leading to loss of FGFR3 expression or function. Studies reporting on these diseases tend to use case studies of individuals rather than cohorts, which limits their broader application. However, individuals with loss of *FGFR3* have not been reported to have any urinary tract defects in infancy or later in life [Rohmann et al., 2006, Toydemir et al., 2006, Makrythanasis et al., 2014]. Thus, despite the expression of *FGFR3* being similar to another growth factor receptor with known urothelial functions, all evidence to date suggests that FGFR3 has no role in the urothelium. It is, however, possible that FGFR3 does have a role which has not yet been discovered.

3.5.7 Potential limitations of this work

There are several potential limitations associated with the work performed in this chapter. Firstly, a relatively small number of ureter tissue samples were used for the assessment of FGFR3 transcript, and also for assessing protein expression of FGFR3. Given that the data that was used showed that FGFR3 transcript expression was highly variable (especially in ureter tissue), this makes it difficult to apply these findings more widely. Ideally, a larger number of ureter samples would have been used. In addition, while both bladder and ureter tissue were used to assess expression of FGFR3 transcript, for FGFR3 protein only ureter tissue was used and expression in bladder tissue was not characterised.

Secondly, there were several drawbacks to the approach used to assess expression of FGFR3 transcript in NHU cells. Reverse transcriptase PCR, rather than quantitative reverse transcriptase PCR was used, meaning that it is not possible to make a quantitative comparison regarding FGFR3 transcript expression with different timepoints of EGFR inhibition. Additionally, only one biological replicate was used.

Finally, when attempting to dissect the effects of EGFR downstream signalling on FGFR3 protein expression, inhibition of MEK and ERK was tested. However, this inhibition of MEK and ERK was assumed and was not additionally validated. It would have been preferable to also show that inhibition of MEK and ERK was successful - for inhibition of MEK, downstream ERK phosphorylation could have been assessed, and for ERK, expression of downstream target genes could have been assessed.

4. Activation and localisation of FGFR3 protein in NHU cells

4.1 Aims and Objectives

In the previous results chapter, EGFR inhibition was established as a reliable method to trigger expression of FGFR3 protein in undifferentiated NHU cells. This FGFR3 was glycosylated, suggesting that it is appropriately trafficked through the Golgi apparatus and endoplasmic reticulum.
In this chapter, the goal was to assess the functionality of FGFR3 protein expressed following EGFR inhibition of NHU cells. This was achieved through several objectives:

- Select and titrate an appropriate ligand for the activation of FGFR3 expressed in undifferentiated NHU cells following inhibition of EGFR
- Assess the activation of FGFR3 by monitoring downstream signalling events including phosphorylation of FRS2 and ERK over time when EGFR is inhibited
- Assess the localisation of FGFR3 within NHU cells and determine whether FGFR3 localisation is altered upon activation by addition of ligand
- Compare the localisation of FGFR3 within NHU cells to FGFR3 in urothelial tissues

4.2 Experimental Design

4.2.1 Use of Fibroblast Growth Factor 9 (FGF9) to activate FGFR3

In the previous chapter, treatment with the EGFR-inhibitor PD153035 for 72 h was shown to reliably trigger the expression of FGFR3 protein. This strategy was employed here to induce FGFR3 protein expression by treating cells for 72 h with the EGFR inhibitor PD153035 prior to the start of the experiment. In any experiments where PD153035 was used, cells were grown in KSFM media which did not include recombinant EGF.
To investigate if ligand activation of expressed FGFR3 was capable of triggering a downstream signalling cascade,exogenous recombinant Fibroblast Growth Factor 9 (FGF9) was used. Tomlinson et al., 2005 previously reported that *FGFR1* and *FGFR2* are expressed in NHU cells in addition to *FGFR3*. Several measures were taken to prevent activation of other FGFRs from confounding these experiments. Expression of FGFR transcript was examined in NHU cells treated with or without PD153035 for 72 h to inhibit EGFR. This transcript data was provided by Raphael Slip and Dr Simon Baker (Jack Birch Unit, University of York) and was generated outside this thesis. Additionally, FGF9 was

chosen to activate FGFR3 as it has been shown to be more specific for FGFR3 versus other FGFRs [Hecht et al., 1995]. Specifically, FGF9 was shown to be approximately 3 times more specific for FGFR3 (K_d = 2.38 nM) than FGFR2 (K_d = 0.78 nM) and was seen to not bind FGFR1 [Hecht et al., 1995].

FGF9 was titrated to find the lowest concentration which gave the maximum FGFR3 activation, as measured by phosphorylation of FRS2 (see below). FGF9 was initially titrated at 30 minutes post-addition, as FRS2 phosphorylation and FGFR3 activation had been consistently demonstrated at this time point in previous studies [Monsonego-Ornan et al., 2000, Monsonego-Ornan et al., 2002, Degnin et al., 2011]. Where cells were treated with FGF9 a vehicle control was used consisting of Dulbecco's phosphate-buffered saline with 0.1% bovine serum albumin, diluted in KSFM to a matching concentration as for FGF9.

In addition, there have been reports that Bovine Pituitary Extract (BPE), a key component of KSFMc contains FGFs [Gambarini and Armelin, 1982, Kent and Bomser, 2003]. Controls were included to test the ability of BPE alone to activate FGFR3.

4.2.2 Localisation of FGFR3 protein in NHU cells with and without activation

In the previous chapter, FGFR3 protein expression in NHU cells was assessed by western blotting. However, since western blotting takes an average of protein expression across the whole cell population, it was unclear how variable FGFR3 expression was across the whole cell population. To determine the proportion of cells which responded to EGFR inhibition by expressing FGFR3 protein, EGFR inhibition experiments were repeated, but instead of harvesting cell lysate for protein, FGFR3 protein expression was examined by indirect immunofluorescence microscopy using antibodies directed against both the N- and C-termini of FGFR3. Primary antibodies were titrated to ensure localisation was specific using RT112 BLCA cell lines, which are known to express FGFR3 protein and acted as a positive control for FGFR3 protein expression [Williams et al., 2013]. Secondary-only controls were included in each experiment to assess background fluorescence from secondary antibodies. Antibodies directed against the N- and C-terminus of FGFR3 were also verified by western blotting.

The mean cell intensity of FGFR3 protein expression was determined by analysing immunofluorescence images using the program ImageJ [Schneider et al., 2012]. This was

used to compare FGFR3 protein expression across a population between treatment conditions.

Immunofluorescence microscopy was also used to determine the localisation of FGFR3 in NHU cells with and without FGFR3 activation. To more precisely understand the localisation of FGFR3 and to determine how FGFR3 was trafficked post-activation, NHU cells were simultaneously labelled with antibodies against the C-terminus of FGFR3 and the lysosomal marker lysosome associated protein 1 (LAMP1) [reviewed by Eskelinen, 2006] or the endoplasmic reticulum marker calnexin [reviewed by Kozlov and Gehring, 2020], and images were overlaid. The location of cell nuclei was visualised using the fluorescent DNA intercalating stain, Hoechst 33258.

Colocalisation of FGFR3 and either calnexin or LAMP1 was quantified using the ImageJ plugin “JACoP” [Bolte and Cordelières, 2006, http://imagej.net/plugins/jacop]. This plugin was used to calculate the Pearson’s R for the correlation of FGFR3 with either positional marker, as well as the Manders’ coefficients (M1 and M2). M1 and M2 provide an estimate of the proportion of FGFR3 which overlapped with Calnexin/LAMP1 (and vice-versa) and is unaffected by the relative intensities of the fluorescence measured [Manders et al., 1992].

4.2.3 Localisation of FGFR3 protein in Urothelial tissues

FGFR3 protein in urothelial tissue was labelled using antibodies directed against both the N- and C-terminus of FGFR3. Antibodies were titrated using positive and negative control tissues known to express (tonsil) and not express (adrenal gland) FGFR3 protein, respectively. Information on expression of FGFR3 protein in various tissues was obtained from Protein Atlas database [Chow et al., 1997, Uhlén M et al., 2015 and https://proteinatlas.org/]. Antibodies directed against the N- and C-terminus of FGFR3 were also verified by western blotting (Chapter 1).

4.3 Results

4.3.1 Expression of *FGFR3* but not other FGFRs increased significantly in NHU cells in response to EGFR inhibition

Before attempting to activate FGFR3 in NHU cells, the change in expression of all FGFRs in response to 72 h of EGFR inhibition with PD153035 was examined. This RNA sequencing data was provided by Raphael Slip and Dr Simon Baker (Jack Birch Unit, University of York) and was generated outside this thesis .*FGFR3* was the only FGFR to be significantly more expressed following EGFR inhibition (FC = 4.91, p<0.001). *FGFR1* and *FGFR2* median expression were both less than 14 TPM regardless of treatment condition (Fig. 4.1). Thus, any FGFR-downstream signalling was most likely to be due to activation of FGFR3 rather than other FGFRs.

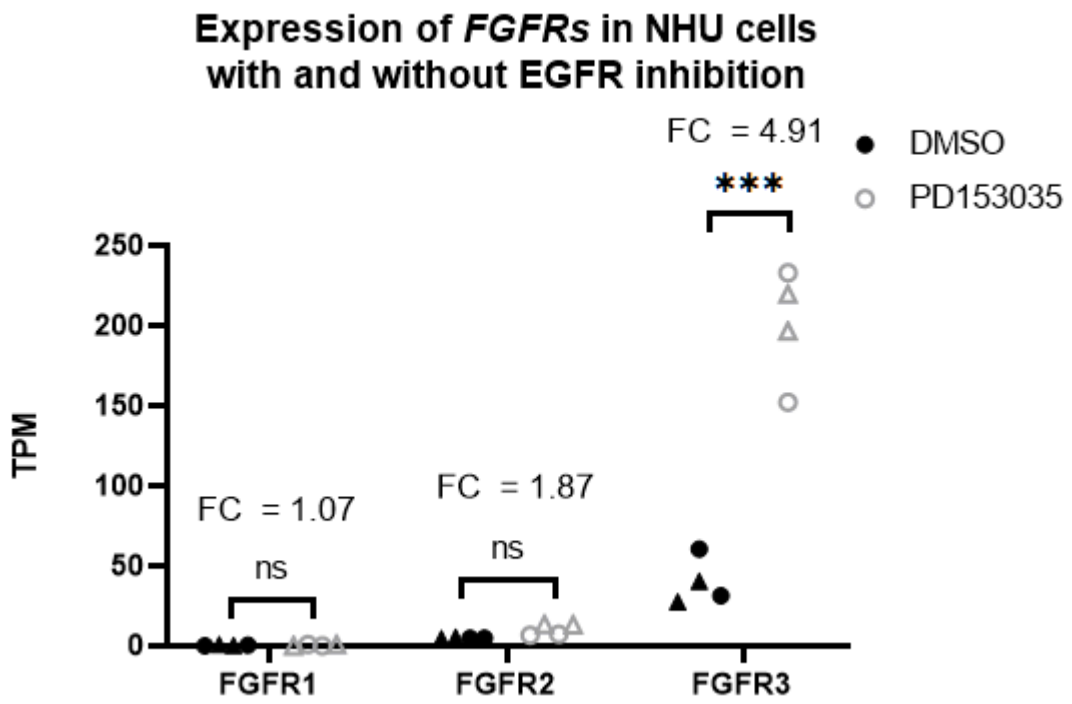

Figure 4.1 - Expression of FGFRs in NHU cells with and without EGFR inhibition - Statistical significance was determined via multiple t-tests with the Holm-Sidak correction for multiple comparisons. TPM; Transcripts per million. Transcript data provided by Raphael Slip and Dr Simon Baker (Jack Birch Unit, University of York) was generated outside this thesis. NHU cells were grown to visual confluence and then maintained for 72 h. Cells were then pre-treated with DMSO for 72 h, before finally receiving treatment of either DMSO vehicle control or PD153035 for 24 h. Experiments were performed on NHU

cell lines Y2996 (Ureter), Y3059 (Ureter), Y569 (Bladder), and Y572 (Bladder). Triangles represent ureter-derived samples and circles represent bladder-derived samples.

4.3.2 Titration of FGF9 for activation of FGFR3 protein

The FGFR3 ligand FGF9 was first titrated to determine the minimum concentration required to maximally activate FGFR3 following a 30-minute treatment, as measured by phosphorylation of FRS2. FRS2 phosphorylation appeared to follow a sigmoidal pattern, with little change in FGFR3 activation between 1 and 100 ng/mL of FGF9. There was a large increase in FRS2 phosphorylation at 300 ng/mL FGF9, after which FRS2 phosphorylation plateaued (Fig. 4.2). Thus, 300 ng/mL FGF9 was chosen for use in further experiments.

When NHU cells were treated by the addition of BPE, a slight increase in FRS2 phosphorylation was observed, approximately equivalent to stimulation with 10 ng/mL of FGF9 (Fig. 4.2). However, this phosphorylation was much less than when NHU cells were stimulated with 300 ng/mL of FGF9.

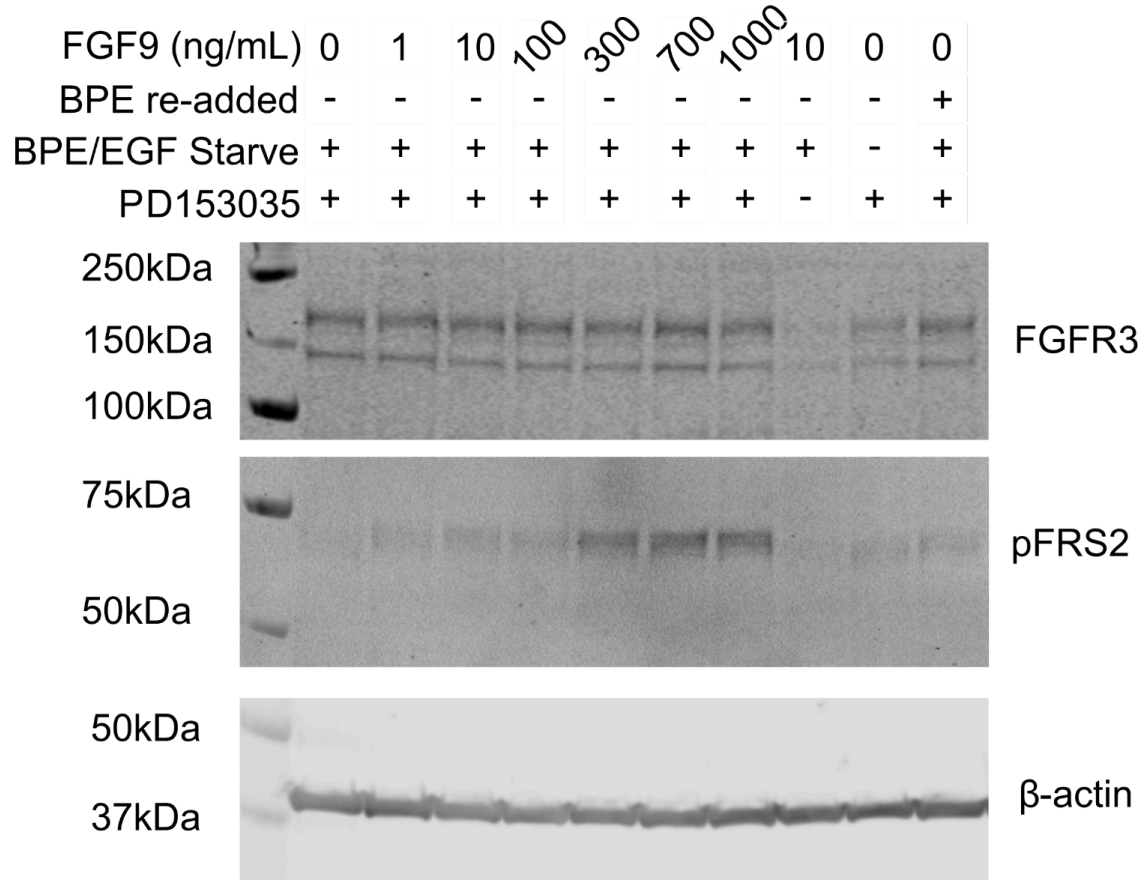

Figure 4.2 - Dose dependent activation of FGFR3 by FGF9 in NHU cells - Undifferentiated NHU cells were treated with 1μM PD153035 for 72 h to trigger FGFR3

protein expression. NHU cells were then treated with increasing concentrations of FGF9 to activate FGFR3 and harvested after 30 minutes. FGFR3 activation was assessed by western blotting for phospho-FRS2. Experiment was performed on NHU cell line Y2324 (single replicate). NHU cells were seeded at 30% visual confluence, then 24 h later indicated treatments were added. From the point at which PD153035 was added to cells, NHU cultures were grown in Keratinocyte Serum-Free Medium supplemented with Cholera toxin only - no BPE or EGF was included.

4.3.3 Activation of FGFR3 protein expressed in EGFR-inhibited NHU cells

To determine the stability/temporal kinetics of FGFR3 activation, EGFR-inhibited NHU cells expressing FGFR3 were treated with FGF9 for between 3 and 120 minutes. FRS2 phosphorylation was strongest at 3 minutes post-activation, after which point FRS2 phosphorylation continued to decrease until 30 minutes (Fig. 4.3a). After 30 minutes FRS2 phosphorylation appeared stable. 3-4 bands were observed for pFRS2 (Fig. 4.3b), agreeing with previous reports that FRS2 has multiple tyrosine phosphorylation sites [Reviewed by Gotoh, 2008]. FRS2 phosphorylation was not seen unless FGF9 was added, suggesting that FGFR3 was not activated in an autocrine fashion NHU cells.

ERK phosphorylation was greatest between 3-5 minutes after FGFR3 activation. ERK was slightly less phosphorylated at 15 minutes, after which ERK phosphorylation was stable for the remainder of the time-course. Very slight p44 ERK phosphorylation was observed in the absence of FGF9 addition. Phosphorylation of AKT was unaffected by FGFR3 activation.

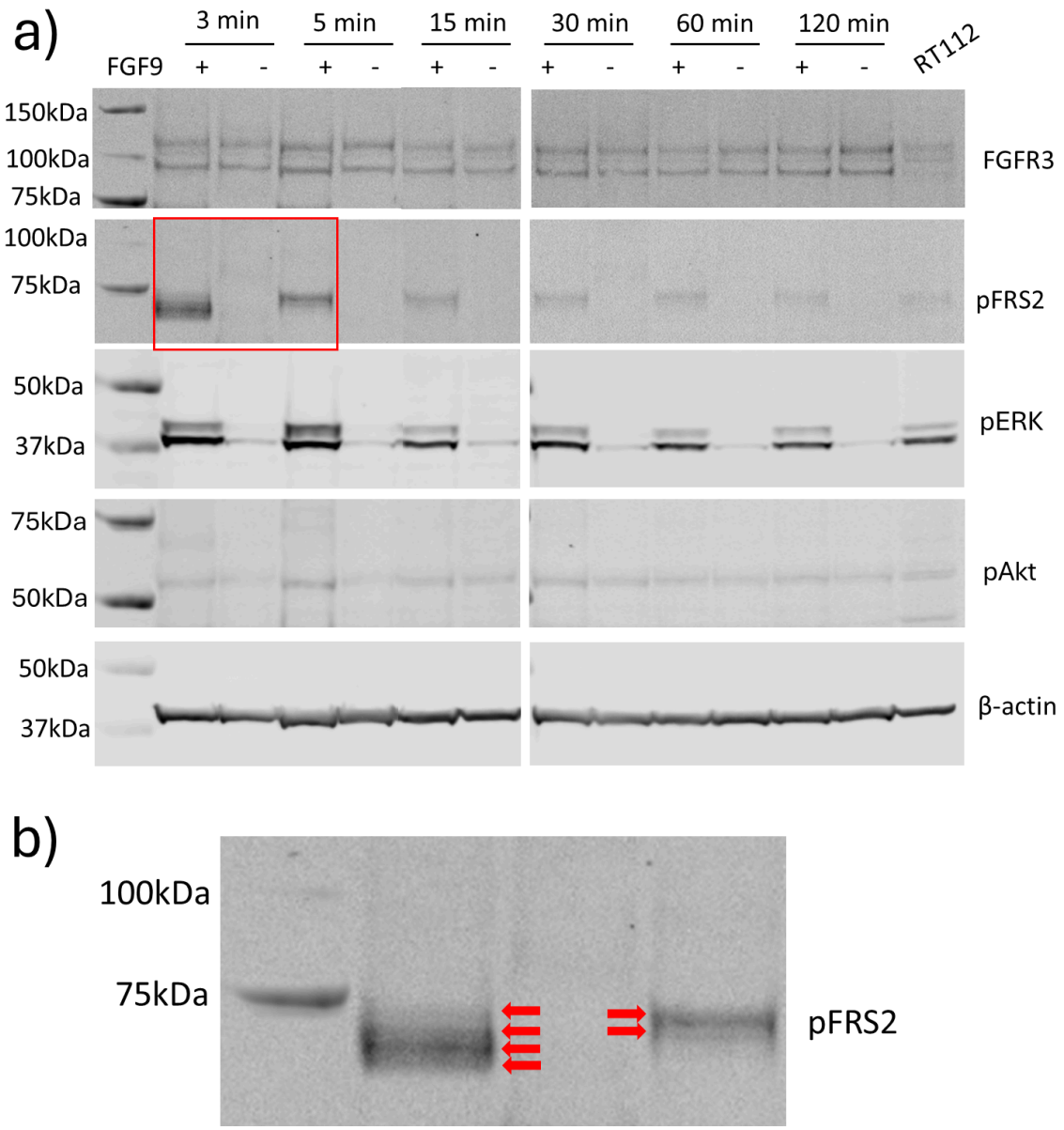

Figure 4.3 - Activation of FGFR3 in EGFR-inhibited NHU cells over a 120 min time-course - (a) Full time-course, (b) zoom-in on pFRS2 showing multiple bands - Red box indicates zoom-in area and red arrows indicate multiple species of phospho-FRS2. NHU cell cultures were treated for 72 h with PD153035 EGFR inhibitor to trigger FGFR3 expression then treated with FGF9 for the time shown to activate FGFR3. Where FGF9 was not added, cells were treated with a 0.1% BSA in DPBS vehicle control. β-actin was blotted as a loading control to ensure equal protein between lanes. RT112 BLCA cell line is a positive control for FGFR3 expression and activity. Independent experiments were performed in NHU cell lines Y1781, Y2698, and Y2843 (3 replicates). AKT phosphorylation was assessed in NHU cell lines Y1781 and Y2843 (2 replicates). NHU cells were seeded at 30% visual confluence, then 24 h later indicated treatments were added. From the point at which PD153035 was added to cells, NHU cultures were grown

in Keratinocyte Serum-Free Medium supplemented with Cholera toxin only - no BPE or EGF was included.

4.3.4 FGFR3 protein localisation in urothelial tissues

4.3.4.1 Titration of FGFR3 antibodies for immunohistochemical labelling of urothelial tissue and selection of controls

Before performing experiments to observe the expression of FGFR3 protein in urothelial tissue, antibodies against the N- and C-terminus of the FGFR3 protein were titrated on ureter tissue, with antibody concentrations being chosen based on manufacturer recommendations (Fig. 4.4 and 4.5). Sections of tissues which were treated with secondary antibody but no primary were included to test specificity of binding to the primary antibodies. From the Protein Atlas online database, tonsil was selected as a positive control tissue which was known to express FGFR3.

Titration of FGFR3 N-terminal antibody

a)

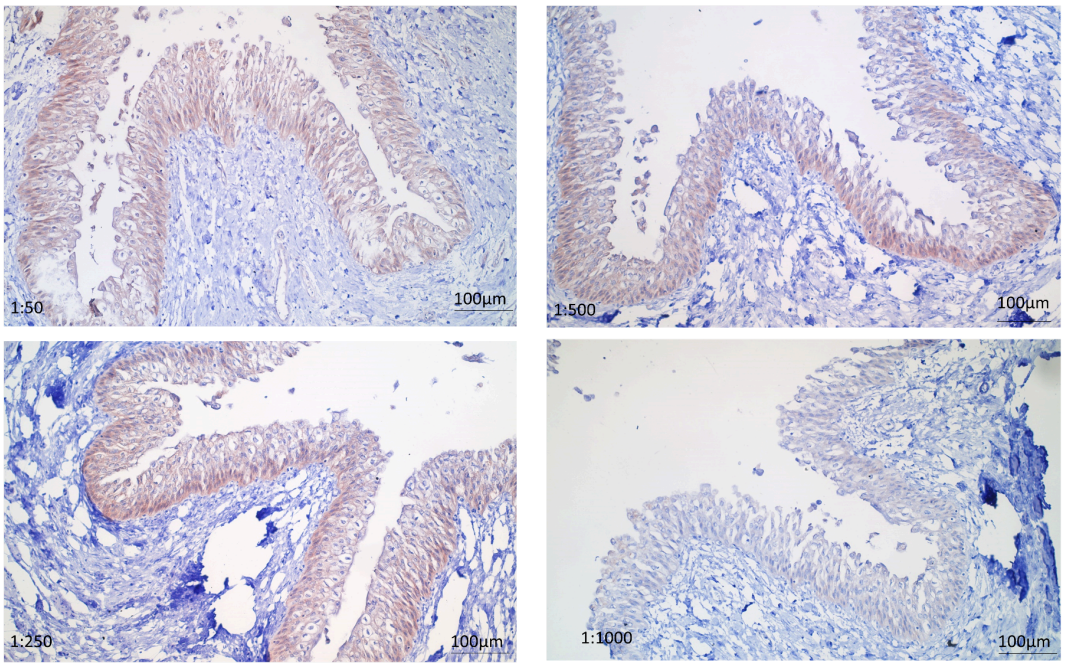

Negative controls: secondary-only

b)

Ureter

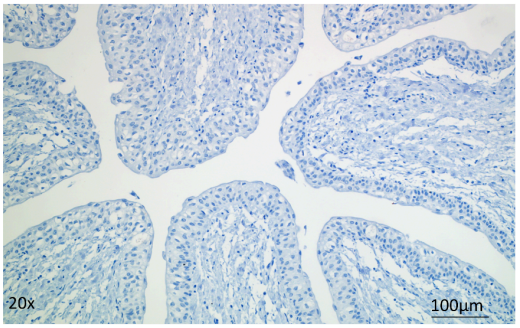

Tonsil

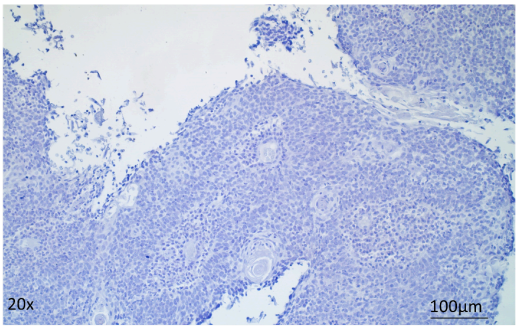

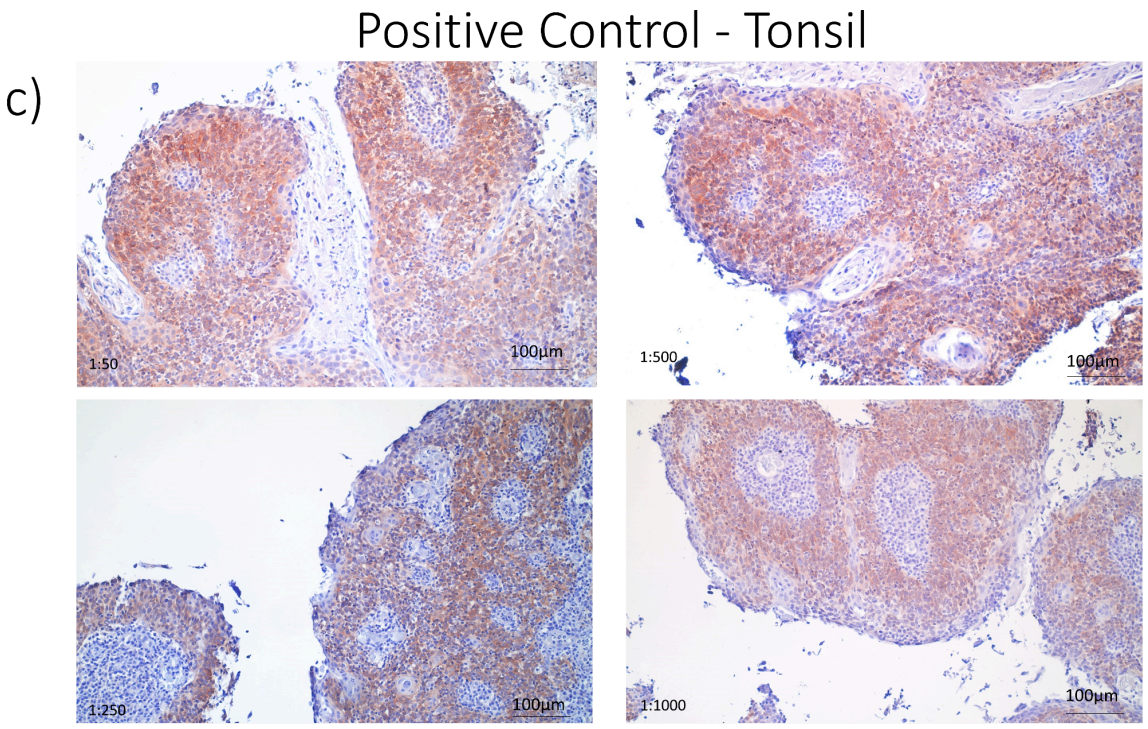

Figure 4.4 - Titration of FGFR3 N-terminal antibody in urothelial and control tissues - Scale bar (black line) represents 100 µm. Sections were labelled with 3,3'-diaminobenzidine followed by horseradish peroxidase and counterstained with haematoxylin and eosin.

Titration of FGFR3 C-terminal antibody

a)

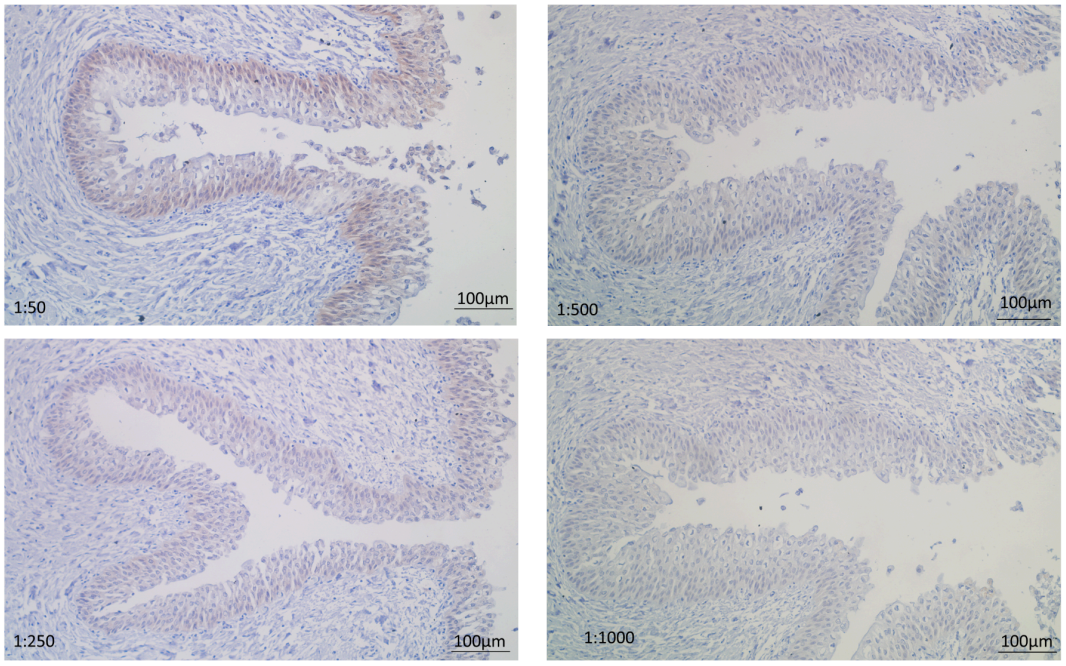

Negative controls: secondary-only

b)

Ureter

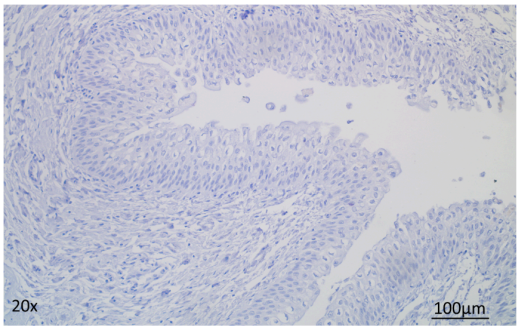

Tonsil

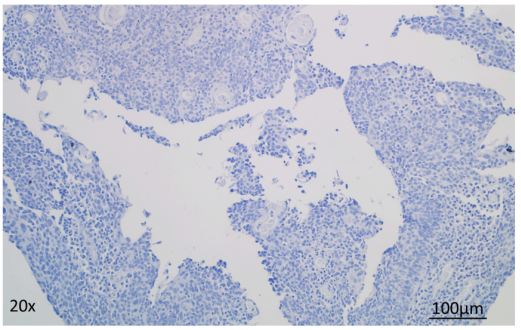

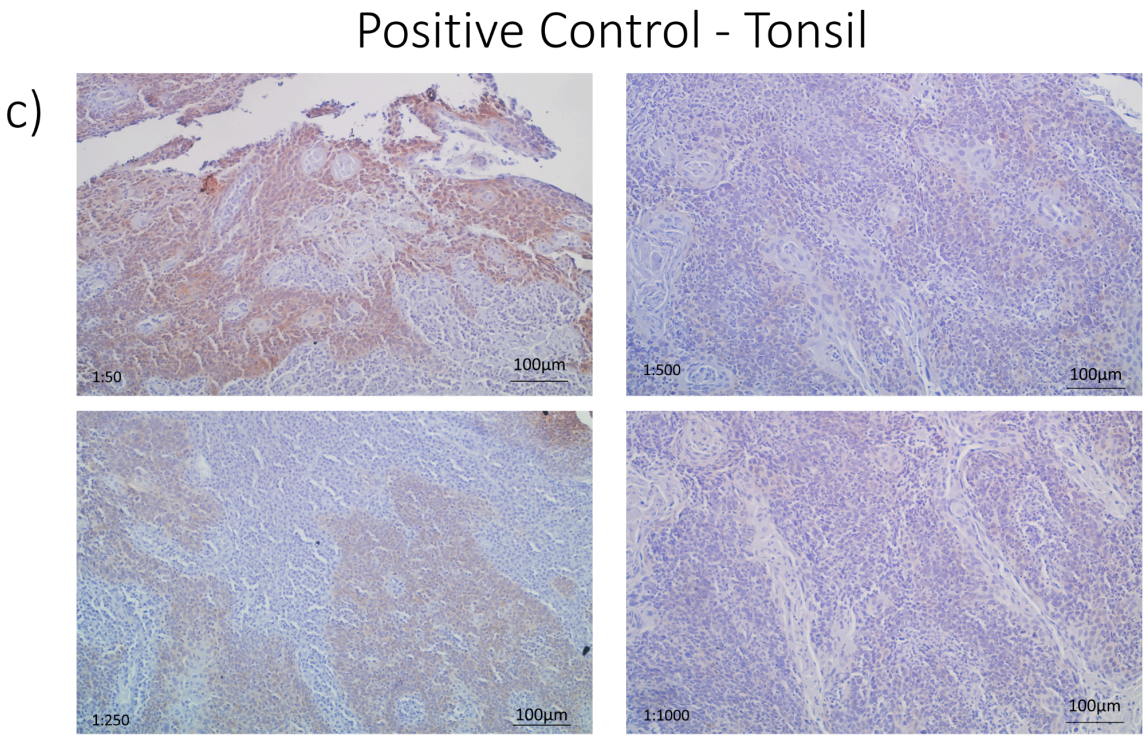

Figure 4.5 - Titration of FGFR3 C-terminal antibody in urothelial and control tissues - Scale bar (black line) represents 100 µm. Sections were labelled with 3,3'-diaminobenzidine followed by horseradish peroxidase and counterstained with haematoxylin and eosin.

4.3.4.2 FGFR3 protein was expressed evenly throughout the layers of the urothelium in six tissue samples

FGFR3 protein expression and localisation were examined in urothelial tissue using antibodies against the N- and C-termini of FGFR3 (Fig. 4.6 and 4.7). Sections of tissues which were treated with secondary antibody but no primary were included to test specificity of binding to the primary antibodies (Fig. 4.7). From the Protein Atlas online database, tonsil was selected as a positive control tissue which was known to express FGFR3. Adrenal gland was selected for a specificity control which did not express FGFR3 protein - this was used to rule out nonspecific binding of FGFR3 antibodies (Fig. 4.7). FGFR3 was expressed evenly throughout the different layers of the urothelium and was not expressed in the underlying stroma (Fig. 4.6). Within cells of urothelial tissue, FGFR3 protein appeared cytoplasmic and was not clearly localised to intercellular borders between cells.

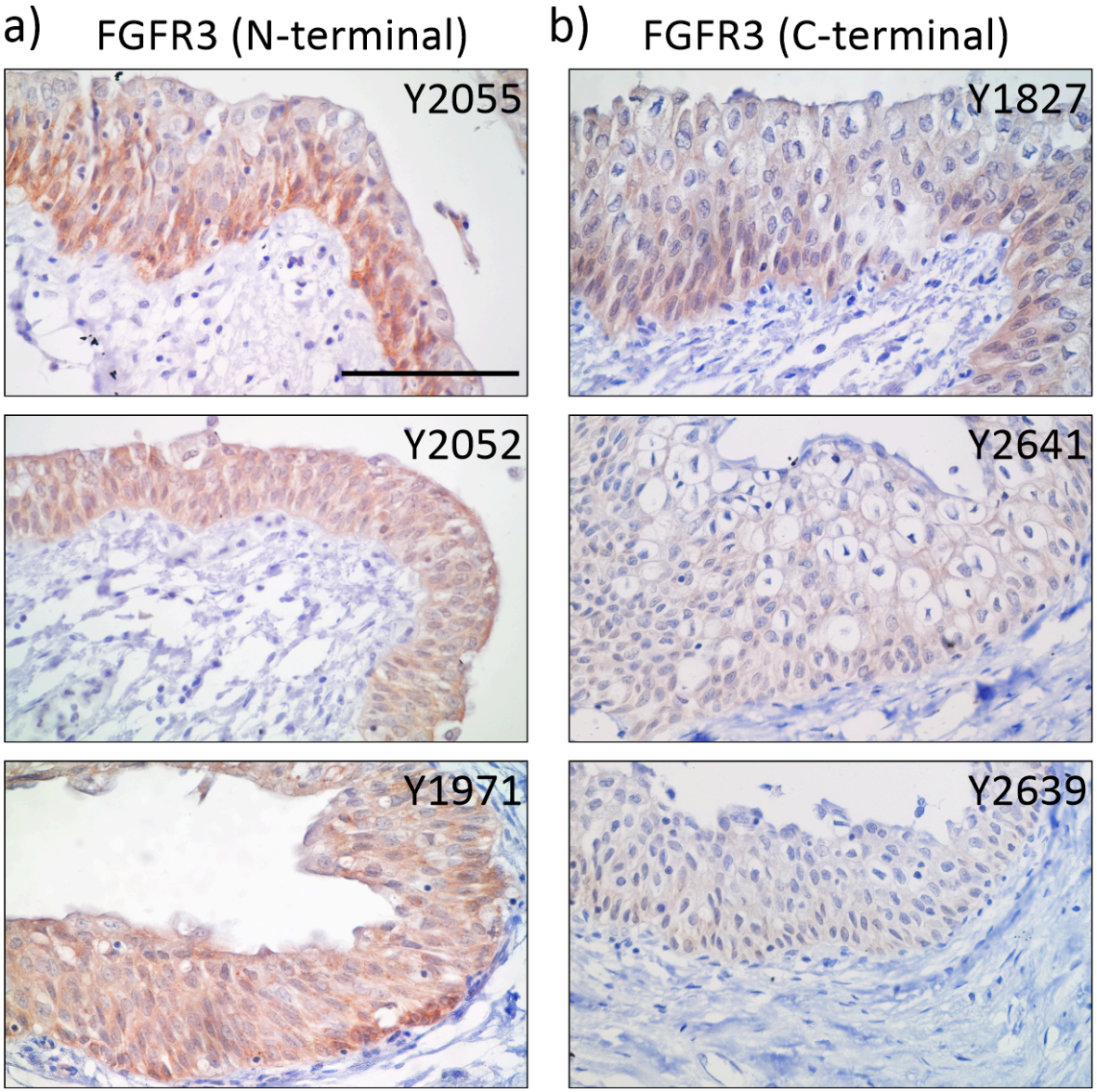

Figure 4.6 - Localisation of FGFR3 protein within urothelial tissue - (a) FGFR3 N-terminal antibody, (b) FGFR3 C-terminal antibody. Scale bar (black line) represents 100 µm. Experiments were performed using tissue from Y2055, Y2052, Y1971, Y1827, Y2641, Y2639 (3 replicates per antibody). Sections were labelled with 3,3'-diaminobenzidine followed by horseradish peroxidase and counterstained with haematoxylin and eosin. Controls are shown in figure 4.7.

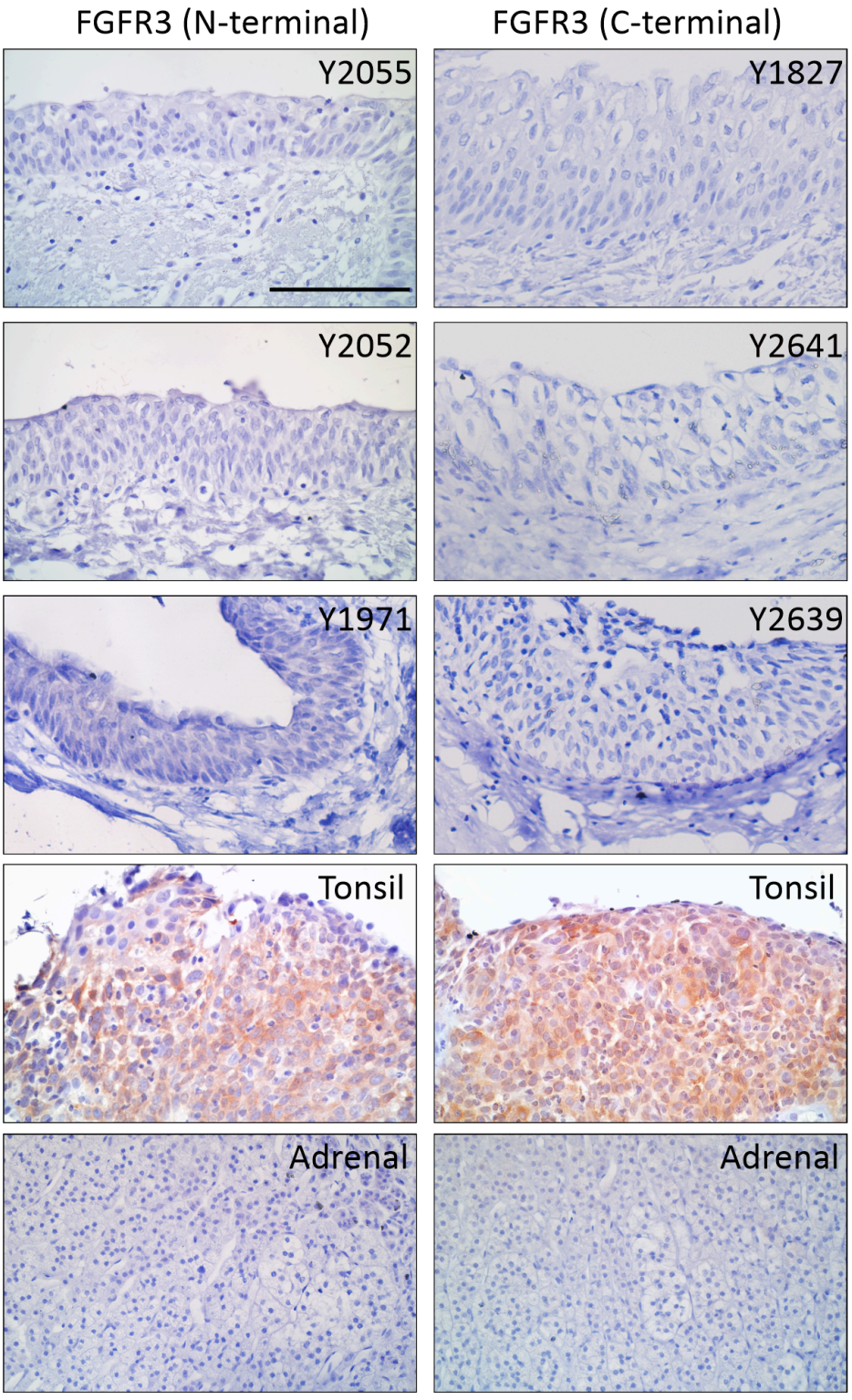

Figure 4.7 - Experimental controls for immunohistochemical analysis of FGFR3 protein within urothelial tissues - Scale bar (black line) represents 100 µm. Experiments were performed using tissue from Y2055, Y2052, Y1971, Y1827, Y2641, Y2639 (3 replicates per antibody). Sections were labelled with 3,3'-diaminobenzidine followed by horseradish peroxidase and counterstained with haematoxylin and eosin. Secondary-only controls were used to confirm specific binding to primary antibodies.

Tonsil was included as a positive control which expressed FGFR3 protein (information from Protein Atlas) and adrenal tissue was included as a specificity control which did not express FGFR3 protein (information from Protein Atlas).

4.3.5 Localisation of FGFR3 protein in NHU cells

4.3.5.1 Titration of FGFR3 antibodies for immunofluorescence labelling of NHU cells and selection of controls

Before performing experiments to observe the expression of FGFR3 protein in NHU, antibodies against the N- and C-terminus of the FGFR3 protein were titrated on RT112 BLCA cells (Fig. 4.8) which were shown to express FGFR3 protein (Chapter 3). Antibodies against Calnexin and LAMP1 were titrated in the same way (Fig. 4.10 and 4.11). Antibody concentrations were selected according to manufacturer instructions. Negative controls were included in which cells were treated with secondary antibody but no primary, to confirm specificity of secondary antibody to the primary antibody. Positive controls for the secondary antibody were included where cells were stained with a known mouse (Ki67) or rabbit (MCM2) primary antibody.

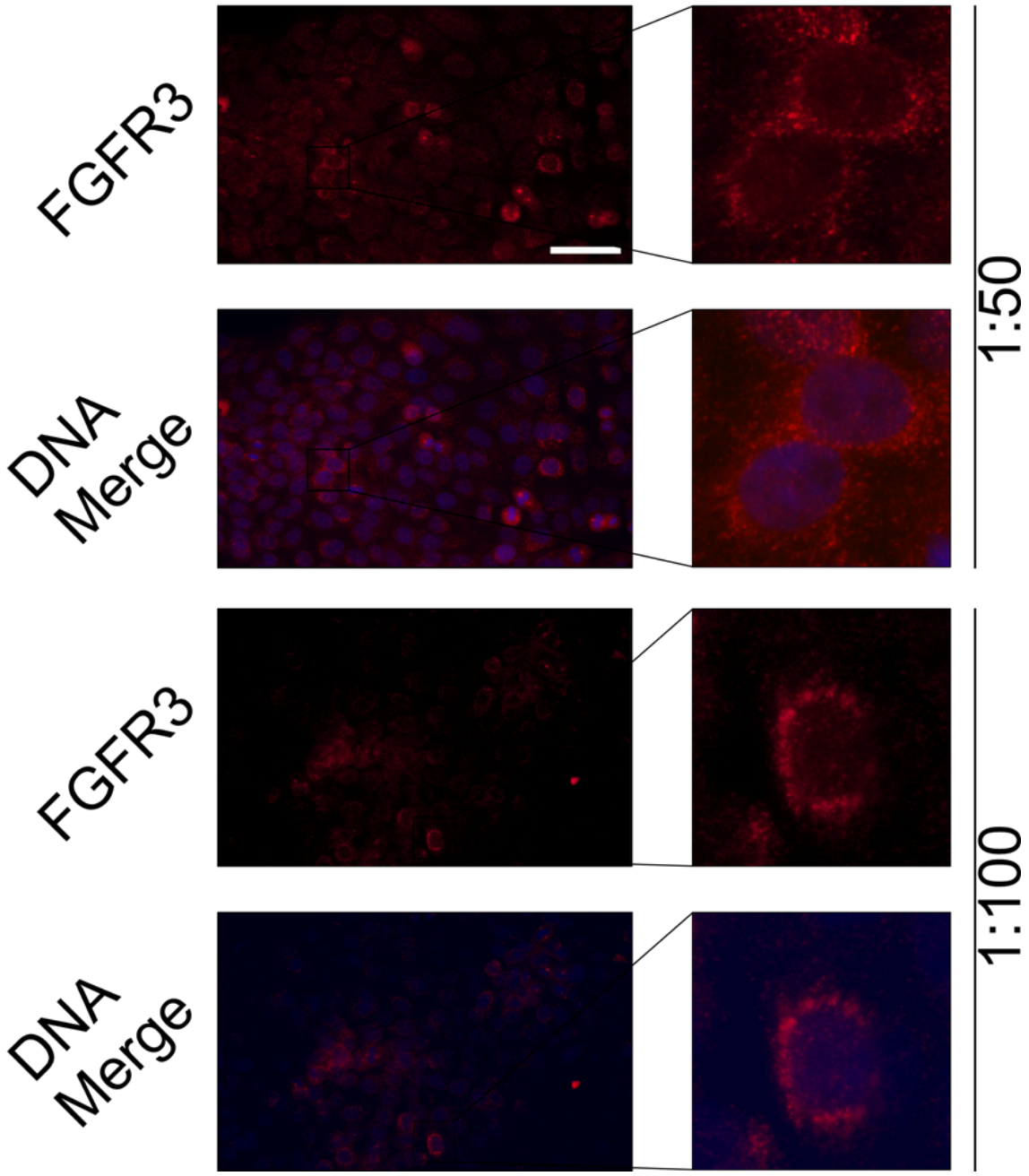
FGFR3
DNA
Merge
FGFR3
DNA
Merge
1:50
1:100

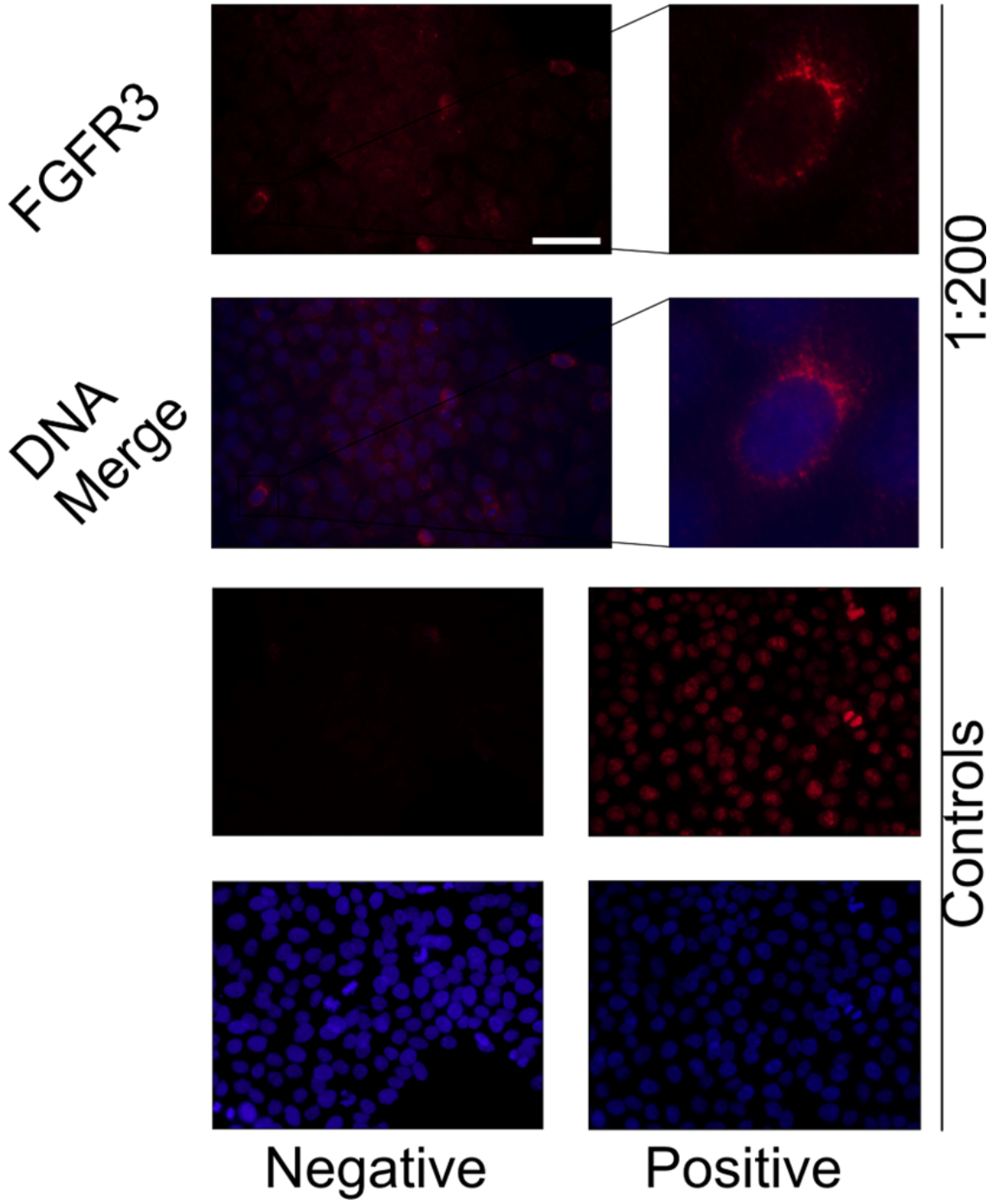

Figure 4.8 - Titration of FGFR3 N-terminal antibody in RT112 BLCA cells - FGFR3 N-terminus shown in red, Hoechst 33258 DNA stain shown in blue. Scale bar (white line) represents 30 μm.

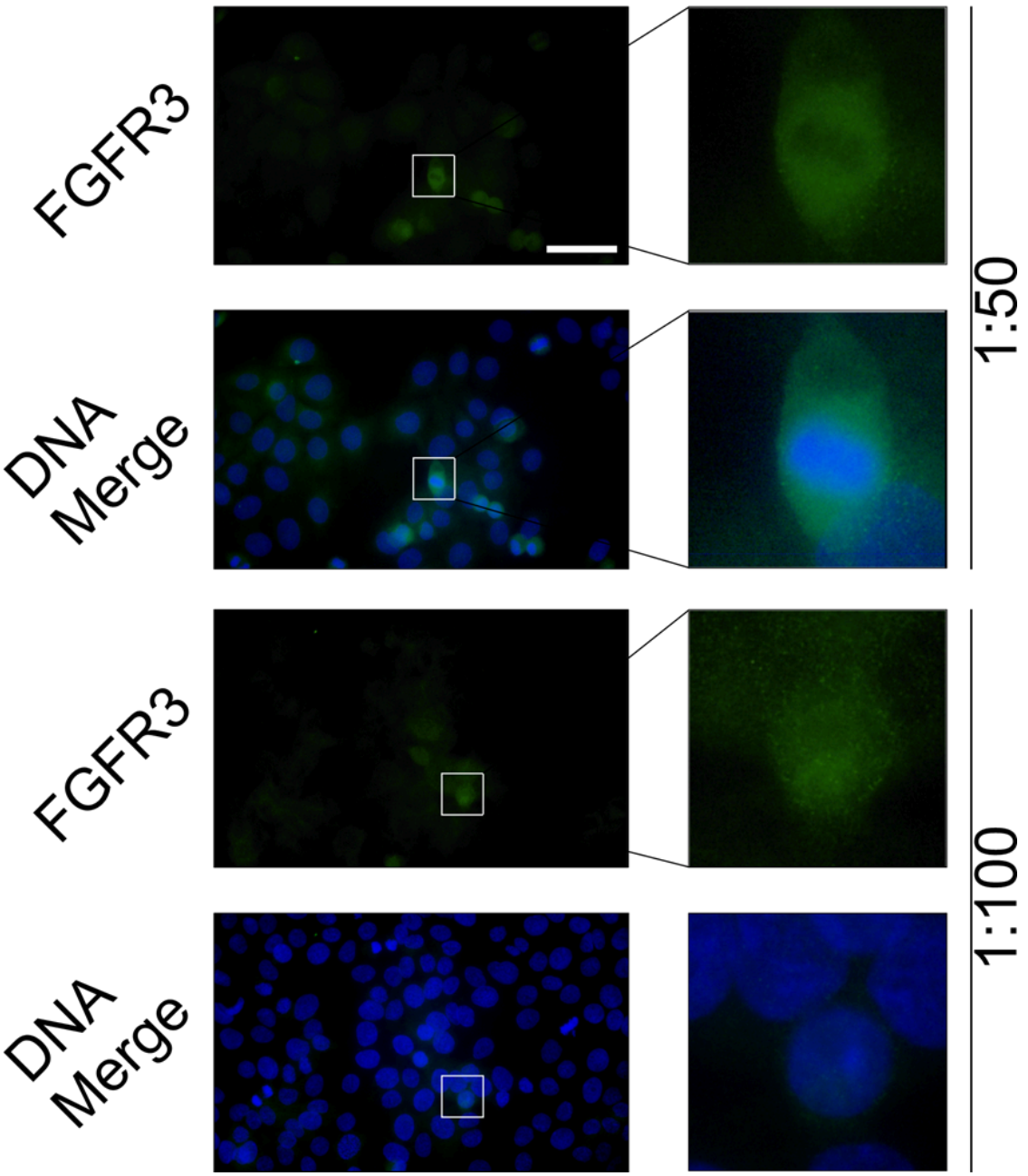
FGFR3
DNA
Merge
1:50
FGFR3
DNA
Merge
1:100

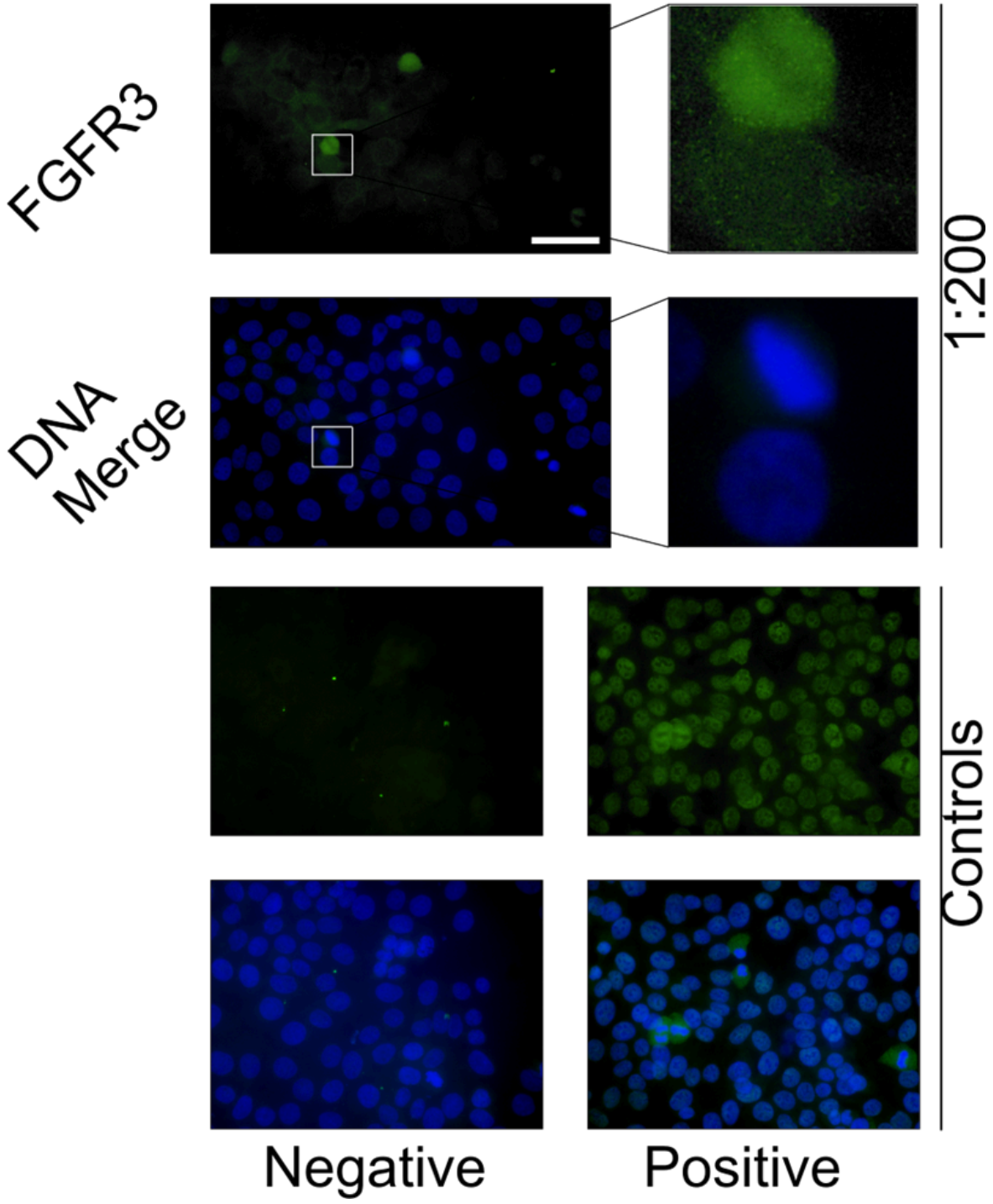

Figure 4.9 - Titration of FGFR3 C-terminal antibody in RT112 BLCA cells - FGFR3 C-terminus shown in green, Hoechst 33258 DNA stain shown in blue. Scale bar (white line) represents 30 μm.

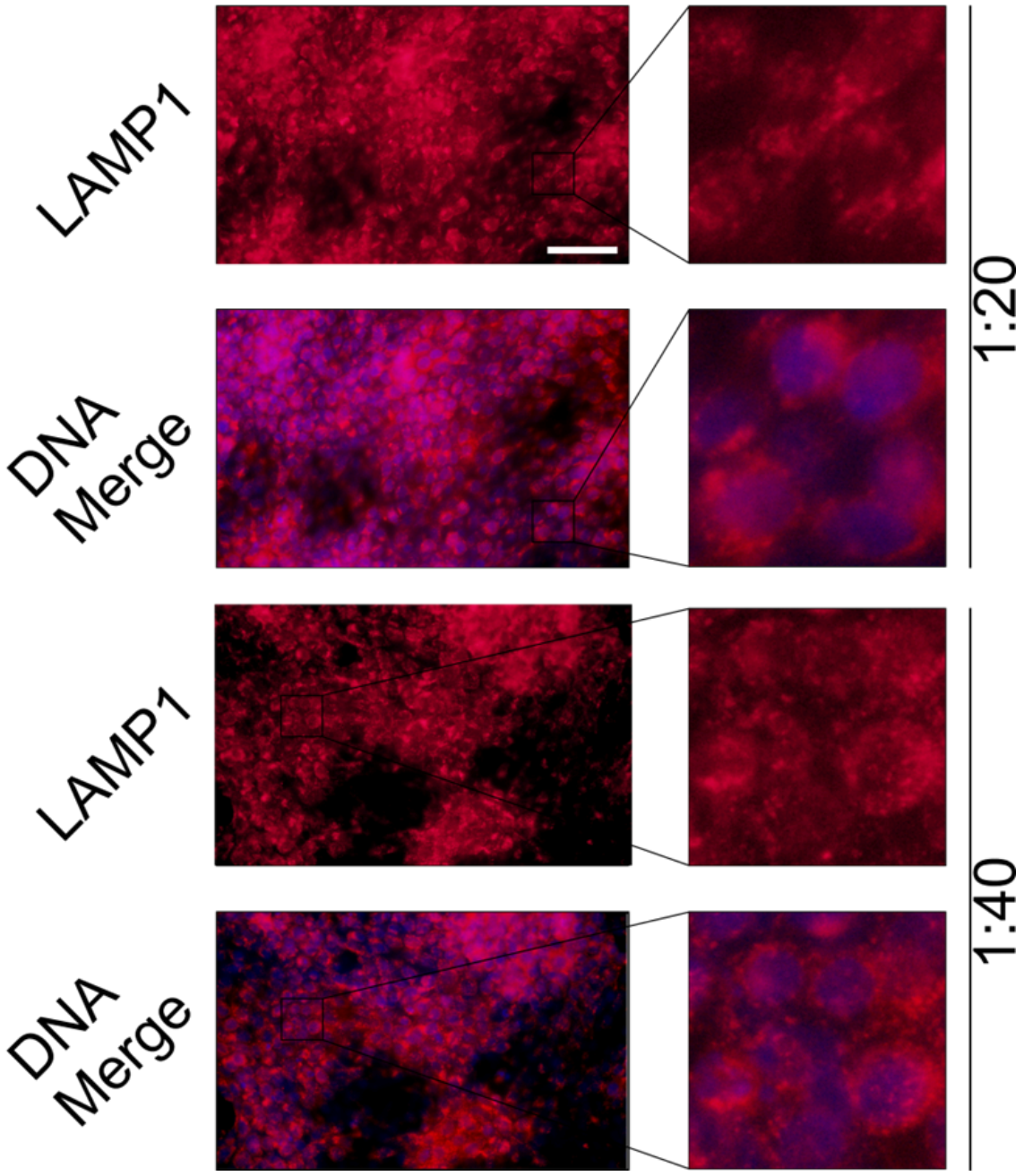
LAMP1
DNA
Merge
LAMP1
DNA
Merge
1:20
1:40

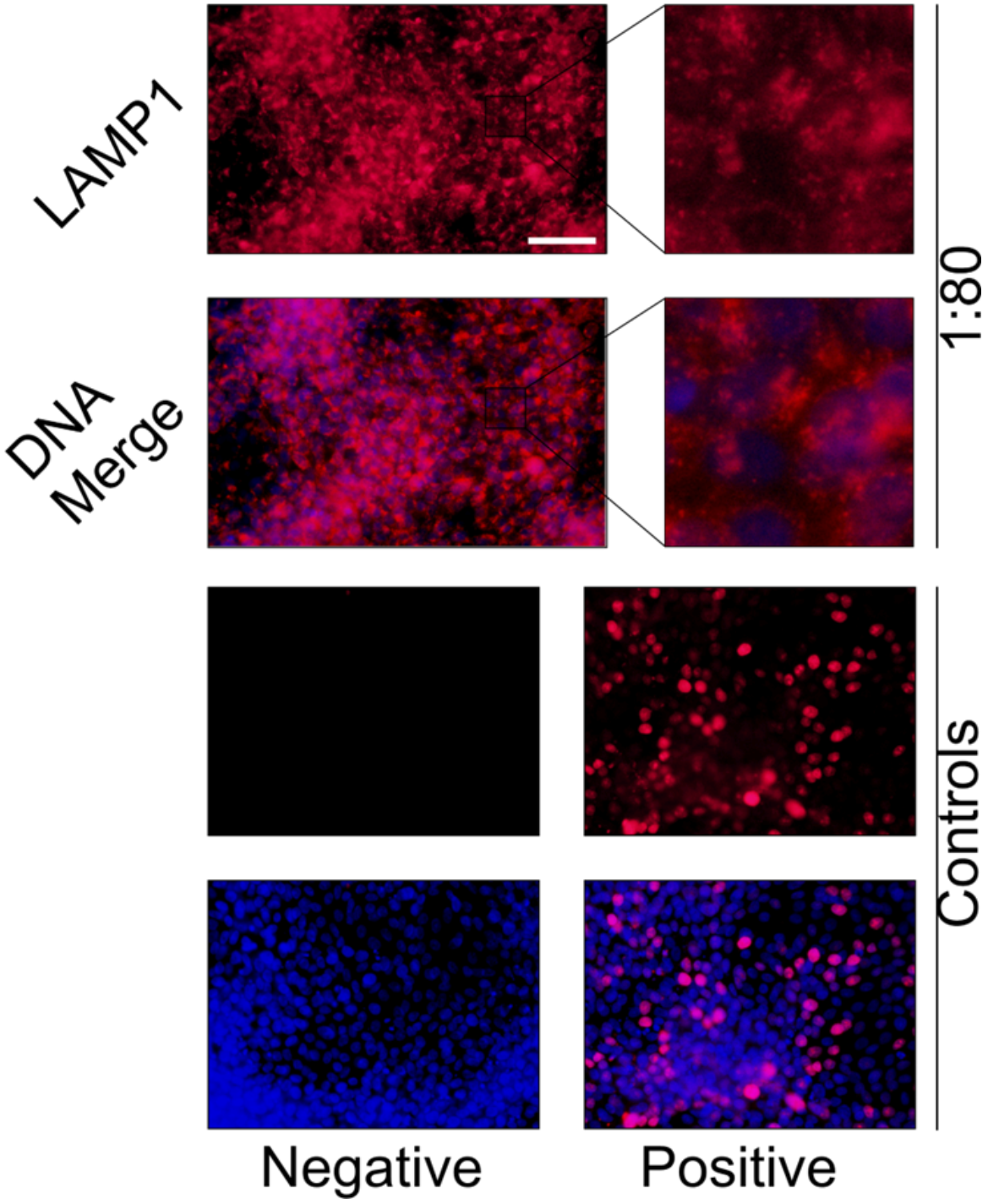

Figure 4.10 - Titration of LAMP1 antibody in RT112 BLCA cells - LAMP1 shown in red, Hoechst 33258 DNA stain shown in blue. Scale bar (white line) represents 30 µm.

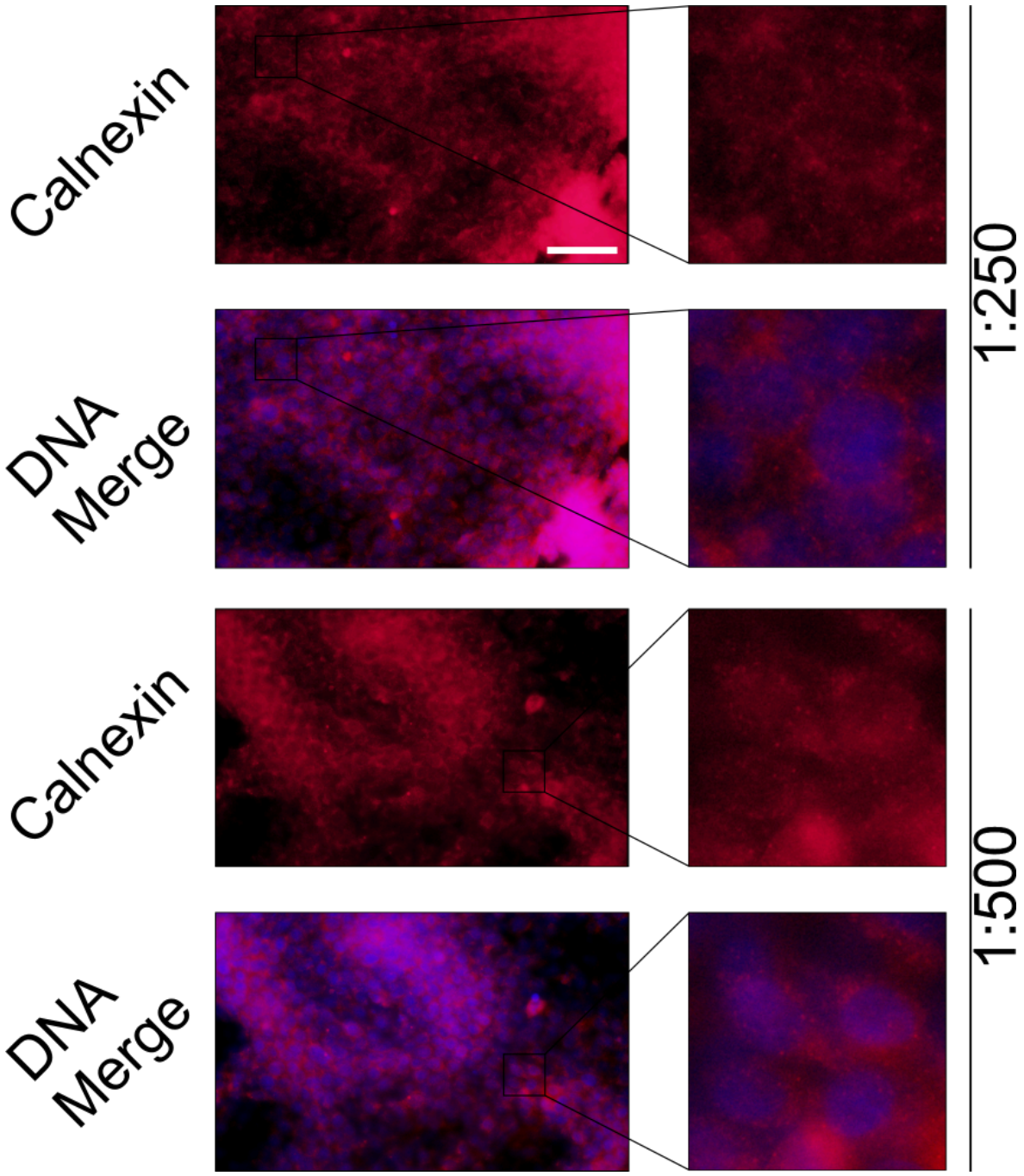
Calnexin
DNA
Merge
Calnexin
DNA
Merge
1:250
1:500

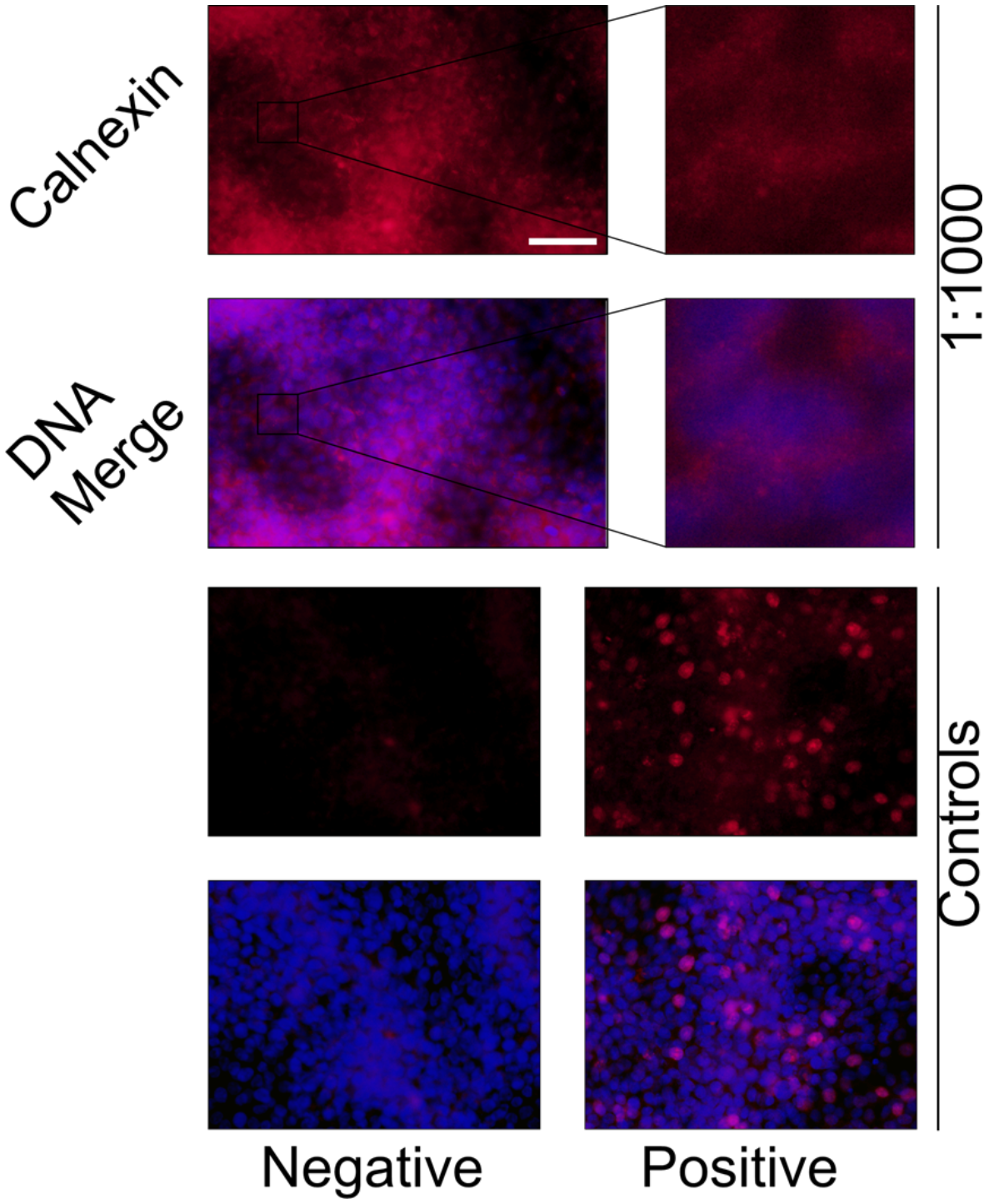

Figure 4.11 - Titration of Calnexin antibody in RT112 BLCA cells - Calnexin shown in red, Hoechst 33258 DNA stain shown in blue. Scale bar (white line) represents 30 µm.

4.3.5.2 FGFR3 protein showed cytoplasmic and perinuclear localisation within EGFR-inhibited NHU cells, regardless of FGFR3 activation status

Firstly, NHU cell cultures were examined to see what proportion of cells expressed FGFR3. Similar to western blotting analysis (Chapter 3) some FGFR3 protein was detected in control NHU cell cultures at confluence, although the mean intensity of

FGFR3 protein expression was significantly greater in NHU cells after EGFR-inhibition with PD153035 (Fig. 4.12). FGFR3 protein expression was highly heterogeneous across the cell population. Treatment with FGF9 for 30 minutes led to significantly decreased mean intensity of FGFR3 protein expression in NHU cells. For both N- and C-terminal FGFR3, mean cell intensity when FGF9 was added was approximately 60% of the mean cell intensity with just PD153035 alone (Fig. 4.12). For both N- and C-terminal FGFR3, the percentage of cells which were FGFR3-positive was greater when NHU cells were treated with PD153035 compared to DMSO controls (Fig. 4.12).

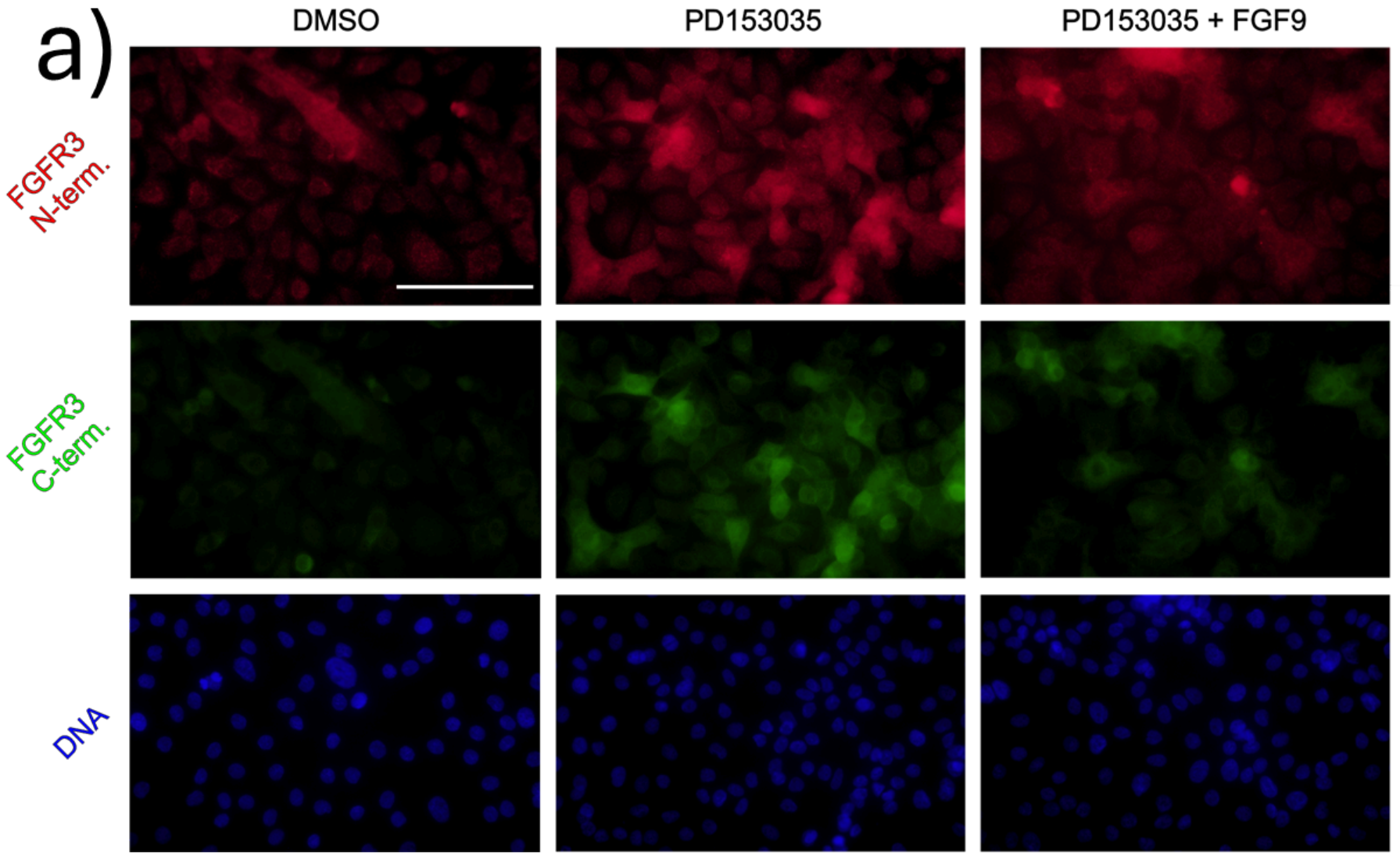
a)
DMSO
PD153035
PD153035 + FGF9
FGFR3 N-term.
FGFR3 C-term.
DNA

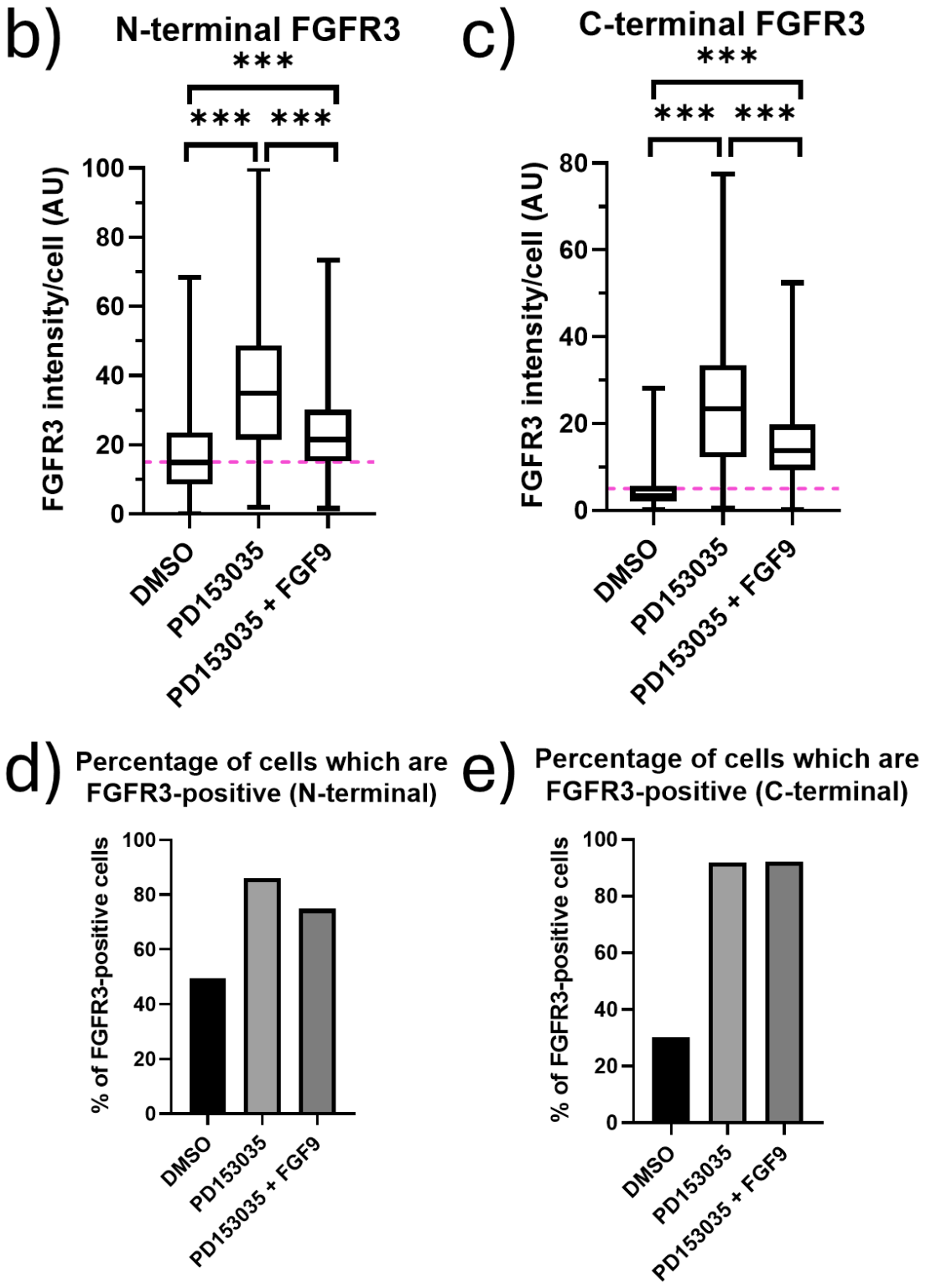

Figure 4.12 - FGFR3 protein expression was variable across a population of NHU cells - (a) Expression of FGFR3 protein visualised by indirect immunofluorescence using antibodies against the N- and C-terminus of FGFR3, (b) FGFR3 intensity per cell visualised using antibodies against the N- and (c) C-terminus of FGFR3, (d) percentage of

cells which were positive for FGFR3 expression when visualised using antibodies against the N- and (e) C-terminus of FGFR3.. Scale bar (white line) represents 50 μm. Brown-Forsythe and Welch ANOVA tests (which do not assume equal standard deviation between groups) were performed to confirm that the three treatment conditions varied significantly from each other. Following this, a Games-Howell's multiple comparisons test was used to examine the degree of significant difference between each group. FGFR3 intensity was measured in at least 600 cells for each condition. Box plot shows the min and max values, as well as the 1st quartile, median and 3rd quartile values (bottom to top). Pink dotted line shows the threshold of intensity used to determine if a cell was FGFR3-positive, used to generate (d) and (e). This threshold was determined by examining images by eye to determine at which intensity value FGFR3 was no longer visible. Experiments were performed on NHU cell line Y1393 (single replicate). NHU cells were seeded at 30% visual confluence, then 24 h later indicated treatments were added. Cells were treated with or without PD153035 for 72 h prior to addition of FGF9 for 30 minutes. From the point at which PD153035 was added to cells, NHU cultures were grown in Keratinocyte Serum-Free Medium supplemented with Cholera toxin only - no BPE or EGF was included. AU; Arbitrary Units.

Visualisation of FGFR3 protein with both N- and C-terminal antibodies simultaneously showed overlap, although N- and C-terminal FGFR3 also both showed distinct localisations (Fig. 4.13). The non-total overlap of FGFR3 N- and C-termini was also reflected in the Pearson's R and Manders' coefficients being less than 1 (Table 4.1). N-terminal FGFR3 appeared to be more cytoplasmic with distinct punctae, while C-terminal FGFR3 was generally more tightly localised to the perinuclear region. The intracellular localisation of FGFR3 did not appear to change with the addition of FGF9, although intensity of FGFR3 expression was reduced (Fig. 4.13)

Comparison of C-terminal FGFR3 with the lysosomal marker LAMP1 or the endoplasmic reticulum marker Calnexin by simultaneous antibody labelling showed some but not complete overlap of localisation (Fig. 4.14 and Fig 4.15). Although FGFR3 localisation overlapped with both positional markers, FGFR3 appeared to co-localise more with calnexin than LAMP1. The Pearson's R was greater for overlap of FGFR3 with calnexin than for FGFR3 and LAMP1, and Manders' coefficients were generally greater for FGFR3 and calnexin also (Table 4.1). Both FGFR3 and calnexin had a relatively diffuse perinuclear location compared to LAMP1, which was localised much more tightly to the perinuclear region (Fig. 4.14 and Fig 4.15).

The localisation pattern of FGFR3 appeared similar in NHU cells as in RT112 BLCA cells, which acted as a positive control for FGFR3 protein expression (Fig. 4.16).

Table 4.1 - Variables representing colocalisation of FGFR3 N- and C-terminus and FGFR3 C-terminus and LAMP1 or Calnexin - Colocalisation of FGFR3 and either calnexin or LAMP1 was quantified using the ImageJ plugin "JACoP" [Bolte and Cordelières, 2006, http://imagej.net/plugins/jacop]. M1 and M2 (Manders' coefficients) represent the proportion of A that overlaps with B and vice-versa, respectively [Manders et al., 1992].

Proteins	Treatment	Pearson's R	M1	M2
FGFR3 N-terminus (A) and FGFR3 C-terminus (B)	**PD153035**	0.856	0.971	0.747
	PD153035 + FGF9	0.834	0.904	0.792
FGFR3	**PD153035**	0.56	0.796	0.555

C-terminus (A) and LAMP1 (B)	**PD153035 + FGF9**	0.573	0.724	0.665
FGFR3 C-terminus A) and Calnexin (B)	**PD153035**	0.792	0.789	0.828
	PD153035 + FGF9	0.784	0.772	0.803

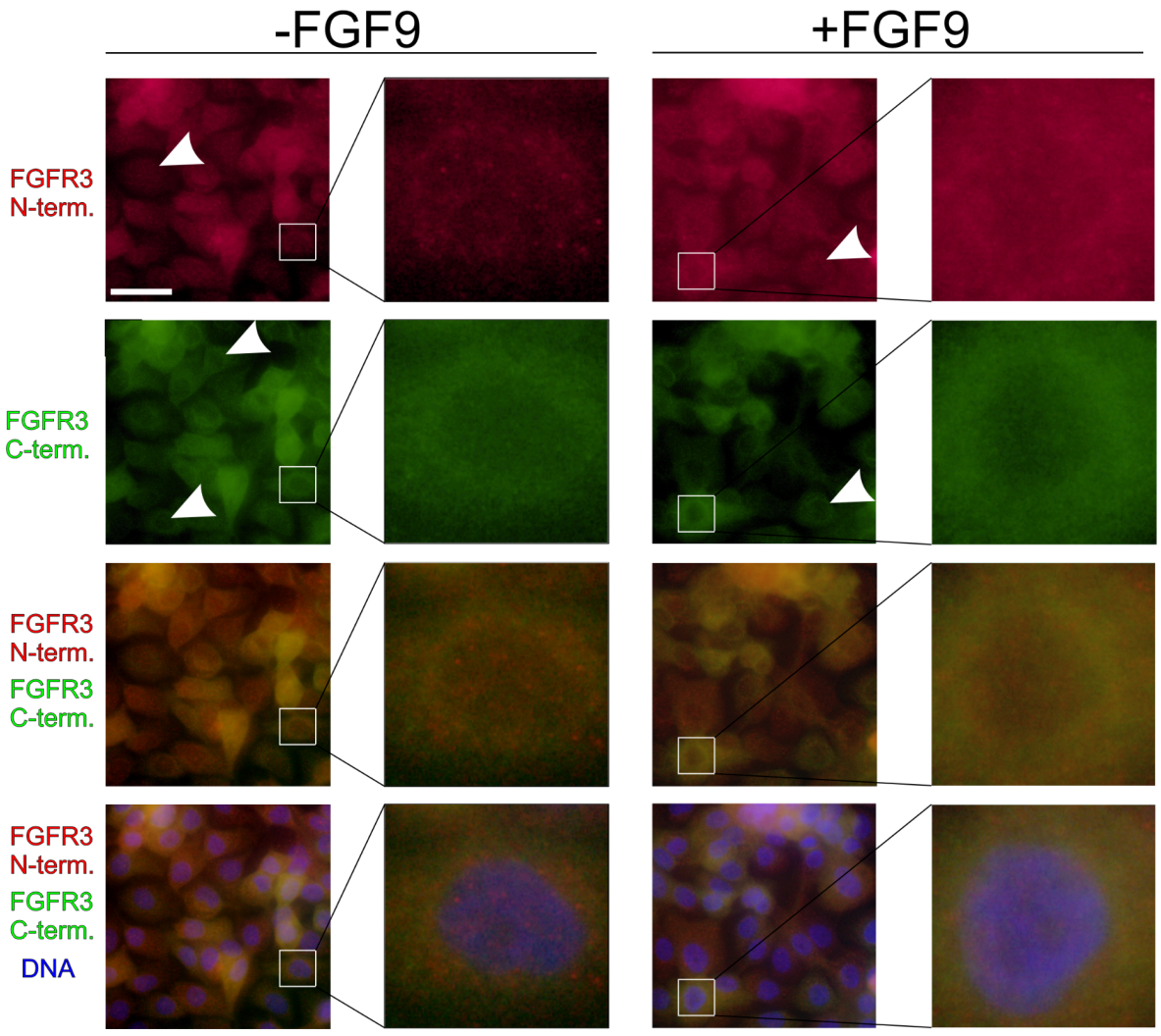

Figure 4.13 - Localisation of FGFR3 within NHU cells - FGFR3 N-terminus shown in red, FGFR3 C-terminus shown in green, Hoechst 33258 DNA stain shown in blue. Scale bar (white line) represents 30 μm. White arrowheads illustrate cells with cytoplasmic (N-terminal) or perinuclear (C-terminal) FGFR3 localisation. Experiments were performed

on NHU cell line Y1393 (single replicate). NHU cells were seeded at 30% visual confluence, then 24 h later indicated treatments were added. Cells were treated with PD153035 for 72 h prior to addition of FGF9 for 30 minutes. From the point at which PD153035 was added to cells, NHU cultures were grown in Keratinocyte Serum-Free Medium supplemented with Cholera toxin only - no BPE or EGF was included. Cells were simultaneously labelled with antibodies against the N-terminus and C-terminus of FGFR3, as well as Hoechst 33258 DNA stain, to assess co-localisation of FGFR3.

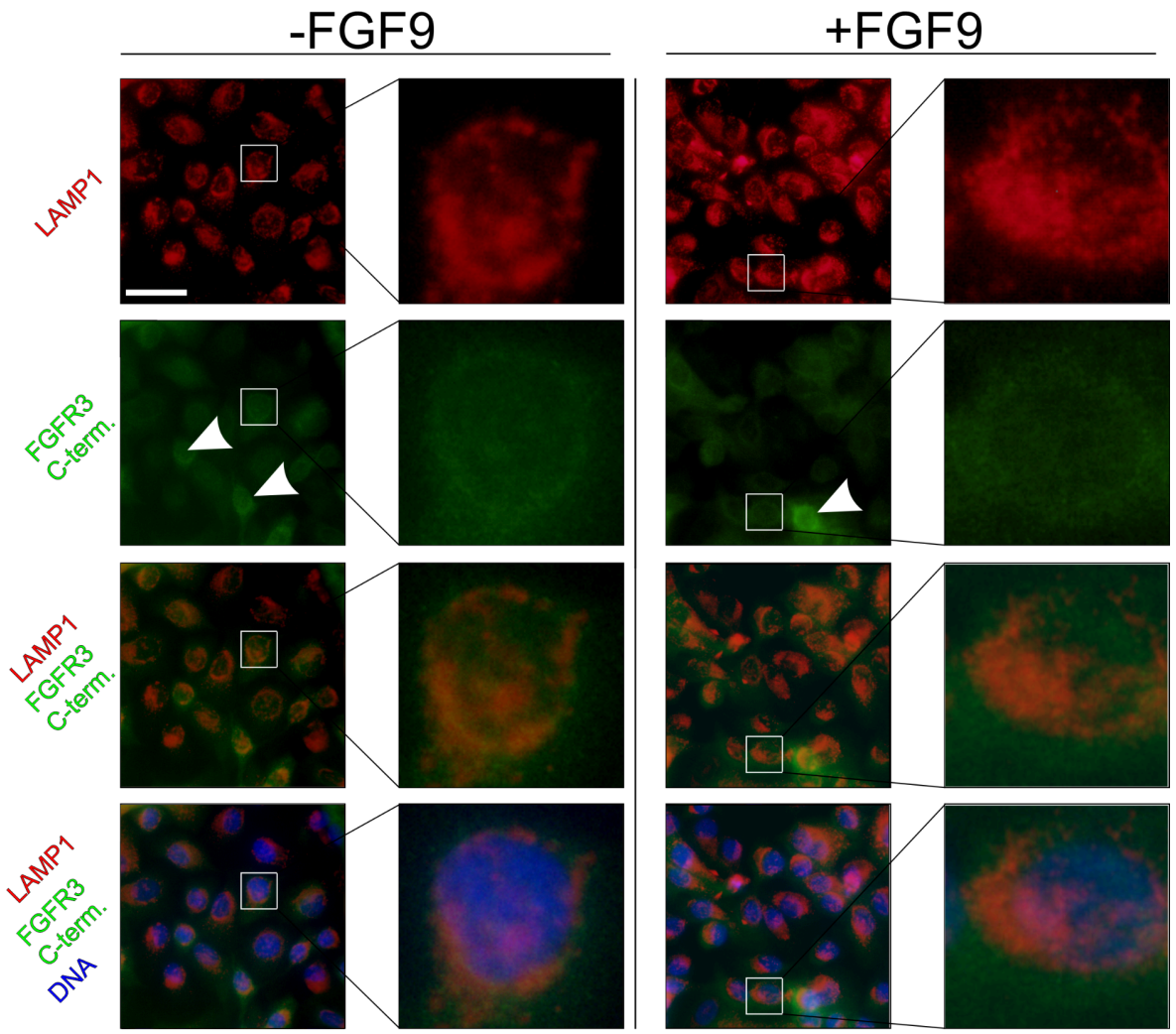

Figure 4.14 - Localisation of FGFR3 within NHU cells compared with lysosomal marker LAMP1 - LAMP1 shown in red, FGFR3 C-terminus shown in green, Hoechst 33258 DNA stain shown in blue. Scale bar (white line) represents 30 μm. White arrowheads illustrate cells with perinuclear FGFR3 localisation. Experiments were performed on NHU cell line Y1393 (single replicate). NHU cells were seeded at 30% visual confluence, then 24 h later indicated treatments were added. Cells were treated with PD153035 for 72 h prior to addition of FGF9 for 30 minutes. From the point at which

PD153035 was added to cells, NHU cultures were grown in Keratinocyte Serum-Free Medium supplemented with Cholera toxin only - no BPE or EGF was included. Cells were simultaneously labelled with antibodies against LAMP1 and the C-terminus of FGFR3, as well as Hoechst 33258 DNA stain, to assess co-localisation of FGFR3 with LAMP1.

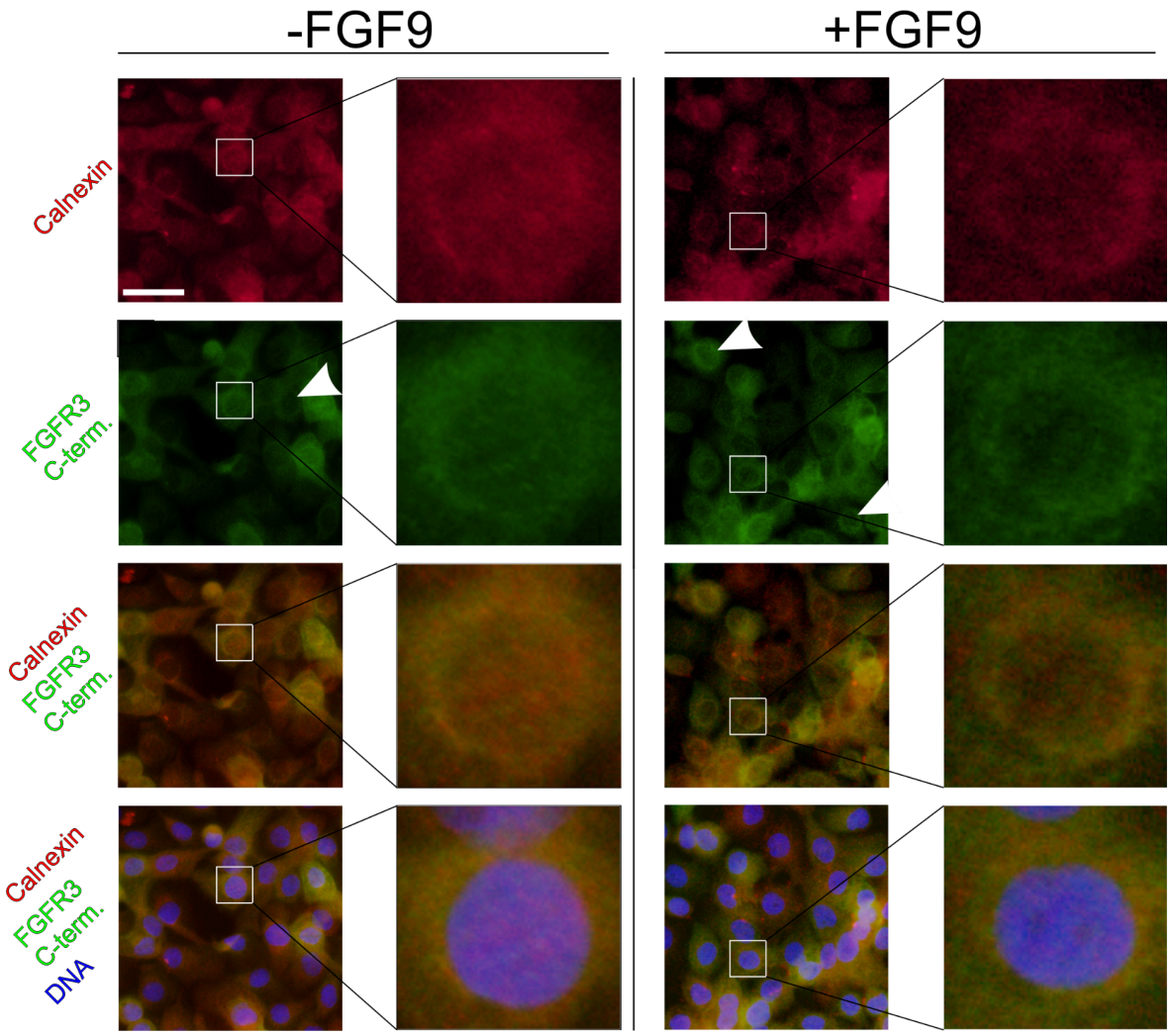

Figure 4.15 - Localisation of FGFR3 within NHU cells compared with endoplasmic reticulum marker calnexin - Calnexin shown in red, FGFR3 C-terminus shown in green, Hoechst 33258 DNA stain shown in blue. Scale bar (white line) represents 30 μm. White arrowheads illustrate cells with perinuclear FGFR3 localisation. Experiments were performed on NHU cell line Y1393 (single replicate). NHU cells were seeded at 30% visual confluence, then 24 h later indicated treatments were added. Cells were treated with t PD153035 for 72 h prior to addition of FGF9 for 30 minutes. From the point at which PD153035 was added to cells, NHU cultures were grown in Keratinocyte Serum-Free Medium supplemented with Cholera toxin only - no BPE or EGF was included. Cells were

simultaneously labelled with antibodies against Calnexin and the C-terminus of FGFR3, as well as Hoechst 33258 DNA stain, to assess co-localisation of FGFR3 with calnexin.

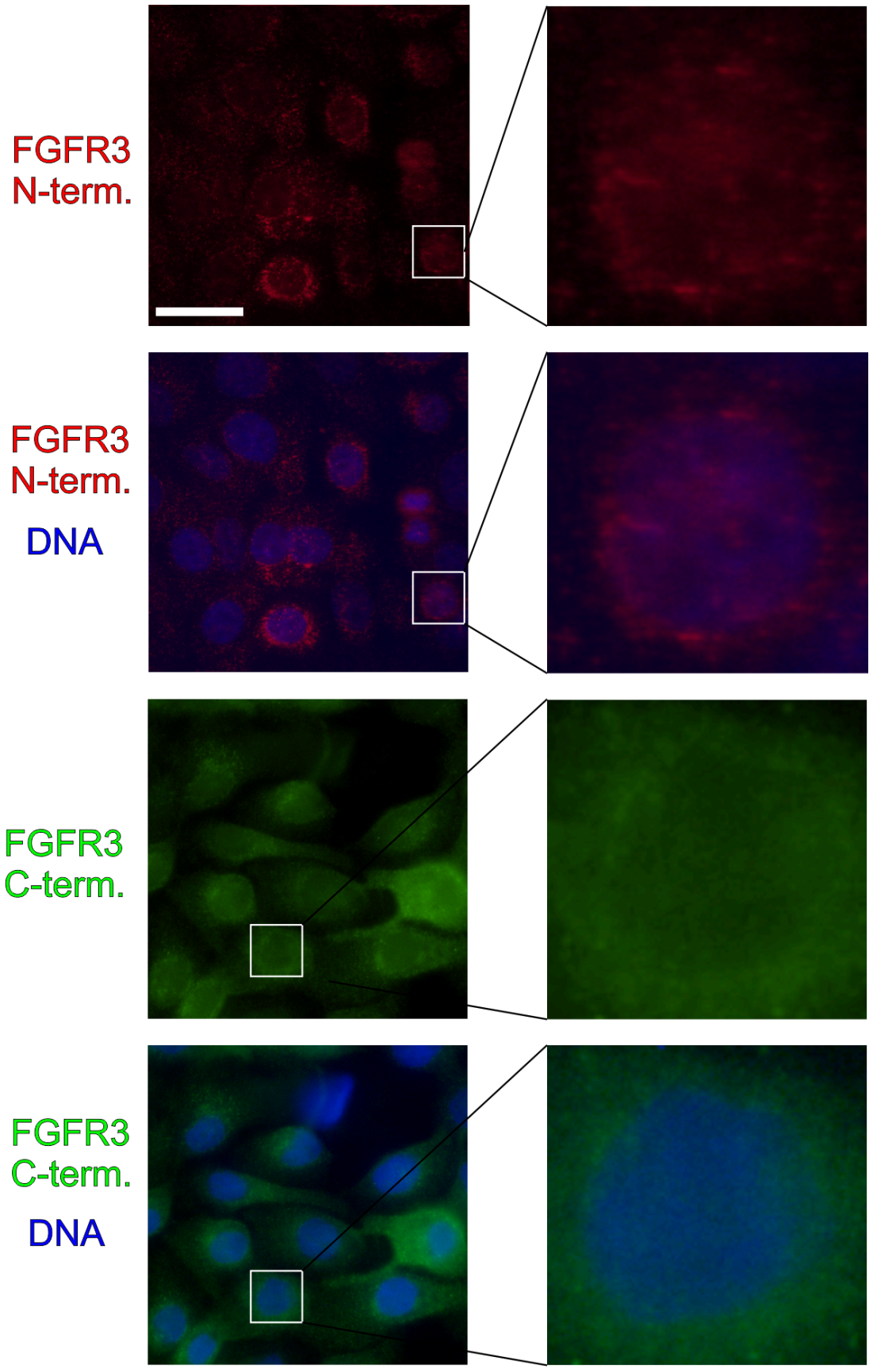

Figure 4.16 - Localisation of FGFR3 within RT112 positive control BLCA cell lines - FGFR3 N-terminus shown in red, FGFR3 C-terminus shown in green, Hoechst 33258 DNA stain shown in blue. Scale bar (white line) represents 30 μm. Images representative of a single replicate.

Localisation of calnexin and LAMP1 was compared in NHU cell cultures treated with DMSO or PD153035 and/or FGF9 to ensure that these experimental treatments did not inadvertently alter the localisation of LAMP1 or calnexin. LAMP1 and calnexin both showed a perinuclear localisation, although calnexin was more diffuse while LAMP1 was more tightly localised to the perinuclear region and had distinct punctae (Fig. 4.17). The localisations of LAMP1 and calnexin were not altered by the addition of PD153035 and/or FGF9.

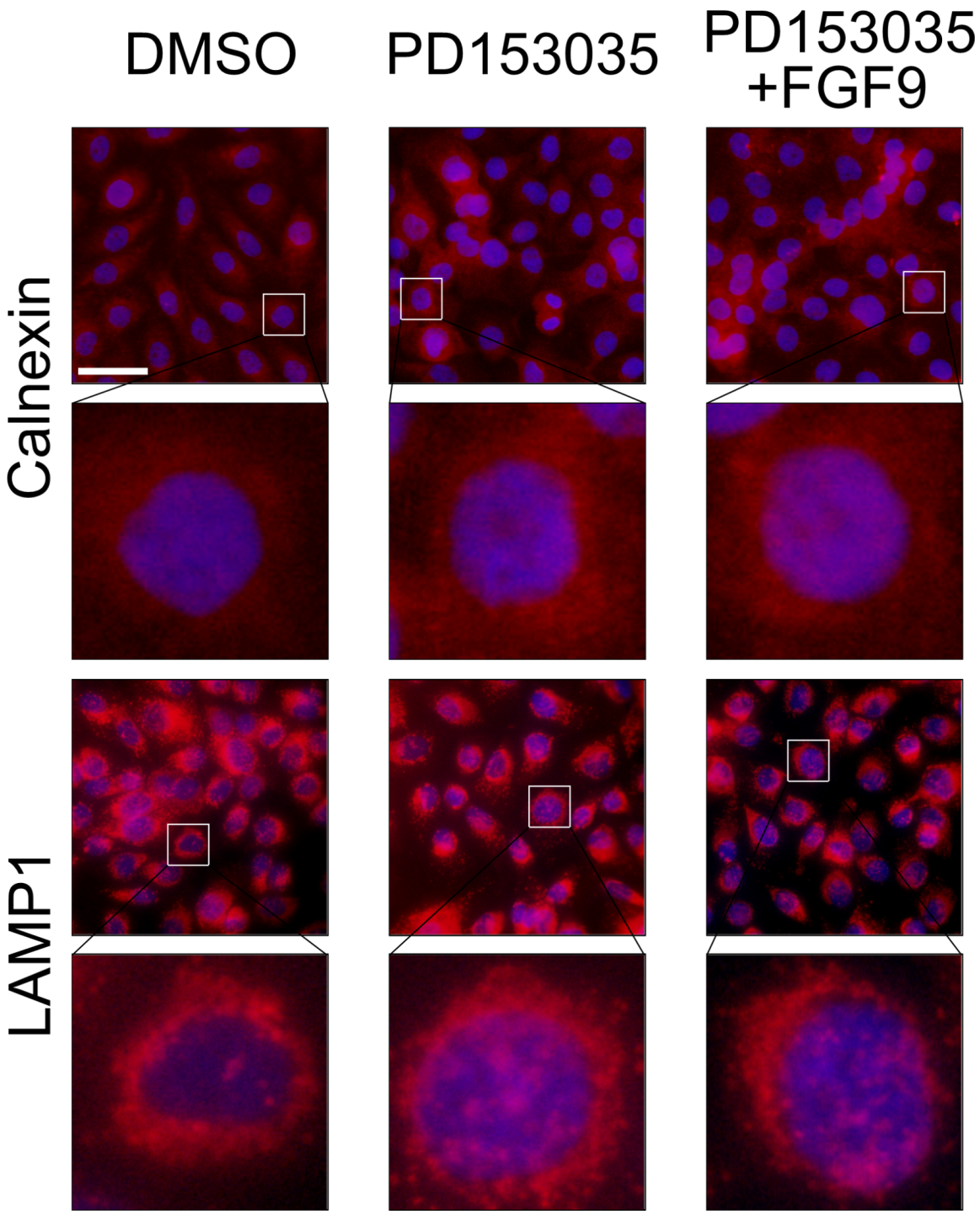

Figure 4.17 - Localisation of LAMP1 and Calnexin in NHU cells treated with and without PD153035 and FGF9 - LAMP1/Calnexin shown in red, Hoechst 33258 DNA stain shown in blue. Scale bar (white line) is 30 μm. Experiments were performed on NHU cell line Y1393 (single replicate).

4.4 - Summary

- When NHU cells derived from ureter or bladder were treated with the EGFR inhibitor PD153035, expression of *FGFR3* but not *FGFR1* or *FGFR2* increased significantly. Hence, EGFR inhibition specifically resulted in the expression of *FGFR3* over other FGFRs.
- FGF9 ligand was able to activate FGF9 protein expressed in FGFR3-expressing (EGFR-inhibited) NHU cells, as assessed by phosphorylation of FRS2.
- FRS2 was not phosphorylated without addition of FGF9.
- FRS2 phosphorylation following FGF9 addition peaked after 3 minutes before rapidly reducing, although was still detectable by western blotting at 120 minutes post-activation.
- ERK phosphorylation peaked at 5 minutes post-activation, but remained obvious at 120 minutes post-activation. Changes in AKT phosphorylation in response to FGFR3 activation was not detected.
- FGFR3 protein showed a diffuse cytoplasmic localisation in urothelial tissue and was evenly distributed throughout all layers of the urothelium, in line with previous reports.
- FGFR3 mean cell intensity was variable within NHU cell cultures, and although FGFR3 protein was detectable without EGFR inhibition, FGFR3 expression was significantly higher in cells which were EGFR-inhibited. Addition of FGF9 to activate FGFR3 reduced FGFR3 mean cell intensity by approximately 40% but did not alter FGFR3 localisation.
- Antibodies against the N- and C-termini of FGFR3 gave partially overlapping localisation both visually and quantitatively. Colocalisation of FGFR3 protein was greater with the endoplasmic reticulum marker calnexin than with the lysosomal marker LAMP1.

4.5 - Discussion

4.5.1 Signalling pathways activated downstream of FGFR3 in NHU cells

In the previous chapter it was observed that FGFR3 was expressed in NHU cells following EGFR inhibition. This FGFR3 was glycosylated, which suggested that it was trafficked through the Golgi Apparatus and Endoplasmic Reticulum, and thus may be functional. That speculation was confirmed in this chapter where it was shown that FGFR3 protein expressed in NHU cells following EGFR inhibition could be activated by addition of the FGFR3 ligand, FGF9. Additionally, slight FGFR3 activation (as measured by phosphorylation of FRS2) was observed with the addition of BPE. This is consistent with previous reports which suggest that FGFs are present within BPE [Gambarini and Armelin, 1982, Kent and Bomser, 2003].

A previous study examined FGFR3 activation with ligands in NHU cells and used retroviral transduction to obtain expression of FGFR3, rather than inhibition of EGFR [Di Martino et al., 2009]. In the 2009 study, the activation time frame of FRS2 downstream of FGFR3 activation was similar to that shown here, however ERK phosphorylation was much less stable - being severely reduced by 15 minutes post-activation. It is possible that this discrepancy could be explained by the differences in experimental setup; di Martino et al. used hTERT-immortalised NHU cells rather than the finite NHU cells used here, and they used FGF1 to activate FGFR3 rather than FGF9. Due to the fact that FGF1 activates all FGFRs, it is possible that some of their results were due to activation of other FGFRs, as they did not assess for expression/activation of other FGFs in their work. The possibility that other FGFRs confounded results here can be safely discounted, as EGFR inhibition with PD153035 was shown to significantly increase expression of only *FGFR3* transcript and not other FGFRs. Alternatively, Di Martino did not include any EGFR inhibition in their treatment of hTERT-immortalised NHU cells - thus it is possible that EGFR activation contributed to the ERK phosphorylation that they observed.

4.5.2 Variability of FGFR3 protein expression withinNHU cell cultures

FGFR3 expression was highly variable across NHU cells, suggesting that not all NHU cells in a culture respond to EGFR inhibition by expressing FGFR3 protein to the same degree. This revealed some FGFR3 protein expression in cells which were not EGFR inhibited, however FGFR3 mean cell intensity was significantly higher in cultures which

had been EGFR inhibited. This was not merely due to non-specific binding of antibodies, as appropriate negative controls were used and titration of antibodies was performed. These results suggest that cell confluence also regulates FGFR3 expression, which was also observed in Results Chapter 1. Previous literature has typically defined NHU cells as representing a homogenous population of cells. For example, Wezel et al., 2014 showed that when urothelial cells are isolated from the basal vs suprabasal portions of urothelium, these cells initially have different growth kinetics and expression of Nerve growth factor receptor (NGFR) when grown in culture. However, after 72-144 h, both basal and suprabasal NHU cell populations had equal growth kinetics and neither population displayed expression of HGFR. Furthermore, both cell populations were equally able to form a functional urothelial barrier and had comparable time to senescence. This would suggest that NHU cells *in vitro* represent a homogeneous population. However, it is not unreasonable to expect expression of certain proteins to vary between cells within a cell culture population. Cross et al., 2005 showed that expression of ZO-1, Occludin, Claudin 1, Claudin 4, CK13 and CK14 proteins were all variable across different cells within an NHU cell culture population when assessed by immunofluorescent imaging.

In Results Chapter 1 it was shown that growth of NHU cells past visual confluence led to a reduction in EGFR activity, as measured by phosphorylation of EGFR and ERK. This coincided with the expression of FGFR3 - hence confluence may trigger FGFR3 expression through the same mechanism as EGFR inhibition. Alternatively, cell confluence may influence FGFR3 expression through alternate mechanisms. A number of signalling pathways have previously shown to be regulated in some way by NHU cell confluence - for example SMAD3 phosphorylation [Fleming et al., 2012] and β-catenin signalling [Georgopoulos et al., 2014]. The ability of cell confluence to trigger FGFR3 expression (although the specific mechanism is unknown) could also explain why *FGFR3* transcript was expressed in urothelial tissue but not NHU cells (Chapter 3). In urothelial tissue cells are essentially always in a confluent state, although confluence in a cell culture context is unlikely to be a one-for-one for confluence in a tissue context.

There was a discrepancy between western blotting and immunofluorescence in terms of the amount of FGFR3 protein detected following activation with FGF9. When probed by western blotting, FGFR3 protein remained constant across the time measured, appearing the same at 3 minutes of FGF9 stimulation vs 30 minutes of FGF9 stimulation. When measured by immunofluorescence the amount of FGFR3 protein was 40% lower 30 minutes after FGF addition. This could potentially be due to a change in epitope availability following FGFR3 activation. This would impede antibody binding when

measuring immunofluorescence, but not in the denaturing conditions in which western blotting takes place.

The observation that FGFR N- and C-termini gave overlapping but distinct localisations is novel, as previous studies have performed indirect immunofluorescence using only one antibody directed against FGFR3. The FGFR3 N- and C-antibodies used here were both verified by western blot and observed FGFR3 expression patterns were supported by RNA-sequencing data. This gives confidence in the observations seen for FGFR3 protein in urothelial cells and tissues.

4.5.3 Localisation of FGFR3 in urothelium

Given that FGFR3 was able to phosphorylate FRS2 - a plasma membrane-bound transducer of FGFR3 signalling - it was expected that FGFR3 protein would be observed at the plasma membrane. However both in NHU cells and in urothelial tissue, FGFR3 appeared to be cytoplasmic/perinuclear rather than clearly localised to the plasma membrane. This is in opposition to the vast majority of studies which have previously examined FGFR3 activation, almost all of which have demonstrated that FGFR3 is present at the plasma membrane when activated [Lievens et al., 2004, Haugsten et al., 2005, Ben-Zvi et al., 2006, Degnin et al., 2011]. The fact that FRS2 became phosphorylated following FGF9 addition and the decrease in intensity of FGFR3 expression 30 minutes post-activation both support activation of FGFR3, even though a change in localisation was not seen. Although it is possible that FGFR3 could be signalling from inside the cell (for example from inside a recycling endosome [reviewed by Ceresa, 2021]), FGFR3 protein must still be at the plasma membrane to be activated by FGF9 in the extracellular environment. Thus, a more likely explanation is that FGFR3 was localised to the plasma membrane, but that this could not be visualised with the techniques used here. An additional way to verify FGFR3 localisation at the plasma membrane in future studies could be to compare FGFR3 localisation with that of a known plasma membrane marker (such as EGFR), similar to the use of LAMP1 and Calnexin as positional markers here.

It was expected, especially in NHU cells stimulated with FGF9, that FGFR3 would co-localise more with LAMP1, as FGFR3 has been reported to traffic to lysosomes following its activation [Monsonego-Ornan et al., 2002, Cho et al., 2003, Haugsten et al., 2005, Bonaventure et al., 2007]. Given that Calnexin is a marker for the endoplasmic reticulum, it was surprising to see an overlap in localisation with FGFR3. The endoplasmic

reticulum represents a location within cells where the initial stages of post-translational modification - particularly glycosylation - of proteins occurs. Typically proteins are trafficked out of the endoplasmic reticulum once modified, and proteins are only retained in the endoplasmic reticulum if they do not fold correctly or modification fails, at which point they are degraded [reviewed by Smirle et al., 2013]. The visual difference between FGFR3 colocalisation with LAMP1 and calnexin was also reflected quantitatively - the Pearson's R representing the correlation of localisation was much greater for FGFR3 and calnexin (average R = 0.788) than for FGFR3 and LAMP1 (average R = 0.567). In fact, for FGFR3 and calnexin the correlation approached that of FGFR3 N- and C-termini (average R = 0.845). Additionally, while M1 (the proportion of FGFR3 overlapping with other protein) was similar for LAMP1 and calnexin, M2 (the proportion of other protein overlapping with FGFR3) was much lower for LAMP1 than for FGFR3. This suggests that while most calnexin overlapped with FGFR3, there was a large proportion of LAMP1 which did not overlap with FGFR3, supporting the hypothesis that most FGFR3 was not present within lysosomes.

In the previous results chapter, deglycosylation of FGFR3 and western blotting supported the idea that non-glycosylated unmodified, immature and fully mature glycosylated species of FGFR3 are present in NHU cells following EGFR inhibition. In this chapter, FGFR3 was activated and could trigger a downstream signalling cascade. These results argue against FGFR3 being retained in the endoplasmic reticulum due to misfolding. Additionally, since FRS2 is located in lipid rafts in the plasma membrane, FGFR3 must be trafficked to the plasma membrane in order to phosphorylate FRS2 [Ridyard and Robins, 2003, Limpert et al., 2007]. A possible explanation for the colocalisation of FGFR3 with Calnexin could be that this FGFR3 represents a population of FGFR3 that is transiently passing through the endoplasmic reticulum. However, this would not explain why FGFR3 mean cell intensity decreased following FGF9 addition, as any FGFR3 in the endoplasmic reticulum would likely not be activated and thus not degraded.

Finally, it is interesting to compare the results found here with those of Lievens and Liboi, 2003. In their study, Lievens and Liboi showed that the FGFR3-K644E mutant is retained in the endoplasmic reticulum and does not mature to the cell surface. They also observed that FGFR3-K644E was active while retained in the endoplasmic reticulum and was able to phosphorylate STAT1. Interpretation of the observations found in this chapter in the context of this previous work could suggest that the FGFR3 seen here was also active from the endoplasmic reticulum of NHU cells. However, there are two problems with this theory. Firstly, Lievens and Liboi observed that whilst FGFR3-K644E was able to

phosphorylate STAT1 from the endoplasmic reticulum, it was unable to phosphorylate FRS2, which is anchored at the cell surface membrane. In contrast to this, it was seen here that activation of FGFR3 with FGF9 resulted in phosphorylation of FRS2. Secondly, for FGFR3 to be signalling from the endoplasmic reticulum in this study, FGF9 would have to have been internalised and transported to the endoplasmic reticulum in order to activate FGFR3, as FRS2 phosphorylation was only seen upon addition of FGF9.

4.5.4 Potential limitations of this study

When examining expression of FGFR3 protein in urothelial tissue via immunohistochemistry, it was not possible to directly compare the localisation of FGFR3 when visualised using N-terminal vs C-terminal antibodies, as was performed in NHU cells via immunofluorescence. This was because different donor tissues were used when examining FGFR3 protein expression with N-terminal vs C-terminal antibodies. In future, it would be beneficial to examine the localisation of N- and C-terminal FGFR3 protein within the same donor sample, in order to compare their relative localisations.

5. Effects of FGFR3 mutational activation in Bladder Cancer and urothelial cells

5.1 Aims and Objectives

Despite the lack of direct evidence that *FGFR3* mutation is able to drive urothelial proliferation, many have suggested that *FGFR3* mutation can lead to hyperplasia or tumour formation by driving tumour growth [di Martino et al., 2009, reviewed by Inamura et al., 2018]. Previous studies have used undifferentiated and proliferative BLCA or normal urothelial cell lines, or have been conducted in mice. Thus, no study has considered how *FGFR3* mutation interacts with the mitotically quiescent differentiated background in which *FGFR3* mutations are likely to occur *in situ*. To address this, *FGFR3* mutation was investigated in ABS-Ca^{2+} differentiated NHU cells. These differentiated NHU cells are mitotically quiescent and so provide a suitable context in which to investigate the potential effects of *FGFR3* mutation on urothelial proliferation, similar to the mitotically quiescent context in which *FGFR3* mutations may occur in urothelial tissue.

If *FGFR3* mutation is responsible for driving urothelium into a hyperplastic state, then it would be expected that in mitotically quiescent differentiated NHU cells, *FGFR3* mutation will drive cell cycle reentry and proliferation leading to a hyperproliferative state. In this chapter, this hypothesis was investigated by overexpression of *FGFR3-S249C* in NHU cells which were then differentiated. This approach was used as it was found in Chapter 3 that ABS-Ca^{2+} differentiated NHU cells did not express FGFR3 protein.
This led to the following objectives:

- Perform analysis of NMIBC and MIBC BLCA datasets to determine the relationship between *FGFR3* mutation status and expression of cell cycle-associated transcripts. Additionally, how does this relationship vary in NMIBC vs MIBC?
- Select NHU cell lines which overexpress *FGFR3-wild-type* and *FGFR3-S249C*. Following differentiation, examine whether FGFR3 mutant activity will force NHU cells back into cell cycle
- Following on from work in Chapter 4, examine the effects of *FGFR3* mutation on the localisation of FGFR3 protein within differentiated NHU cells

5.2 Experimental Design

5.2.1 Experimental use of *FGFR3*-transduced NHU cell lines

In order to investigate whether *FGFR3* mutation could influence proliferation in NHU cells, transduced cells were differentiated with ABS-Ca^{2+} treatment (ABS-Ca^{2+} differentiated NHU cells; hence referred to as “differentiated NHU cells”, Fig. 5.1). In addition, FGFR3 protein localisation in NHU cells was examined via immunofluorescence microscopy, and signalling downstream of FGFR3 was examined at the phospho-protein level. For the investigation of FGFR3 downstream signalling, NHU cells were treated with the EGFR inhibitor PD153035 for 30 minutes to eliminate ERK activity downstream of EGFR (Chapter 3). This allowed for examination of the contribution of FGFR3 alone to ERK activity. In Chapter 3 it was shown that FGFR3 protein was typically expressed in NHU cells following 48-72 h of EGFR inhibition - hence 30 minutes of EGFR inhibition used here would be unlikely to lead to expression of additional FGFR3 protein. Following EGFR inhibition, FGFR3 was activated by the addition of FGF9 (Chapter 4).
The ureter-derived NHU cells lines Y2654, Y2712 and Y2946 were used for transduction. The generation of FGFR3-expressing transduced NHU cells is covered in detail at the end of Chapter 2.

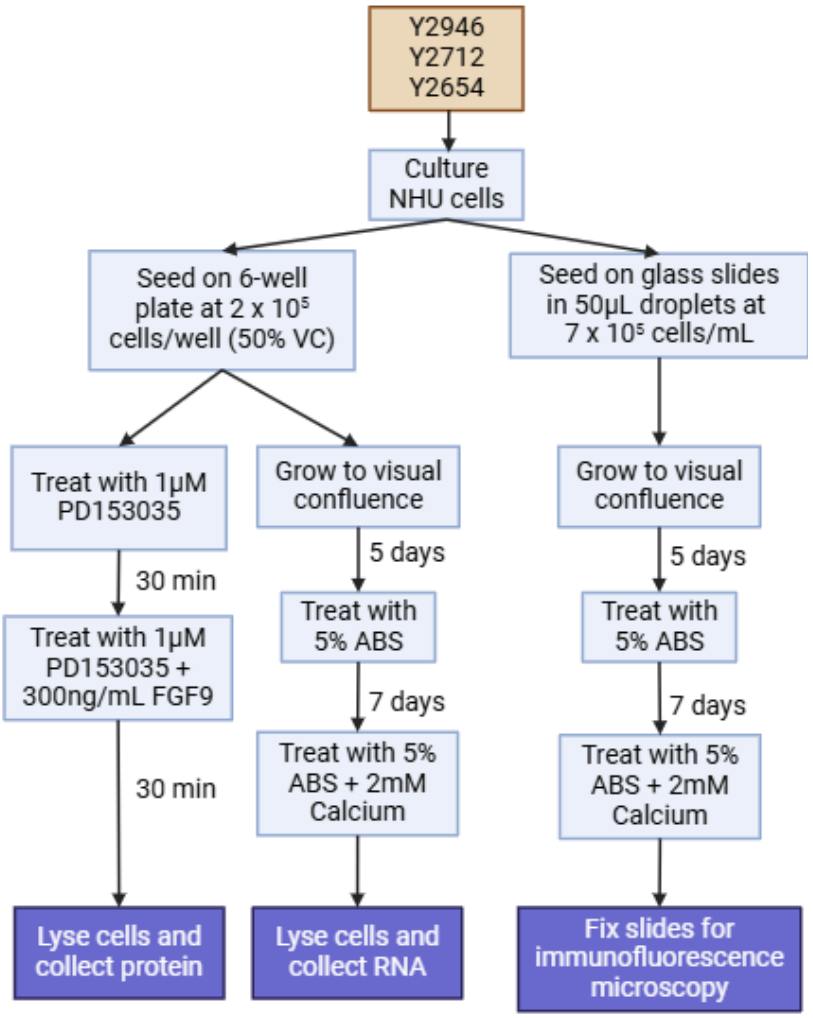

Figure 5.1 - Experimental schematic for treatment of *FGFR3*-overexpressing NHU cell lines - VC; visual confluence.

5.2.2 Use of *MKI67* transcript and Ki67 protein as markers of urothelial proliferation

Differentiation of NHU cells using serum and calcium has been shown to cause exit from the cell cycle and mitotic quiescence, with reported nuelcar Ki67 labelling indices of 1-3%. [Baker et al., 2022]. Thus *FGFR3*-overexpressing NHU cells were differentiated to assess whether FGFR3 mutation could force differentiated NHU cells to become proliferative, as would be expected if *FGFR3* mutation was a tumour-initiating event. Two methods were used to assess NHU cell proliferation, both involving the cell cycle marker *MKI67* [Gerdes et al., 1991].

MKI67 transcript was compared in pLXSP vector control, wild-type FGFR3 and FGFR3-S249C-overexpressing differentiated NHU cells using quantitative

reverse-transcriptase (RT) PCR. RT-negative controls were included to confirm lack of non-specific amplification and/or genomic DNA contamination. The number of cycles required to amplify *MKI67* transcript in each case was normalised to the housekeeping gene *GAPDH* to control for loading of RNA, RNA concentration and cell density.
Ki67 protein was measured by immunofluorescence in pLXSP vector control, wild-type FGFR3 and FGFR3-S249C overexpressing differentiated NHU cells. This was used to calculate a “Nuclear Ki67 index”, expressed as the percentage of nuclei which were positive for Ki67 expression. This nuclear Ki67 index was used as a measure of the percentage of cells which were in cell cycle. The nuclear Ki67 index was also calculated for three non-transduced, undifferentiated NHU cell control cultures at visual confluence.

5.2.3 Assessment of proliferation status in bladder cancer cohorts

To test if *FGFR3* mutation was associated with increased tumour cell cycle activity, RNA expression of a panel of cell cycle-associated genes (*MKI67, MCM2, PLK1, BUB1, PCNA* and *E2F*) selected from the literature (Table 5.1) [reviewed by Jurikova et al., 2016] was investigated in *FGFR3* wild-type vs *FGFR3* mutant tumours from the UROMOL NMIBC [Lindskrog et al., 2021] and TCGA MIBC [Robertson et al., 2017] cohorts. The six genes chosen have roles in DNA replication, cell division or cell cycle progression, are expressed in cells going through the cell cycle, and their expression has been shown to correlate with cell division rates [Perou et al., 1999, Cho et al., 2001, Whitfield et al., 2012, Locard-Paulet et al., 2022]. In addition, all six proliferation marker genes were verified against the online database of cell cycle-associated genes Cyclebase, which showed that expression of the selected genes peaked at various points of the cell cycle [Santos et al., 2015].

Table 5.1 - Genes chosen as markers of cell cycle activity

Gene	Cell cycle expression	References
BUB1	Peaks in M phase	Davenport et al., 1999, Whitfield et al., 2002, Santos et al., 2015
E2F1	Peaks in G1/S phase	Whitfield et al., 2002, Balciunaite et al., 2005, Santos et al., 2015
MCM2	Peaks in G1/S phase	Perou et al., 1999, Whitfield

		et al., 2002, Whitfield et al., 2002, Santos et al., 2015
MKI67	Peaks in G2/M phase	Gerdes et al., 1991, Perou et al., 1999, Ross et al., 2000, Santos et al., 2015
PCNA	Peaks in G1/S phase	Cho et al., 2001, Whitfield et al., 2002, Santos et al., 2015
PLK1	Peaks in M phase	Cho et al., 2001, Whitfield et al., 2002, Santos et al., 2015

As well as comparing the expression of cell cycle-associated genes between all *FGFR3* wild-type and mutant tumours, tumours were also stratified based on molecular subtype, stage and grade. This was to distinguish the effects of *FGFR3* mutation from the effects of tumour molecular subtype etc, to see if *FGFR3* mutation was independently associated with proliferation marker expression in NMIBC and MIBC tumours. When comparing *FGFR3* mutant and wild-type tumours by molecular subtype, for UROMOL tumours all subtypes were considered. However for TCGA tumours only Luminal Papillary (LumP) and Basal/Squamous (Ba/Sq) tumours were assessed, as other subtypes did not contain enough *FGFR3* mutant tumours for statistical analysis.

5.3 Results

5.3.1 Phenotype of FGFR3-overexpressing NHU cells in culture

NHU cell lines were generated which overexpressed a pLXSP vector control, wild-type FGFR3 (FGFR3-WT), or mutant-active FGFR3 (FGFR3-S249C). Three independent NHU cell lines derived from ureter tissue were transduced: Y2946, Y2653, and Y2712. pLXSP vector control was included to account for the effect of transduction and selection alone on NHU cells.

In general, undifferentiated FGFR3-overexpressing cells appeared healthy and indistinguishable from non-transduced NHU cells. There was a variation in cell size, with transduced cells sometimes appearing larger and more vacuolar (Fig. 5.2, white arrowheads). These observations were the same for NHU cells which were transduced with *FGFR3* as well as NHU cells which were transduced with pLXSP vector only. FGFR3-expressing cells did not show obvious gaps between cells or become stratified at confluence (Fig. 5.2, black arrowheads)
When transduced NHU cells were differentiated, cells became stratified with some floating cells as has previously been demonstrated for non-transduced NHU cells (Fig 5.3, white arrowheads). While there was some variation in cell appearance between NHU cell lines, FGFR3-overexpressing cells were not different in appearance from pLXSP vector controls (Fig. 5.3).

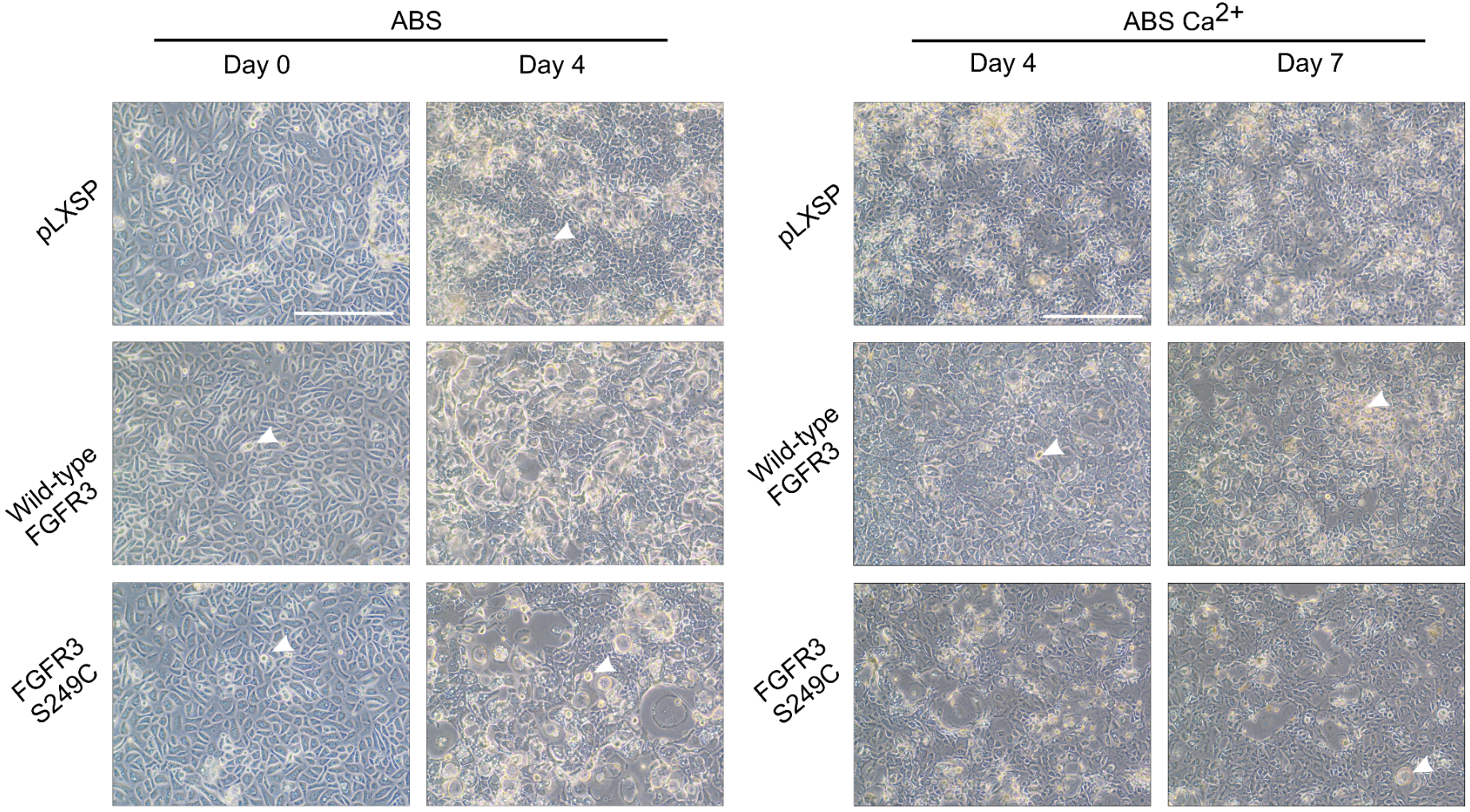

Figure 5.2 - Phase contrast images of undifferentiated transduced NHU cells in culture - Scale bar is 200 μm. White arrowheads mark large vacuolar cells. Tight cell junctions without gaps are marked with black arrowheads.

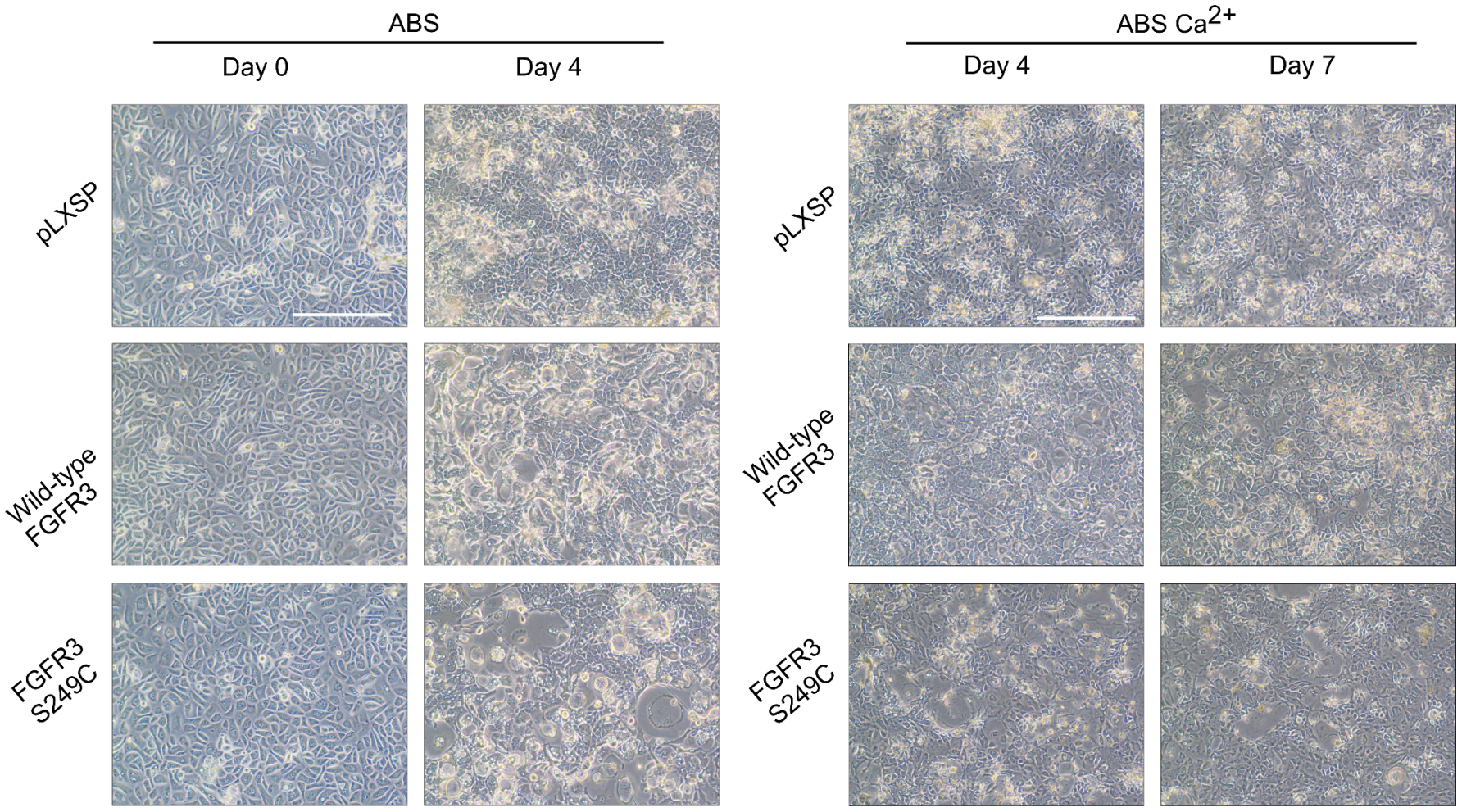

Figure 5.3 - Phase contrast images of Y2946 transduced NHU cells in culture during differentiation - Scale bar is 200 µm. Images are representative of all three transduced NHU cell lines. Floating cells are marked with white arrowheads.

5.3.2 Assessment of FGFR3 protein overexpression and activity in transduced NHU cells

Western blotting confirmed that FGFR3 protein was over-expressed in wild-type FGFR3 and FGFR3 S249C mutant transduced NHU cell lines, as well as a lack of FGFR3 protein expression in the pLXSP vector control (Fig. 5.4a). FRS2 was phosphorylated only in the presence of FGF9 in wild-type FGFR3 NHU cells, but was phosphorylated regardless of FGF9 addition in FGFR3 S249C NHU cells, confirming the presence of the activating S249C mutation (Fig. 5.4a-b).

Transduced NHU cells were treated with PD153035 to inhibit EGFR activity and prevent autocrine phosphorylation of ERK. This showed that wild-type FGFR3 was able to phosphorylate ERK when activated by FGF9, but S249C FGFR3 was able to phosphorylate ERK regardless of FGF9 addition (Fig. 5.4c).

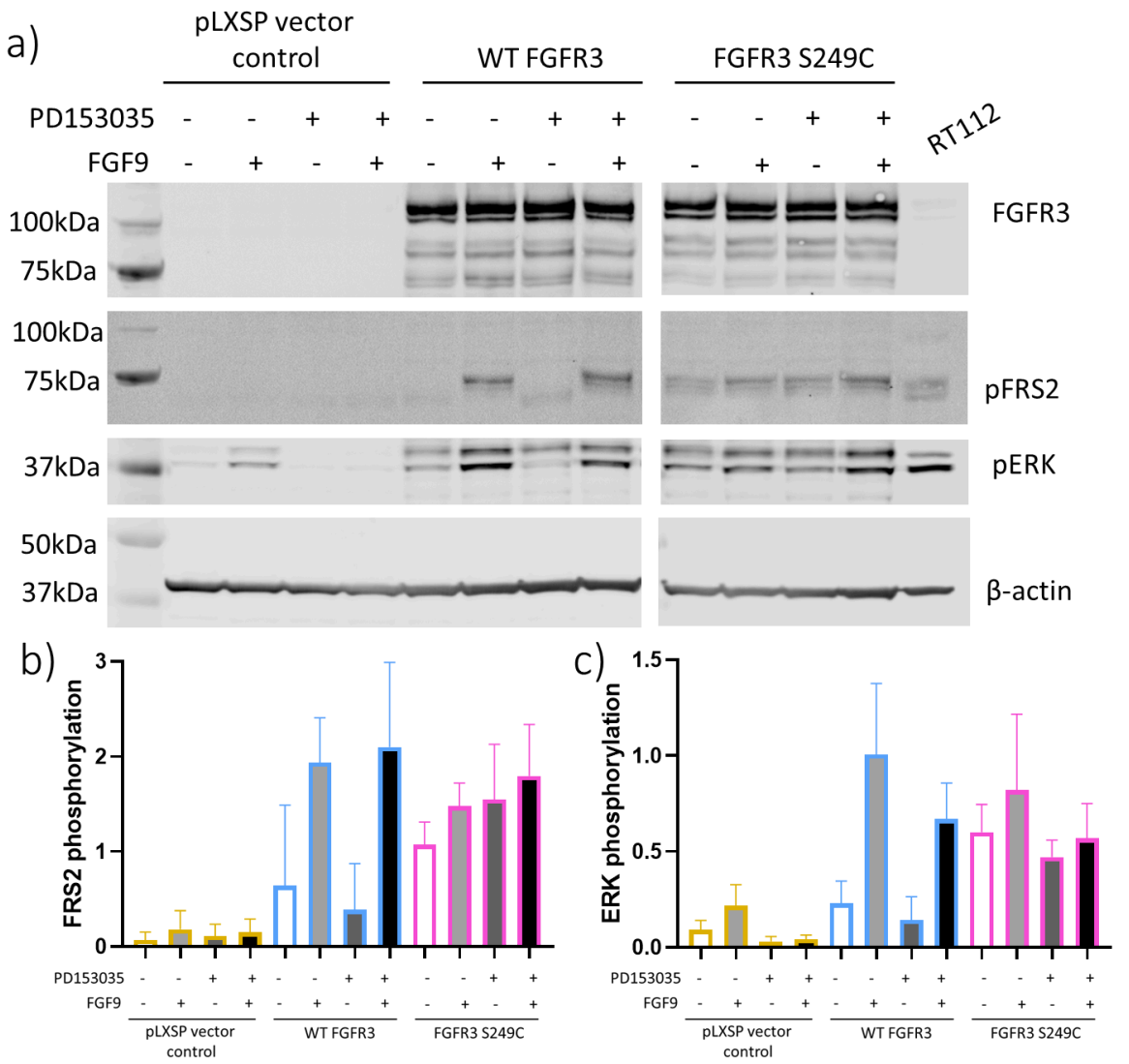

Figure 5.4 - Expression and activation of FGFR3 in transduced NHU cells - β-actin was blotted as a loading control to ensure equal protein between lanes. Lysate from RT112 BLCA cell line was loaded as a positive control for FGFR3 expression and activity; RT112 FGFR3 expression was much lower than FGFR3-overexpressing NHU cells. PD13035 EGFR inhibitor was added for 30 minutes at 1 μM to reduce ERK phosphorylation downstream of EGFR activity, followed by 30 minutes of PD153035 plus FGF9 at 300 ng/mL for 30 minutes to activate FGFR3. For densitometry purposes, phosphorylation of ERK and FRS2 in NHU cells was normalised to an RT112 control lysate. Independent experiments were performed in NHU cell lines Y2946, Y2653 and Y2712 - Y2712 is shown in (a) and data from multiple lines are compiled in (b) and (c). FRS2 phosphorylation was not verified for Y2653. Error bars represent standard deviation.

5.3.3 Overexpression of wild-type or S249C mutant FGFR3 did not significantly alter proliferation of differentiated NHU cells

Differentiated NHU cells which overexpressed wild-type or S249C constitutively-active FGFR3 did not show significantly increased expression of *MKI67,* and in 2 out of 3 NHU cell lines assessed, *MKI67* expression was lower when FGFR3 was expressed versus the vector-only control (Fig. 5.5). Hence, overexpression of *FGFR3-S249C* was insufficient to drive proliferation in mitotically-quiescent differentiated NHU cells.

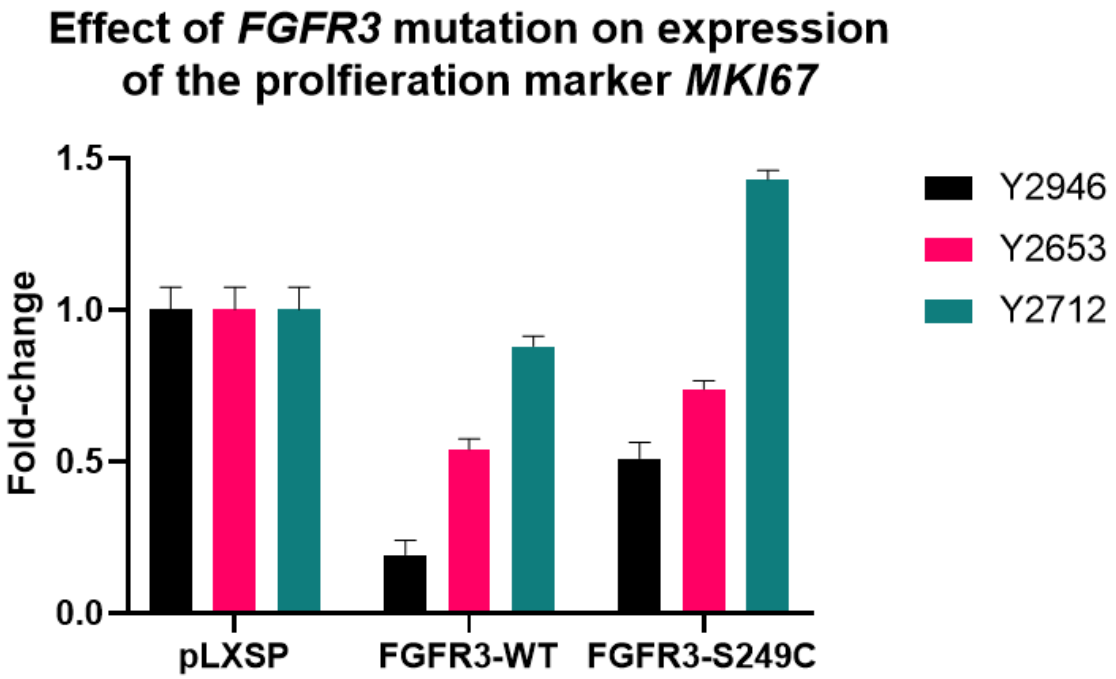

Figure 5.5 - Expression of proliferation marker *MKI67* was not significantly changed by overexpression of wild-type or S249C mutant FGFR3 vs vector-only controls - Each NHU cell line was tested with three technical replicates - error bars represent one standard deviation on the mean. The number of cycles required to amplify *MKI67* transcript in each case was normalised to the housekeeping gene *GAPDH* to control for loading of RNA, RNA concentration and cell density. Fold change was calculated by normalising *MKI67* expression in FGFR3-WT and FGFR3-S249C expressing cells to pLXSP-expressing cells for each cell line.

Overexpression of wild-type or S249C FGFR3 also did not significantly alter the percentage of cells with Ki67-positive nuclei (Fig. 5.6). Transduced NHU cells which were differentiated had a mean nuclear Ki67 index of 3.30%, compared with a mean of 49.9% in three non-transduced, undifferentiated reference NHU cell cultures grown to visual

confluence (Fig. 5.6). Hence, overexpression of *FGFR3-S249C* in differentiated NHU cells was insufficient to drive an increase in nuclear Ki67 index to proliferative levels.

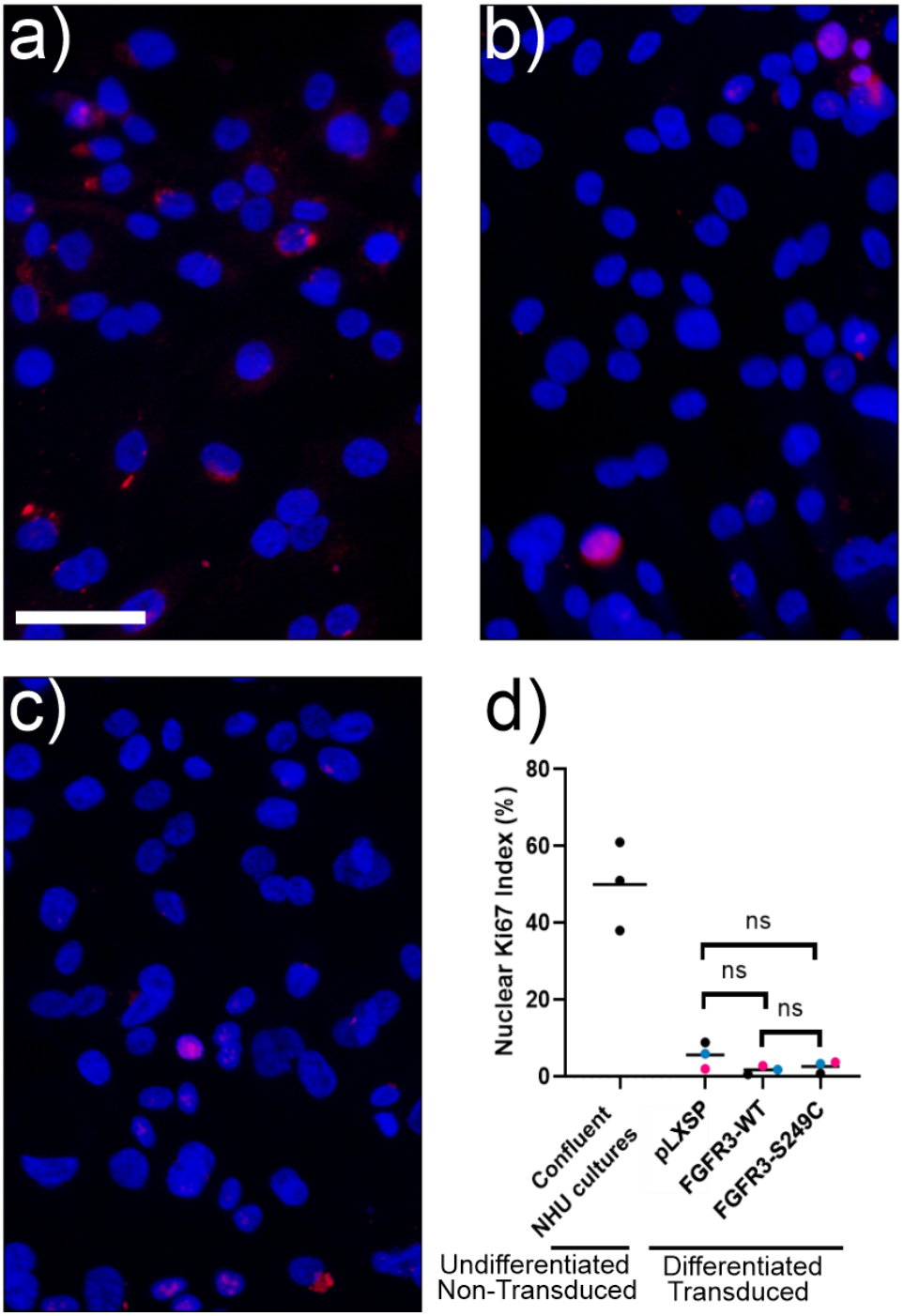

Figure 5.6 - Nuclear Ki67 index of transduced differentiated NHU cells was not significantly changed by overexpression of wild-type or S249C mutant FGFR3 vs vector-only controls - Indirect immunofluorescence labelling of Ki67 (red) in (a) pLXSP, (b) FGFR3-WT or (c) FGFR3-S249C transduced ABS-Ca^{2+} differentiated NHU cells, (d) Nuclear Ki67 index, expressed as percentage of cell nuclei positively labelled for Ki67. DNA was labelled with Hoechst 33258 (blue). Scale bar (white line) represents 30 μm.

Black line represents the mean. Each dot represents the percentage of cells with Ki67-positive nuclei; Transduced NHU cell lines (right) are distinguished by colour. Dunn's multiple comparisons test was used to determine statistical significance. Images are representative of three transduced NHU cell lines. Nuclear Ki67 index was calculated for three reference confluent cultures (Y1237, Y1393 and Y2324). These cultures were undifferentiated and had not been transduced.

5.3.4 Localisation of mutant FGFR3 and wild-type FGFR3 in differentiated NHU cells

FGFR3 protein localisation was assessed using antibodies against the N- and C-terminus of the FGFR3 protein. No FGFR3 protein was detected in the pLXSP control cells (Fig. 5.10).

Both N- and C-terminal FGFR3 had a similar localisation, appearing to be concentrated in the perinuclear region (Fig. 5.7 and 5.8). Intensity of both N- and C-terminal FGFR3 was variable between cells, suggesting that NHU cells in a population did not have uniform expression of FGFR3.

N-terminal FGFR3 protein appeared to be particularly concentrated around the perinuclear region of NHU cells, with clear punctae throughout the cell (Fig. 5.7). FGFR3 localisation did not appear different in NHU cells expressing FGFR3-WT compared to those expressing FGFR3-S249C. C-terminal FGFR3 appeared less concentrated in the perinuclear region and more cytoplasmic than N-terminal FGFR (Fig. 5.8). In addition, the number of punctae throughout the cell appeared much greater for C-terminal FGFR3 than N-terminal FGFR3. Thus, *FGFR3* mutation status did not influence the localisation of FGFR3 protein within differentiated NHU cells.

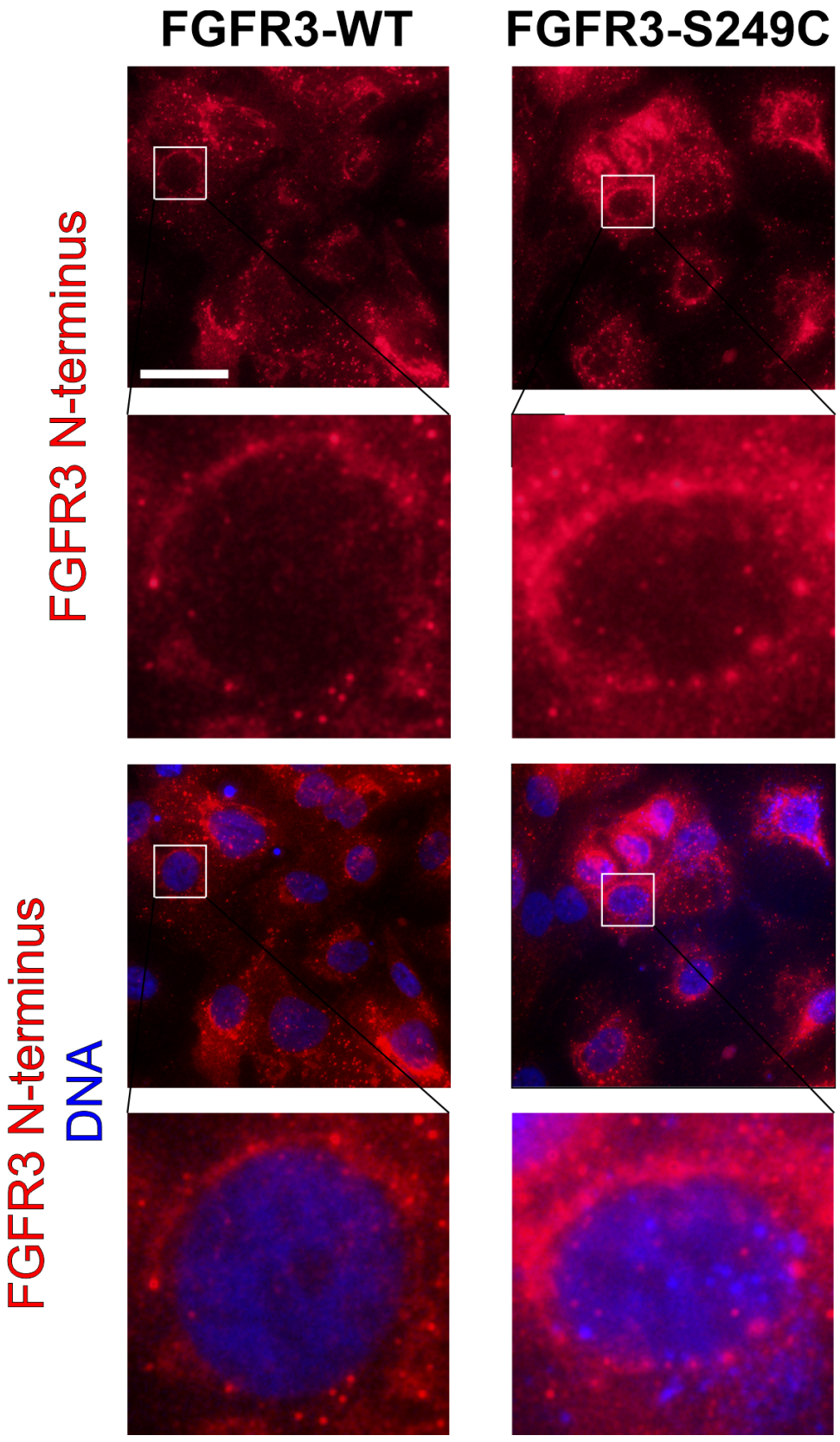

Figure 5.7 - N-terminal localisation of both wild-type and S249C mutant FGFR3 protein was perinuclear in differentiated NHU cells - FGFR3 N-terminus shown in red, Hoechst 33258 DNA stain shown in blue. Scale bar (white line) represents 30 μm. Experiments were performed on NHU cell line Y2946 (single replicate). Images taken in

pLXSP, FGFR3-WT and FGFR3-S249C conditions used matched exposure times. Cells were permeabilised prior to fixation.

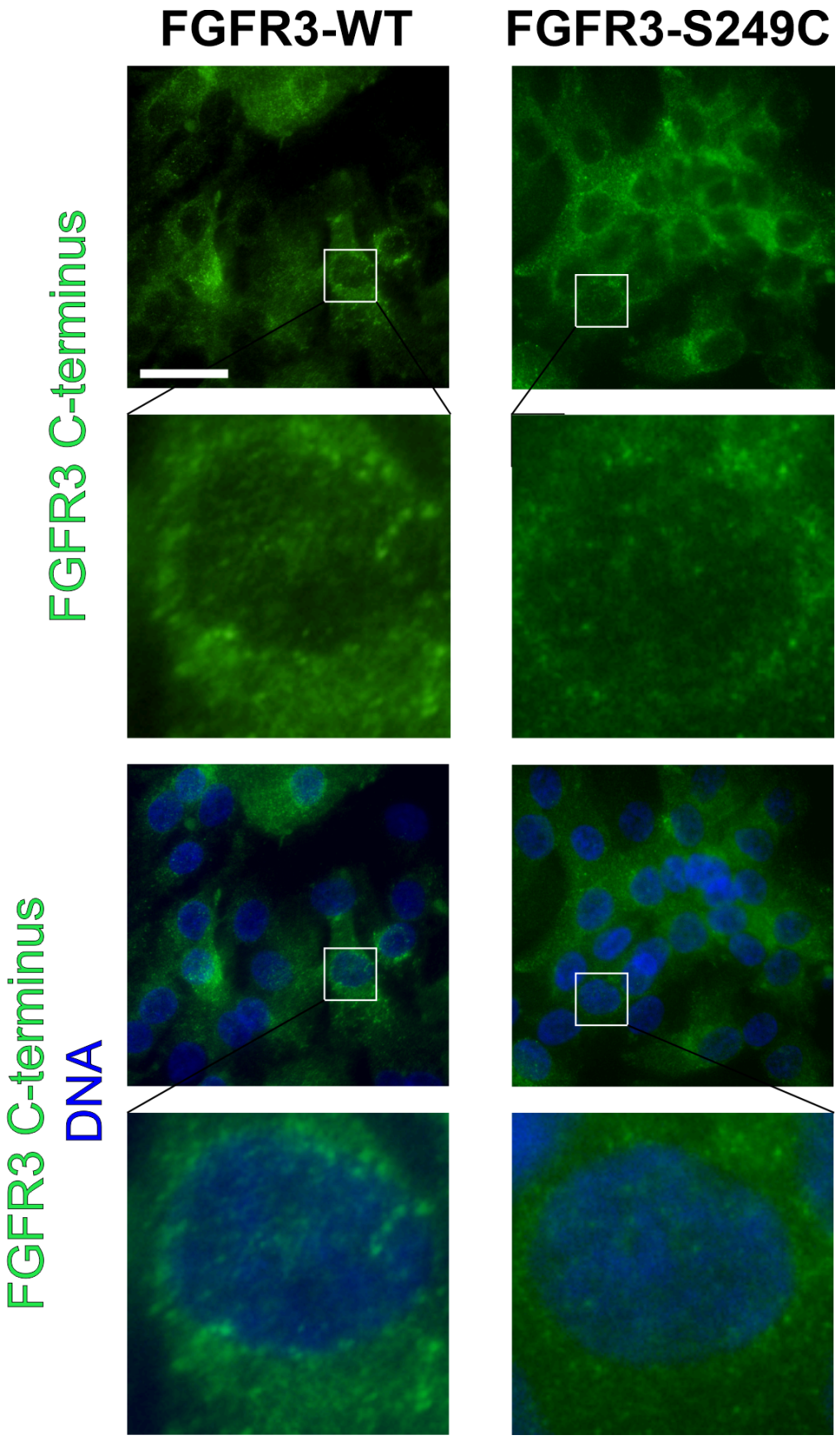

Figure 5.8 - C-terminal localisation of both wild-type and S249C mutant FGFR3 protein was cytoplasmic and perinuclear in differentiated NHU cells - FGFR3 C-terminus shown in green, Hoechst 33258 DNA stain shown in blue Scale bar (white line) represents 30 µm. Experiments were performed on NHU cell line Y2946 (single replicate). Images taken in pLXSP, FGFR3-WT and FGFR3-S249C conditions used matched exposure times. Cells were permeabilised prior to fixation.

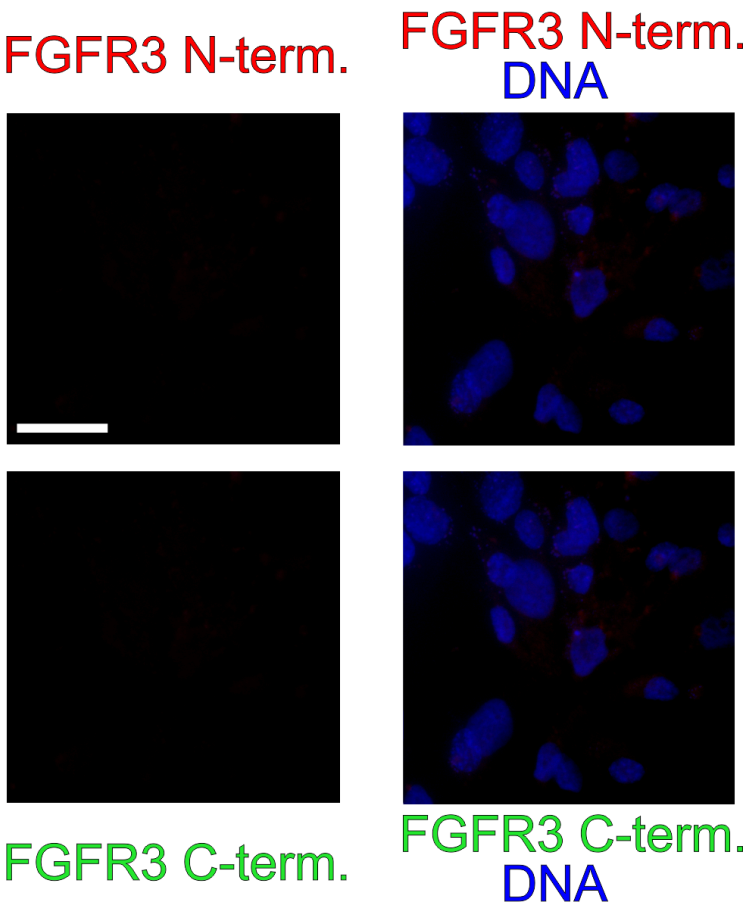

Figure 5.9 - FGFR3 immunofluorescence in pLXSP vector-only control NHU cells - FGFR3 N-terminus shown in red, FGFR3 C-terminus shown in green, Hoechst 33258 DNA stain shown in blue. Scale bar (white line) represents 30 µm. Experiments were performed on NHU cell line Y2946 (single replicate). Images taken in pLXSP, FGFR3-WT and FGFR3-S249C conditions used matched exposure times. Cells were permeabilised prior to fixation.

5.3.5 *FGFR3* mutations were associated with significantly lower expression of cell cycle-associated transcripts in NMIBC and MIBC

In UROMOL NMIBC tumours *FGFR3* mutation was associated with significantly lower expression of all six cell cycle-associated transcripts when all tumours were compared (Fig. 5.10).

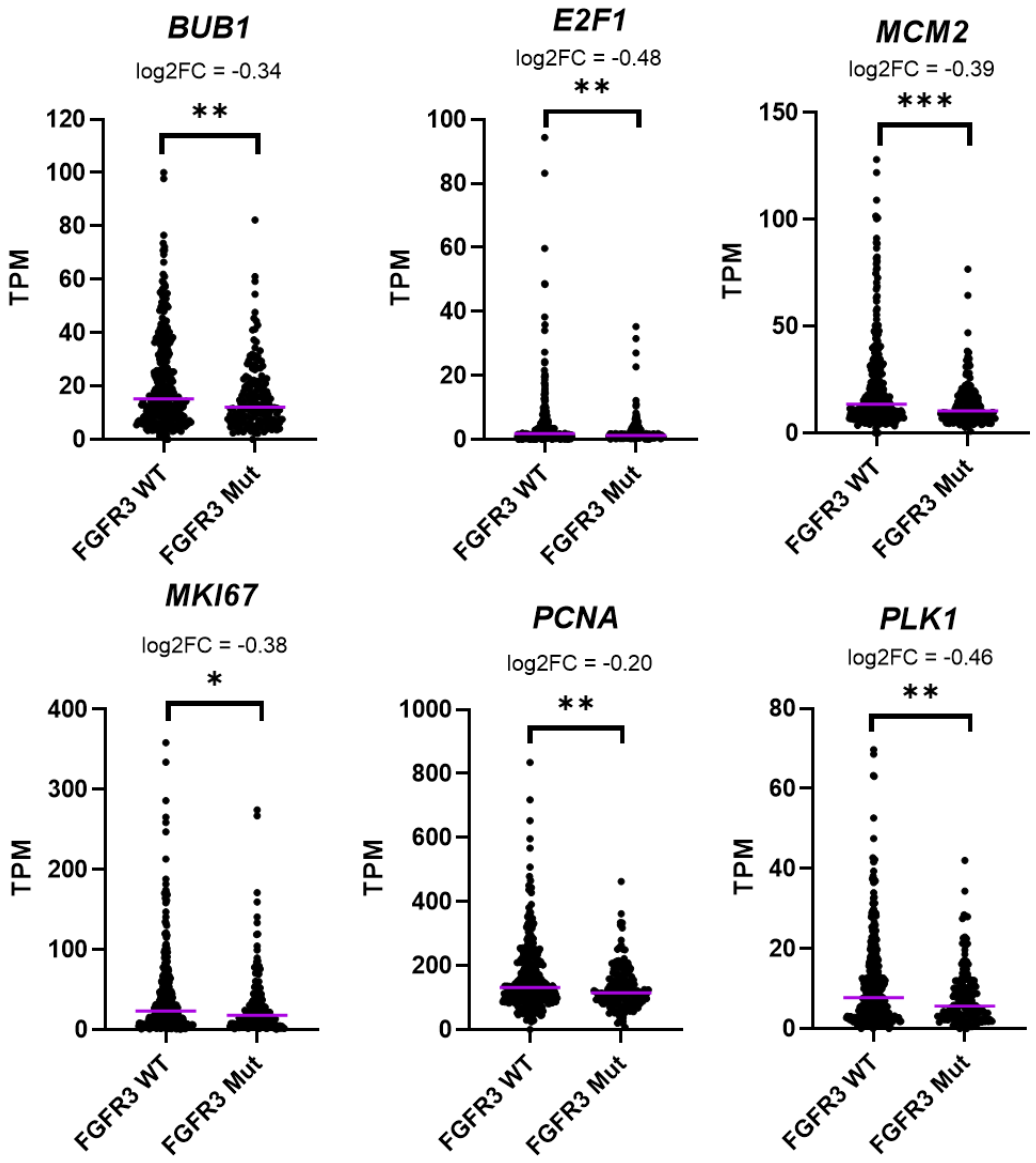

Figure 5.10 - *FGFR3* mutations were associated with significantly lower expression of cell cycle-associated transcripts in UROMOL NMIBC tumours - Kruskal-Wallis test was used to determine statistical significance. log2FC represents the log2 fold-change on the median for *FGFR3* wild-type versus *FGFR3* mutant tumours. Purple line represents the median value. Analysis included 334 *FGFR3* wild-type and 171 *FGFR3* mutant tumours.

When NMIBC tumours were stratified by molecular subtype, *FGFR3* mutation was associated with lower expression of cell cycle transcripts mostly in Class 2a, although *FGFR3* mutation itself was associated with Class 1 and Class 3 tumours (Fig. 5.11). In the other molecular subtypes present in the UROMOL cohort, median expression of the six cell cycle-associated transcript was lower than Class 2a, and *FGFR3* mutations were not associated with lower expression.

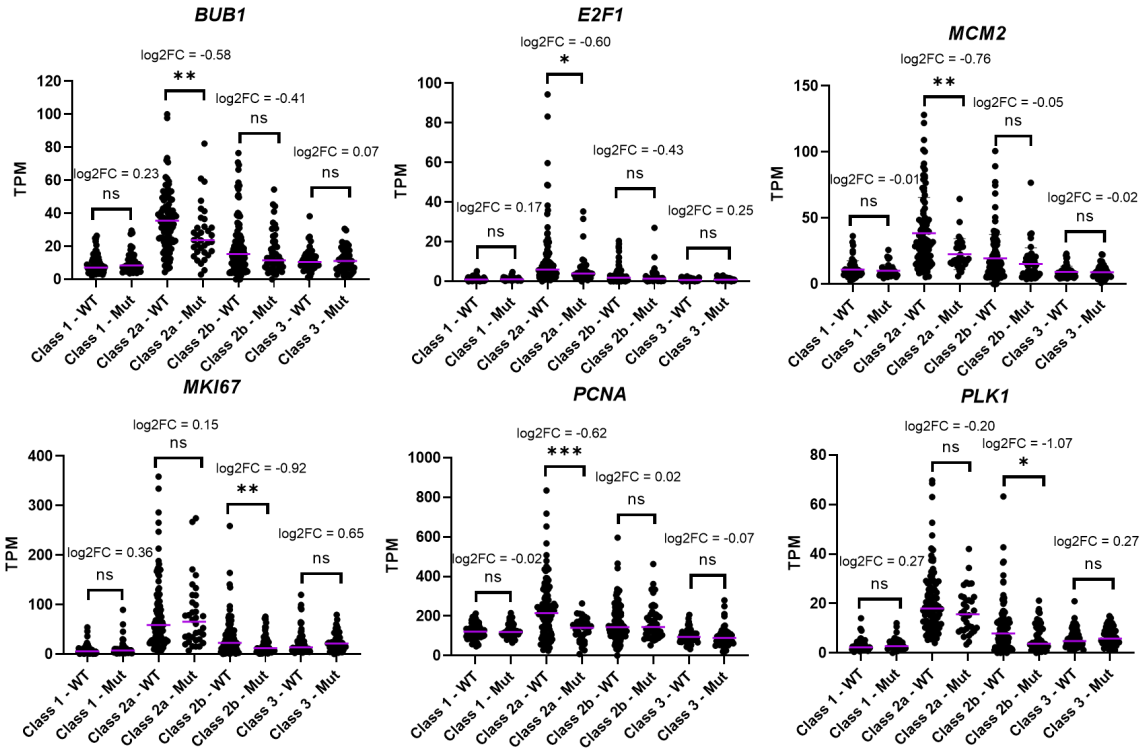

Figure 5.11 - *FGFR3* mutations were associated with significantly lower expression of cell cycle-associated transcripts in Class 2a and Class 2b UROMOL NMIBC tumours - Kruskal-Wallis test was used to determine statistical significance. log2FC represents the log2 fold-change on the median for *FGFR3* wild-type versus *FGFR3* mutant tumours. Purple line represents the median value. Class 1 tumours contained 63 *FGFR3* wild-type tumours and 36 *FGFR3* mutant tumours, Class 2a contained 103 *FGFR3* wild-type tumours and 34 *FGFR3* mutant tumours, Class 2b contained 111 *FGFR3* wild-type tumours and 50 *FGFR3* mutant tumours, Class 3 contained 55 *FGFR3* wild-type tumours and 51 *FGFR3* mutant tumours.

When tumours were grouped by stage (Ta and T1), *FGFR3* mutation was associated with significantly lower expression of cell cycle transcripts in T1 tumours (Fig. 5.12). Ta tumours had lower median expression of cell cycle transcripts, and there was no

difference in cell cycle transcript expression whether *FGFR3* was mutated or not. In T1 tumours cell cycle transcript expression was higher, and *FGFR3* mutations were associated with significantly lower expression of cell cycle transcripts (although still higher than in Ta tumours). A similar pattern was seen when tumours were stratified by grade (low-grade and high-grade; Fig. 5.13).

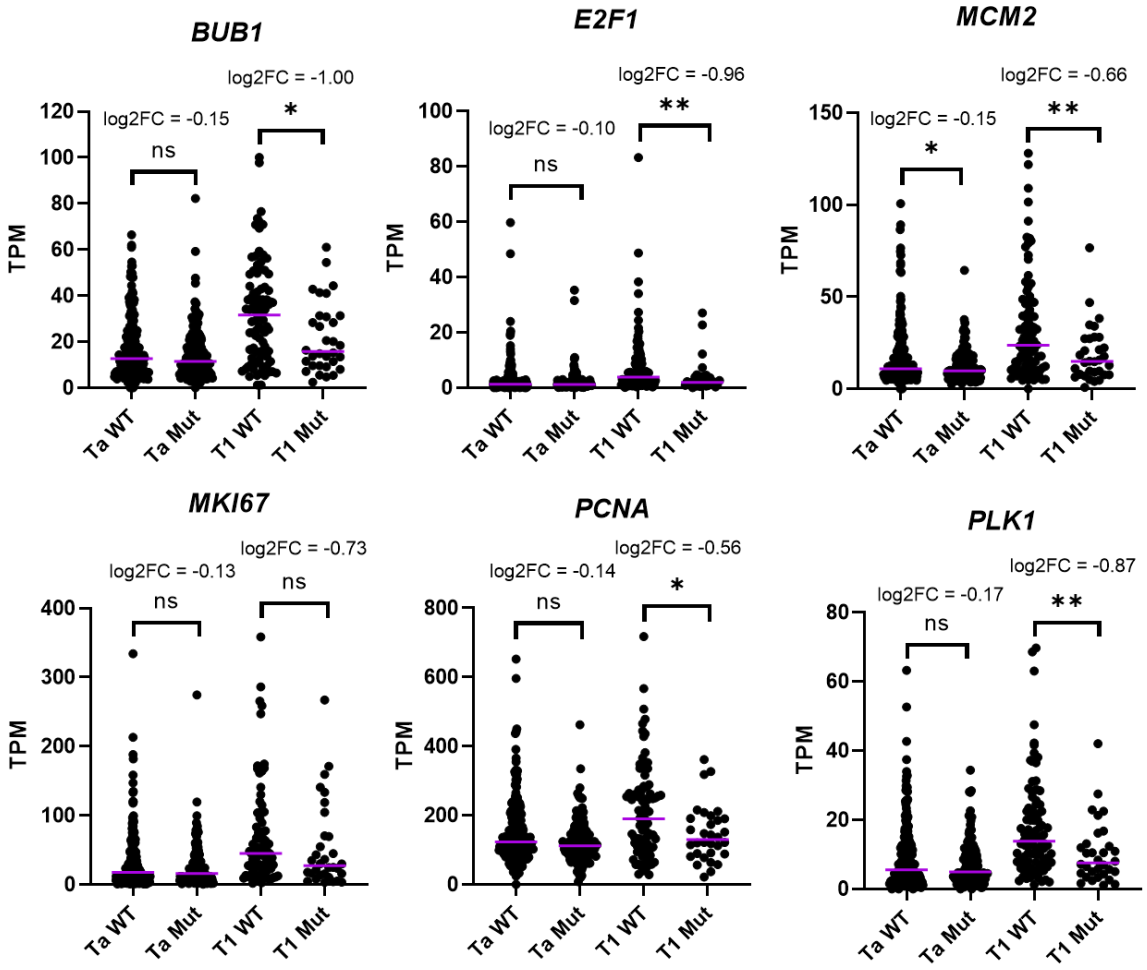

Figure 5.12 - *FGFR3* mutations were associated with significantly lower expression of cell cycle-associated transcripts in Stage T1 UROMOL NMIBC tumours - Kruskal-Wallis test was used to determine statistical significance. log2FC represents the log2 fold-change on the median for *FGFR3* wild-type versus *FGFR3* mutant tumours. Purple line represents the median value. Ta tumours contained 240 *FGFR3* wild-type tumours and 139 *FGFR3* mutant tumours, T1 tumours contained 90 *FGFR3* wild-type tumours and 32 *FGFR3* mutant tumours.

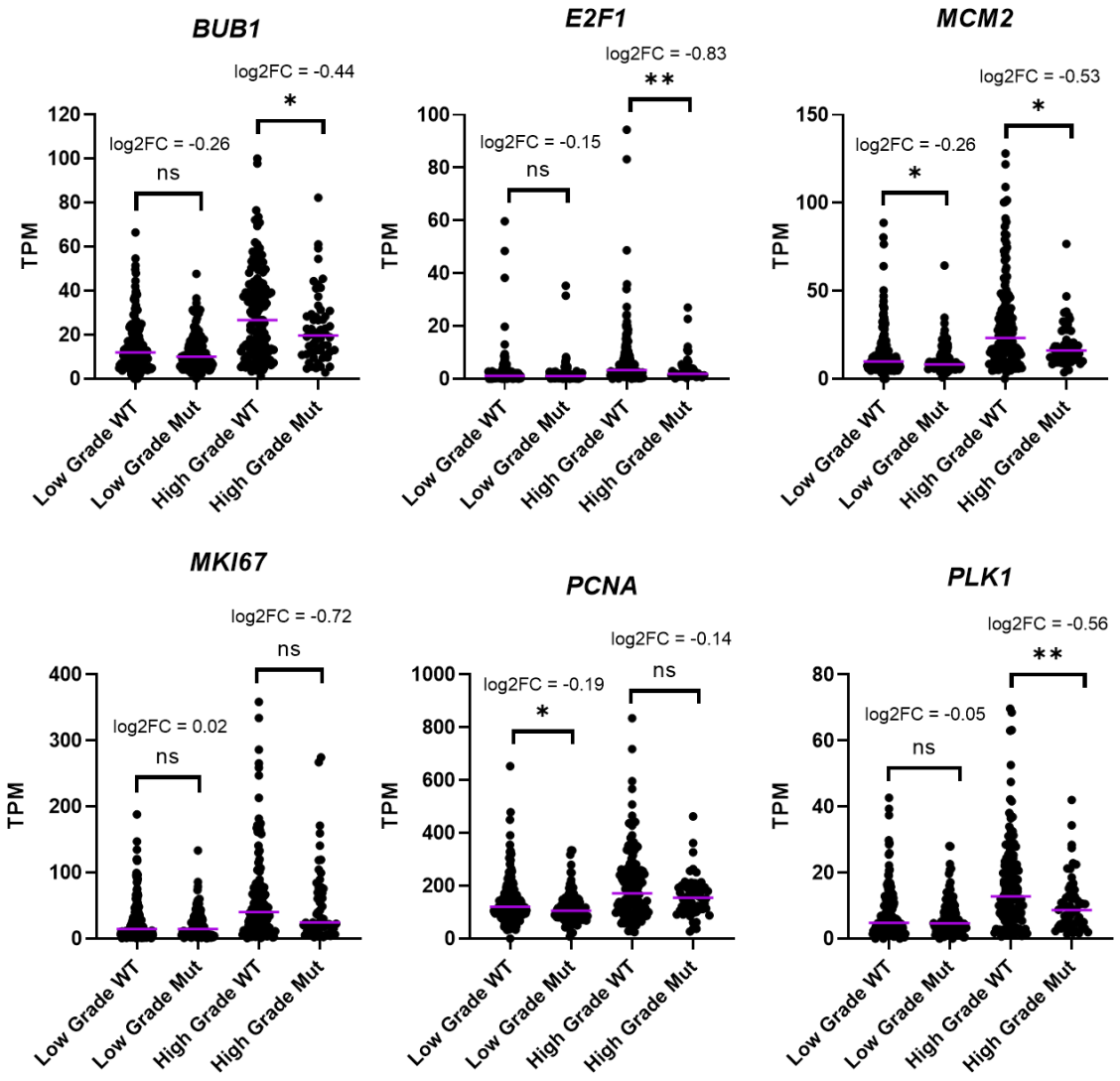

Figure 5.13 - *FGFR3* mutations were associated with significantly lower expression of cell cycle-associated transcripts in mostly high-grade vs low-grade UROMOL NMIBC tumours - Kruskal-Wallis test was used to determine statistical significance. log2FC represents the log2 fold-change on the median for *FGFR3* wild-type versus *FGFR3* mutant tumours. Purple line represents the median value. Low grade tumours contained 187 *FGFR3* wild-type tumours and 115 *FGFR3* mutant tumours, high grade tumours contained 145 *FGFR3* wild-type tumours and 56 *FGFR3* mutant tumours.

In TCGA MIBC tumours, when all tumours were compared, those carrying *FGFR3* mutations were associated with significantly lower expression of all six cell cycle transcripts (Fig. 5.14).

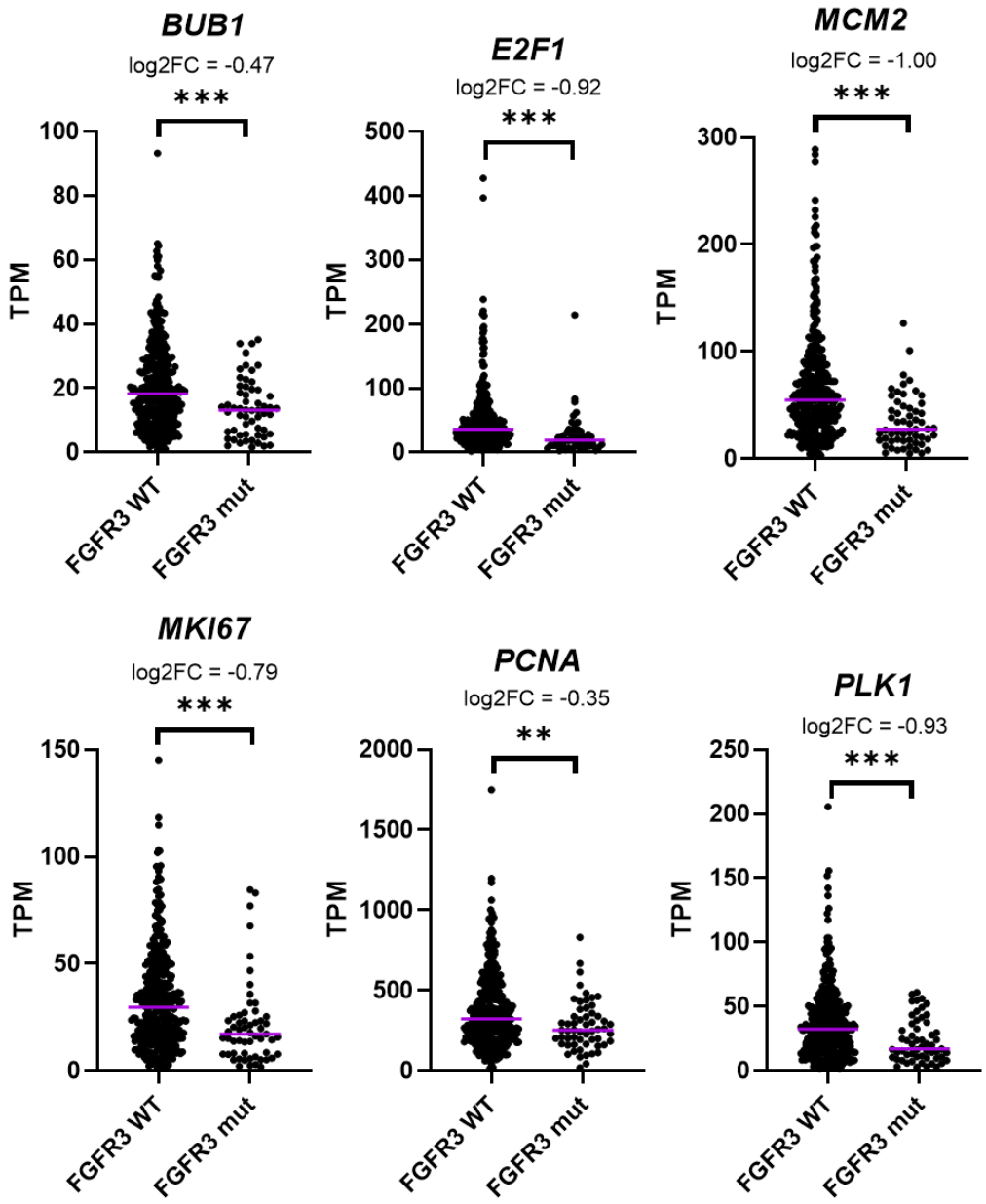

Figure 5.14 - *FGFR3* mutations were associated with significantly lower expression of cell cycle-associated transcripts in TCGA MIBC tumours - Kruskal-Wallis test was used to determine statistical significance. log2FC represents the log2 fold-change on the median for *FGFR3* wild-type versus *FGFR3* mutant tumours. Purple line represents the median value. Analysis included 347 *FGFR3* wild-type and 57 *FGFR3* mutant tumours.

When the effect of *FGFR3* mutations was examined within the LumP and Ba/Sq molecular subtypes, most genes did not show significant changes with *FGFR3* mutation status (Fig. 5.15). Within Ba/Sq tumours, none of the six cell cycle transcripts showed significant changes. Within the LumP subtype, *E2F1*, *MCM2* and *MKI67* were all significantly lower in *FGFR3* mutant tumours compared to *FGFR3* wiltype tumours.

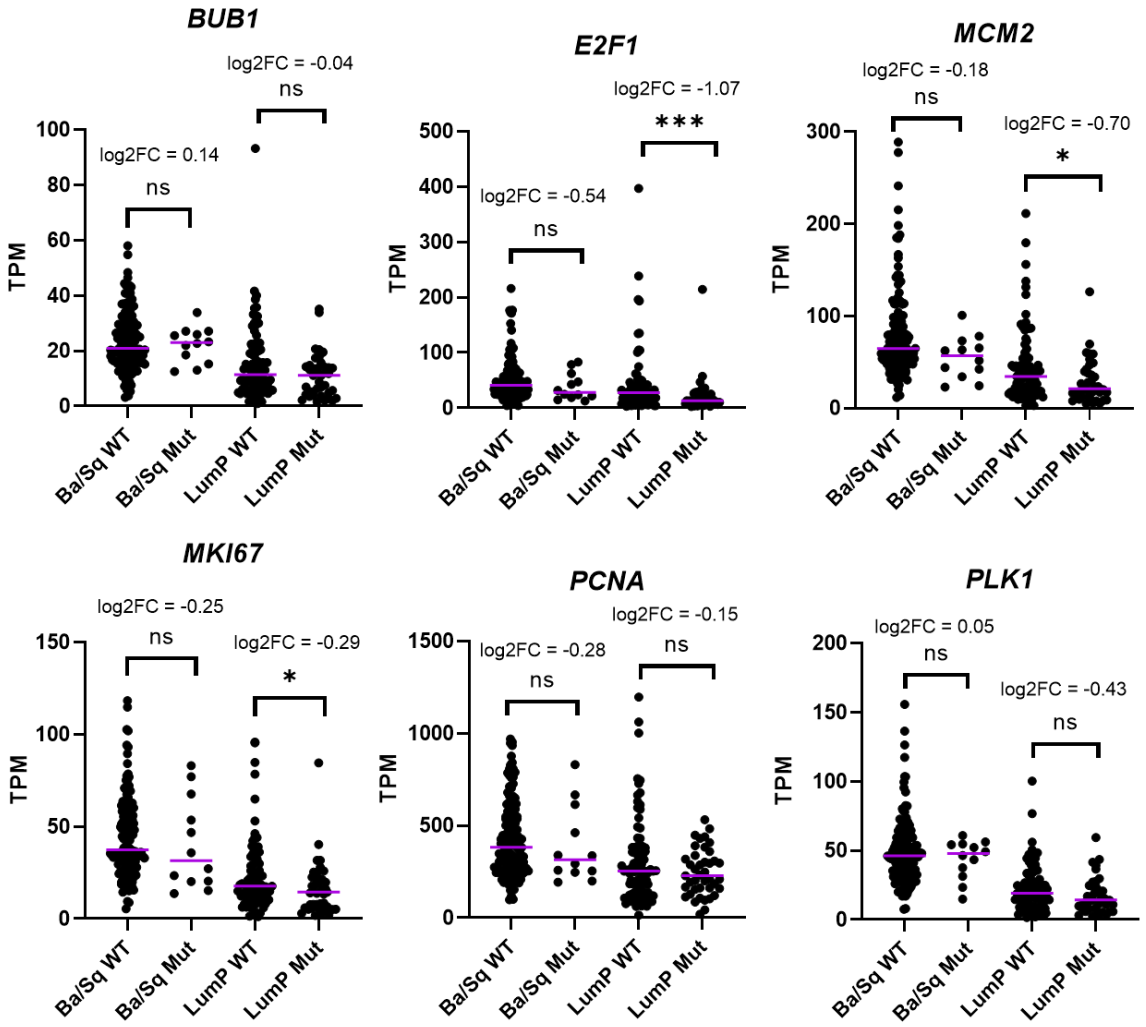

Figure 5.15 - *FGFR3* mutations were associated with significantly lower expression of cell cycle-associated transcripts in LumP but not Ba/Sq TCGA MIBC tumours - Kruskal-Wallis test was used to determine statistical significance. log2FC represents the log2 fold-change on the median for *FGFR3* wild-type versus *FGFR3* mutant tumours. Purple line represents the median value. Ba/Sq tumours included 140 *FGFR3* wild-type and 13 *FGFR3* mutant tumours, LumP tumours included 88 *FGFR3* wild-type and 42 *FGFR3* mutant tumours.

When MIBC tumours were stratified by stage, all six cell cycle-associated genes were significantly lower in *FGFR3* mutant tumours in stage 2 and stage 3 tumours, but not stage 4 tumours (Fig. 5.16). *BUB1* expression was significantly lower in stage 2 *FGFR3* mutant tumours only.

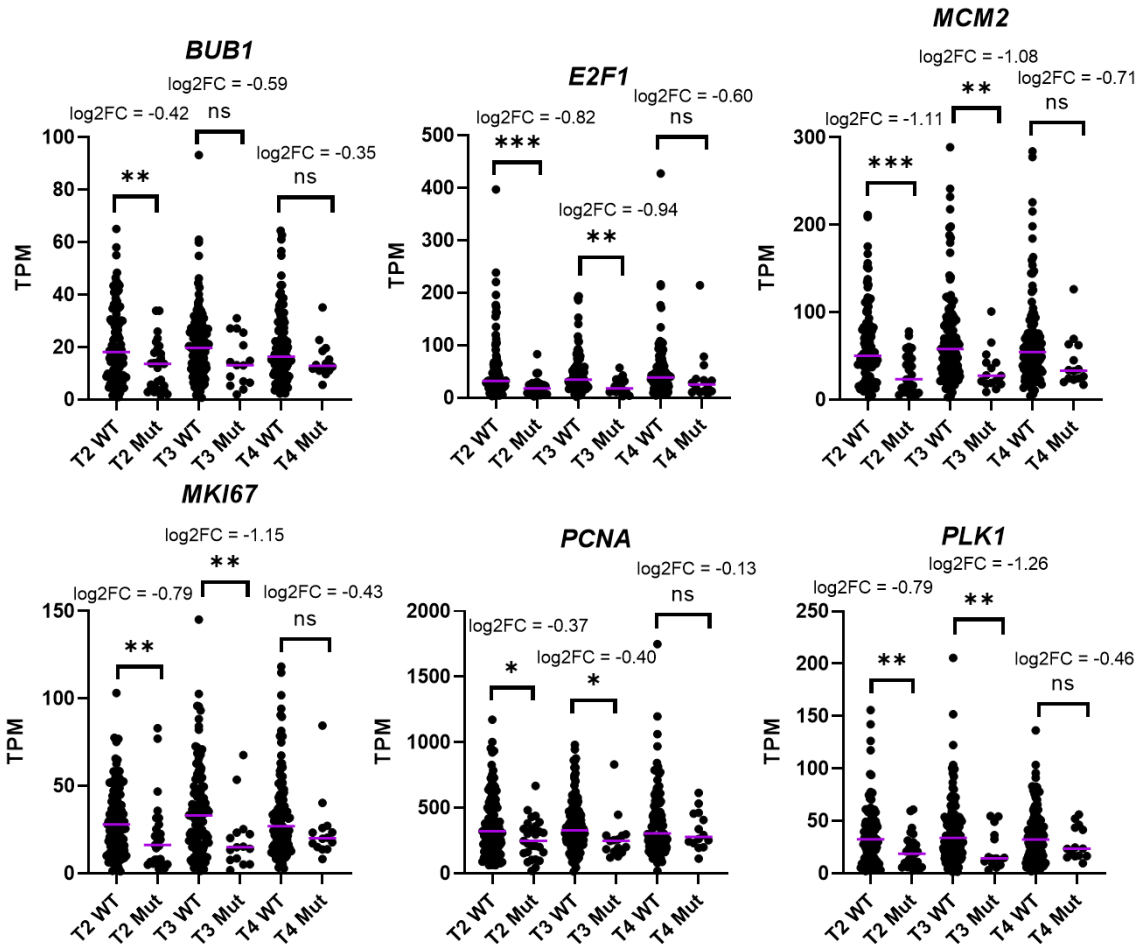

Figure 5.16 - *FGFR3* mutations were associated with significantly lower expression of cell cycle-associated transcripts in TCGA MIBC tumours regardless of tumour stage - Kruskal-Wallis test was used to determine statistical significance. log2FC represents the log2 fold-change on the median for *FGFR3* wild-type versus *FGFR3* mutant tumours. Purple line represents the median value. T2 tumours included 104 *FGFR3* wild-type and 28 *FGFR3* mutant tumours, T3 tumours included 125 *FGFR3* wild-type and 16 *FGFR3* mutant tumours, T4 tumours included 120 *FGFR3* wild-type and 15 *FGFR3* mutant tumours.

5.4 Summary

- Overexpression of wild-type mutant-active FGFR3 protein in differentiated NHU cells did not increase expression of *MKI67* transcript or the proportion of cells which were positive for Ki67 protein. Hence it was shown for the first time in a differentiated mitotically quiescent cell model of urothelial tissue, *FGFR3* activating mutation did not drive urothelial proliferation.
- When overexpressed in NHU cells, FGFR3 protein had a perinuclear localisation, and FGFR3 mutation status did not alter localisation of FGFR3 protein. This was similar to the localisation of FGFR3 expressed following EGFR inhibition of NHU cells in Chapter 4.
- Similarly to NHU cell models, analysis of UROMOL NMIBC and TCGA MIBC cohorts found that *FGFR3* mutation was associated with significantly lower expression of cell cycle-associated transcripts.
- In both NMIBC and MIBC *FGFR3* mutations were associated with lower expression of cell cycle associated transcripts in more-differentiated molecular subtypes (Class 2a and LumP respectively). However, when stratifying by stage only T1 tumours had significantly lower expression of cell cycle-associated genes with *FGFR3* mutation status. By contrast in MIBC tumours T2-3 but not T4 tumours had significantly lower expression of cell-cycle associated genes associated with *FGFR3* mutation status.

5.5 Discussion

5.5.1 Is *FGFR3* mutation capable of driving urothelial proliferation? Contradictions in the literature

Ahmad et al first reported that *FGFR3* mutations could co-operate with *K-Ras* and *B-catenin* mutations to cause tumours in skin and lung tissue, but not in the bladder. This finding in itself suggests that the bladder is different in some way and forms tumours less readily than other tissues [Ahmad et al., 2011c]. This was supported by the observation that mice which expressed mutant *FGFR3* had increased ERK phosphorylation in the urothelium but no hyperplasia or tumour thickening. Thus, even though ERK signalling was taking place downstream of mutant *FGFR3*, no proliferation resulted.

The idea that *FGFR3* mutations alone are unable to lead to tumours in the urothelium are part of a wider group of papers which together suggest that the urothelium has a number of “anti-tumour” mechanisms. Typically, studies have found that multiple oncogenic mutations must be combined to “overcome” the anti-tumour mechanisms, or an oncogenic mutation when combined with loss of a tumour suppressor can lead to BLCA. For example, Ahmad et al., 2011a showed that while β-catenin overexpression in mice resulted in hyperplasia, the additional loss of the tumour suppressor PTEN was required for tumour formation to occur. In fact, when β-catenin overexpression occurred alone, regions of hyperplasia showed increased expression of PTEN. From this, the authors concluded that PTEN had become activated in response to β-catenin overexpression, as a tumour suppressor mechanism. Similarly, Ahmad et al., 2011b found that expression of mutant-active HRAS led to hyperplasia, but was unable to cause tumour formation without loss of the tumour suppressor p21. As was seen for β-catenin overexpression and subsequent PTEN activation, p21 expression was increased in the areas of hyperplasia following HRAS mutation.

The “anti-tumour” nature of the bladder urothelium was further substantiated by the observation that mice which expressed *FGFR3-S249C* showed increased expression of the tumour-suppressor proteins p16, p19, p21 and p53 [Zhou et al., 2016]. When these anti-tumour mechanisms were disabled by expression of SV40 antigen, *FGFR3-S249C* transduced mice developed high-grade papillary tumours. A different study showed that expression of *FGFR3-S249C* in TERT-NHU cells resulted in increased expression of the tumour suppressor protein Rb [di Martino et al., 2009].

Thus the majority of studies suggest that while *FGFR3* mutation can activate downstream pro-proliferative signalling, tumour suppressor mechanisms are activated in response, and this ultimately prevents proliferation or tumour formation in urothelium.

Shi et al reported that when expression of *FGFR3-S249C* was driven in the urothelium of mice by placing *FGFR3* under the control of a Uroplakin II promoter, mice developed hyperplasia by 6 months and low-grade papillary BLCAs by 15 months [Shi et al., 2022]. This was contrasted to the work of four other studies - for example Foth et al saw no urothelial abnormalities (i.e. no hyperplasia, no tumours) when mice were sacrificed at 12 months [Foth et al., 2018]. Currently, how Shi et al observed tumour formation in mice transduced with *FGFR3-S249C* when previous studies have not is unexplained. Shi et al proposed that since frequency of tumour incidence was correlated to *FGFR3-S249C* transgene expression, that lack of tumour formation in previous studies was due to expression of *FGFR3-S249C* being too low. Given that previous studies have not quantified expression of the *FGFR3-S249C* transgene, this hypothesis is impossible to refute.

More interesting is the relationship observed by Shi et al between tumour formation and the expression of tumour suppressor genes. It was seen that hyperplasias and tumours that formed following expression of *FGFR3-S249C* showed reduced expression of p53 and p27 tumour suppressor proteins compared to controls [Shi et al., 2022]. This is in contrast to previous results showing that expression of activating mutations of *FGFR3* in mice or urothelial cells resulted in a compensatory increase in expression of tumour suppressor proteins involved such as Rb, p16, p19, p21 and p53 [di Martino et al., 2009, Zhou et al., 2016]. Furthermore, the controls used by Shi et al for this analysis were taken from control littermate mice, rather than from areas of normal urothelium in the mice that developed tumours. Hence, it is possible that the mice that went on to develop tumours had an existing reduction in expression of tumour suppressor proteins and that this allowed the formation of tumours following expression of *FGFR3-S249C,* as has previously demonstrated [Zhou et al., 2016].

5.5.2 *FGFR3* mutations were associated with lower expression of proliferation marker transcripts in both NMIBC and MIBC

In UROMOL NMIBC tumours, molecular subtype clearly had an effect on expression of cell cycle activity, as Class 2a tumours had greater expression of cell cycle-associated genes [Hedegaard et al., 2016, Lindskrog et al., 2021]. *FGFR3* mutations were associated

with the luminal Class 1 tumours and basal Class 3 tumours. However, *FGFR3* mutation status was associated with significantly lower expression of cell cycle transcripts in Class 2a tumours. Similarly, expression of cell cycle transcripts was generally lower in low-grade/stage tumours than high-grade/stage tumours [Hedegaard et al., 2016, Lindskrog et al., 2021] , but *FGFR3* mutation was independently associated with significantly lower expression of cell cycle transcripts in high-grade/stage tumours. Thus, in NMIBC tumours *FGFR3* mutation was associated with lower expression of cell cycle transcripts in tumours with relatively higher expression of those transcripts.
In MIBC, *FGFR3* mutations were associated with the luminal LumP tumours. Additionally, the association of *FGFR3* mutation with reduced expression of cell cycle transcripts was less obvious than in NMIBC. When tumours were stratified into the LumP and Ba/Sq molecular subtypes the median expression of cell-cycle associated transcripts was lower in *FGFR3* mutation tumours, but this was only significant in LumP tumours. Thus in both NMIBC and MIBC, *FGFR3* mutations were associated most strongly with lower cell cycle transcript expression in luminal tumours.

Whereas in NMIBC *FGFR3* mutation was associated with reduced cell cycle transcript expression in high grade/stage tumours in MIBC the reverse was seen, as *FGFR3* mutation was associated with significantly lower expression of cell cycle transcripts in stage 2 and stage 3 tumours, but not stage four tumours. It is possible that by the time a tumour has advanced to stage 4, it has acquired so many growth-promoting mutations that *FGFR3* mutation makes no difference to cell cycle activity. It has previously been shown that in BLCA higher grade and/or stage is associated with a greater number of somatic mutations and copy number changes [Cazier et al., 2014, Wu et al., 2020]. Alternatively, this could suggest that *FGFR3* mutations have different roles in BLCA depending on the biological background. Whereas in NMIBC *FGFR3* mutations seem to oppose urothelial proliferation, especially in late-stage MIBC it is possible that *FGFR3* may no longer oppose tumour growth. In a similar fashion, Foth et al demonstrated that *FGFR3* mutations acted to suppress inflammation early on in tumour formation, but that *FGFR3* mutations switched to promoting inflammation once tumours were established [Foth et al., 2018].

5.5.3 *FGFR3* mutations have been associated with reduced proliferation in other tissues

It is worth noting that while this is the first report that *FGFR3* mutations are associated with lower proliferation in BLCA, it has been suggested that *FGFR3* mutations may have a

protective role in pancreatic cancer [Lafitte et al., 2013]. This is based on the observation that overexpression of *FGFR3* in the epithelial-like pancreatic cancer cell lines Capan-2 and BxPC-3 resulted in decreased proliferation, and reduced tumour growth when these cell lines were used to establish xenografts in mice [Lafitte et al., 2013]. Furthermore, FGFR3 is known to suppress proliferation in chondrocytes, pancreatic epithelial cells and intestinal crypt cells [Rozenblatt-Rozen et al., 2002, Arnaud-Dabernat et al., 2007, Arnaud-Dabernat et al., 2008, reviewed by Krejci, 2014].

5.5.4 Lack of PIK3K activation downstream of FGFR3 - implications for BLCA

The absence of PI3K activation downstream of FGFR3 activation seen here has also been reported elsewhere. A study in which FGFR3-S249C protein was expressed in NHU cells also found that active FGFR3 did not phosphorylate AKT [Di Martino et al., 2009]. Also, mice expressing mutant-active FGFR3 in their urothelium were found to have increased ERK phosphorylation, but no AKT phosphorylation was seen [Ahmad et al., 2011].

The fact that FGFR3 activation did not seem to affect activation of the PI3K-AKT pathway is interesting in the context of bladder cancer, where mutations in *PIK3CA* (the gene encoding the PI3K catalytic p110α subunit) are significantly associated with *FGFR3* mutations [Lopez-Knowles et al., 2006, Kompier et al., 2010, Sjodahl et al., 2011, Jaunpere et al., 2012, Duenas et al., 2015, Nassar et al., 2019]. Additionally, studies in mice as well as *in silico* modelling of tumour invasiveness found that combining *FGFR3* mutation with PI3K activation results in increased tumorigenesis/invasiveness [Foth et al., 2014, Remy et al., 2015].

Together these results suggest that even when activated by mutation FGFR3 does not signal to the PI3K-AKT pathway in urothelium, instead preferentially signalling through the MAPK pathway. Since mutant FGFR3 does not signal to PI3K, there would be an advantage to tumours which also gain a *PIK3CA* mutation and thus achieve active MAPK and PI3K signalling downstream of FGFR3.

5.5.5 Potential limitations of this study

Firstly, the characterisation of FGFR3-expressing NHU cells performed in this study was relatively limited in scope. Given the associations between *FGFR3* mutations and more-differentiated tumours in MIBC [Choi et al., 2014, Eriksson et al., 2014, Kamoun et al., 2020], it would be beneficial in future to assess whether FGFR3-S249C-expressing

NHU cells show any changes for example in expression of urothelial differentiation markers. This is important to consider when looking at the effects that FGFR3 mutation might have on cell cycle status of cells - in tumours it was shown that *FGFR3* mutant tumours typically had lower expression of markers of cell cycle activity. It is not unreasonable to speculate that *FGFR3* mutation could decrease cell cycle activity by promoting urothelial differentiation, which itself *in vitro* is associated with reduced proliferation and exit from the cell cycle [Varley et al., 2005, Baker et al., 2022].

Secondly, the analysis here only considered the relationship between *FGFR3* mutations and expression of cell cycle-associated genes. However *FGFR3* mutations in BLCA do not exist in a vacuum - what this means practically is that in BLCA tumours *FGFR3* mutations are unlikely to exist in a wildtype background as has been performed here. For example, tumours with an *FGFR3* mutation are much less likely to have a *TP53* mutation or *EGFR* amplification. Hence, while *FGFR3* mutations were found to be significantly associated with lower expression of cell cycle-associated genes, this may not be a direct result of mutant FGFR3 activity. Rather, a lack of expression/activity of some other gene, or a lack of another mutation may result in lower proliferation.

6. Discussion

6.1 Thesis Overview

The work of this thesis has sought to increase understanding of *FGFR3* in the normal urothelium and in bladder cancer. The following specific research questions were focused on:

- What are the effects of activating *FGFR3* mutation in a mitotically quiescent, differentiated normal urothelial background?
    - Can *FGFR3* mutation drive urothelial proliferation?
- What factors influence the expression of FGFR3 transcript and protein in normal urothelium?
    - How does expression of FGFR3 transcript and protein vary in NHU cells compared to urothelial tissue?
    - How does FGFR3 expression vary between bladder and ureter tissue?

To examine the effects of *FGFR3* mutational activation in normal urothelium, mutant *FGFR3* was expressed in Normal Human Urothelial (NHU) cells. NHU cells provide a genetically normal background which can be manipulated to mimic the mitotic quiescence of *in situ* urothelium, making them a highly-appropriate system in which to study *FGFR3* alteration. Urothelial proliferation status was examined, supplemented by analysis of NMIBC and MIBC datasets to look for associations between *FGFR3* mutation status and cell cycle activity. NHU cells were also used to test the effects of EGFR activity and urothelial differentiation on FGFR3 expression.

Expression of *FGFR3-S249C*, the most common *FGFR3* mutation in BLCA [Shi et al., 2019], was unable to force differentiated NHU cells into a proliferative state. This was in spite of the fact that FGFR3-S249C successfully phosphorylated FRS2 and signalled into the MAP kinase pathway. Similarly, bioinformatic analysis showed that in both NMIBC and MIBC cohorts, *FGFR3* mutation was associated with significantly lower expression of several cell-cycle associated genes.

Both FGFR3 transcript and protein had much greater expression in urothelial tissue than in NHU cells. FGFR3 protein was expressed in undifferentiated NHU cells following

inhibition of EGFR or downstream MAP kinase pathway signalling. Differentiation of NHU cells did not result in FGFR3 expression, and once NHU cells were differentiated they no longer responded to EGFR inhibition by expressing FGFR3 protein.

6.2 Different acquisition and roles of *FGFR3* mutations in NMIBC vs MIBC

FGFR3 is one of the most common mutations in BLCA, occurring in approximately 70% of NMIBC and 20% of MIBC [Mahe et al., 2018]. *FGFR3* mutations are associated with low grade and stage disease [Billerey et al., 2001, Hernandez et al., 2006, Lamy et al., 2006, Tomlinson et al., 2007a, Junker et al., 2008], as well as improved prognosis of BLCA [van Rhijn et al., 2003, van Oers et al., 2007, van Rhijn et al., 2010, Robertson et al., 2017, Teo et al., 2020, Van Rhijn et al., 2020, Mertens et al., 2022]. As such, *FGFR3* mutations have been described to have a “protective effect”, and at one point it was believed that *FGFR3* mutant NMIBC could not progress to MIBC [van Rhijn et al., 2003, Hernandez et al., 2006, Burger et al., 2008, van Rhijn et al., 2010, Jiang et al., 2022]. All of these observations are however juxtaposed by the fact that *FGFR3* mutations do occur in MIBC [Robertson et al., 2017, Kamoun et al., 2020]. The observation that *FGFR3* mutations appear in MIBC is also at odds with the results shown in this thesis that *FGFR3* mutations are associated with reduced rates of proliferation in BLCA.

It is currently contested as to whether all MIBC are formed from NMIBC that has progressed, or whether MIBC can arise *de novo* without first existing as NMIBC. The latter hypothesis is based on the observation that approximately 20% of BLCA patients present with MIBC with no previous history of disease [reviewed by Raghavan, 2003]. Similarly, it is possible that *FGFR3* mutations occur *de novo* in MIBC, rather than *FGFR3* mutant NMIBC tumours progressing to MIBC. In this scenario, continuing APOBEC mutagenic activity in MIBC results in *FGFR3* mutations [Robertson et al., 2017, Shi et al., 2019, Rao et al., 2023], rather than *FGFR3*-mutant NMIBC tumours progressing to MIBC (Fig. 6.1).

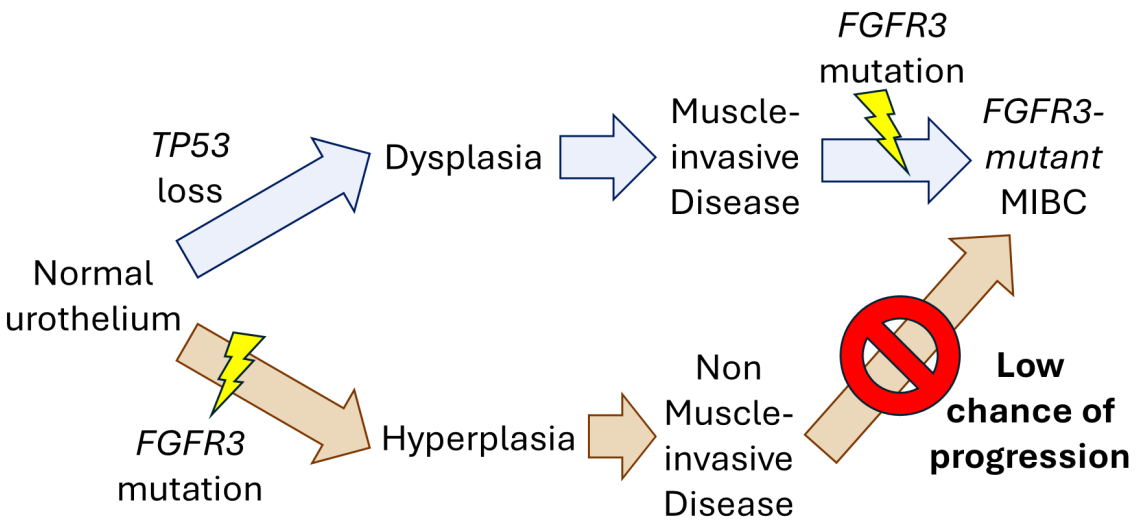

Figure 6.1 - Schematic representation of how *FGFR3* mutations may occur independently in NMIBC and MIBC rather than progressing from NMIBC

The fact that *FGFR3* mutation did not drive urothelial proliferation (Chapter 5) is somewhat surprising given the high frequency of *FGFR3* mutations in BLCA [Neuzillet et al., 2012] and the fact that FGFR3 tyrosine kinase inhibitors have shown clinical benefit when administered to BLCA patients with tumours harbouring *FGFR3* mutations. Both of these observations would suggest that *FGFR3* mutation is providing a selective advantage to tumours, likely in the form of supporting tumour growth. These observations can be reconciled with the results presented here by accepting that *FGFR3* mutations have different roles in BLCA, depending on when they are acquired. However, it is also possible that some of the clinical benefit provided by FGFR3 tyrosine kinase inhibitors could be due to off-target effects on other receptor tyrosine kinases.

When *FGFR3* mutations are acquired can be somewhat inferred by the frequency of *FGFR3* mutations in different stages of BLCA development. Within BLCA, *FGFR3* mutations are much more common in NMIBC than in MIBC. A meta-analysis by Neuzillet et al based on eight previous studies concluded that *FGFR3* mutations were most common in Ta tumours, and the incidence of *FGFR3* mutations statistically decreased as tumour stage increased (Incidence of *FGFR3* mutations: Ta; 65%, T1; 30%, T2-4; 11%) [Neuzillet et al., 2012]. The UROMOL and TCGA cohorts had similar results, both showing that *FGFR3* mutations were always less frequent as tumour stage increased, and were less frequent in MIBC than NMIBC [Robertson et al., 2017, Lindskrog et al., 2021]. Thus based on these findings *FGFR3* mutations are most common in Ta tumours.

It is impossible to say definitively that *FGFR3* mutations detected in Ta tumours occurred in those Ta tumours and not in normal or hyperplastic urothelium that has progressed. However, evidence suggests that incidence of *FGFR3* mutations is much greater in Ta tumours than either normal urothelium or hyperplasias. Several studies have sequenced histologically-normal urothelium from patients with BLCA [Lawson et al., 2020, Li et al., 2020] or no urothelial malignancies [Otto et al., 2009] and found no evidence of *FGFR3* mutation.

The above reports of a lack of *FGFR3* mutations in normal urothelial tissue are contrasted by a report by Hayashi et al who detected *FGFR3* mutations in normal urothelial samples taken from patients with NMIBC at an incidence of 17% [Hayashi et al., 2022]. The authors themselves admitted that small sample size (just 23 patients) means these results should be interpreted with caution, however they then compared their results with those of Li et al., 2020 and Lawson et al., 2020. A key difference in these studies is that Hayashi et al. obtained normal urothelium from NMIBC patients, while both Li et al. and Lawson et al. used normal urothelium from MIBC patients. Hayashi et al. went on to claim that the differences in mutations found in normal urothelium between these studies may be indicative that different normal urothelial mutations alter the route BLCA takes, supporting the “two pathways” model [Spruck et al., 1994, Bakkar et al., 2003, van Rhijn et al., 2004]. Interestingly, the analysis of Hayashi et al. showed that NMIBC patients with *FGFR3* mutations in their tumours had *FGFR3* mutations in their corresponding normal urothelium, while MIBC patients did not. This supports the hypothesis presented above that *FGFR3* mutations found in MIBC tumours have occurred *de novo* rather than originating from NMIBCs which have advanced.

In terms of *FGFR3* mutations in hyperplasias, the reported incidence is much lower than in Ta tumours. Van Oers et al reported *FGFR3* mutations in 23% of flat urothelial hyperplasias examined, and Cheng et al reported the same incidence of *FGFR3* mutations in papillary urothelial hyperplasia [van Oers et al., 2006, Cheng et al., 2023]. In summary, these reports support a model in which *FGFR3* mutations do not occur in normal urothelium, but rather in hyperplastic lesions or in low-stage tumours. Here FGFR3 activity is able to drive proliferation and clonal expansion, which would explain the high frequency of *FGFR3* mutations in Ta tumours [Neuzuillet et al., 2012]. This is supported by results presented in this thesis (Chapter 5) that *FGFR3* mutation was unable to drive proliferation in mitotically quiescent differentiated normal urothelial cells. From T1 stage onwards though, it is possible that *FGFR3* mutations become disadvantageous to the tumour in some way and so are selected against. This is supported by (1) results shown

here (Chapter 5) that *FGFR3* mutations were associated with significantly lower expression of cell cycle-associated genes in T1, T2 and T3 tumours and (2) observations that incidence of *FGFR3* mutation significantly decreases as tumour stage increases [Neuzillet et al., 2012]. Given that *FGFR3* mutations are inversely related to both stage and grade, a logical question might be whether *FGFR3* mutation acts to oppose tumour invasiveness which is associated with basal biology (see section 6.3).

6.3 The link between *FGFR3* mutations, urothelial differentiation, and immunosuppression in MIBC

Numerous studies have demonstrated that *FGFR3* mutations are associated with more-differentiated MIBC subtypes with poor immune responses and/or low immune infiltration in tumours [Sweiss et al., 2016, Robinson et al., 2019, Lindskrog et al., 2021, Su et al., 2021]. Several clinical trials have also demonstrated that MIBC patients with *FGFR3* mutations have worse survival outcomes when treated with immune checkpoint inhibitors, compared to *FGFR3* wild type patients [Loriot et al., 2019, Santiago-Walker et al., 2019, Song et al., 2023, Okato et al., 2024]. The relationship between *FGFR3* and urothelial differentiation in BLCA is undefined; it is unproven whether *FGFR3* expression is driven by urothelial differentiation, or whether FGFR3 activity can somehow influence urothelial differentiation. However, it was shown here that urothelial differentiation of NHU cells was unable to trigger expression of FGFR3 protein. This would suggest that the association of *FGFR3* expression and activity in more differentiated BLCA tumours is due to FGFR3 - i.e. *FGFR3* activity drives or keeps tumours in more-differentiated state, rather than the differentiated state of tumours driving the expression of *FGFR3*.

It has been suggested that *FGFR3* mutation may be linked to both immunosuppression and urothelial differentiation through interaction with Peroxisome proliferator-activated receptor gamma (PPARγ). PPARγ is a transcription factor whose activity is crucial for urothelial differentiation *in vitro* and in mouse models [Varley et al., 2004a, Fishwick et al., 2017, Liu et al., 2019, Tate et al., 2021]. Alongside *FGFR3* mutations, increased PPARγ transcriptional activity is associated with luminal MIBC tumours that have low immune activity [Choi et al., 2014, Sweiss et al., 2016, Robertson et al., 2017, Kamoun et al., 2020, Rose et al., 2021]. PPARγ activity has also been shown to be crucial for suppressing activity of the key immune component NFkB in the urothelium of mice following wounding [Liu et al., 2019,] and expression of overactive PPARγ in bladder tumours of mice reduced the immune response and suppressed NFkB signalling [Tate et al., 2021].

Thus modulation of PPARγ activity could link *FGFR3* mutation to both urothelial differentiation and the immune desert phenotype in MIBC (Fig. 6.2). However, so far the association reported between *FGFR3* mutation and PPARγ activity has been almost entirely correlational in nature. There is a single report which supports the idea that *FGFR3* mutation drives increased PPARγ activity. Okato et al generated tumours in mice by knocking out the function of *Transformation related protein 53 (Trp53)*. A subset of mice were also given tumours by knocking out *Trp53* function in addition to expression of *FGFR3-S249C*. Mice which expressed *FGFR3-S249C* had much greater expression of *PPARG*, and also showed increased transcriptional activity of PPARγ and increased PPARγ regulon activity, based on gene expression [Okato et al., 2024]. The authors did not suggest a mechanism for how *FGFR3* mutation may influence PPARγ expression and activity, and such a mechanism has not been suggested elsewhere in the literature.

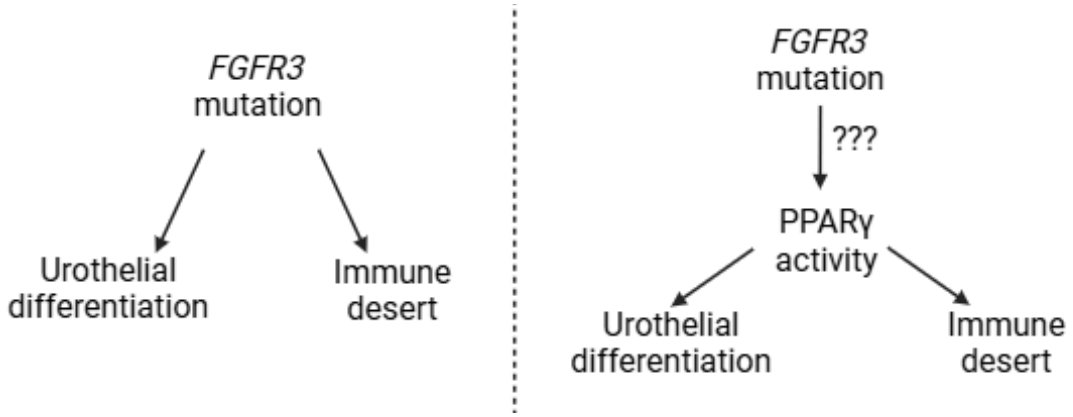

Figure 6.2 - PPARγ would theoretically link *FGFR3* mutation to both the luminal differentiation and immune desert phenotypes in MIBC tumours

Finally, there is an additional possibility as to the role of *FGFR3* mutations and their effects within BLCA - simply that *FGFR3* is a passenger mutation. Mutations in cancer are typically grouped into either “driver” mutations (those which drive formation and/or evolution of the tumour e.g. by driving proliferation or allowing immune evasion) and “passenger” mutations (those which seemingly have no role in the tumour and thus are considered incidental). BLCA is one of the most mutated cancers [Alexandrov et al., 2014], and not all of these mutations may play a functional role in tumour formation or progression. While the majority of evidence presented in this thesis and within the literature suggests that *FGFR3* mutations play an active role in BLCA, there has been some debate as to whether *FGFR3* may be a passenger mutation [Al-Almadie et al., 2011, Shi et al., 2019, Shi et al., 2020], and the potential for a driver vs passenger effect for *FGFR3* mutations vs *FGFR3* overexpression [van Rhijn et al., 2020]. In particular, the

work of Shi et al showed that *FGFR3* S249C mutations are overrepresented in BLCA due to the activity of APOBEC enzymes, rather than increased tumorigenicity of those mutations [Shi et al., 2019]. This is consistent with the possibility of *FGFR3* acting as a passenger mutation in BLCA.

6.4 Limitations of this study

The work performed here investigated the role of *FGFR3* mutations in urothelial cancer and the urothelium as whole was performed mostly on tissues of a ureteric origin, rather than tissue from the bladder. Ureter and bladder are morphologically similar tissues which both contain urothelium, however they have different embryological origins [reviewed by Liaw et al., 2018]. Additionally, *FGFR3* mutations are frequent in cancers of both the bladder and the ureter [Audinet et al., 2019, Necchi et al., 2021].

Due to the difficulties in obtaining human bladder tissue and culturing urothelial cells from it, ureteric urothelium has long been used as a substitute [Hutton et al., 1993, Southgate et al., 1994, de Boer et al., 1996, Bindels et al., 2002, Daher et al., 2003, Varley et al., 2005, di Martino et al., 2014]. Only one previous study has directly compared NHU cells derived from bladder and ureteric urothelium - Southgate et al examined expression of several urothelial differentiation markers in urothelial tissue from both ureter and bladder, as well as in NHU cells derived from both ureter and bladder tissue [Southgate et al., 2007]. The authors observed that urothelial tissue from bladder and ureter appeared morphologically similar, and both showed very low expression of the proliferation marker Ki67. Importantly, ureter and bladder urothelium showed similar localisation and expression patterns of the urothelial differentiation markers CK7, CK20 and UPK3a, as well as Claudins 4, 5, and 7.

6.5 Strengths of this study

A possible limitation of previous studies is that they have always been conducted either in mice or in human cell lines that are poorly representative of the differentiated mitotically-quiescent background of normal human urothelium. To overcome these limitations, NHU cells were used here to study the effects of *FGFR3-S249C* expression in a differentiated mitotically quiescent human urothelial background. *In* vitro cell culture does provide some limitations however, when it comes to studying the factors which influence FGFR3 expression in normal urothelium. For example, the observation that EGFR/ERK activity opposed FGFR3 protein expression in undifferentiated but not in differentiated NHU cells was confusing. Also, why was FGFR3 transcript expression

greater in urothelial tissue than in NHU cells? It is possible that *FGFR3* expression is influenced by paracrine signalling between the urothelium and stroma. Paracrine signalling between the urothelium and stroma is well-evidenced both in development and wound repair and has been reported for Bone Morphogenic Protein [Mysorekar et al., 2002, Mysorekar et al., 2009], Sonic Hedgehog [Shin et al., 2011], and retinoic acid signalling [Gandhi et al., 2013]. FGFRs generally are considered to signal in a paracrine fashion [reviewed by Itoh and Ornitz, 2011] and so it is also possible that once expressed, FGFR3 protein is activated by signals from the stroma which could not be captured here. The theory of paracrine signalling between the urothelium and stroma to control or activate FGFR3 is not supported by any literature - however this is due to a lack of investigation rather than any reports disproving the hypothesis. In future, it could be beneficial to co-culture NHU cells with stromal cells or establish 3D cell culture models to capture potential paracrine interactions [reviewed by Vasutin et al., 2019].

6.6 Future Work

Firstly, the link between *FGFR3* mutation and increased PPARγ activity is correlational in nature and somewhat speculative. Future research should seek to identify whether *FGFR3* mutation can cause increased PPARγ activity. Experiments could be performed in the system developed here in which NHU cells overexpress wild-type and S249C FGFR3. By examining expression of *PPARG*, markers of PPARγ activity and/or urothelial differentiation in NHU cells expressing *FGFR3-S249C* a functional link could potentially be built between *FGFR3* mutation and increased PPARγ activity. For example, to test if the effects of *FGFR3* mutation are mediated by PPARγ, PPARγ inhibition or knockdown experiments could be performed in NHU cells which express *FGFR3* S249C. Phenotypes previously reported to be associated with *FGFR3* mutation (such as immune suppression or increased urothelial differentiation) could then be examined for.

Secondly, future work should continue to expand on the remaining questions on the relationship of FGFR3 with EGFR and PPARγ. The fact that *FGFR3* mutation is associated with PPARγ activity (a marker of urothelial differentiation), and that EGFR (a marker of basal/squamous differentiation) opposes FGFR3 expression suggests that FGFR3 is somehow linked to urothelial differentiation in BLCA. However, this is currently unclear. Research could look to identify the specific mechanism by which EGFR activity represses expression of FGFR3, and whether this is at the level of FGFR3 transcription or translation. Additionally, it would be interesting to see if FGFR3 activity can suppress

EGFR expression. This could provide another way for *FGFR3* mutation to oppose basal biology and drive luminal differentiation in MIBC tumours.

Finally, current research on *FGFR3* mutations is being applied in two main ways in BLCA - in therapies targeted against FGFR3, and as a biomarker for detecting BLCA. *FGFR3* mutations are used to identify patients who may benefit from FGFR tyrosine kinase inhibitors. Currently only one FGFR tyrosine kinase inhibitor (Erdafitinib) has been approved for use in patients, and this is only in the context of metastatic BLCA. Interestingly, it was found here that these are the only tumours in which *FGFR3* mutations were not found to be associated with lower cell cycle activity. Thus, work here loosely suggests that targeted therapies for FGFR3 in BLCA may only be of benefit to patients with metastatic disease. Hence, it may be more beneficial to focus future research on FGFR3 on using the presence of *FGFR3* mutations as a non-invasive test for BLCA, or to direct more personalised treatment plans for patients.

6.7 Conclusions

Firstly, it was shown here for the first time that *FGFR3* mutation is unable to drive proliferation in a mitotically quiescent, differentiated normal human urothelial cell background. Additionally, in T1-T3 tumours *FGFR3* mutation was associated with lower expression of cell cycle-associated genes. These results suggest that *FGFR3* mutation is not sufficient to drive BLCA or hyperplasia formation in normal urothelium. Rather, *FGFR3* mutation may drive proliferation once hyperplasia or Ta tumours have already formed.

Secondly, EGFR activity was found to repress expression of FGFR3 transcript and protein. This is consistent with observations that *FGFR3* expression is associated with luminal MIBC tumours which tend to have lower EGFR activity, as opposed to basal/squamous tumours which have high EGFR activity. RNA-sequencing revealed that expression of *FGFR3*, but not *FGFR1* or *FGFR2* significantly increased in NHU cells following EGFR inhibition.

Thirdly, urothelial differentiation did not drive expression of FGFR3. This suggests that in the association of FGFR3 and urothelial differentiation that occurs in MIBC, *FGFR3* somehow drives urothelial differentiation rather than the other way around. Specific mechanisms by which EGFR represses FGFR3 and how *FGFR3* mutation may drive urothelial differentiation remain to be elucidated.

7. Appendix

Appendix A - Representative uncropped western blots

FGFR3

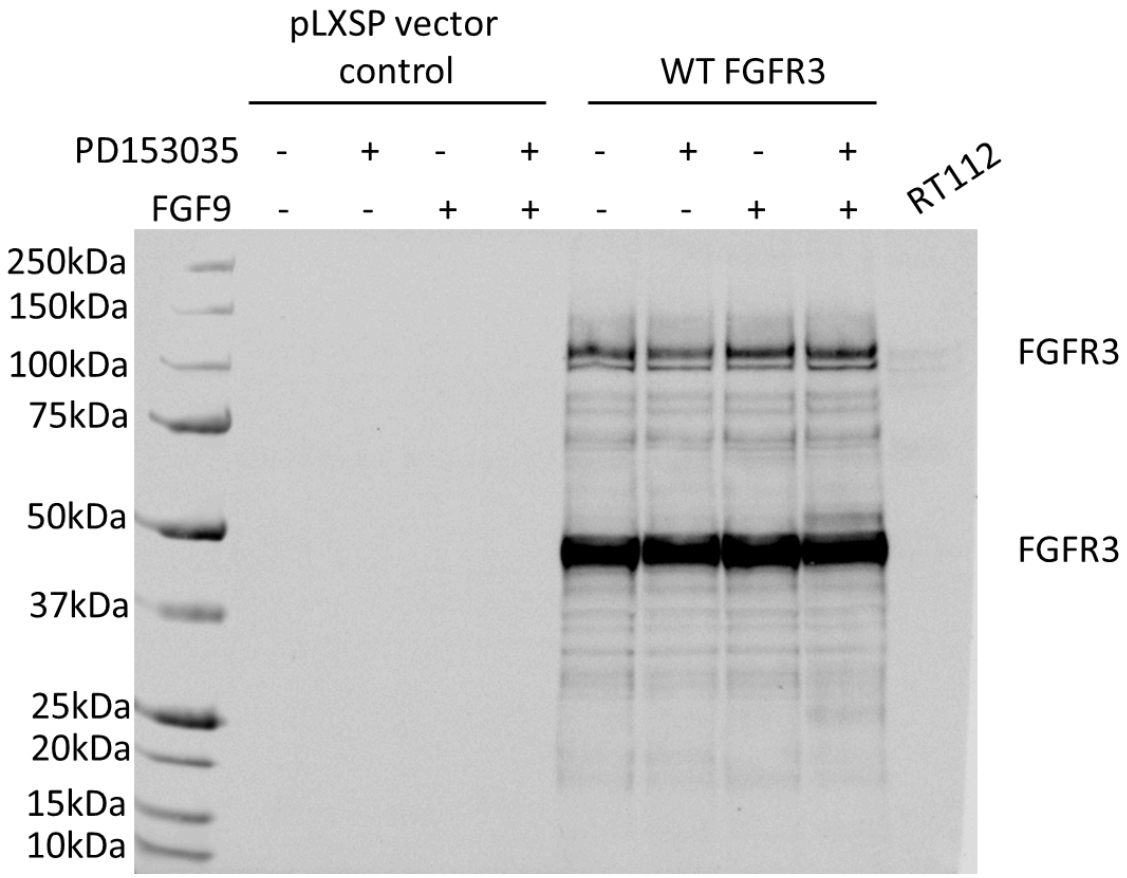

Phospho-ERK

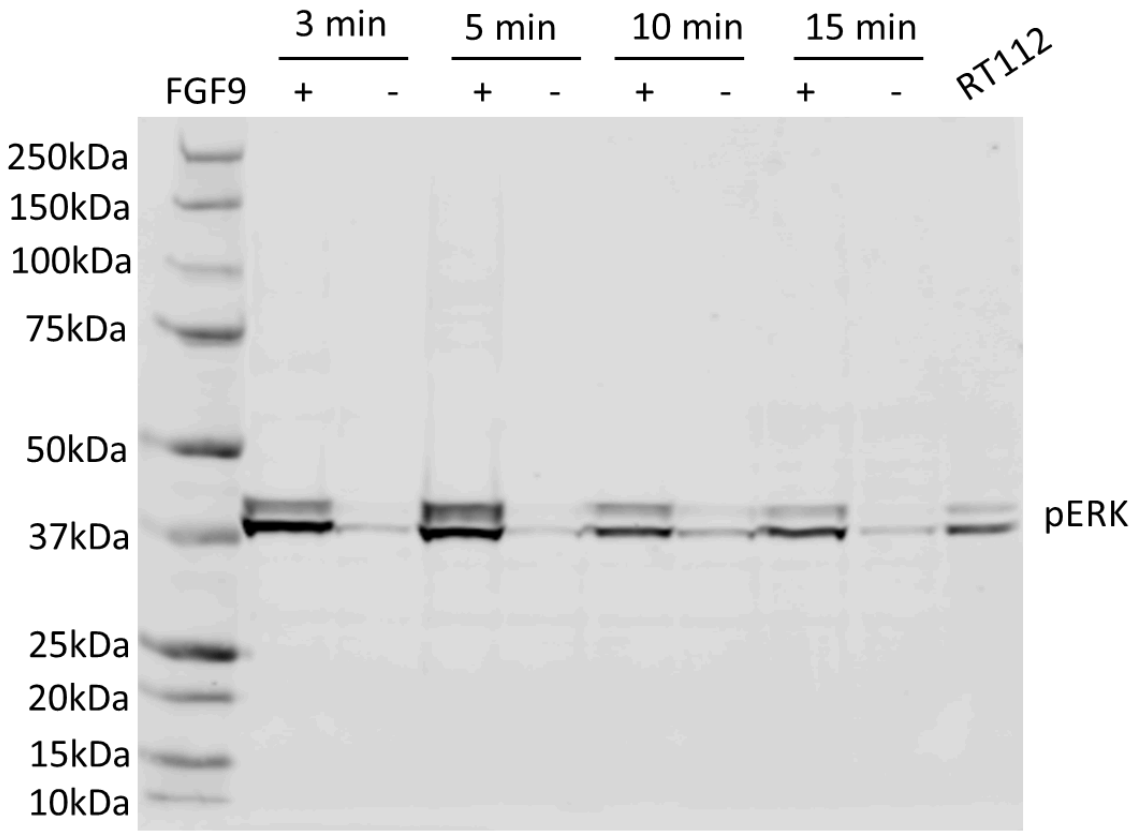
3 min
5 min
10 min
15 min
FGF9
+ - + - + - + -
RT112
250kDa
150kDa
100kDa
75kDa
50kDa
37kDa
25kDa
20kDa
15kDa
10kDa
pERK

Phospho-FRS2

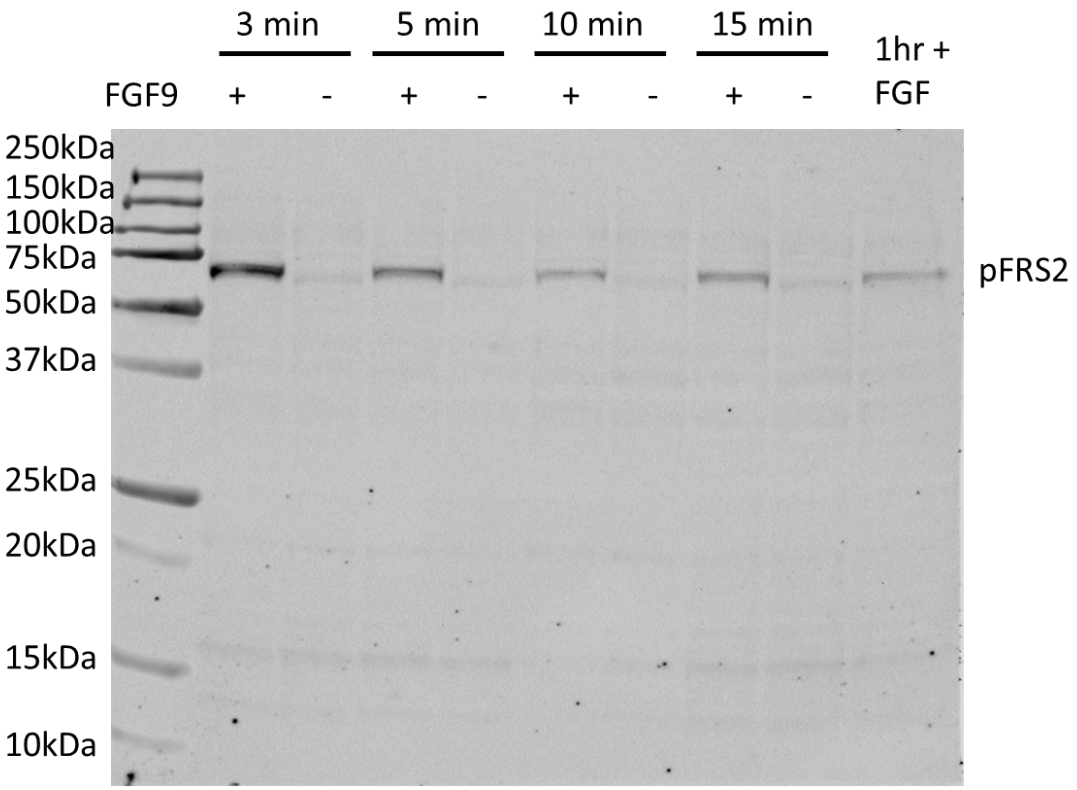

Phospho-EGFR

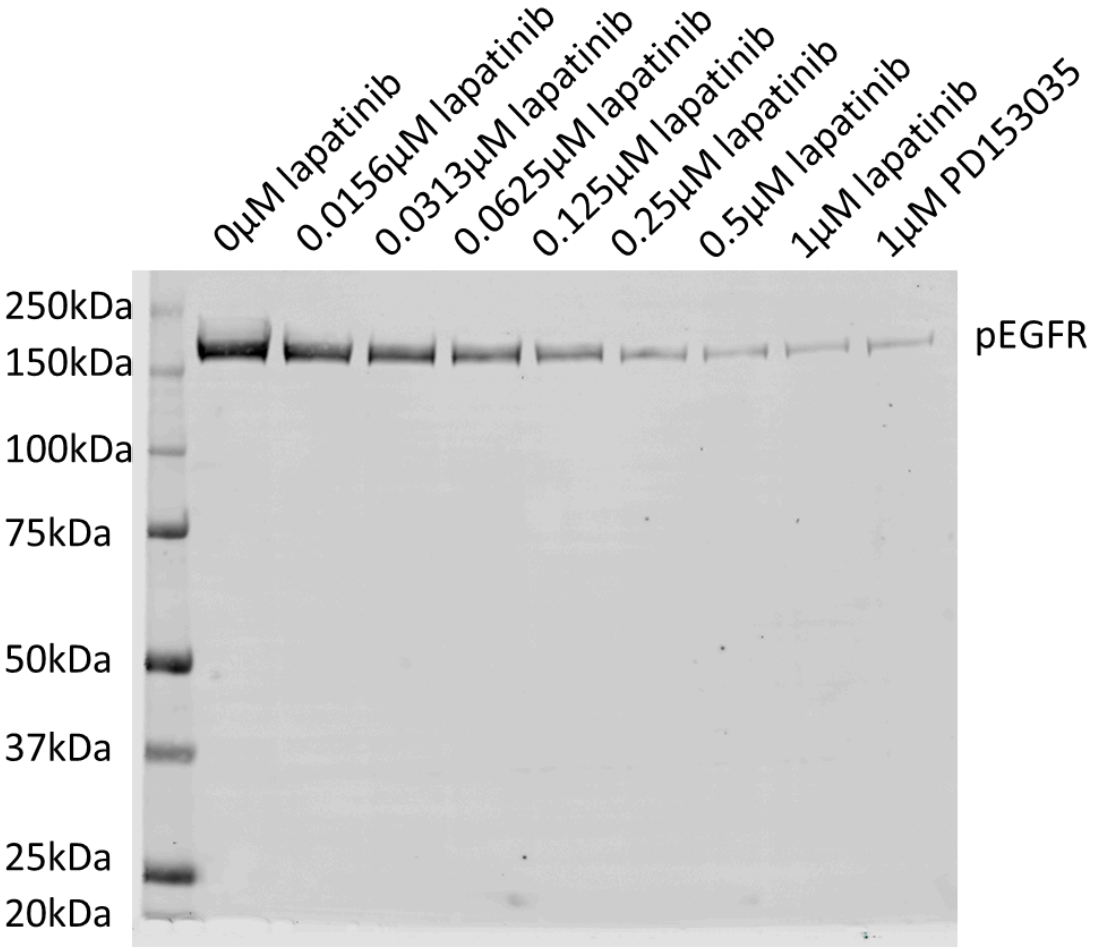

Phospho-Akt

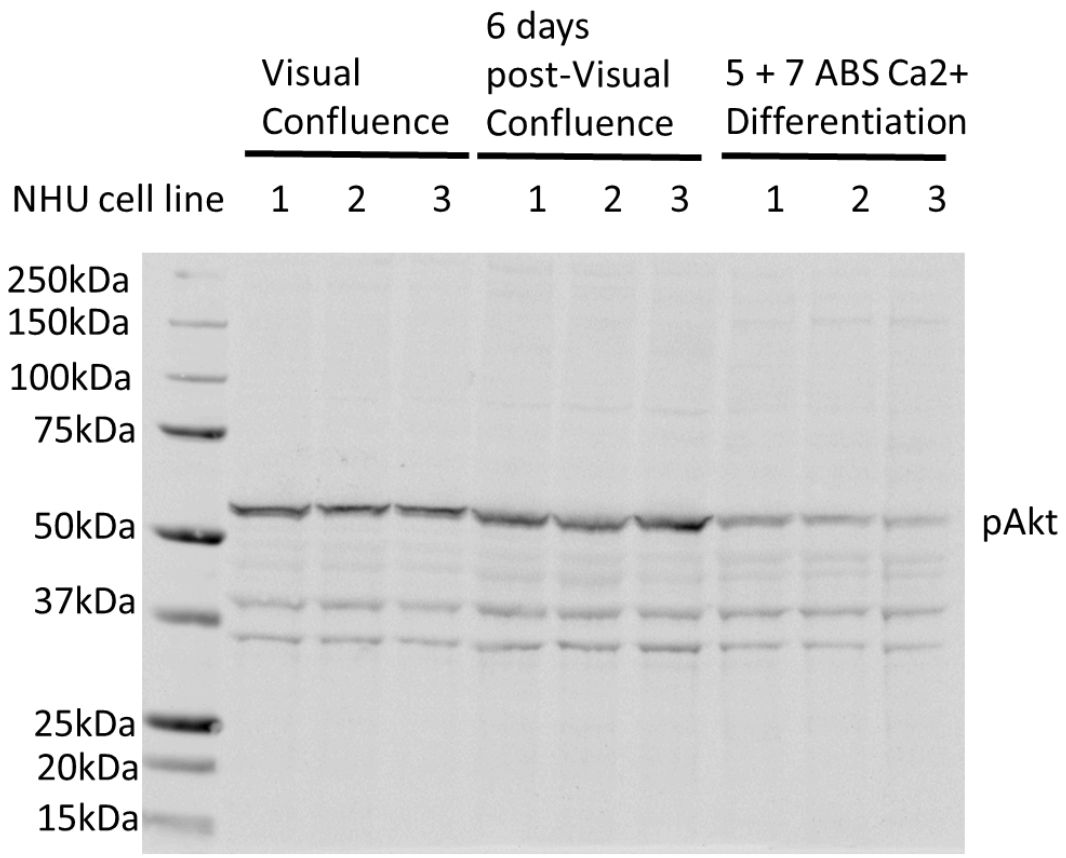
Visual Confluence
6 days post-Visual Confluence
5 + 7 ABS Ca2+ Differentiation
NHU cell line
1 2 3 1 2 3 1 2 3
250kDa
150kDa
100kDa
75kDa
50kDa
37kDa
25kDa
20kDa
15kDa
pAkt

Phospho-ERBB2

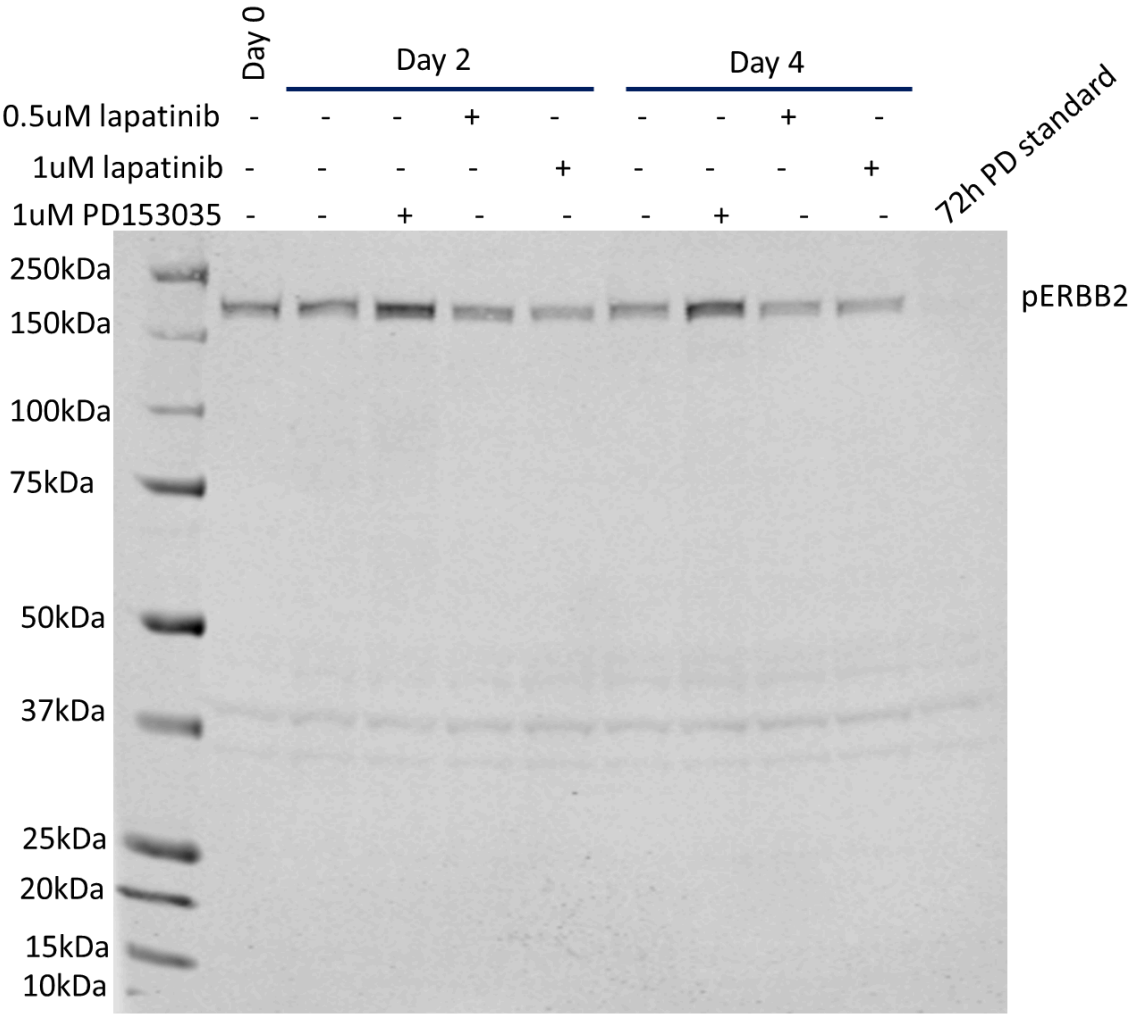

ZO-3

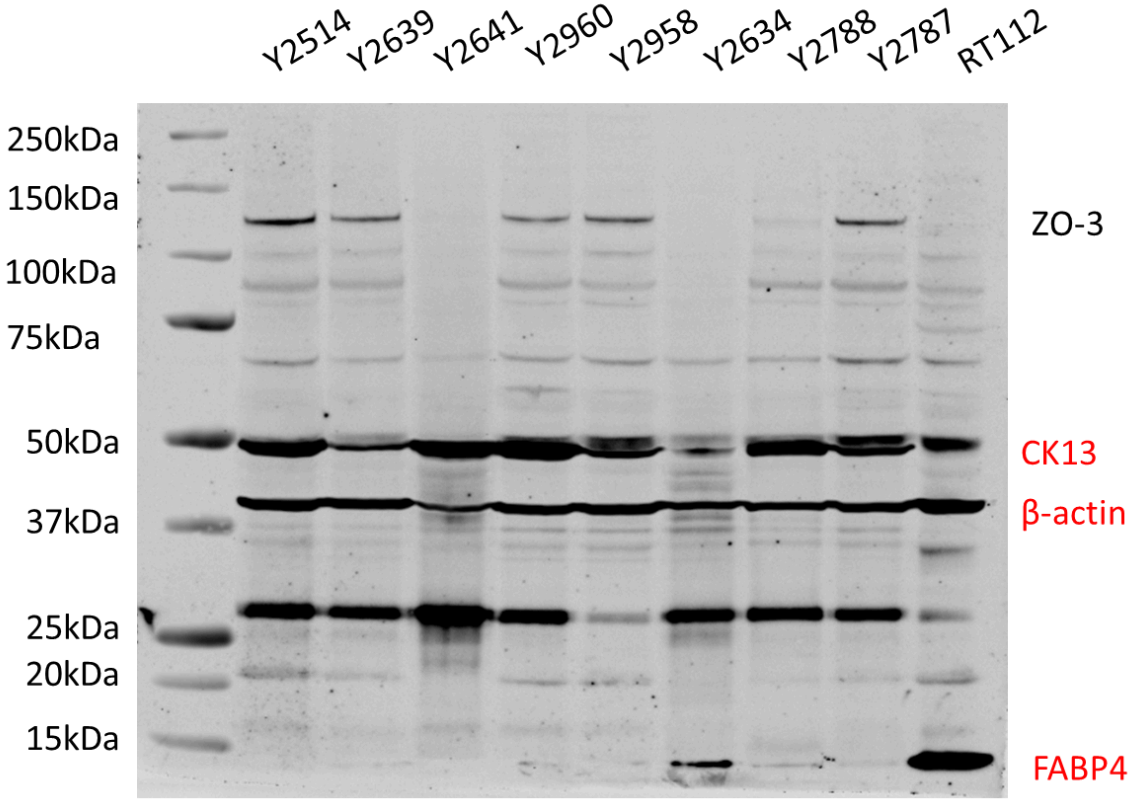
Y2514
Y2639
Y2641
Y2960
Y2958
Y2634
Y2788
Y2787
RT112
250kDa
150kDa
100kDa
75kDa
50kDa
37kDa
25kDa
20kDa
15kDa
ZO-3
CK13
β-actin
FABP4

Cytokeratin 13

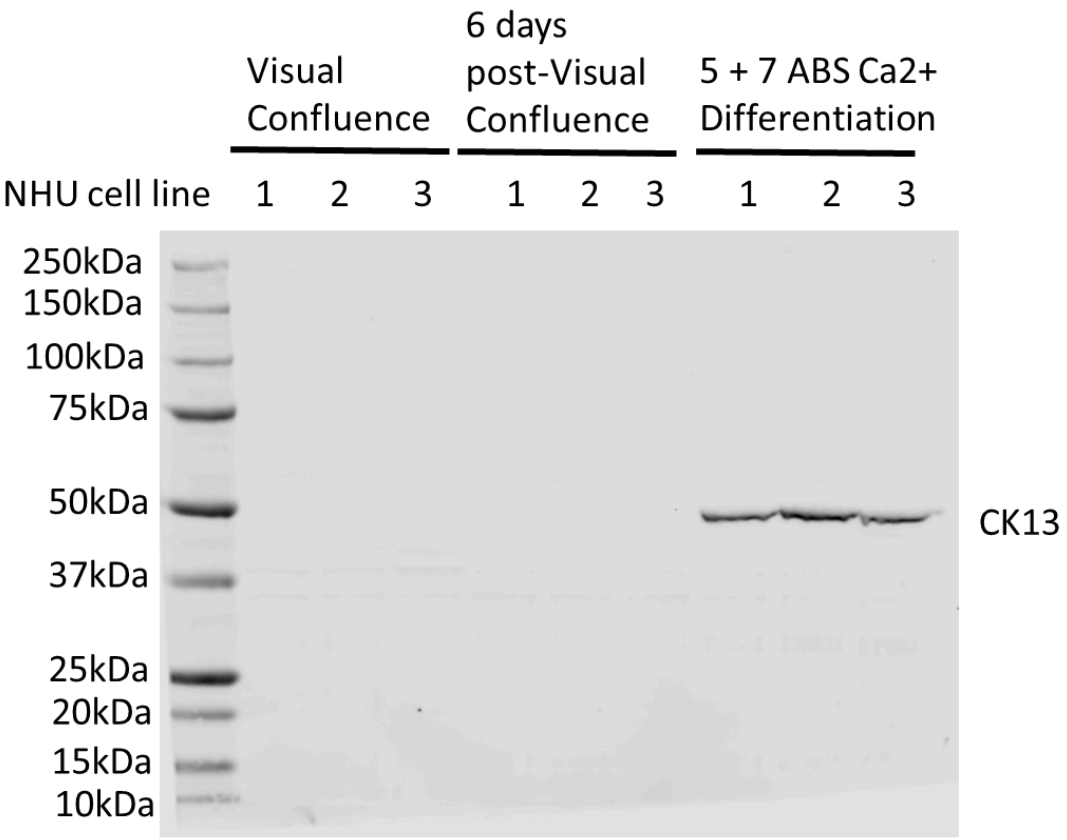

Cytokeratin 14

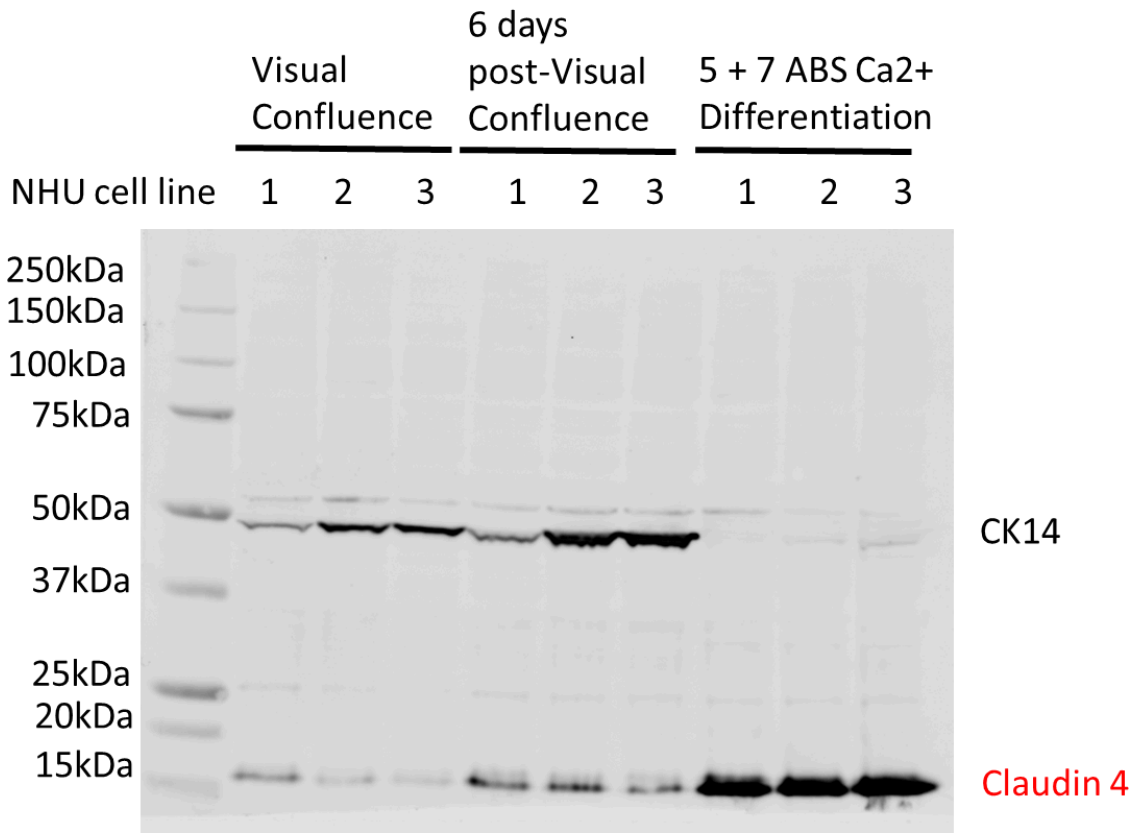

B-actin

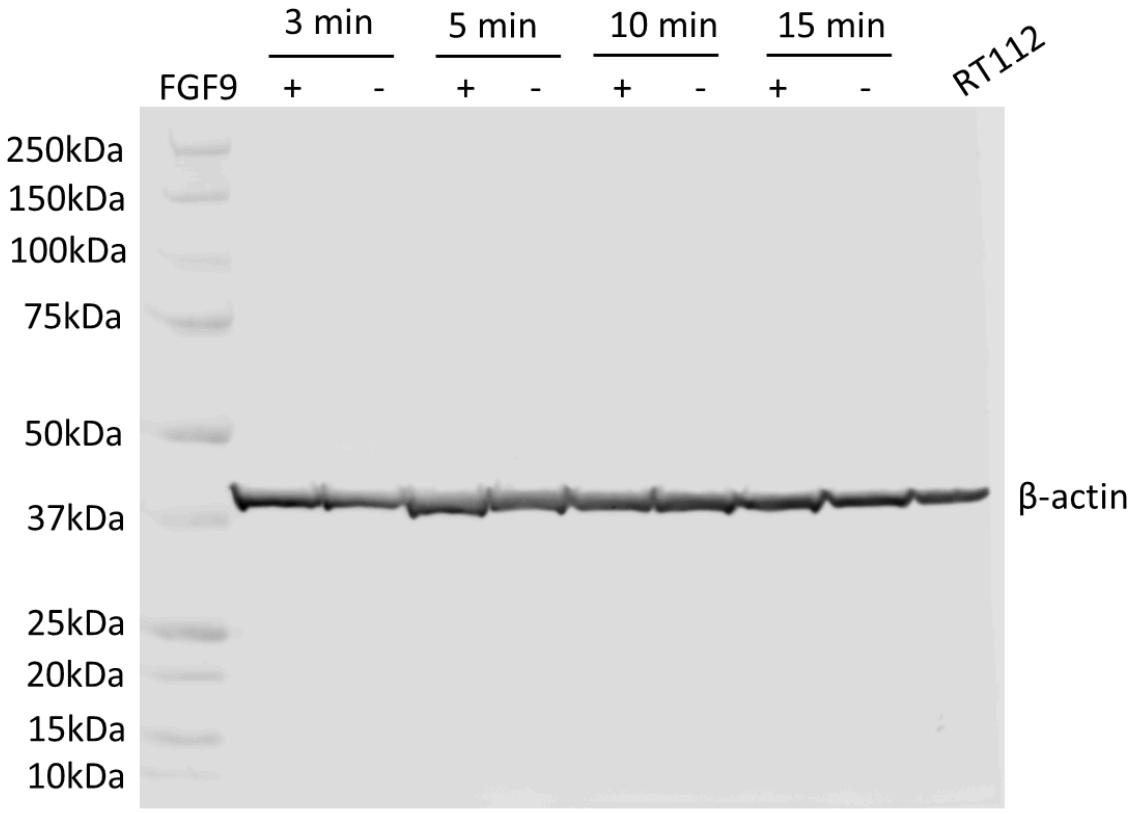
3 min
5 min
10 min
15 min
FGF9
+ - + - + - + -
RT112
250kDa
150kDa
100kDa
75kDa
50kDa
37kDa
25kDa
20kDa
15kDa
10kDa
β-actin

Appendix B - Titration of Cetuximab and Lapatinib in NHU cells

For 30-minute titrations of EGFR (family) antagonists cetuximab and lapatinib, NHU cells were serum starved overnight to reduce background EGFR signalling, then pre-treated with the antagonist for 30 minutes prior to a 30-minute treatment with EGF and antagonist before harvesting cells for western blotting.

Titration of Cetuximab

Cetuximab was titrated between 0.5 and 2 ug/mL, as per manufacturer recommendations. Two titrations were performed; one 30-minute treatment (Fig. G1, a) and a 72h-hour treatment (fig. G1, b). The ability of cetuximab to inhibit EGFR was measured by western blotting for ERK and EGFR phosphorylation. NHU cells were treated with PD153035 as a positive control for successful EGFR inhibition, as PD153035 has previously been shown to be effective at inhibiting EGFR in NHU cells [Varley et al., 2004].
At 30 minutes, 1 ug/mL cetuximab was able to reduce ERK and EGFR phosphorylation, although not as much as PD153035; 72h treatment showed a similar result. Increasing EGFR inhibition was seen with concentrations of cetuximab greater than 1 ug/mL, but potential toxicity was observed at these concentrations. At 2 ug/mL, cells showed a spindle-like morphology and became large and vacuolated (Fig. G1, b). Hence 1 ug/mL cetuximab was selected for use in further experiments.

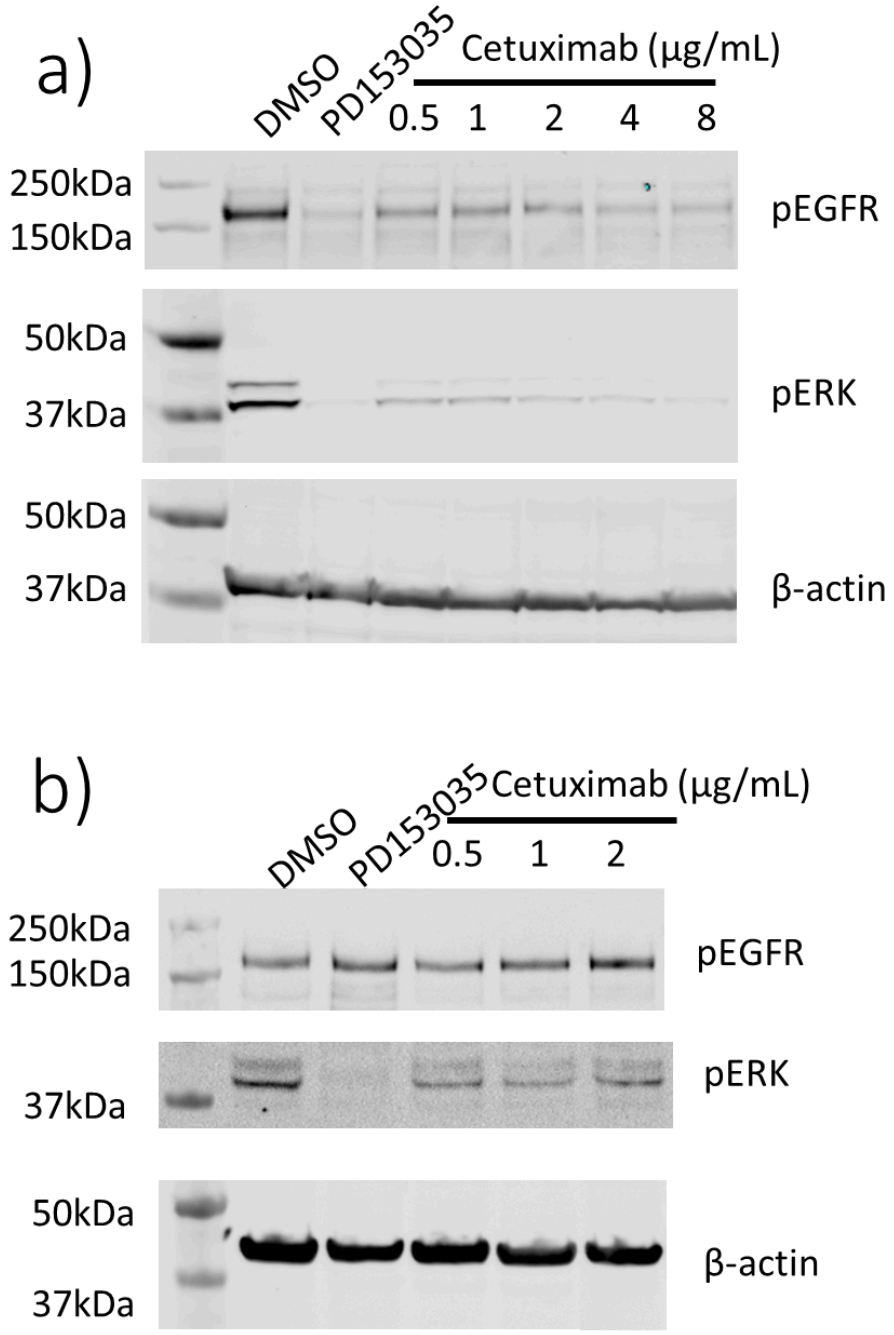

Figure G1 - Titration of cetuximab in undifferentiated NHU cells - (a) Titration of cetuximab using a 30-minute treatment, (b) titration of cetuximab using a 72 h treatment with media changed 48 h after cetuximab addition. A DMSO vehicle control was included. Effect of EGFR inhibition was assessed by western blotting for EGFR and ERK phosphorylation. PD153035 was used at 1 µM as a positive control for EGFR inhibition. Experiments were performed in NHU cell line Y1781.

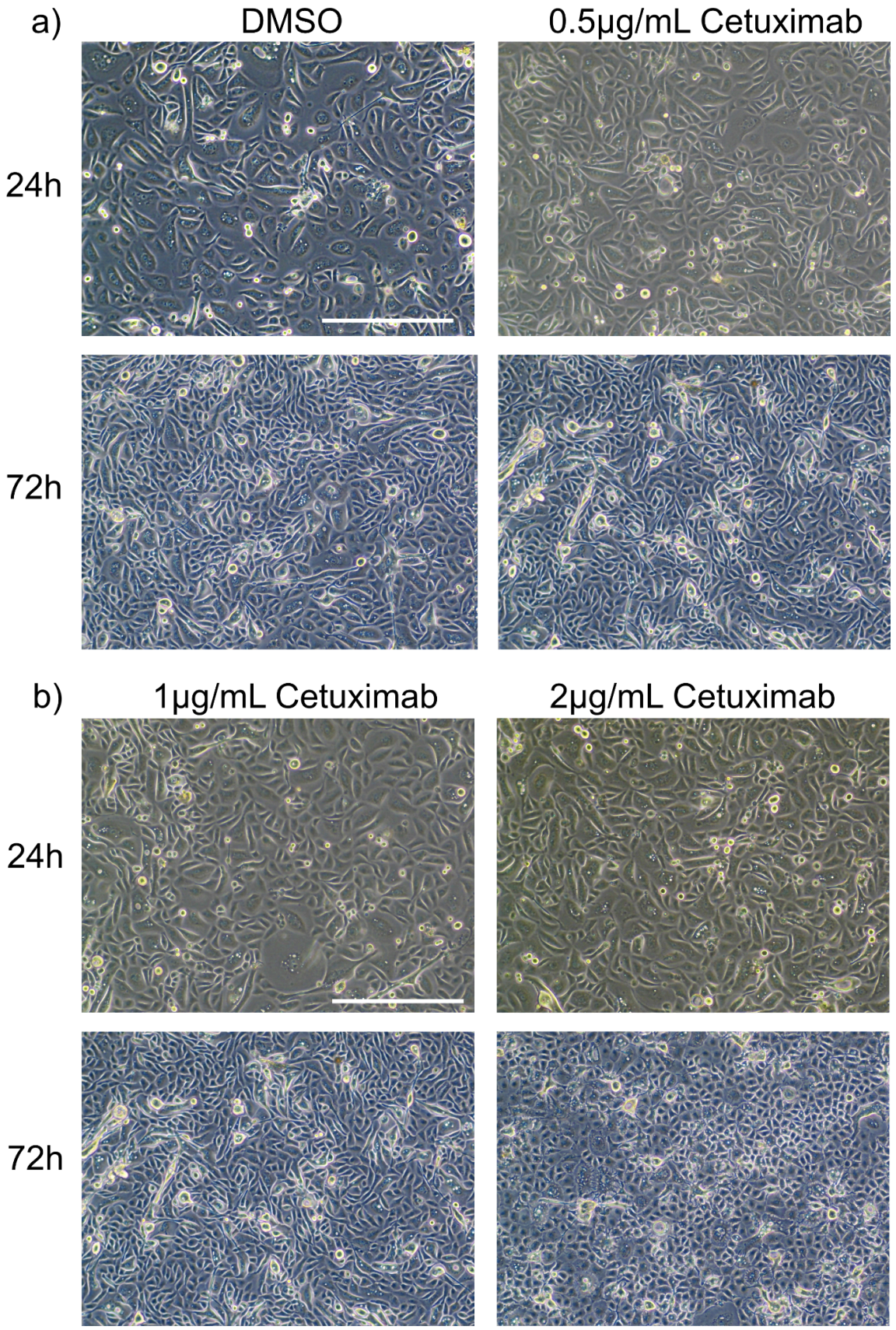

Figure G2 - Brightfield images of cells treated with cetuximab - Scale bar (white line) is 200 µm. A DMSO vehicle control was included. A smaller, spindle-like morphology can

be seen for NHU cells treated with 2 μg/mL cetuximab for 72 h, potentially indicating toxicity.

Titration of Lapatinib

For experiments where the aim was to inhibit ERK signalling in ABS-Ca^{2+} differentiated NHU cells, an EFR-family inhibitor (rather than an EGFR-only inhibitor) was required as ABS-Ca^{2+} differentiated NHU cells express ERBB2 and ERBB3 in addition to EGFR (see Appendix).

Lapatinib was titrated between 0.0156 and 1 μM, with concentrations being halved each time. Titrations were performed in both undifferentiated NHU cells (where EGFR signalling dominates and ERBB2 and ERBB3 expression is much lower) and ABS-Ca^{2+} differentiated NHU cells (where ERBB2 and ERBB3 have greatly increased expression). In undifferentiated NHU cells two titrations were performed; one 30-minute treatment (fig. G3, a) and a 72 h-hour treatment (Fig. G3, b). The ability of lapatinib to inhibit EGFR was compared to PD153035, by western blotting for ERK and EGFR phosphorylation.

At 30 minutes, 0.25 μM lapatinib gave maximal reduction of ERBB2 phosphorylation, and further increasing lapatinib concentration did not give greater inhibition (Fig. G3, a). Treatment of NHU cells with 0.5μM lapatinib was able to reduce ERK and EGFR phosphorylation to the same degree as PD153035. Hence, 0.5 and 1μM lapatinib were selected for further experiments.

NHU cells were treated with 0.5 or 1 μM lapatinib for 72 h and the reduction in ERK phosphorylation was compared to 72 h of PD153035 treatment to see if inhibition was maintained over a longer time-frame. (Fig. G3, b). Lapatinib reduced ERK phosphorylation versus the DMSO control at all time-points, although the degree of inhibition varied between time-points - at 24 h and 72 h lapatinib greatly reduced ERK phosphorylation versus DMSO control, but 48 h of lapatinib treatment gave only a very small reduction in ERK phosphorylation. Whereas at 30 minutes lapatinib was able to inhibit ERK to the same degree as PD153035, at 24-72 h, reduction in ERK phosphorylation was always much greater with PD153035 than lapatinib.

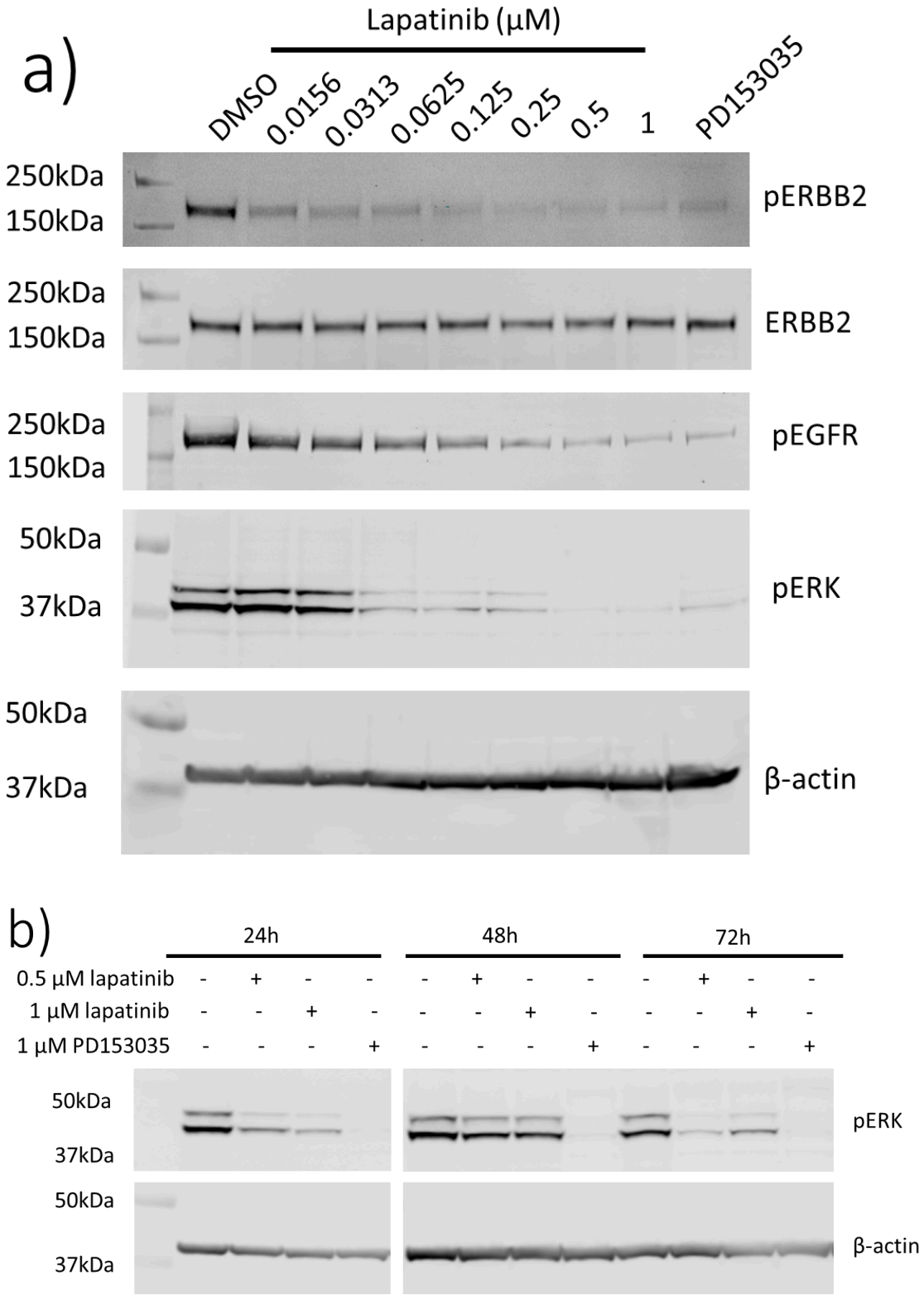

Figure G3 - Titration of lapatinib in undifferentiated NHU cells - (a) Titration of lapatinib using a 30-minute treatment, (b) titration of lapatinib using a 24-72h treatment. 30-minute titration of Lapatinib was performed in NHU cell line Y1781 and 24-72h treatment was performed in NHU cell line Y2863.

A 30-minute titration of lapatinib in ABS-Ca^{2+} differentiated NHU cells gave similar results to in undifferentiated NHU cells; reduction of ERBB2 phosphorylation was maximal at 0.5-1 μM lapatinib (Fig. G4, a).

Following this, ABS-Ca^{2+} differentiated NHU cells were treated with 0.5 or 1 μM lapatinib, either alone or in combination with PD153035, for 48 h and 96 h (fig. 4, b). Treatment with PD153035 for 48-96h did not affect ERK phosphorylation but resulted in increased ERBB2 phosphorylation. Lapatinib treatment at 0.5 μM or 1 μM did not reduce ERBB2 phosphorylation, although did reduce ERK phosphorylation vs day 0 and time-matched vehicle controls. However, lapatinib could not fully abolish ERK phosphorylation. The ability of lapatinib to reduce ERK phosphorylation appeared much greater with 48h of treatment versus 96 h of treatment.

Experiments in both undifferentiated and ABS-Ca^{2+} differentiated NHU cells showed that while 30 minutes of lapatinib was sufficient to abolish ERK phosphorylation, lapatinib appeared less effective at longer-term inhibition of EGFR family signalling. Thus lapatinib was combined with PD153035 in further long-term inhibition experiments.

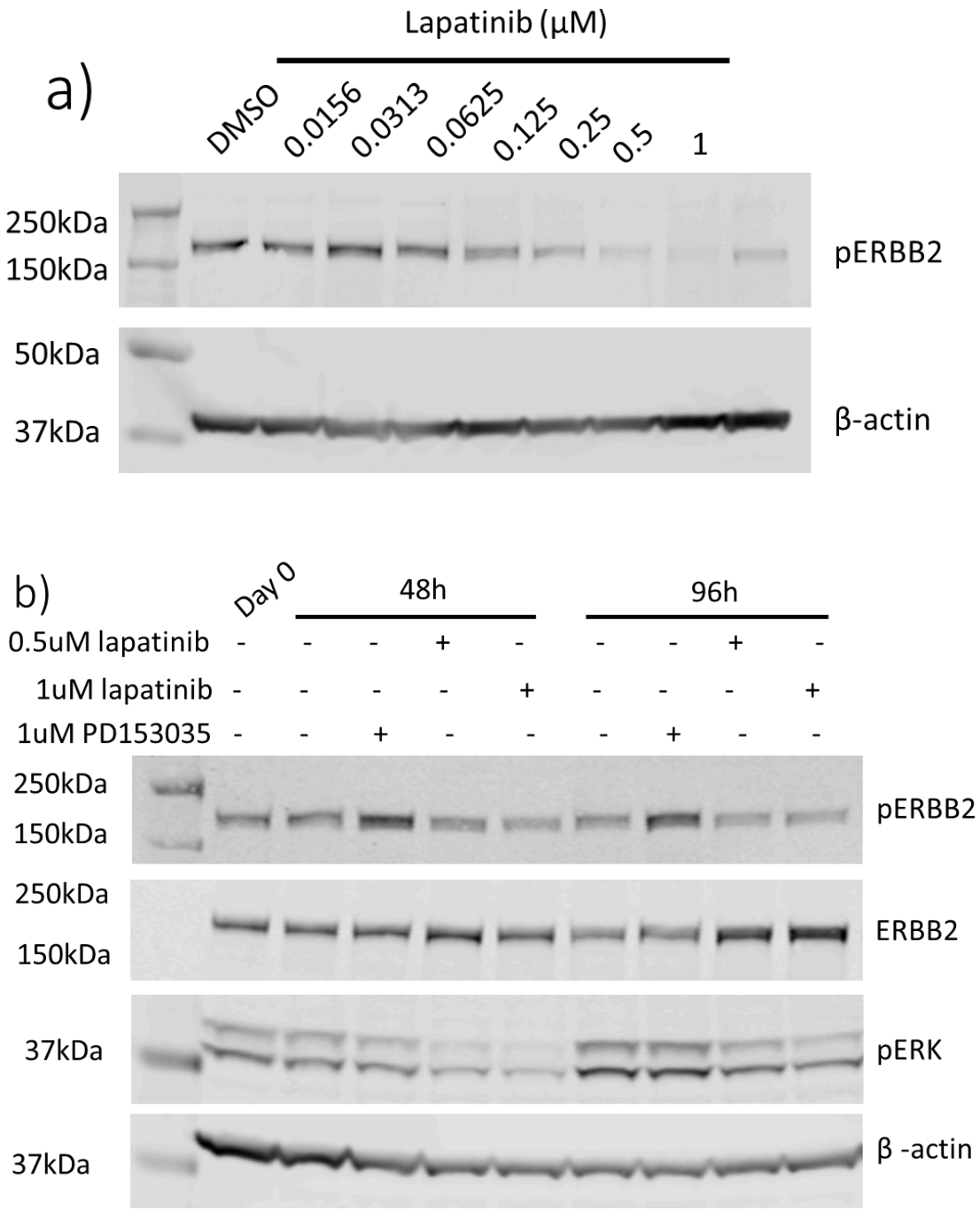

Fig G4 - Titration of lapatinib in ABS-Ca^{2+} differentiated NHU cells - (a) Titration of lapatinib using a 30-minute treatment, (b) titration of lapatinib using a 48 h or 96 h treatment. Growth medium was changed 48 h before cells were harvested. For (b), Day 0 represents untreated NHU cells from the same NHU line which were ABS-Ca^{2+} differentiated and then immediately harvested - in addition to this there is also a DMSO vehicle control at each timepoint. 30-minute titration of Lapatinib was performed in NHU cell line Y2843 and 48-96h treatment was performed in Y2863.

Appendix C - Original assessment of FGFR3 protein expression in all 8 donor samples

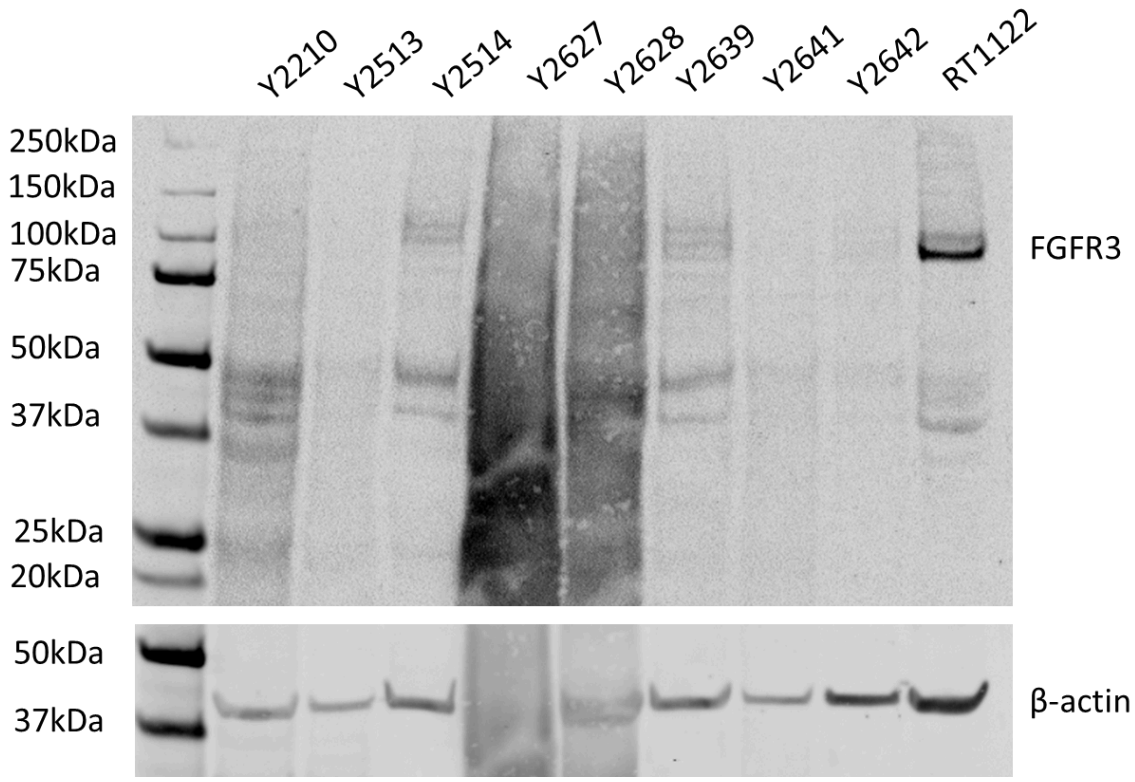

Figure C1 - FGFR3 protein expression varied across urothelial tissue samples - Western blot of urothelial tissue separated from stroma. Lysates were taken from freshly-isolated ureteric urothelium (n = 8). 20 µg of protein was loaded for each sample. β-actin was used as a loading control to ensure equal protein between lanes. Lysate from the RT112 BLCA cell line was loaded as a positive control for FGFR3 expression.

8. References

Acharya, P. et al., 2004. Distribution of the tight junction proteins ZO-1, occludin, and claudin-4, -8, and -12 in bladder epithelium. *American Journal of Physiology. Renal Physiology,* August, Volume 287, p. F305–318.

Adar, R., Monsonego-Ornan, E., David, P. & Yayon, A., 2002. Differential activation of cysteine-substitution mutants of fibroblast growth factor receptor 3 is determined by cysteine localization. *Journal of Bone and Mineral Research: The Official Journal of the American Society for Bone and Mineral Research,* May, Volume 17, p. 860–868.

Ahmadi, H. & Daneshmand, S., 2021. Multiparametric cystoscopy: is the future here yet?. *Translational Andrology and Urology,* January, Volume 10, pp. 1-6.

Ahmad, I. et al., 2011. β-Catenin activation synergizes with PTEN loss to cause bladder cancer formation. *Oncogene,* January, Volume 30, p. 178–189.

Ahmad, I. et al., 2011. Ras mutation cooperates with β-catenin activation to drive bladder tumourigenesis. *Cell Death & Disease,* March, Volume 2, p. e124–e124.

Ahmad, I. et al., 2011. K-Ras and -catenin mutations cooperate with Fgfr3 mutations in mice to promote tumorigenesis in the skin and lung, but not in the bladder. *Disease Models & Mechanisms,* April, Volume 4, pp. 548-555.

Al‐Ahmadie, H. A. et al., 2011. Somatic mutation of fibroblast growth factor receptor‐3 (FGFR3) defines a distinct morphological subtype of high‐grade urothelial carcinoma. *The Journal of Pathology,* May, Volume 224, p. 270–279.

Alexandrov, L. B. et al., 2013. Signatures of mutational processes in human cancer. *Nature,* August, Volume 500, p. 415–421.

Alonso, A., Ikinger, U. & Kartenbeck, J., 2009. Staining patterns of keratins in the human urinary tract.. *PubMed,* November, Volume 24, pp. 1425-37.

Al-Zalabani, A. H. et al., 2016. Modifiable risk factors for the prevention of bladder cancer: a systematic review of meta-analyses. *European Journal of Epidemiology,* March, Volume 31, pp. 811-851.

Aminoltejari, K. & Black, P. C., 2020. Radical cystectomy: a review of techniques, developments and controversies. *Translational Andrology and Urology,* December, Volume 9, p. 3073–3081.

Arnaud-Dabernat, S. et al., 2007. FGFR3 Is a Negative Regulator of the Expansion of Pancreatic Epithelial Cells. *Diabetes,* January, Volume 56, pp. 96-106.

Arnaud-Dabernat, S., Yadav, D. & Sarvetnick, N., 2008. FGFR3 contributes to intestinal crypt cell growth arrest. *Journal of Cellular Physiology,* Volume 216, pp. 261-268.

Ascione, C. M. et al., 2023. Role of FGFR3 in bladder cancer: Treatment landscape and future challenges. *Cancer Treatment Reviews,* April, Volume 115, p. 102530.

Audenet, F. et al., 2019. Clonal Relatedness and Mutational Differences between Upper Tract and Bladder Urothelial Carcinoma. *European Urology,* February, Volume 25, pp. 967-976.

Avivi, A., Yayon, A. & Givol, D., 1993. A novel form of FGF receptor-3 using an alternative exon in the immunoglobulin domain III. *FEBS Letters,* September, Volume 330, pp. 249-252.

Bagai, S. et al., 2002. Fibroblast Growth Factor-10 Is a Mitogen for Urothelial Cells. *Journal of Biological Chemistry,* June, Volume 277, pp. 23828-23837.

Bagrodia, A. et al., 2016. Genomic Biomarkers for the Prediction of Stage and Prognosis of Upper Tract Urothelial Carcinoma. *The Journal of Urology,* June, Volume 195, pp. 1684-1689.

Baker, S. C. et al., 2022. Induction of APOBEC3-mediated genomic damage in urothelium implicates BK polyomavirus (BKPyV) as a hit-and-run driver for bladder cancer. *Oncogene,* February, Volume 41, pp. 2139-2151.

Bakkar, A. A. et al., 2003. FGFR3 and TP53 Gene Mutations Define Two Distinct Pathways in Urothelial Cell Carcinoma of the Bladder. *Cancer Research,* December, Volume 63, pp. 8108-8112.

Balar, A. V. et al., 2017. First-line pembrolizumab in cisplatin-ineligible patients with locally advanced and unresectable or metastatic urothelial cancer (KEYNOTE-052): a multicentre, single-arm, phase 2 study. *The Lancet Oncology,* November, Volume 18, pp. 1483-1492.

Barbisan, F. et al., 2008. Strong immunohistochemical expression of fibroblast growth factor receptor 3, superficial staining pattern of cytokeratin 20, and low proliferative activity define those papillary urothelial neoplasms of low malignant potential that do not recur. *Cancer,* February, Volume 112, pp. 636-644.

Baskin, L. S. et al., 1997. Growth factors in bladder wound healing. *The Journal of Urology,* June, Volume 157, p. 2388–2395.

Baumgart, E. et al., 2007. Identification and Prognostic Significance of an Epithelial-Mesenchymal Transition Expression Profile in Human Bladder Tumors. *Clinical Cancer Research,* March, Volume 13, pp. 1685-1694.

Beer, H. D. et al., 2000. Fibroblast growth factor (FGF) receptor 1-IIIb is a naturally occurring functional receptor for FGFs that is preferentially expressed in the skin and the brain. *The Journal of Biological Chemistry,* May, Volume 275, p. 16091–16097.

Ben-Zvi, T., Yayon, A., Gertler, A. & Monsonego-Ornan, E., 2006. Suppressors of cytokine signaling (SOCS) 1 and SOCS3 interact with and modulate fibroblast growth factor receptor signaling. *Journal of Cell Science,* January, Volume 119, pp. 380-387.

Bernard-Pierrot, I. et al., 2005. Oncogenic properties of the mutated forms of fibroblast growth factor receptor 3b. *Carcinogenesis,* December, Volume 27, pp. 740-747.

Bethune, G., Bethune, D., Ridgway, N. & Xu, Z., 2010. Epidermal growth factor receptor (EGFR) in lung cancer: an overview and update. *Journal of thoracic disease,* Volume 2, pp. 48-51.

Billerey, C. et al., 2001. Frequent FGFR3 Mutations in Papillary Non-Invasive Bladder (pTa) Tumors. *The American Journal of Pathology,* June, Volume 158, p. 1955–1959.

Bindels, E. M. J. et al., 2002. Functions of epidermal growth factor-like growth factors during human urothelial reepithelialization in vitro and the role of erbB2. *Urological Research,* September, Volume 30, p. 240–247.

Bitgood, M. J. & McMahon, A. P., 1995. Hedgehog and Bmp genes are coexpressed at many diverse sites of cell-cell interaction in the mouse embryo. *Developmental Biology,* November, Volume 172, p. 126–138.

Biton, A. et al., 2014. Independent Component Analysis Uncovers the Landscape of the Bladder Tumor Transcriptome and Reveals Insights into Luminal and Basal Subtypes. *Cell Reports,* November, Volume 9, pp. 1235-1245.

Blehm, K. N. et al., 2006. Mutations within the kinase domain and truncations of the epidermal growth factor receptor are rare events in bladder cancer: implications for therapy. *Clinical Cancer Research: An Official Journal of the American Association for Cancer Research,* August, Volume 12, p. 4671–4677.

Bocharov, E. et al., 2013. Structure of FGFR3 Transmembrane Domain Dimer: Implications for Signaling and Human Pathologies. *Structure,* November, Volume 21, p. 2087–2093.

Böck, M. et al., 2014. Identification of ELF3 as an early transcriptional regulator of human urothelium. *Developmental Biology,* February, Volume 386, p. 321–330.

Böhle, A., Jocham, D. & Bock, P. R., 2003. Intravesical bacillus Calmette-Guerin versus mitomycin C for superficial bladder cancer: a formal meta-analysis of comparative studies on recurrence and toxicity. *The Journal of Urology,* January, Volume 169, p. 90–95.

Bonaventure, J., Gibbs, L., Horne, W. C. & Baron, R., 2007. The localization of FGFR3 mutations causing thanatophoric dysplasia type I differentially affects phosphorylation, processing and ubiquitylation of the receptor. *FEBS Journal,* May, Volume 274, pp. 3078-3093.

Booth, D. G., Hood, F. E., Prior, I. A. & Royle, S. J., 2011. A TACC3/ch-TOG/clathrin complex stabilises kinetochore fibres by inter-microtubule bridging. *The EMBO Journal,* February, Volume 30, pp. 906-919.

Brausi, M. et al., 2014. Side Effects of Bacillus Calmette-Guérin (BCG) in the Treatment of Intermediate- and High-risk Ta, T1 Papillary Carcinoma of the Bladder: Results of the EORTC Genito-Urinary Cancers Group Randomised Phase 3 Study Comparing One-third

Dose with Full Dose and 1 Year with 3 Years of Maintenance BCG. *European Urology,* January, Volume 65, pp. 69-76.

Breyer, J. et al., 2017. In stage pT1 non-muscle-invasive bladder cancer (NMIBC), high KRT20 and low KRT5 mRNA expression identify the luminal subtype and predict recurrence and survival. *Virchows Archiv,* January, Volume 470, pp. 267-274.

Burger, M. et al., 2008. Prediction of Progression of Non–Muscle-Invasive Bladder Cancer by WHO 1973 and 2004 Grading and by FGFR3 Mutation Status: A Prospective Study. *European Urology,* October, Volume 54, pp. 835-844.

Camps, M. et al., 1998. Catalytic Activation of the Phosphatase MKP-3 by ERK2 Mitogen-Activated Protein Kinase. *Science,* May, Volume 280, pp. 1262-1265.

Cancer Research, U. K., 2020. *Survival | Bladder cancer.* s.l.:s.n.

Cancer Research, U. K., 2022. *Stages of bladder cancer.* s.l.:s.n.

Casalini, P., Iorio, M. V., Galmozzi, E. & Ménard, S., 2004. Role of HER receptors family in development and differentiation. *Journal of Cellular Physiology,* January, Volume 200, pp. 343-350.

Catto, J. W. F. et al., 2009. Distinct microRNA alterations characterize high- and low-grade bladder cancer. *Cancer Research,* November, Volume 69, p. 8472–8481.

Ceresa, B. P., 2021. Prime time for the recycling endosome. *The EMBO Journal,* June.Volume 40.

Chadalapaka, G., Jutooru, I. & Safe, S., 2012. Celastrol decreases specificity proteins (Sp) and fibroblast growth factor receptor-3 (FGFR3) in bladder cancer cells. *Carcinogenesis,* February, Volume 33, pp. 886-894.

Chai, T. C. et al., 2000. Bladder stretch alters urinary heparin-binding epidermal growth factor and antiproliferative factor in patients with interstitial cystitis. *The Journal of Urology,* May, Volume 163, p. 1440–1444.

Chaux, A. et al., 2012. High epidermal growth factor receptor immunohistochemical expression in urothelial carcinoma of the bladder is not associated with EGFR mutations in exons 19 and 21: a study using formalin-fixed, paraffin-embedded archival tissues. *Human Pathology,* October, Volume 43, pp. 1590-1595.

Chen, F. & Hristova, K., 2011. The Physical Basis of FGFR3 Response to fgf1 and fgf2. *Biochemistry,* September, Volume 50, p. 8576–8582.

Cheng, J. et al., 2002. Overexpression of epidermal growth factor receptor in urothelium elicits urothelial hyperplasia and promotes bladder tumor growth. *Cancer Research,* July, Volume 62, p. 4157–4163.

Cheng, X. et al., 2021. Single-cell analysis reveals urothelial cell heterogeneity and regenerative cues following cyclophosphamide-induced bladder injury. *Cell Death & Disease,* May.Volume 12.

Chen, J. et al., 2005. Constitutively activated FGFR3 mutants signal through PLCgamma-dependent and -independent pathways for hematopoietic transformation. *Blood,* July, Volume 106, p. 328–337.

Chen, L. et al., 1999. Gly369Cys mutation in mouse FGFR3 causes achondroplasia by affecting both chondrogenesis and osteogenesis. *The Journal of Clinical Investigation,* December, Volume 104, p. 1517–1525.

Chen, X. et al., 2022. Mutant p53 in cancer: from molecular mechanism to therapeutic modulation. *Cell Death & Disease,* November.Volume 13.

Chew, N. J. et al., 2020. FGFR3 signaling and function in triple negative breast cancer. *Cell Communication and Signaling,* January.Volume 18.

Chodak, G. W. et al., 1988. Increased Levels of Fibroblast Growth Factor-like Activity in Urine from Patients with Bladder or Kidney Cancer. *Cancer Research,* Volume 48, p. 2083–2088.

Choi, W. et al., 2014. Identification of Distinct Basal and Luminal Subtypes of Muscle-Invasive Bladder Cancer with Different Sensitivities to Frontline Chemotherapy. *Cancer Cell,* February, Volume 25, pp. 152-165.

Cho, J. Y. et al., 2003. Defective lysosomal targeting of activated fibroblast growth factor receptor 3 in achondroplasia. *Proceedings of the National Academy of Sciences,* December, Volume 101, pp. 609-614.

Chopra, B., Hinley, J., Oleksiewicz, M. B. & Southgate, J., 2008. Trans-species comparison of PPAR and RXR expression by rat and human urothelial tissues. *Toxicologic Pathology,* April, Volume 36, p. 485–495.

Cho, R. J. et al., 2001. Transcriptional regulation and function during the human cell cycle. *Nature Genetics,* January, Volume 27, pp. 48-54.

Chow, N. H. et al., 2001. Expression profiles of ErbB family receptors and prognosis in primary transitional cell carcinoma of the urinary bladder. *Clinical Cancer Research: An Official Journal of the American Association for Cancer Research,* July, Volume 7, p. 1957–1962.

Chow, N. H. et al., 1998. Urinary excretion of transforming growth factor-alpha in patients with transitional cell carcinoma. *Anticancer research,* May, Volume 18, p. 2053–2057.

Chow, N.-H.et al., 1997. Expression patterns of erbB receptor family in normal urothelium and transitional cell carcinoma. *Virchows Archiv,* June, Volume 430, pp. 461-466.

Collaboration, A. B. C. (. M.-a., 2005. Adjuvant Chemotherapy in Invasive Bladder Cancer: A Systematic Review and Meta-Analysis of Individual Patient Data. *European Urology,* August, Volume 48, p. 189–201.

Collaboration, A. B. C. (. M.-a., 2005. Neoadjuvant Chemotherapy in Invasive Bladder Cancer: Update of a Systematic Review and Meta-Analysis of Individual Patient Data. *European Urology,* August, Volume 48, pp. 202-206.

Collaboration, A. B. C. M., 2006. Adjuvant chemotherapy for invasive bladder cancer (individual patient data). *Cochrane Database of Systematic Reviews,* April.

Colvin, J. S. et al., 1996. Skeletal overgrowth and deafness in mice lacking fibroblast growth factor receptor 3. *Nature Genetics,* April, Volume 12, pp. 390-397.

Costa, R. et al., 2016. FGFR3-TACC3 fusion in solid tumors: mini review. *Oncotarget,* July, Volume 7, p. 55924–55938.

Cross, W. R., Eardley, I., Leese, H. J. & Southgate, J., 2005. A biomimetic tissue from cultured normal human urothelial cells: analysis of physiological function. *American Journal of Physiology. Renal Physiology,* August, Volume 289, p. F459–468.

Dadhania, V. et al., 2016. Meta-Analysis of the Luminal and Basal Subtypes of Bladder Cancer and the Identification of Signature Immunohistochemical Markers for Clinical Use. *EBioMedicine,* October, Volume 12, pp. 105-117.

Daher, A. et al., 2003. Epidermal Growth Factor Receptor Regulates Normal Urothelial Regeneration. *Laboratory Investigation,* September, Volume 83, p. 1333–1341.

Dai, S. et al., 2019. Fibroblast Growth Factor Receptors (FGFRs): Structures and Small Molecule Inhibitors. *Cells,* June, Volume 8, p. 614.

Damrauer, J. S. et al., 2014. Intrinsic subtypes of high-grade bladder cancer reflect the hallmarks of breast cancer biology. *Proceedings of the National Academy of Sciences of the United States of America,* February, Volume 111, p. 3110–3115.

Davis, R. et al., 2012. Diagnosis, Evaluation and Follow-Up of Asymptomatic Microhematuria (AMH) in Adults: AUA Guideline. *Journal of Urology,* December, Volume 188, pp. 2473-2481.

de Boer, W. I., Schuller, A. G., Vermey, M. & van der Kwast, T. H., 1994. Expression of growth factors and receptors during specific phases in regenerating urothelium after acute injury in vivo. *The American Journal of Pathology,* November, Volume 145, p. 1199–1207.

de Boer, W. I. et al., 1996. Functions of fibroblast and transforming growth factors in primary organoid-like cultures of normal human urothelium.. *Laboratory investigation; a journal of technical methods and pathology,* August, 75(2), p. 147–156.

De La Rosette, J. et al., 2002. Changing Patterns of Keratin Expression could be Associated with Functional Maturation of the Developing Human Bladder. *The Journal of Urology,* August, Volume 168, pp. 709-717.

Degnin, C. R., Laederich, M. B. & Horton, W. A., 2011. Ligand activation leads to regulated intramembrane proteolysis of fibroblast growth factor receptor 3. *Molecular Biology of the Cell,* October, Volume 22, p. 3861–3873.

Deng, C. et al., 1996. Fibroblast Growth Factor Receptor 3 Is a Negative Regulator of Bone Growth. *Cell,* March, Volume 84, p. 911–921.

di Martino, E., Kelly, G., Roulson, J.-A. & Knowles, M. A., 2014. Alteration of Cell–Cell and Cell–Matrix Adhesion in Urothelial Cells: An Oncogenic Mechanism for Mutant FGFR3. *Molecular Cancer Research,* September, Volume 13, pp. 138-148.

di Martino, E. et al., 2009. Mutant fibroblast growth factor receptor 3 induces intracellular signaling and cellular transformation in a cell type- and mutation-specific manner. *Oncogene,* September, Volume 28, pp. 4306-4316.

Dobruch, J. et al., 2016. Gender and Bladder Cancer: A Collaborative Review of Etiology, Biology, and Outcomes. *European Urology,* February, Volume 69, pp. 300-310.

Dueñas, M. et al., 2015. PIK3CA gene alterations in bladder cancer are frequent and associate with reduced recurrence in non-muscle invasive tumors. *Molecular Carcinogenesis,* July, Volume 54, p. 566–576.

Dueñas, M. et al., 2016. BMP-4 production by bladder cancer cells favors tumor progression and promotes the development of a pro-tumoral immune environment. *Annals of Oncology,* November, Volume 27, p. viii10.

Eckstein, M. et al., 2018. mRNA-Expression of KRT5 and KRT20 Defines Distinct Prognostic Subgroups of Muscle-Invasive Urothelial Bladder Cancer Correlating with Histological Variants. *International Journal of Molecular Sciences,* October, Volume 19, p. 3396.

Eriksson, P. et al., 2015. Molecular subtypes of urothelial carcinoma are defined by specific gene regulatory systems. *BMC Medical Genomics,* May.Volume 8.

Fei, D. L. et al., 2012. Hedgehog Signaling Regulates Bladder Cancer Growth and Tumorigenicity. *Cancer research,* August, Volume 72, pp. 4449-4458.

Fishwick, C. et al., 2017. Heterarchy of transcription factors driving basal and luminal cell phenotypes in human urothelium. *Cell Death & Differentiation,* May, Volume 24, p. 809–818.

Fleming, J. M. et al., 2012. Differentiation-Associated Reprogramming of the Transforming Growth Factor β Receptor Pathway Establishes the Circuitry for Epithelial Autocrine/Paracrine Repair. *PLoS ONE,* December, Volume 7, p. e51404.

Foth, M. et al., 2014. Fibroblast growth factor receptor 3 activation plays a causative role in urothelial cancer pathogenesis in cooperation withPtenloss in mice. *The Journal of Pathology,* March, Volume 233, pp. 148-158.

Foth, M. et al., 2018. FGFR3 mutation increases bladder tumourigenesis by suppressing acute inflammation. *The Journal of Pathology,* September, Volume 246, pp. 331-343.

Freedman, N. D., 2011. Association Between Smoking and Risk of Bladder Cancer Among Men and Women. *JAMA,* August, Volume 306, p. 737.

Freeman, M. R. et al., 1997. Heparin-binding EGF-like growth factor is an autocrine growth factor for human urothelial cells and is synthesized by epithelial and smooth muscle cells in the human bladder. *The Journal of Clinical Investigation,* March, Volume 99, p. 1028–1036.

FRÖMTER, E. B. E. R. H. A. R. D. & DIAMOND, J. A. R. E. D., 1972. Route of Passive Ion Permeation in Epithelia. *Nature New Biology,* January, Volume 235, pp. 9-13.

Fujii, Y. et al., 2021. Molecular classification and diagnostics of upper urinary tract urothelial carcinoma. *Cancer Cell,* June, Volume 39, pp. 793-809.e8.

Gakis, G., 2020. Management of Muscle-invasive Bladder Cancer in the 2020s: Challenges and Perspectives. *European Urology Focus,* January.

Gandhi, D. et al., 2013. Retinoid Signaling in Progenitors Controls Specification and Regeneration of the Urothelium. *Developmental Cell,* September, Volume 26, p. 469–482.

Garcia del Muro, X. et al., 2000. Prognostic value of the expression of E-cadherin and β-catenin in bladder cancer. *European Journal of Cancer,* February, Volume 36, pp. 357-362.

Georgopoulos, N. T., Kirkwood, L. A. & Southgate, J., 2014. A novel bidirectional positive feedback loop between Wnt/β-catenin and EGFR/ERK: role of context-specific signalling crosstalk in modulating epithelial tissue regeneration. *Journal of Cell Science,* January.

Georgopoulos, N. T. et al., 2011. Immortalisation of normal human urothelial cells compromises differentiation capacity. *European Urology,* July, Volume 60, p. 141–149.

Gerdes, J. et al., 1991. Immunobiochemical and molecular biologic characterization of the cell proliferation-associated nuclear antigen that is defined by monoclonal antibody Ki-67.. *The American Journal of Pathology,* April, Volume 138, p. 867–873.

Gibbs, L. & Legeai-Mallet, L., 2007. FGFR3 intracellular mutations induce tyrosine phosphorylation in the Golgi and defective glycosylation. *Biochimica et Biophysica Acta (BBA) - Molecular Cell Research,* April, Volume 1773, pp. 502-512.

Guercio, B. J. et al., 2023. Clinical and Genomic Landscape of FGFR3-Altered Urothelial Carcinoma and Treatment Outcomes with Erdafitinib: A Real-World Experience. *Clinical cancer research,* September, Volume 29, pp. 4586-4595.

Guerrero-Ramos, F. et al., 2022. Predicting Recurrence and Progression in Patients with Non-Muscle-Invasive Bladder Cancer: Systematic Review on the Performance of Risk Stratification Models. *Bladder cancer,* December, Volume 8, pp. 339-357.

Hadari, Y. R., Kouhara, H., Lax, I. & Schlessinger, J., 1998. Binding of Shp2 Tyrosine Phosphatase to FRS2 Is Essential for Fibroblast Growth Factor-Induced PC12 Cell Differentiation. *Molecular and Cellular Biology,* July, Volume 18, pp. 3966-3973.

Hanafusa, H., Torii, S., Yasunaga, T. & Nishida, E., 2002. Sprouty1 and Sprouty2 provide a control mechanism for the Ras/MAPK signalling pathway. *Nature Cell Biology,* October, Volume 4, pp. 850-858.

Han, R. F. & Pan, J. G., 2006. Can intravesical bacillus Calmette-Guérin reduce recurrence in patients with superficial bladder cancer? A meta-analysis of randomized trials. *Urology,* June, Volume 67, pp. 1216-1223.

Haradhvala, N. et al., 2016. Mutational Strand Asymmetries in Cancer Genomes Reveal Mechanisms of DNA Damage and Repair. *Cell,* January, Volume 164, pp. 538-549.

Haraguchi, R. et al., 2012. The Hedgehog Signal Induced Modulation of Bone Morphogenetic Protein Signaling: An Essential Signaling Relay for Urinary Tract Morphogenesis. *PLoS ONE,* July, Volume 7, p. e42245.

Haraguchi, R. et al., 2007. Molecular analysis of coordinated bladder and urogenital organ formation by Hedgehog signaling. *Development,* February, Volume 134, pp. 525-533.

Harnden, P., Eardley, I., Joyce, A. D. & Southgate, J., 1996. Cytokeratin 20 as an objective marker of urothelial dysplasia. *BJU International,* December, Volume 78, pp. 870-875.

Harnden, P., Mahmood, N. & Southgate, J., 1999. Expression of cytokeratin 20 redefines urothelial papillomas of the bladder. *The Lancet,* March, Volume 353, pp. 974-977.

Harnden, P. & Southgate, J., 1997. Cytokeratin 14 as a marker of squamous differentiation in transitional cell carcinomas.. *Journal of Clinical Pathology,* December, Volume 50, p. 1032–1033.

Harrison, P. W. et al., 2023. Ensembl 2024. *Nucleic acids research,* November, Volume 52, pp. D891-D899.

Hart, K. C., Robertson, S. C. & Donoghue, D. J., 2001. Identification of Tyrosine Residues in Constitutively Activated Fibroblast Growth Factor Receptor 3 Involved in Mitogenesis, Stat Activation, and Phosphatidylinositol 3-Kinase Activation. *Molecular Biology of the Cell,* April, Volume 12, pp. 931-942.

Hart, K. C. et al., 2000. Transformation and Stat activation by derivatives of FGFR1, FGFR3, and FGFR4. *Oncogene,* July, Volume 19, p. 3309–3320.

Hashimoto, U. et al., 2024. N-glycan on N262 of FGFR3 regulates the intracellular localization and phosphorylation of the receptor. *Biochimica et biophysica acta. G, General subjects/Biochimica et biophysica acta. General subjects (Online),* April, Volume 1868, pp. 130565-130565.

hashmi, A. A. et al., 2018. Prognostic significance of epidermal growth factor receptor (EGFR) over expression in urothelial carcinoma of urinary bladder. *BMC Urology,* June.Volume 18.

Haugsten, E. M. et al., 2005. Different intracellular trafficking of FGF1 endocytosed by the four homologous FGF receptors. *Journal of Cell Science,* September, Volume 118, pp. 3869-3881.

Haugsten, E. M. et al., 2011. Clathrin- and Dynamin-Independent Endocytosis of FGFR3 – Implications for Signalling. *PLoS ONE,* July, Volume 6, p. e21708.

Hayashi, Y. et al., 2022. Targeted-sequence of normal urothelium and tumor of patients with non-muscle invasive bladder cancer. *Scientific Reports,* October.Volume 12.

Hecht, D. et al., 1995. Identification of Fibroblast Growth Factor 9 (FGF9) as a High Affinity, Heparin Dependent Ligand for FGF Receptors 3 and 2 but not for FGF Receptors 1 and 4. *Growth Factors,* January, Volume 12, pp. 223-233.

He, H.-c.et al., 2011. Expression of Hedgehog Pathway Components is Associated with Bladder Cancer Progression and Clinical Outcome. *Pathology & Oncology Research,* August, Volume 18, pp. 349-355.

Hernandez, S. et al., 2005. FGFR3 and Tp53 Mutations in T1G3 Transitional Bladder Carcinomas: Independent Distribution and Lack of Association with Prognosis. *Clinical Cancer Research,* August, Volume 11, pp. 5444-5450.

Hernández, S. et al., 2006. Prospective Study of FGFR3 Mutations As a Prognostic Factor in Nonmuscle Invasive Urothelial Bladder Carcinomas. *Journal of Clinical Oncology,* August, Volume 24, pp. 3664-3671.

Herrera-Abreu, M. T. et al., 2013. Parallel RNA Interference Screens Identify EGFR Activation as an Escape Mechanism in FGFR3-Mutant Cancer. *Cancer Discovery,* June, Volume 3, pp. 1058-1071.

Hinley, J. et al., 2022. Barrier forming potential of epithelial cells from the exstrophic bladder. *American Journal of Pathology,* March.

Holzmann, K. et al., 2012. Alternative Splicing of Fibroblast Growth Factor Receptor IgIII Loops in Cancer. *Journal of Nucleic Acids,* Volume 2012, pp. 1-12.

Hudolin, T. et al., 2019. Bone morphogenic proteins‐2, ‐4, ‐6 and 7 in non‐muscle invasive bladder cancer. *Oncology Letters,* December.

Hung, T.-T.et al., 2008. Molecular profiling of bladder cancer: Involvement of the TGF-β pathway in bladder cancer progression. *Cancer Letters,* June, Volume 265, pp. 27-38.

Hurst, C. D. et al., 2017. Genomic Subtypes of Non-invasive Bladder Cancer with Distinct Metabolic Profile and Female Gender Bias in KDM6A Mutation Frequency. *Cancer Cell,* November, Volume 32, p. 701–715.e7.

Hurst, C. D. et al., 2021. Stage-stratified molecular profiling of non-muscle-invasive bladder cancer enhances biological, clinical, and therapeutic insight. *Cell Reports Medicine,* December, Volume 2, p. 100472.

Hustler, A. et al., 2018. Differential transcription factor expression by human epithelial cells of buccal and urothelial derivation. *Experimental Cell Research,* August, Volume 369, pp. 284-294.

Hutton, K. A. R., Trejdosiewicz, L. K., Thomas, D. F. M. & Southgate, J., 1993. Urothelial Tissue Culture for Bladder Reconstruction: An Experimental Study. *The Journal of Urology,* August, Volume 150, pp. 721-725.

Inamura, K., 2018. Bladder Cancer: New Insights into Its Molecular Pathology. *Cancers,* April, Volume 10, p. 100.

Institute, N. C., 2023. *Bladder Cancer Prognosis and Survival Rates - NCI.* s.l.:s.n.

Islam, S. S. et al., 2015. Sonic hedgehog (Shh) signaling promotes tumorigenicity and stemness via activation of epithelial-to-mesenchymal transition (EMT) in bladder cancer. *Molecular Carcinogenesis,* March, Volume 55, pp. 537-551.

Itoh, N. & Ornitz, D. M., 2010. Fibroblast growth factors: from molecular evolution to roles in development, metabolism and disease. *Journal of Biochemistry,* October, Volume 149, p. 121–130.

Iwata, T., Li, C., Deng, X. & Francomano, C., 2001. Highly activated Fgfr3 with the K644M mutation causes prolonged survival in severe dwarf mice. *Human Molecular Genetics,* June, Volume 10, pp. 1255-1264.

Jacobi, N., Seeboeck, R., Hofmann, E. & Eger, A., 2017. ErbB Family Signalling: A Paradigm for Oncogene Addiction and Personalized Oncology. *Cancers,* April, Volume 9, p. 33.

Jafari, N. V. & Rohn, J. L., 2022. The urothelium: a multi-faceted barrier against a harsh environment. *Mucosal Immunology,* November, Volume 15, pp. 1127-1142.

Jang, J.-H., 2002. Identification and characterization of soluble isoform of fibroblast growth factor receptor 3 in human SaOS-2 osteosarcoma cells. *Biochemical and Biophysical Research Communications,* March, Volume 292, p. 378–382.

Jang, T. J., Cha, W. H. & Lee, K. S., 2010. Reciprocal correlation between the expression of cyclooxygenase-2 and E-cadherin in human bladder transitional cell carcinomas. *Virchows Archiv: An International Journal of Pathology,* September, Volume 457, p. 319–328.

Jenkins, D., Winyard, P. J. D. & Woolf, A. S., 2007. Immunohistochemical analysis of Sonic hedgehog signalling in normal human urinary tract development. *Journal of Anatomy,* November, Volume 211, pp. 620-629.

Jiang, H. et al., 2014. miR-99a promotes proliferation targeting FGFR3 in human epithelial ovarian cancer cells. *Biomedicine & Pharmacotherapy,* March, Volume 68, p. 163–169.

Jiang, S. & Redelman-Sidi, G., 2022. BCG in Bladder Cancer Immunotherapy. *Cancers,* June, Volume 14, p. 3073.

Jimenez, R. E. et al., 2001. Her-2/neu overexpression in muscle-invasive urothelial carcinoma of the bladder: prognostic significance and comparative analysis in primary and metastatic tumors. *Clinical Cancer Research: An Official Journal of the American Association for Cancer Research,* August, Volume 7, p. 2440–2447.

Jing, Y. et al., 2014. Activated androgen receptor promotes bladder cancer metastasis via Slug mediated epithelial-mesenchymal transition. *Cancer Letters,* June, Volume 348, pp. 135-145.

Johnston, C. L., Cox, H. C., Gomm, J. J. & Coombes, R. C., 1995. Fibroblast Growth Factor Receptors (FGFRs) Localize in Different Cellular Compartments. *Journal of Biological Chemistry,* December, Volume 270, pp. 30643-30650.

Jost, S. P., 1989. Cell cycle of normal bladder urothelium in developing and adult mice. *Virchows Archiv B Cell Pathology Including Molecular Pathology,* January, Volume 57, pp. 27-36.

Jost, S. P., Gosling, J. A. & Dixon, J. S., 1989. The morphology of normal human bladder urothelium. *Journal of Anatomy,* December, Volume 167, p. 103–115.

Juanpere, N. et al., 2012. Mutations in FGFR3 and PIK3CA, singly or combined with RAS and AKT1, are associated with AKT but not with MAPK pathway activation in urothelial bladder cancer. *Human Pathology,* October, Volume 43, pp. 1573-1582.

Junker, K. et al., 2008. Fibroblast Growth Factor Receptor 3 Mutations in Bladder Tumors Correlate with Low Frequency of Chromosome Alterations. *Neoplasia,* January, Volume 10, pp. 1-7.

Juríková, M., Danihel, Ľ., Polák, Š. & Varga, I., 2016. Ki67, PCNA, and MCM proteins: Markers of proliferation in the diagnosis of breast cancer. *Acta Histochemica,* June, Volume 118, p. 544–552.

Kamoun, A. et al., 2020. A Consensus Molecular Classification of Muscle-invasive Bladder Cancer. *European Urology,* April, Volume 77, p. 420–433.

Kanai, M., Göke, M., Tsunekawa, S. & Podolsky, D. K., 1997. Signal Transduction Pathway of Human Fibroblast Growth Factor Receptor 3: IDENTIFICATION OF A NOVEL 66-kDa PHOSPHOPROTEIN *. *Journal of Biological Chemistry,* March, Volume 272, p. 6621–6628.

Kashibuchi, K. et al., 2007. The prognostic value of E-cadherin, α-, β- and γ-catenin in bladder cancer patients who underwent radical cystectomy. *International Journal of Urology,* August, Volume 14, pp. 789-794.

Kassouf, W. et al., 2008. Distinctive Expression Pattern of ErbB Family Receptors Signifies an Aggressive Variant of Bladder Cancer. *Journal of Urology,* January, Volume 179, pp. 353-358.

Kastritis, E. et al., 2008. Somatic mutations of adenomatous polyposis coli gene and nuclear b-catenin accumulation have prognostic significance in invasive urothelial carcinomas: Evidence for Wnt pathway implication. *International Journal of Cancer,* October, Volume 124, pp. 103-108.

KEEGAN, K. A. T. H. L. E. E. N., JOHNSON, D. A. N. I. E. L. E., WILLIAMS, L. T. & HAYMAN, M. J., 1991. Characterization of the FGFR‐3 Gene and Its Gene Product. *Annals of the New York Academy of Sciences,* December, Volume 638, p. 400–402.

Keegan, K., Johnson, D. E., Williams, L. T. & Hayman, M. J., 1991. Isolation of an additional member of the fibroblast growth factor receptor family, FGFR-3. *Proceedings of the National Academy of Sciences of the United States of America,* February, Volume 88, p. 1095–1099.

Kimball, E. S. et al., 1984. Distinct high-performance liquid chromatography pattern of transforming growth factor activity in urine of cancer patients as compared with that of normal individuals. *Cancer Research,* August, Volume 44, p. 3613–3619.

Kim, M.-S.et al., 2006. Evidence for alternative candidate genes near RB1 involved in clonal expansion of in situ urothelial neoplasia. *Laboratory Investigation; a Journal of Technical Methods and Pathology,* February, Volume 86, p. 175–190.

Kitagawa, K. et al., 2019. Possible correlation of sonic hedgehog signaling with epithelial–mesenchymal transition in muscle-invasive bladder cancer progression. *Journal of cancer research and clinical oncology,* July, Volume 145, pp. 2261-2271.

Kolawa, A., D'Souza, A. & Tulpule, V., 2023. Overview, Diagnosis, and Perioperative Systemic Therapy of Upper Tract Urothelial Carcinoma. *Cancers,* September, Volume 15, p. 4813.

Kompier, L. C. et al., 2010. FGFR3, HRAS, KRAS, NRAS and PIK3CA Mutations in Bladder Cancer and Their Potential as Biomarkers for Surveillance and Therapy. *PLoS ONE,* November, Volume 5, p. e13821.

Kouhara, H. et al., 1997. A Lipid-Anchored Grb2-Binding Protein That Links FGF-Receptor Activation to the Ras/MAPK Signaling Pathway. *Cell,* May, Volume 89, pp. 693-702.

Kreft, M. E., Hudoklin, S., Jezernik, K. & Romih, R., 2010. Formation and maintenance of blood–urine barrier in urothelium. *Protoplasma,* June, Volume 246, pp. 3-14.

Krejci, P., 2014. The paradox of FGFR3 signaling in skeletal dysplasia: Why chondrocytes growth arrest while other cells over proliferate. *Mutation Research/Reviews in Mutation Research,* January, Volume 759, pp. 40-48.

Lafitte, M. et al., 2013. FGFR3 has tumor suppressor properties in cells with epithelial phenotype. *Molecular Cancer,* July.Volume 12.

Lamy, A. et al., 2006. Molecular Profiling of Bladder Tumors Based on the Detection of FGFR3 and TP53 Mutations. *Journal of Urology,* December, Volume 176, pp. 2686-2689.

Lawson, A. R. J. et al., 2020. Extensive heterogeneity in somatic mutation and selection in the human bladder. *Science,* October, Volume 370, p. 75–82.

Leary, J. B. et al., 2024. Frequency and Nature of Genomic Alterations in ERBB2-Altered Urothelial Bladder Cancer. *Targeted Oncology,* April, Volume 19, pp. 447-458.

Lee, Y.-C.et al., 2017. Knock-in human FGFR3 achondroplasia mutation as a mouse model for human skeletal dysplasia. *Scientific Reports,* February.Volume 7.

Lenis, A. T., Lec, P. M., Chamie, K. & MSHS, 2020. Bladder Cancer. *JAMA,* November, Volume 324, p. 1980.

Liang, Y. et al., 2016. Conditional ablation of TGF-β signaling inhibits tumor progression and invasion in an induced mouse bladder cancer model. *Scientific Reports,* July, Volume 6, p. 29479.

Liaw, A. et al., 2018. Development of the human bladder and ureterovesical junction. *Differentiation,* September, Volume 103, p. 66–73.

Li, C. et al., 1999. A Lys644Glu substitution in fibroblast growth factor receptor 3 (FGFR3) causes dwarfism in mice by activation of STATs and ink4 cell cycle inhibitors. *Human Molecular Genetics,* January, Volume 8, pp. 35-44.

Lievens, P. M.-J. & Liboi, E., 2003. The Thanatophoric Dysplasia Type II Mutation Hampers Complete Maturation of Fibroblast Growth Factor Receptor 3 (FGFR3), Which Activates Signal Transducer and Activator of Transcription 1 (STAT1) from the Endoplasmic Reticulum. *Journal of Biological Chemistry,* May, Volume 278, pp. 17344-17349.

Lievens, P. M.-J., Mutinelli, C., Baynes, D. & Liboi, E., 2004. The kinase activity of fibroblast growth factor receptor 3 with activation loop mutations affects receptor trafficking and signaling. *The Journal of Biological Chemistry,* October, Volume 279, p. 43254–43260.

Li, E., You, M. & Hristova, K., 2006. FGFR3 Dimer Stabilization Due to a Single Amino Acid Pathogenic Mutation. *Journal of Molecular Biology,* February, Volume 356, p. 600–612.

Limpert, A. S., Karlo, J. C. & Landreth, G. E., 2007. Nerve Growth Factor Stimulates the Concentration of TrkA within Lipid Rafts and Extracellular Signal-Regulated Kinase Activation through c-Cbl-Associated Protein. *Molecular and Cellular Biology,* August, Volume 27, pp. 5686-5698.

Lindgren, D. et al., 2010. Combined Gene Expression and Genomic Profiling Define Two Intrinsic Molecular Subtypes of Urothelial Carcinoma and Gene Signatures for Molecular Grading and Outcome. *Cancer Research,* April, Volume 70, pp. 3463-3472.

Lindskrog, S. V. et al., 2021. An integrated multi-omics analysis identifies prognostic molecular subtypes of non-muscle-invasive bladder cancer. *Nature Communications,* April, Volume 12, p. 2301.

Lin, J.-F.et al., 2019. Benzyl isothiocyanate suppresses IGF1R, FGFR3 and mTOR expression by upregulation of miR-99a-5p in human bladder cancer cells. *International Journal of Oncology,* March.

Lin, J., Zhao, H. & Sun, T.-T., 1995. A tissue-specific promoter that can drive a foreign gene to express in the suprabasal urothelial cells of transgenic mice.. *Proceedings of the National Academy of Sciences of the United States of America,* January, Volume 92, pp. 679-683.

Lipponen, P. & Eskelinen, M., 1994. Expression of epidermal growth factor receptor in bladder cancer as related to established prognostic factors, oncoprotein (c-erbB-2, p53) expression and long-term prognosis.. *British Journal of Cancer,* June, Volume 69, p. 1120–1125.

Li, R. et al., 2020. Macroscopic somatic clonal expansion in morphologically normal human urothelium. *Science,* October, Volume 370, p. 82–89.

Liu, C. et al., 2019. Pparg promotes differentiation and regulates mitochondrial gene expression in bladder epithelial cells. *Nature Communications,* October.Volume 10.

Li, Y. et al., 2010. Inhibition of TGF-beta receptor I by siRNA suppresses the motility and invasiveness of T24 bladder cancer cells via modulation of integrins and matrix metalloproteinase. *International Urology and Nephrology,* June, Volume 42, p. 315–323.

Lobban, E. D. et al., 1998. Uroplakin gene expression by normal and neoplastic human urothelium. *The American Journal of Pathology,* December, Volume 153, p. 1957–1967.

Locard‐Paulet, M., Palasca, O. & Jensen, L. J., 2022. Identifying the genes impacted by cell proliferation in proteomics and transcriptomics studies. *PLOS Computational Biology,* October, Volume 18, pp. e1010604-e1010604.

Lombardi, B. et al., 2017. Unique signalling connectivity of FGFR3-TACC3 oncoprotein revealed by quantitative phosphoproteomics and differential network analysis. *Oncotarget,* October, Volume 8, pp. 102898-102911.

López-Knowles, E. et al., 2006. PIK3CA Mutations Are an Early Genetic Alteration Associated with FGFR3 Mutations in Superficial Papillary Bladder Tumors. *Cancer Research,* August, Volume 66, pp. 7401-7404.

Loriot, Y. et al., 2019. Erdafitinib in Locally Advanced or Metastatic Urothelial Carcinoma. *New England Journal of Medicine,* July, Volume 381, pp. 338-348.

MacLennan, G. T., Kirkali, Z. & Cheng, L., 2007. Histologic Grading of Noninvasive Papillary Urothelial Neoplasms. *European Urology,* April, Volume 51, pp. 889-898.

Mahe, M. et al., 2018. An FGFR3/MYC positive feedback loop provides new opportunities for targeted therapies in bladder cancers. *EMBO Molecular Medicine,* April.Volume 10.

Majewski, T. et al., 2019. Whole-Organ Genomic Characterization of Mucosal Field Effects Initiating Bladder Carcinogenesis. *Cell Reports,* February, Volume 26, p. 2241–2256.e4.

Makrythanasis, P. et al., 2014. A Novel Homozygous Mutation in FGFR3 Causes Tall Stature, Severe Lateral Tibial Deviation, Scoliosis, Hearing Impairment, Camptodactyly, and Arachnodactyly. *Human Mutation,* June, Volume 35, pp. 959-963.

Mantovani, F., Collavin, L. & Del Sal, G., 2018. Mutant p53 as a guardian of the cancer cell. *Cell Death & Differentiation,* December, Volume 26, pp. 199-212.

Marsit, C. J. et al., 2005. Epigenetic Inactivation of SFRP Genes and TP53 Alteration Act Jointly as Markers of Invasive Bladder Cancer. *Cancer Research,* August, Volume 65, pp. 7081-7085.

Martin, B., 1972. Cell replacement and differentiation in transitional epithelium: a histological and autoradiographic study of the guinea-pig bladder and ureter. *J. Anat,* Volume 112, pp. 433-455.

Marzouka, N.-a.-d.et al., 2018. A validation and extended description of the Lund taxonomy for urothelial carcinoma using the TCGA cohort. *Scientific Reports,* February.Volume 8.

Mason, R. A. et al., 2009. EGFR pathway polymorphisms and bladder cancer susceptibility and prognosis. *Carcinogenesis,* April, Volume 30, pp. 1155-1160.

Mata, D. A. et al., 2020. Genetic and epigenetic landscape of IDH-wildtype glioblastomas with FGFR3-TACC3 fusions. *Acta Neuropathologica Communications,* November.Volume 8.

McConkey, D. J. et al., 2010. Molecular genetics of bladder cancer: Emerging mechanisms of tumor initiation and progression. *Urologic Oncology: Seminars and Original Investigations,* July, Volume 28, pp. 429-440.

McEwen, D. G. et al., 1999. Fibroblast Growth Factor Receptor 3 Gene Transcription Is Suppressed by Cyclic Adenosine 3′,5′-Monophosphate. *Journal of Biological Chemistry,* October, Volume 274, pp. 30934-30942.

McEwen, D. G. & Ornitz, D. M., 1998. Regulation of the Fibroblast Growth Factor Receptor 3 Promoter and Intron I Enhancer by Sp1 Family Transcription Factors. *Journal of Biological Chemistry,* February, Volume 273, pp. 5349-5357.

Mellon, J. K. et al., 1996. C-ERBB-2 in Bladder Cancer: Molecular Biology, Correlation with Epidermal Growth Factor Receptors and Prognostic Value. *The Journal of Urology,* January, Volume 155, pp. 321-326.

Mellon, K. et al., 1995. Long-term outcome related to epidermal growth factor receptor status in bladder cancer. *The Journal of Urology,* March, Volume 153, p. 919–925.

Mertens, L. S. et al., 2022. Prognostic markers in invasive bladder cancer: FGFR3 mutation status versus P53 and KI-67 expression: a multi-center, multi-laboratory analysis in 1058 radical cystectomy patients. *Urologic Oncology,* March, Volume 40, p. 110.e1–110.e9.

Messing, E. M., 1990. Clinical implications of the expression of epidermal growth factor receptors in human transitional cell carcinoma. *Cancer Research,* April, Volume 50, p. 2530–2537.

Messing, E. M., Hanson, P., Ulrich, P. & Ertürk, E., 1987. Epidermal Growth Factor—Interactions with Normal and Malignant Urothelium: In Vivo and in Situ Studies. *The Journal of Urology,* November, Volume 138, pp. 1329-1335.

Mitri, Z., Constantine, T. & O'Regan, R., 2012. The HER2 Receptor in Breast Cancer: Pathophysiology, Clinical Use, and New Advances in Therapy. *Chemotherapy Research and Practice,* Volume 2012, pp. 1-7.

Miyazaki, Y., Oshima, K., Fogo, A. & Ichikawa, I., 2003. Evidence that bone morphogenetic protein 4 has multiple biological functions during kidney and urinary tract development. *Kidney International,* March, Volume 63, pp. 835-844.

Mohammadi, M., Schlessinger, J. & Hubbard, S. R., 1996. Structure of the FGF Receptor Tyrosine Kinase Domain Reveals a Novel Autoinhibitory Mechanism. *Cell,* August, Volume 86, pp. 577-587.

Moll, R., Löwe, A., Laufer, J. & Franke, W. W., 1992. Cytokeratin 20 in human carcinomas. A new histodiagnostic marker detected by monoclonal antibodies. *The American journal of pathology,* Volume 140, pp. 427-47.

Moll, R., Schiller, D. L. & Franke, W. W., 1990. Identification of protein IT of the intestinal cytoskeleton as a novel type I cytokeratin with unusual properties and expression patterns.. *Journal of Cell Biology,* August, Volume 111, pp. 567-580.

Monsonego-Ornan, E. et al., 2000. The Transmembrane Mutation G380R in Fibroblast Growth Factor Receptor 3 Uncouples Ligand-Mediated Receptor Activation from Down-Regulation. *Molecular and Cellular Biology,* January, Volume 20, p. 516–522.

Monsonego-Ornan, E. et al., 2000. The Transmembrane Mutation G380R in Fibroblast Growth Factor Receptor 3 Uncouples Ligand-Mediated Receptor Activation from Down-Regulation. *Molecular and Cellular Biology,* January, Volume 20, pp. 516-522.

Monsonego-Ornan, E., Adar, R., Rom, E. & Yayon, A., 2002. FGF receptors ubiquitylation: dependence on tyrosine kinase activity and role in downregulation. *FEBS letters,* September, Volume 528, p. 83–89.

Moore, L. D., Le, T. & Fan, G., 2012. DNA Methylation and Its Basic Function. *Neuropsychopharmacology,* July, Volume 38, pp. 23-38.

Mooso, B. A. et al., 2015. The role of EGFR family inhibitors in muscle invasive bladder cancer: a review of clinical data and molecular evidence. *The Journal of Urology,* January, Volume 193, p. 19–29.

Moss, T. J. et al., 2017. Comprehensive Genomic Characterization of Upper Tract Urothelial Carcinoma. *European Urology,* October, Volume 72, pp. 641-649.

Murgue, B. et al., 1994. Identification of a novel variant form of fibroblast growth factor receptor 3 (FGFR3 IIIb) in human colonic epithelium. *Cancer Research,* October, Volume 54, p. 5206–5211.

Murphy, N. et al., 2022. Predictive molecular biomarkers for determining neoadjuvant chemosensitivity in muscle invasive bladder cancer. *Oncotarget,* November, Volume 13, p. 1188–1200.

Mushtaq, J., Thurairaja, R. & Nair, R., 2019. Bladder cancer. *Surgery (Oxford),* September, Volume 37, pp. 529-537.

Mysorekar, I. U. et al., 2009. Bone Morphogenetic Protein 4 Signaling Regulates Epithelial Renewal in the Urinary Tract in Response to Uropathogenic Infection. *Cell Host & Microbe,* May, Volume 5, p. 463–475.

Mysorekar, I. U., Mulvey, M. A., Hultgren, S. J. & Gordon, J. I., 2002. Molecular Regulation of Urothelial Renewal and Host Defenses during Infection with Uropathogenic Escherichia coli. *Journal of Biological Chemistry,* March, Volume 277, p. 7412–7419.

Narla, S. T. et al., 2021. Loss of Fibroblast Growth Factor Receptor 2 (FGFR2) Leads to Defective Bladder Urothelial Regeneration after Cyclophosphamide Injury. *American Journal of Pathology,* April, Volume 191, pp. 631-651.

Nassar, A. H. et al., 2018. Enrichment of FGFR3-TACC3 Fusions in Patients With Bladder Cancer Who Are Young, Asian, or Have Never Smoked. *JCO Precision Oncology,* November.pp. 1-11.

Nassar, A. H. et al., 2019. Mutational Analysis of 472 Urothelial Carcinoma Across Grades and Anatomic Sites. *Clinical Cancer Research: An Official Journal of the American Association for Cancer Research,* April, Volume 25, p. 2458–2470.

Neal, D. E. et al., 1990. The epidermal growth factor receptor and the prognosis of bladder cancer. *Cancer,* April, Volume 65, pp. 1619-1625.

Necchi, A. et al., 2021. Comprehensive Genomic Profiling of Upper-tract and Bladder Urothelial Carcinoma. *European Urology Focus,* November, Volume 7, p. 1339–1346.

Nedjadi, T. et al., 2018. Sonic Hedgehog Expression is Associated with Lymph Node Invasion in Urothelial Bladder Cancer. *Pathology & Oncology Research,* October, Volume 25, pp. 1067-1073.

Nelson, K. N. et al., 2016. Oncogenic Gene Fusion FGFR3-TACC3 Is Regulated by Tyrosine Phosphorylation. *Molecular Cancer Research,* February, Volume 14, pp. 458-469.

Network, T. C. G. A. R., 2014. Comprehensive molecular characterization of urothelial bladder carcinoma. *Nature,* January, Volume 507, pp. 315-322.

Neuzillet, Y. et al., 2012. A Meta-Analysis of the Relationship between FGFR3 and TP53 Mutations in Bladder Cancer. *PLoS ONE,* December, Volume 7, p. e48993.

Nguyen, P. L. et al., 1994. Expression of Epidermal Growth Factor Receptor in Invasive Transitional Cell Carcinoma of the Urinary Bladder:A Multivariate Survival Analysis. *American Journal of Clinical Pathology,* February, Volume 101, pp. 166-176.

Nh, C. et al., 1997. Significance of urinary epidermal growth factor and its receptor expression in human bladder cancer. *Anticancer research,* March.Volume 17.

O'Brien, J., Hayder, H., Zayed, Y. & Peng, C., 2018. Overview of MicroRNA Biogenesis, Mechanisms of Actions, and Circulation. *Frontiers in Endocrinology,* August.Volume 9.

O'BRIEN, T. S. et al., 1995. Urinary basic fibroblast growth factor in patients with bladder cancer and benign prostatic hypertrophy. *British Journal of Urology,* September, Volume 76, pp. 311-314.

Ohkubo, Y. et al., 2004. Fibroblast Growth Factor Receptor 1 Is Required for the Proliferation of Hippocampal Progenitor Cells and for Hippocampal Growth in Mouse. *Journal of Neuroscience,* July, Volume 24, pp. 6057-6069.

Okato, A. et al., 2024. FGFR inhibition augments anti–PD-1 efficacy in murine FGFR3-mutant bladder cancer by abrogating immunosuppression. *The Journal of Clinical Investigation,* January, Volume 134, p. e169241.

Ong, S. H., Lim, Y. P., Low, B. C. & Guy, G. R., 1997. SHP2 associates directly with tyrosine phosphorylated p90 (SNT) protein in FGF-stimulated cells. *Biochemical and Biophysical Research Communications,* September, Volume 238, p. 261–266.

Ornitz, D. M. & Itoh, N., 2015. The Fibroblast Growth Factor signaling pathway. *Wiley Interdisciplinary Reviews. Developmental Biology,* May, Volume 4, p. 215–266.

Ornitz, D. M. & Marie, P. J., 2015. Fibroblast growth factor signaling in skeletal development and disease. *Genes & Development,* July, Volume 29, pp. 1463-1486.

Ornitz, D. M. et al., 1996. Receptor Specificity of the Fibroblast Growth Factor Family. *Journal of Biological Chemistry,* June, Volume 271, pp. 15292-15297.

Orr-Urtreger, A. et al., 1993. Developmental localization of the splicing alternatives of fibroblast growth factor receptor-2 (FGFR2). *Developmental Biology,* August, Volume 158, p. 475–486.

Otto, W. et al., 2009. No mutations of FGFR3 in normal urothelium in the vicinity of urothelial carcinoma of the bladder harbouring activating FGFR3 mutations in patients with bladder cancer. *International Journal of Cancer,* July, Volume 125, p. 2205–2208.

Papafotiou, G. et al., 2016. KRT14 marks a subpopulation of bladder basal cells with pivotal role in regeneration and tumorigenesis. *Nature Communications,* June.Volume 7.

Parker, B. C. et al., 2013. The tumorigenic FGFR3-TACC3 gene fusion escapes miR-99a regulation in glioblastoma. *The Journal of Clinical Investigation,* January.

Park, S., Reuter, V. E. & Hansel, D. E., 2018. Non-urothelial carcinomas of the bladder. *Histopathology,* December, Volume 74, pp. 97-111.

Patel, V. G., Oh, W. K. & Galsky, M. D., 2020. Treatment of muscle‐invasive and advanced bladder cancer in 2020. *CA: A Cancer Journal for Clinicians,* August, Volume 70, pp. 404-423.

Paur, J. et al., 2015. Fibroblast growth factor receptor 3 isoforms: Novel therapeutic targets for hepatocellular carcinoma?. *Hepatology,* October, Volume 62, pp. 1767-1778.

Pederzoli, F. et al., 2019. Incremental Utility of Adjuvant Chemotherapy in Muscle-invasive Bladder Cancer: Quantifying the Relapse Risk Associated with Therapeutic Effect. *European Urology,* October, Volume 76, p. 425–429.

Pereira, E. R., Jones, D., Jung, K. & Padera, T. P., 2015. The lymph node microenvironment and its role in the progression of metastatic cancer. *Seminars in Cell & Developmental Biology,* February, Volume 38, pp. 98-105.

Perou, C. M. et al., 1999. Distinctive gene expression patterns in human mammary epithelial cells and breast cancers. *Proceedings of the National Academy of Sciences of the United States of America,* August, Volume 96, p. 9212–9217.

Perou, C. M. et al., 2000. Molecular portraits of human breast tumours. *Nature,* August, Volume 406, pp. 747-752.

Petros, F. G., 2020. Epidemiology, clinical presentation, and evaluation of upper-tract urothelial carcinoma. *Translational Andrology and Urology,* August, Volume 9, p. 1794798–1791798.

Pietzak, E. J. et al., 2017. Next-generation Sequencing of Nonmuscle Invasive Bladder Cancer Reveals Potential Biomarkers and Rational Therapeutic Targets. *European Urology,* December, Volume 72, pp. 952-959.

Popov, Z. et al., 2004. Prognostic value of EGF receptor and tumor cell proliferation in bladder cancer: therapeutic implications. *Urologic Oncology,* Volume 22, p. 93–101.

Porten, S., Leapman, M. & Greene, K., 2015. Intravesical chemotherapy in non-muscle-invasive bladder cancer. *Indian Journal of Urology,* Volume 31, p. 297.

Qing, J. et al., 2009. Antibody-based targeting of FGFR3 in bladder carcinoma and t(4;14)-positive multiple myeloma in mice. *Journal of Clinical Investigation,* May, Volume 119, pp. 1216-1229.

Raghavan, D., 2003. Chemotherapy and cystectomy for invasive transitional cell carcinoma of bladder. *Urologic Oncology: Seminars and Original Investigations,* November, Volume 21, p. 468–474.

Rao, N. et al., 2023. Analysis of Several Common APOBEC-type Mutations in Bladder Tumors Suggests Links to Viral Infection. *Cancer Prevention Research,* July, Volume 16, p. 561–570.

Rebouissou, S. et al., 2014. EGFR as a potential therapeutic target for a subset of muscle-invasive bladder cancers presenting a basal-like phenotype. *Science Translational Medicine,* July, Volume 6, p. 244ra91.

Reinhold, M. I., McEwen, D. G. & Naski, M. C., 2004. Fibroblast Growth Factor Receptor 3 Gene: Regulation by Serum Response Factor. *Molecular Endocrinology,* January, Volume 18, pp. 241-251.

Remy, E. et al., 2015. A Modeling Approach to Explain Mutually Exclusive and Co-Occurring Genetic Alterations in Bladder Tumorigenesis. *Cancer Research,* September, Volume 75, pp. 4042-4052.

Rhijn, v. et al., 2010. Molecular Grade (FGFR3/MIB-1) and EORTC Risk Scores Are Predictive in Primary Non–Muscle-Invasive Bladder Cancer. *European Urology,* September, Volume 58, pp. 433-441.

Rhijn, v. et al., 2010. The Pathologist's Mean Grade Is Constant and Individualizes the Prognostic Value of Bladder Cancer Grading. *European Urology,* June, Volume 57, pp. 1052-1057.

Richelda, R. et al., 1997. A novel chromosomal translocation t(4; 14)(p16.3; q32) in multiple myeloma involves the fibroblast growth-factor receptor 3 gene. *Blood,* November, Volume 90, p. 4062–4070.

Ridyard, M. S. & Robbins, S. M., 2003. Fibroblast Growth Factor-2-induced Signaling through Lipid Raft-associated Fibroblast Growth Factor Receptor Substrate 2 (FRS2). *Journal of Biological Chemistry,* April, Volume 278, pp. 13803-13809.

Rinaldetti, S. et al., 2022. High-Content Drug Discovery Targeting Molecular Bladder Cancer Subtypes. *International Journal of Molecular Sciences,* September, Volume 23, p. 10605.

Robertson, A. G. et al., 2017. Comprehensive Molecular Characterization of Muscle-Invasive Bladder Cancer. *Cell,* Volume 171, pp. 540-556.e25.

Robinson, B. D. et al., 2019. Upper tract urothelial carcinoma has a luminal-papillary T-cell depleted contexture and activated FGFR3 signaling. *Nature Communications,* July, Volume 10, p. 2977.

Rohmann, E. et al., 2006. Mutations in different components of FGF signaling in LADD syndrome. *Nature Genetics,* April, Volume 38, p. 414–417.

Ronchetti, D. et al., 2001. Deregulated FGFR3 mutants in multiple myeloma cell lines with t(4;14): comparative analysis of Y373C, K650E and the novel G384D mutations. *Oncogene,* June, Volume 20, pp. 3553-3562.

Rosen, R. D. & Sapra, A., 2020. *TNM Classification.* s.l.:StatPearls Publishing.

Rose, T. L. et al., 2021. Fibroblast growth factor receptor 3 alterations and response to immune checkpoint inhibition in metastatic urothelial cancer: a real world experience. *British Journal of Cancer,* July, Volume 125, pp. 1251-1260.

Røtterud, R., Fosså, S. D. & Nesland, J. M., 2007. Protein networking in bladder cancer: immunoreactivity for FGFR3, EGFR, ERBB2, KAI1, PTEN, and RAS in normal and malignant urothelium. *Histology and Histopathology,* April, Volume 22, p. 349–363.

Rousseau, F. et al., 1996. Missense FGFR3 mutations create cysteine residues in thanatophoric dwarfism type I (TD1). *Human Molecular Genetics,* April, Volume 5, pp. 509-512.

Rozenblatt-Rosen, O. et al., 2002. Induction of chondrocyte growth arrest by FGF: transcriptional and cytoskeletal alterations. *Journal of Cell Science,* February, Volume 115, pp. 553-562.

Rozen, S. G., 2020. Mutational selection in normal urothelium. *Science,* October, Volume 370, p. 34–35.

Sami, M. M. et al., 2023. Expression of epidermal growth factor receptor and human epidermal growth factor receptor 2 in urothelial bladder carcinoma in an Egyptian cohort: Clinical implication and prognostic significance. *Rivista Urologia,* January, Volume 90, pp. 248-260.

Santiago-Walker, A. E. et al., 2019. Predictive value of fibroblast growth factor receptor (FGFR) mutations and gene fusions on anti-PD-(L)1 treatment outcomes in patients (pts) with advanced urothelial cancer (UC).. *Journal of Clinical Oncology,* March, Volume 37, p. 419–419.

Santos, A., Wernersson, R. & Jensen, L. J., 2014. Cyclebase 3.0: a multi-organism database on cell-cycle regulation and phenotypes. *Nucleic Acids Research,* November, Volume 43, pp. D1140-D1144.

Sarkar, S., Ryan, E. L. & Royle, S. J., 2017. FGFR3–TACC3 cancer gene fusions cause mitotic defects by removal of endogenous TACC3 from the mitotic spindle. *Open Biology,* August, Volume 7, p. 170080.

Schmoldt, A., Benthe, H. F. & Haberland, G., 1975. Digitoxin metabolism by rat liver microsomes.. *Biochemical pharmacology,* September, 24(17), p. 1639–1641.

Scotet, E. & Houssaint, E., 1995. The choice between alternative IIIb and IIIc exons of the FGFR-3 gene is not strictly tissue-specific. *Biochimica Et Biophysica Acta,* November, Volume 1264, p. 238–242.

Seiler, R. et al., 2017. Impact of Molecular Subtypes in Muscle-invasive Bladder Cancer on Predicting Response and Survival after Neoadjuvant Chemotherapy. *European Urology,* October, Volume 72, pp. 544-554.

Senol, S. et al., 2015. Prognostic significance of survivin, β-catenin and p53 expression in urothelial carcinoma. *Bosnian Journal of Basic Medical Sciences,* August.Volume 15.

Sfakianos, J. P. et al., 2015. Genomic Characterization of Upper Tract Urothelial Carcinoma. *European Urology,* December, Volume 68, p. 970–977.

Shariat, S. F., Karam, J. A., Lotan, Y. & Karakiewizc, P. I., 2008. Critical Evaluation of Urinary Markers for Bladder Cancer Detection and Monitoring. *Reviews in Urology,* Volume 10, p. 120–135.

Sharma, S. & Baysal, B. E., 2017. Stem-loop structure preference for site-specific RNA editing by APOBEC3A and APOBEC3G. *PeerJ,* December, Volume 5, p. e4136.

Shaw, N. J., Georgopoulos, N. T., Southgate, J. & Trejdosiewicz, L. K., 2005. Effects of loss of p53 and p16 function on life span and survival of human urothelial cells. *International journal of cancer,* April, Volume 116, pp. 634-639.

Shigeta, K. et al., 2022. Profiling the Biological Characteristics and Transitions through Upper Tract Tumor Origin, Bladder Recurrence, and Muscle-Invasive Bladder Progression in Upper Tract Urothelial Carcinoma. *International journal of molecular sciences,* May, Volume 23, pp. 5154-5154.

SHIINA, H. I. R. O. A. K. I. et al., 2002. β-Catenin Mutations Correlate with Over Expression of C-myc and Cyclin D1 Genes in Bladder Cancer. *Journal of Urology,* November, Volume 168, pp. 2220-2226.

Shi, M.-J.et al., 2022. FGFR3 Mutational Activation Can Induce Luminal-like Papillary Bladder Tumor Formation and Favors a Male Sex Bias. *European Urology,* October.

Shi, M.-J.et al., 2020. Identification of new driver and passenger mutations within APOBEC-induced hotspot mutations in bladder cancer. *Genome Medicine,* September.Volume 12.

Shi, M.-J.et al., 2019. APOBEC-mediated Mutagenesis as a Likely Cause of FGFR3 S249C Mutation Over-representation in Bladder Cancer. *European Urology,* July, Volume 76, pp. 9-13.

Shin, K. et al., 2011. Hedgehog/Wnt feedback supports regenerative proliferation of epithelial stem cells in bladder. *Nature,* March, Volume 472, pp. 110-114.

Shin, K. et al., 2014. Hedgehog Signaling Restrains Bladder Cancer Progression by Eliciting Stromal Production of Urothelial Differentiation Factors. *Cancer Cell,* October, Volume 26, pp. 521-533.

Simeonova, P. P. et al., 2000. Arsenic mediates cell proliferation and gene expression in the bladder epithelium: association with activating protein-1 transactivation. *Cancer Research,* July, Volume 60, p. 3445–3453.

Sjödahl, G. et al., 2011. A systematic study of gene mutations in urothelial carcinoma; inactivating mutations in TSC2 and PIK3R1. *PloS One,* April, Volume 6, p. e18583.

Sjodahl, G. et al., 2012. A Molecular Taxonomy for Urothelial Carcinoma. *Clinical Cancer Research,* May, Volume 18, pp. 3377-3386.

Slaughter, D. P., Southwick, H. W. & Smejkal, W., 1953. “Field cancerization” in oral stratified squamous epithelium. Clinical implications of multicentric origin. *Cancer,* September, Volume 6, p. 963–968.

Smirle, J. et al., 2013. Cell Biology of the Endoplasmic Reticulum and the Golgi Apparatus through Proteomics. *Cold Spring Harbor Perspectives in Biology,* January, Volume 5, pp. a015073-a015073.

Smith, N. J. et al., 2015. The human urothelial tight junction: claudin 3 and the ZO-1α+ switch. *Bladder,* Volume 2, p. e9.

Sobin, L. H., Gospodarowicz, M. K. & Wittekind, C., 2009. *TNM Classification of Malignant Tumours.* s.l.:John Wiley & Sons.

Sochet, A. A. et al., 2020. Plasma and Urinary FGF-2 and VEGF-A Levels Identify Children at Risk for Severe Bleeding after Pediatric Cardiopulmonary Bypass: A Pilot Study.. *Medical research archives,* January.Volume 8.

Society, A. C., 2024. *Key Statistics for Bladder Cancer.* s.l.:s.n.

Song, Y. et al., 2023. Fibroblast growth factor receptor 3 mutation attenuates response to immune checkpoint blockade in metastatic urothelial carcinoma by driving immunosuppressive microenvironment. *Journal for ImmunoTherapy of Cancer,* September, Volume 11, pp. e006643-e006643.

Sorokin, A., Lemmon, M. A., Ullrich, A. & Schlessinger, J., 1994. Stabilization of an active dimeric form of the epidermal growth factor receptor by introduction of an inter-receptor disulfide bond. *The Journal of Biological Chemistry,* April, Volume 269, p. 9752–9759.

Southgate, J., Harnden, P. & Trejdosiewicz, L. K., 1999. Cytokeratin expression patterns in normal and malignant urothelium: a review of the biological and diagnostic implications. *Histology and Histopathology,* April, Volume 14, p. 657–664.

Southgate, J., Hutton, K. A., Thomas, D. F. & Trejdosiewicz, L. K., 1994. Normal human urothelial cells in vitro: proliferation and induction of stratification. *Laboratory Investigation; a Journal of Technical Methods and Pathology,* Volume 71, p. 583–594.

Southgate, J., Masters, J. R. W. & Trejdosiewicz, L. K., 2002. Culture of Human Urothelium. *Culture of Specialized Cells,* April.pp. 381-399.

Southgate, J. et al., 2007. Differentiation potential of urothelium from patients with benign bladder dysfunction. *BJU International,* June, Volume 99, pp. 1506-1516.

Spruck, C. H. et al., 1994. Two molecular pathways to transitional cell carcinoma of the bladder. *Cancer Research,* February, Volume 54, p. 784–788.

Steinberg, R. L., Thomas, L. J., Mott, S. L. & O'Donnell, M. A., 2016. Bacillus Calmette-Guérin (BCG) Treatment Failures with Non-Muscle Invasive Bladder Cancer: A Data-Driven Definition for BCG Unresponsive Disease. *Bladder Cancer,* April, Volume 2, pp. 215-224.

St-Germain, J. et al., 2014. Differential regulation of FGFR3 by PTPN1 and PTPN2. *Proteomics,* December, Volume 15, pp. 419-433.

Stoehr, R. et al., 2002. No evidence for involvement of β-catenin and APC in urothelial carcinomas. *International journal of oncology,* May.

Stojnev, S. et al., 2019. Prognostic Impact of Canonical TGF-β Signaling in Urothelial Bladder Cancer. *Medicina,* June, Volume 55, p. 302.

Suda, K. et al., 2023. Distinct effects of Fgf7 and Fgf10 on the terminal differentiation of murine bladder urothelium revealed using an organoid culture system. *BMC urology,* October.Volume 23.

Su, X. et al., 2021. Comprehensive integrative profiling of upper tract urothelial carcinomas. *Genome Biology,* January.Volume 22.

Sverrisson, E. F. et al., 2014. Clinicopathological correlates of Gli1 expression in a population-based cohort of patients with newly diagnosed bladder cancer. *Urologic oncology,* July, Volume 32, pp. 539-545.

Swanton, C., McGranahan, N., Starrett, G. J. & Harris, R. S., 2015. APOBEC Enzymes: Mutagenic Fuel for Cancer Evolution and Heterogeneity. *Cancer Discovery,* June, Volume 5, pp. 704-712.

Sweis, R. F. et al., 2016. Molecular Drivers of the Non-T-cell-Inflamed Tumor Microenvironment in Urothelial Bladder Cancer. *Cancer Immunology Research,* May, Volume 4, pp. 563-568.

Swiatkowski, S. et al., 2003. Activities of MAP-Kinase Pathways in Normal Uroepithelial Cells and Urothelial Carcinoma Cell Lines. *Experimental cell research,* January, Volume 282, pp. 48-57.

Sylvester, R. J. et al., 2006. Predicting recurrence and progression in individual patients with stage Ta T1 bladder cancer using EORTC risk tables: a combined analysis of 2596 patients from seven EORTC trials. *European Urology,* March, Volume 49, pp. 466–465; discussion 475-477.

Syrigos, K. N. et al., 1998. ALTERED gamma-CATENIN EXPRESSION CORRELATES WITH POOR SURVIVAL IN PATIENTS WITH BLADDER CANCER. *Investigative Urology,* November, Volume 160, pp. 1889-1893.

Szarvas, T., Módos, O., Horváth, A. & Nyirády, P., 2016. Why are upper tract urothelial carcinoma two different diseases?. *Translational Andrology and Urology,* October, Volume 5, p. 636–647.

Szybowska, P. et al., 2021. Negative Regulation of FGFR (Fibroblast Growth Factor Receptor) Signaling. *Cells,* May, Volume 10, p. 1342.

Tadeo, V. et al., 2017. BMP4 Induces M2 Macrophage Polarization and Favors Tumor Progression in Bladder Cancer. *Clinical Cancer Research,* December, Volume 23, pp. 7388-7399.

Tang, D. H. & Chang, S. S., 2015. Management of carcinoma in situ of the bladder: best practice and recent developments. *Therapeutic Advances in Urology,* August, Volume 7, pp. 351-364.

Tan, T. Z. et al., 2019. Molecular Subtypes of Urothelial Bladder Cancer: Results from a Meta-cohort Analysis of 2411 Tumors. *European Urology,* March, Volume 75, p. 423–432.

Tash, J. A., David, S. G., Vaughan ED, E. D. & Herzlinger, D. A., 2001. Fibroblast growth factor-7 regulates stratification of the bladder urothelium. *The Journal of Urology,* December, Volume 166, p. 2536–2541.

Tate, T. et al., 2021. Pparg signaling controls bladder cancer subtype and immune exclusion. *Nature Communications,* October.Volume 12.

Tavormina, P. L. et al., 1995. Thanatophoric dysplasia (types I and II) caused by distinct mutations in fibroblast growth factor receptor 3. *Nature Genetics,* March, Volume 9, p. 321–328.

Teo, M. Y. et al., 2020. Fibroblast Growth Factor Receptor 3 Alteration Status is Associated with Differential Sensitivity to Platinum-based Chemotherapy in Locally Advanced and Metastatic Urothelial Carcinoma. *European Urology,* December, Volume 78, p. 907–915.

Terada, M. et al., 2001. Fibroblast growth factor receptor 3 lacking the Ig IIIb and transmembrane domains secreted from human squamous cell carcinoma DJM-1 binds to FGFs. *Molecular cell biology research communications: MCBRC,* November, Volume 4, p. 365–373.

Tomiyama, E. et al., 2022. Comparison of molecular profiles of upper tract urothelial carcinoma vs. urinary bladder cancer in the era of targeted therapy: a narrative review. *Translational andrology and urology,* December, Volume 11, pp. 1747-1761.

Tomlinson, D. C., Baldo, O., Harnden, P. & Knowles, M. A., 2007. FGFR3 protein expression and its relationship to mutation status and prognostic variables in bladder cancer. *The Journal of Pathology,* Volume 213, pp. 91-98.

Tomlinson, D. C., Hurst, C. D. & Knowles, M. A., 2007. Knockdown by shRNA identifies S249C mutant FGFR3 as a potential therapeutic target in bladder cancer. *Oncogene,* March, Volume 26, pp. 5889-5899.

Tomlinson, D. C. et al., 2005. Alternative Splicing of Fibroblast Growth Factor Receptor 3 Produces a Secreted Isoform That Inhibits Fibroblast Growth Factor–Induced Proliferation and Is Repressed in Urothelial Carcinoma Cell Lines. *Cancer Research,* November, Volume 65, pp. 10441-10449.

Tosoni, I. et al., 2000. Clinical significance of interobserver differences in the staging and grading of superficial bladder cancer. *BJU International,* January, Volume 85, pp. 48-53.

Toydemir, R. M. et al., 2006. A Novel Mutation in FGFR3 Causes Camptodactyly, Tall Stature, and Hearing Loss (CATSHL) Syndrome. *The American Journal of Human Genetics,* November, Volume 79, pp. 935-941.

Tsai, T.-F.et al., 2020. Benzyl isothiocyanate promotes miR-99a expression through ERK/AP-1-dependent pathway in bladder cancer cells. *Environmental Toxicology,* January, Volume 35, p. 47–54.

Turo, R. et al., 2015. FGFR3 Expression in Primary Invasive Bladder Cancers and Matched Lymph Node Metastases. *Journal of Urology,* January, Volume 193, pp. 325-330.

Uhlen, M. et al., 2015. Tissue-based map of the human proteome. *Science,* January, Volume 347, pp. 1260419-1260419.

Urakami, S. et al., 2006. Combination Analysis of Hypermethylated Wnt-Antagonist Family Genes as a Novel Epigenetic Biomarker Panel for Bladder Cancer Detection. *Clinical Cancer Research,* April, Volume 12, pp. 2109-2116.

Urakami, S. et al., 2006. Epigenetic Inactivation of Wnt Inhibitory Factor-1 Plays an Important Role in Bladder Cancer through Aberrant Canonical Wnt/ -Catenin Signaling Pathway. *Clinical Cancer Research,* January, Volume 12, pp. 383-391.

van den Bosch, S. & Alfred Witjes, J., 2011. Long-term Cancer-specific Survival in Patients with High-risk, Non–muscle-invasive Bladder Cancer and Tumour Progression: A Systematic Review. *European Urology,* September, Volume 60, pp. 493-500.

van Oers, J. M. M. et al., 2006. Chromosome 9 deletions are more frequent than FGFR3 mutations in flat urothelial hyperplasias of the bladder. *International Journal of Cancer,* September, Volume 119, p. 1212–1215.

van Oers, J. M. M. et al., 2007. FGFR3 mutations and a normal CK20 staining pattern define low-grade noninvasive urothelial bladder tumours. *European Urology,* September, Volume 52, p. 760–768.

van Rhijn, B. W. G. et al., 2020. FGFR3 Mutation Status and FGFR3 Expression in a Large Bladder Cancer Cohort Treated by Radical Cystectomy: Implications for Anti-FGFR3 Treatment?†. *European Urology,* November, Volume 78, pp. 682-687.

van Rhijn, B. W. G. et al., 2002. Frequent FGFR3 mutations in urothelial papilloma. *The Journal of Pathology,* July, Volume 198, pp. 245-251.

van Rhijn, B. W. G. et al., 2004. FGFR3 and P53 characterize alternative genetic pathways in the pathogenesis of urothelial cell carcinoma. *Cancer Research,* March, Volume 64, p. 1911–1914.

van Rhijn, B. W. G. et al., 2003. Molecular Grading of Urothelial Cell Carcinoma With Fibroblast Growth Factor Receptor 3 and MIB-1 is Superior to Pathologic Grade for the Prediction of Clinical Outcome. *Journal of Clinical Oncology,* May, Volume 21, pp. 1912-1921.

van Rhijn, B. W. et al., 2001. The fibroblast growth factor receptor 3 (FGFR3) mutation is a strong indicator of superficial bladder cancer with low recurrence rate. *Cancer Research,* February, Volume 61, p. 1265–1268.

Varley, C. et al., 2005. Autocrine regulation of human urothelial cell proliferation and migration during regenerative responses in vitro. *Experimental Cell Research,* May, Volume 306, pp. 216-229.

Varley, C. L., Bacon, E. J., Holder, J. C. & Southgate, J., 2008. FOXA1 and IRF-1 intermediary transcriptional regulators of PPARγ-induced urothelial cytodifferentiation. *Cell Death & Differentiation,* August, Volume 16, pp. 103-114.

Varley, C. L. et al., 2006. PPARγ-regulated tight junction development during human urothelial cytodifferentiation. *Journal of Cellular Physiology,* Volume 208, pp. 407-417.

Varley, C. L. et al., 2004. Role of PPARgamma and EGFR signalling in the urothelial terminal differentiation programme. *Journal of Cell Science,* April, Volume 117, p. 2029–2036.

Varley, C. L. et al., 2004. Activation of peroxisome proliferator-activated receptor-gamma reverses squamous metaplasia and induces transitional differentiation in normal human urothelial cells. *The American Journal of Pathology,* May, Volume 164, p. 1789–1798.

Vishnu, P., Mathew, J. & Tan, W., 2011. Current therapeutic strategies for invasive and metastatic bladder cancer. *OncoTargets and Therapy,* July.p. 97.

Volkmer, J.-P.et al., 2012. Three differentiation states risk-stratify bladder cancer into distinct subtypes. *Proceedings of the National Academy of Sciences of the United States of America,* February, Volume 109, p. 2078–2083.

Waingankar, N. et al., 2019. The impact of pathologic response to neoadjuvant chemotherapy on conditional survival among patients with muscle-invasive bladder cancer. *Urologic Oncology: Seminars and Original Investigations,* September, Volume 37, pp. 572.e21-572.e28.

Wang, G. J., Brenner-Anantharam, A., Vaughan, E. D. & Herzlinger, D., 2008. Antagonism of BMP4 Signaling Disrupts Smooth Muscle Investment of the Ureter and Ureteropelvic Junction. *Journal of Urology,* April, Volume 181, pp. 401-407.

Wang, Y. et al., 1999. A mouse model for achondroplasia produced by targeting fibroblast growth factor receptor 3. *Proceedings of the National Academy of Sciences,* April, Volume 96, pp. 4455-4460.

Ware, K. E. et al., 2010. Rapidly Acquired Resistance to EGFR Tyrosine Kinase Inhibitors in NSCLC Cell Lines through De-Repression of FGFR2 and FGFR3 Expression. *PLoS ONE,* November, Volume 5, pp. e14117-e14117.

Warrick, J. I. et al., 2019. Intratumoral Heterogeneity of Bladder Cancer by Molecular Subtypes and Histologic Variants. *European Urology,* January, Volume 75, p. 18–22.

Webster, M. K., D'Avis, P. Y., Robertson, S. C. & Donoghue, D. J., 1996. Profound ligand-independent kinase activation of fibroblast growth factor receptor 3 by the activation loop mutation responsible for a lethal skeletal dysplasia, thanatophoric dysplasia type II.. *Molecular and Cellular Biology,* August, Volume 16, pp. 4081-4087.

Webster, M. K. & Donoghue, D. J., 1996. Constitutive activation of fibroblast growth factor receptor 3 by the transmembrane domain point mutation found in achondroplasia. *The EMBO journal,* February, Volume 15, p. 520–527.

Wei, H. et al., 2012. Genetic Variations in the Transforming Growth Factor Beta Pathway as Predictors of Bladder Cancer Risk. *PLoS ONE,* December, Volume 7, p. e51758.

Weinstein, M., Xu, X., Ohyama, K. & Deng, C. X., 1998. FGFR-3 and FGFR-4 function cooperatively to direct alveogenesis in the murine lung. *Development,* September, Volume 125, pp. 3615-3623.

Wezel, F., Pearson, J. & Southgate, J., 2014. Plasticity ofIn Vitro-Generated Urothelial Cells for Functional Tissue Formation. *Tissue Engineering Part A,* May, Volume 20, p. 1358–1368.

Whitfield, M. L., George, L. K., Grant, G. D. & Perou, C. M., 2006. Common markers of proliferation. *Nature Reviews Cancer,* February, Volume 6, pp. 99-106.

Wieduwilt, M. J. & Moasser, M. M., 2008. The epidermal growth factor receptor family: Biology driving targeted therapeutics. *Cellular and Molecular Life Sciences,* February, Volume 65, pp. 1566-1584.

Wijewardhane, N., Dressler, L. & Ciccarelli, F. D., 2021. Normal Somatic Mutations in Cancer Transformation. *Cancer Cell,* February, Volume 39, p. 125–129.

Wilhelm-Benartzi, C. S. et al., 2011. Association of secondhand smoke exposures with DNA methylation in bladder carcinomas. *Cancer Causes & Control,* June, Volume 22, pp. 1205-1213.

Williams, S. V., Hurst, C. D. & Knowles, M. A., 2012. Oncogenic FGFR3 gene fusions in bladder cancer. *Human Molecular Genetics,* November, Volume 22, pp. 795-803.

Wong, A. et al., 2002. FRS2 attenuates FGF receptor signaling by Grb2- mediated recruitment of the ubiquitin ligase Cbl. *Proceedings of the National Academy of Sciences,* May, Volume 99, pp. 6684-6689.

WU, D. E. Y. A. O. et al., 2014. microRNA-99a inhibiting cell proliferation, migration and invasion by targeting fibroblast growth factor receptor 3 in bladder cancer. *Oncology Letters,* February, Volume 7, pp. 1219-1224.

Wuechner, C. et al., 1996. Developmental expression of splicing variants of fibroblast growth factor receptor 3 (FGFR3) in mouse. *The International Journal of Developmental Biology,* December, Volume 40, p. 1185–1188.

Wu, X. R., Manabe, M., Yu, J. & Sun, T. T., 1990. Large scale purification and immunolocalization of bovine uroplakins I, II, and III. Molecular markers of urothelial differentiation. *The Journal of Biological Chemistry,* November, Volume 265, p. 19170–19179.

Xie, Y. et al., 2020. FGF/FGFR signaling in health and disease. *Signal Transduction and Targeted Therapy,* September.Volume 5.

Xu, X. et al., 1998. Fibroblast growth factor receptor 2 (FGFR2)-mediated reciprocal regulation loop between FGF8 and FGF10 is essential for limb induction. *Development,* February, Volume 125, pp. 753-765.

Yang, B. et al., 2014. In vitro comparative evaluation of recombinant growth factors for tissue engineering of bladder in patients with neurogenic bladder. *Journal of Surgical Research,* January, Volume 186, pp. 63-72.

Yeh, B. K. et al., 2003. Structural basis by which alternative splicing confers specificity in fibroblast growth factor receptors. *Proceedings of the National Academy of Sciences,* February, Volume 100, pp. 2266-2271.

Yu, J., Carroll, T. J. & McMahon, A. P., 2002. Sonic hedgehog regulates proliferation and differentiation of mesenchymal cells in the mouse metanephric kidney. *Development,* November, Volume 129, pp. 5301-5312.

Yu, J. et al., 1990. Uroplakin I: a 27-kD protein associated with the asymmetric unit membrane of mammalian urothelium.. *Journal of Cell Biology,* September, Volume 111, pp. 1207-1216.

Yu, K. et al., 2003. Conditional inactivation of FGF receptor 2 reveals an essential role for FGF signaling in the regulation of osteoblast function and bone growth. *Development,* July, Volume 130, pp. 3063-3074.

Yu, S. H. et al., 2024. FGFR3 Mutations in Urothelial Carcinoma: A Single-Center Study Using Next-Generation Sequencing. *Journal of Clinical Medicine,* February, Volume 13, p. 1305.

Zhang, C.-O., Li, Z.-L. & Kong, C.-Z., 2005. APF, HB-EGF, and EGF biomarkers in patients with ulcerative vs. non-ulcerative interstitial cystitis. *BMC Urology,* April.Volume 5.

Zhang, D. et al., 2006. FGF-10 and its receptor exhibit bidirectional paracrine targeting to urothelial and smooth muscle cells in the lower urinary tract. *American Journal of Physiology-Renal Physiology,* August, Volume 291, pp. F481-F494.

Zhang, X. et al., 2006. Receptor Specificity of the Fibroblast Growth Factor Family. *Journal of Biological Chemistry,* April, Volume 281, pp. 15694-15700.

Zhou, H. et al., 2016. FGFR3b Extracellular Loop Mutation Lacks Tumorigenicity In Vivo but Collaborates with p53/pRB Deficiency to Induce High-grade Papillary Urothelial Carcinoma. *Scientific Reports,* May, Volume 6, p. 25596.

Zhou, W. et al., 2009. FGF-receptor substrate 2 functions as a molecular sensor integrating external regulatory signals into the FGF pathway. *Cell Research,* October, Volume 19, p. 1165–1177.

Zhu, S. et al., 2020. Traditional Classification and Novel Subtyping Systems for Bladder Cancer. *Frontiers in Oncology,* February.Volume 10.